

Precipitation of CaCO_3 in natural and man-made aquatic environments - Mechanisms, analogues, and proxies

Martin Dietzel*, Ronny Boch

Graz University of Technology, Institute of Applied Geosciences, Rechbauerstrasse 12, 8010 Graz, Austria



ARTICLE INFO

Handling Editor: Astrid Holzheid

Keywords:

CaCO_3 formation
Calcite
Amorphous calcium carbonate
Environmental archives
Monitoring
Element and isotope fractionation
Environmental proxy
Calcareous deposits
Carbon dioxide
Geomicrobiology
Crystal growth and inhibition

ABSTRACT

Calcium carbonate precipitates occur in diverse and widespread aquatic environments, both from marine to terrestrial natural surroundings and from anthropogenic to engineered settings. In aquatic media, calcium and carbonate ions react to form hydrous and anhydrous CaCO_3 -containing solids in types of amorphous and crystalline phases, with calcite, aragonite and dolomite being the most frequent carbonate minerals in the Earth's crust. Understanding the CaCO_3 formation kinetics and mechanisms is key to exploring and evaluating individual aspects of biomineralization, speleothem and travertine growth, lime-/dolostone genesis, diagenetic pathways, climate reconstruction, CO_2 sequestration, tailored synthesis, unwanted scaling, mediated cementation, (geo) chemical forensics, etc. Although the literature dealing with CaCO_3 abundance, formation conditions, reaction mechanisms, nano- and macrostructures, elemental and isotope proxies is extensive, a comprehensive and up-to-date review of the highly diverse environments of CaCO_3 precipitation from aqueous media is valuable due to the tremendous increase in our knowledge about (i) CaCO_3 formation settings, analogues, reaction dynamics, and (potential) applications, (ii) novel high-precision, temporally and spatially highly-resolved analytical techniques, and (iii) monitoring, tracing and modeling tools. The present review on the formation of CaCO_3 in natural and man-made aquatic environments focuses on a systematic compilation and assessment of (i) reaction kinetics, mechanisms, and pathways of carbonate precipitation, (ii) analytical tools and proxies for tracking and reconstructing the solid-fluid-gas interactions and physico(bio)chemical environmental conditions during CaCO_3 precipitation, and (iii) natural and man-made analogs for the precipitation settings. The present review approach is not encyclopedic, but aims at a diverse array of environmental settings, the complex and coupled reaction pathways, state-of-the-art elemental and isotopic environmental proxies, and novel monitoring and modeling concepts for CaCO_3 precipitation.

1. Introduction

In natural environments, calcium carbonate bearing rocks are omnipresent in inorganic and biogenic sediments and sedimentary rocks, like skeletons of diverse organisms, microbial mats, ooids, calcrete, travertine, calcareous tufa, veins and filling of voids, evaporites,

saline lake deposits, speleothems and diagenetic cements: A schematic overview of widespread natural settings is given in Fig. 1 (see also section 8.1). A large number of former recapitulatory contributions display and highlight the relevance of the individual natural CaCO_3 deposits from sedimentary to diagenetic surroundings in aspects of their occurrences, structures, compositions and formation conditions (e.g. Bissell

Abbreviations: ACC, Amorphous calcium carbonate; ACMC, Amorphous calcium magnesium carbonate; BCC, Basic calcium carbonate; HMC, High Mg-calcite; LMC, Low Mg-calcite; VHMC, Very high Mg-calcite; T, Temperature ($^{\circ}\text{C}$); P, Pressure (atm); Pco_2 , Partial pressure of CO_2 (atm); K_s , Solubility constant; $[i]$, Molar concentration of component i ; γ_i , Activity coefficient of component i ; (i), Thermodynamic activity of component i ; Ω , Saturation degree; SI, Saturation index; D, Elemental distribution coefficient; α , Isotope fractionation factor; DIC, Dissolved inorganic carbon; DOC, Dissolved organic carbon; DCOM, Dissolved or colloidal organic matter; CAS, Carbonate associated sulfate; CCD, Carbonate compensation depth; $\mu\text{-CT}$, Micro-computer tomography; MICP, Microbial-induced carbonate precipitation; EICP, Enzyme-induced carbonate precipitation; MIC, Minimum inhibitor concentration; CCM, Cryogenic cave minerals; ASM, Asian summer monsoon; CCS, Carbon capture and storage; EGS, Enhanced geothermal systems; CPG, CO_2 Plume geothermal systems; CCUS, Carbon capture utilization and storage; CAES, Compressed air energy storage; DACSS, Direct air capture with synthetic sorbents; CDR, Carbon dioxide removal; scCO_2 , Supercritical state CO_2 ; DNA and RNA, (Deoxy)ribonucleic acid; EPS, Extracellular polymeric substances; SISAL, Speleothem isotopes synthesis and analyses.

* Corresponding author.

E-mail addresses: martin.dietzel@tugraz.at (M. Dietzel), ronny.boch@tugraz.at (R. Boch).

and Chilingar, 1967; Lippmann, 1973; Barthurst, 1971, 1975; Scholle et al., 1983; Morse and Mackenzie, 1990; Reeder, 1990; Tucker et al., 1990; Wright, 1992; Mackenzie, 2003; Schlager, 2005; Alonso-Zarza and Tanner, 2010; Deocampo, 2010; Flügel, 2010; Westphal et al., 2010; Fairchild and Baker, 2012; Swart et al., 2012; Arvidson and Morse, 2014; Swart, 2015; James and Jones, 2015; Zamanian et al., 2016; Gilbert et al., 2019; Fantle et al., 2020; Immenhauser, 2022; Dickson, 2023). The precipitation of CaCO_3 in aquatic media is also a common issue in anthropogenic and engineering settings comprising manufacturing of inorganic binder, scaling in water pipes, draining of infrastructure and hydrogeothermal systems, mineralization during CO_2 sequestration, tailored mineral synthesis, ion removal/recovering, archeometrical tasks, healthcare and medical applications, etc. (e.g. Tegethoff, 2001; Fujiwara et al., 2010; Power et al., 2013; Van Driessche et al., 2017; Chen et al., 2019; Hashizume, 2022; Oriols et al., 2022; see schematic overview in Fig. 2; see also section 8.2). Although CaCO_3 formation is highly divers in respect to its origin and precipitation conditions, nearly all of these environmental settings are associated with an aqueous medium and some induced gradients and disturbed equilibria of physicochemical parameters - like temperature, pressure or pH - and/or an exchange of chemical components with interrelated gas and solid phases.

In natural and man-made deposits the most abundant calcium and carbonate containing minerals are calcite (trigonal CaCO_3) and dolomite ($\text{CaMg}(\text{CO}_3)_2$). Both minerals comprise about 90 wt% of solid carbonate in the Earth's crust. In a simple approach the surroundings of CaCO_3 formation can be subdivided by their primary precipitation from an aqueous solution at low or high concentration of dissolved components, i.e. karstic spring or drinking water and seawater or brines from geothermal power plants, respectively. In any case, the formation and dissolution phenomena of CaCO_3 significantly affect the elemental cycles of e.g. Ca, Mg, Sr, C and S in the Earth's crust or in a given man-made surrounding.

Accordingly, elemental and (stable) isotope distribution of CaCO_3 precipitates are used to reconstruct the environmental conditions during their (trans)formation and thus evaluating e.g. the Earth's history of geochemical cycles and climate changes from past to the future (e.g. Sr/Ca, $^{44}\text{Ca}/^{40}\text{Ca}$ ratios as environmental proxies: Farkas et al., 2007; Gussone et al., 2020). Doing so, the paleo-seawater composition can be reconstructed and evaluated in terms of a carbonate factory and the evolution of CaCO_3 from its sedimentary realm to diagenetic

transformation reactions (e.g. Henderson, 2002; Armenteros, 2010; Swart, 2015; Turchyn and Depaolo, 2019; Wang et al., 2023a; see section 8.1.1). In another scenario, knowledge about how CO_2 trapping/degassing affect precipitation/dissolution of CaCO_3 minerals - and thus their elemental and isotope signals - is highly required to assess weathering rates, (paleo)climate changes, elemental fluxes, operating conditions, etc. (e.g. James and Jones, 2015; Boch et al., 2017a). Subsequent to CaCO_3 deposition, complex reaction pathways throughout diagenesis may yield in lithification to form limestone/dolostone to be traced by distinct environmental proxy signals (Armenteros, 2010; Swart, 2015). Under elevated temperatures and pressures, metamorphism may yield in the formation of marble, although not being a focus herein. Considering man-made settings, the CaCO_3 formation environments are numerous and highly divers spanning from cement industry to pharmaceutical productions (see section 8.2.1), where the evaluation and tracing of CaCO_3 mineral formation can be particularly realized by experimental and monitoring approaches with highly sound tools in order to understand and develop strategies of tailored CaCO_3 formation/inhibition (e.g. Jimoh et al., 2018; Hickman et al., 2019).

For all of the above surroundings an advanced understanding of the individual precipitation kinetics and mechanisms of CaCO_3 is essential to recover the causes and history of CaCO_3 formation pathways as well as to tailor its precipitation. Reaction mechanisms as well as elemental and isotope fractionation effects can be excellently revealed in settings with active CaCO_3 precipitation by *in-situ* and online monitoring approaches, where - besides the solid CaCO_3 reaction product - the reactive solution and the coexisting gas phase have to be considered in the context of a combined physicochemical system. Accordingly, travertine and unwanted scale formation was classically investigated by *in-situ* monitoring and thermodynamic modeling of aqueous-gaseous CO_2 exchange, as well as of nucleation and crystal growth and via the evolution of individual elemental and isotope signals (e.g. Dandurand et al., 1982; Dietzel et al., 1992; Boch et al., 2015).

The present review on precipitation of CaCO_3 in natural and man-made aquatic environments aims to give a comprehensive overview about the concepts of the $\text{CaCO}_3\text{-CO}_2\text{-H}_2\text{O}$ system (section 2), (non-) classical carbonate nucleation and precipitation pathways (section 3), individual and combined driving and inhibiting forces for CaCO_3 formation (section 4), CaCO_3 microstructure and fabrics indicative for its formation conditions (section 5), biological influences on CaCO_3 deposition (section 6), tracing of CaCO_3 formation by elemental and isotope

8.1. Natural environments

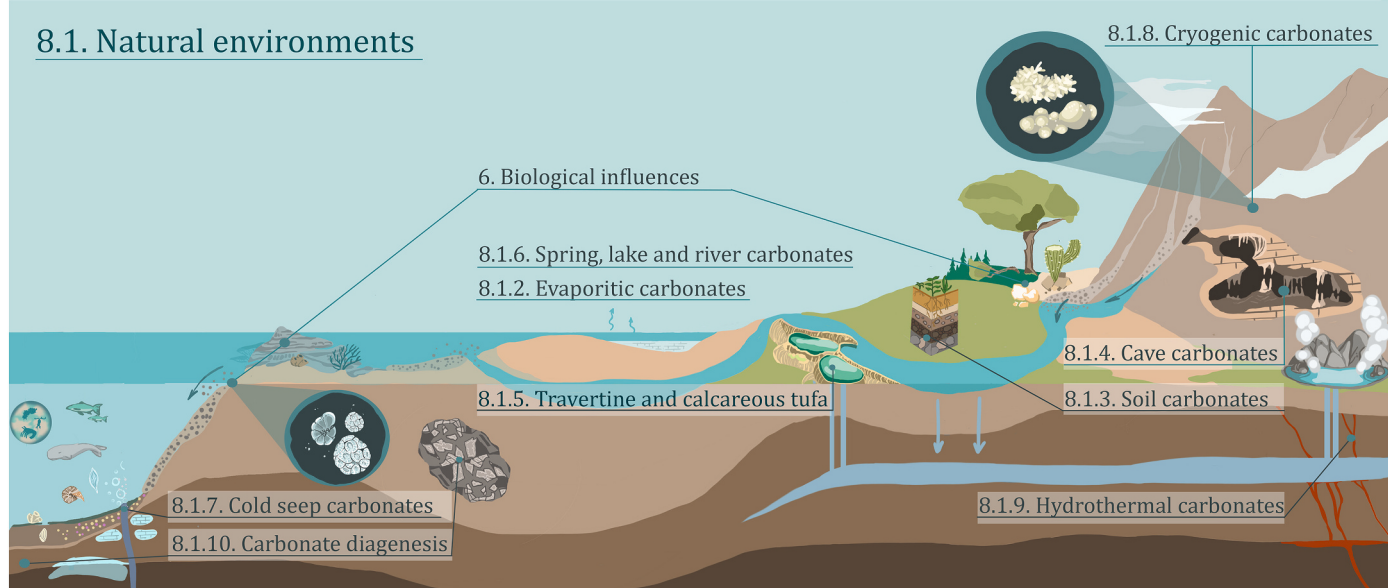


Fig. 1. Schematic overview about CaCO_3 precipitation in natural aquatic environments.

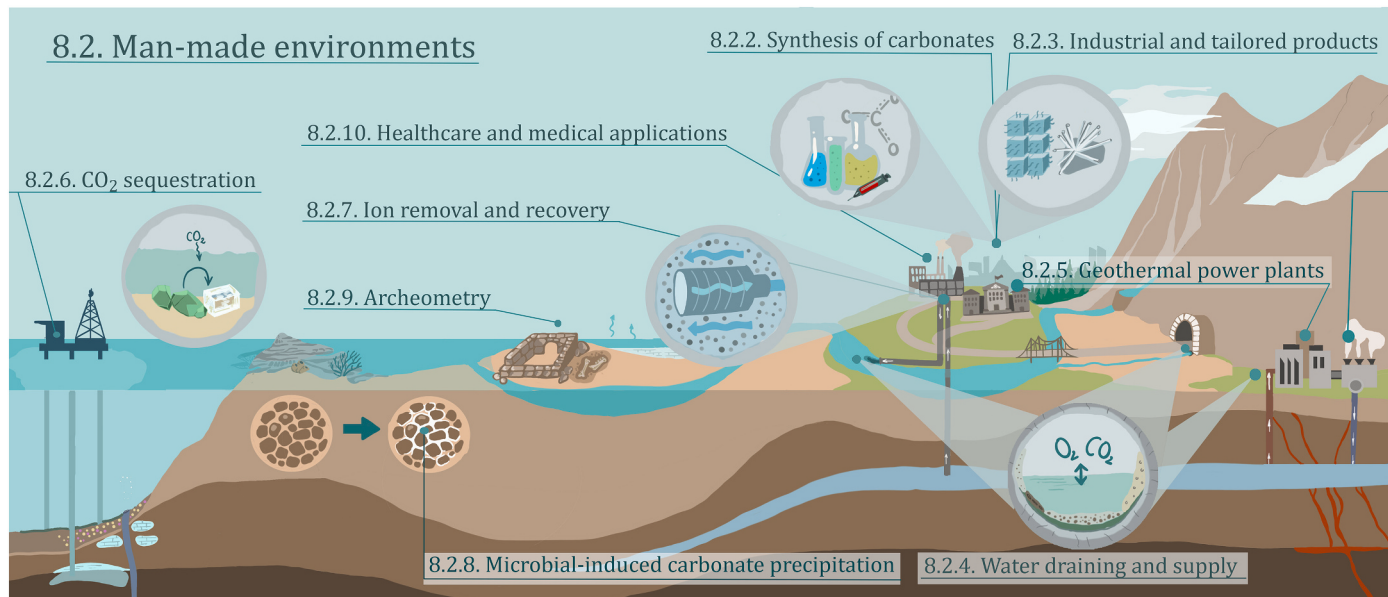


Fig. 2. Schematic overview about CaCO₃ precipitation in man-made aquatic environments.

proxies (section 7), natural and man-made CaCO₃ formation environments to be used as environmental archives and for technical applications (section 8), and environmental monitoring concepts of CaCO₃ nucleation and growth (section 9). The present approach is not encyclopedic and does not introduce the basics of the carbonate system, so it is intended more for experienced readers and scientists than for the beginner.

2. The CaCO₃-CO₂-H₂O system

Review articles and textbooks dealing with the (geo)chemistry of the CaCO₃-CO₂-H₂O system have been manifold throughout the past (e.g. Garrels and Christ, 1965; Lippmann, 1973; Loewenthal and Marais, 1976; Usdowski, 1982; Reeder and Barber, 1983 Morse and Mackenzie, 1990; Stumm and Morgan, 1996; Appelo and Postma, 2005; Morse et al., 2007; MacKenzie and Andersson, 2013; Du and Amstad, 2020), where the main reaction mechanisms for CaCO₃ formation are properly developed. The present contribution provides a brief overview and update of current knowledge with foci on most relevant and novel conclusions on CaCO₃ stabilities and formation mechanisms.

CaCO₃ containing solids comprise of crystalline and amorphous phases, which basically consist of cations (e.g. Mg²⁺ and Sr²⁺ besides Ca²⁺) and triangular carbonate groups (CO₃²⁻) as anions. In individual cases, additional components such as OH⁻, SO₄²⁻, and H₂O can be incorporated (see section 7.1). However, the anhydrous *pure* CaCO₃ polymorphs comprise - with increasing order of their solubility - the minerals calcite, aragonite, and vaterite (e.g. Morse et al., 2007). In contrast to calcite and aragonite with well-defined crystal structures and coordination numbers [6] and [9] of the Ca ion in respect to O ions, the structure of vaterite is still not completely understood but addressed to nanoscale intergrowth of two polytypes (e.g. Burgess and Bryce, 2015; Christy, 2017). Hydrous *pure* CaCO₃ minerals are hemihydrate CaCO₃·½H₂O (Zou et al., 2019 and Schmidt et al., 2024; intermediate hydrated phase), monohydrocalcite (CaCO₃·H₂O), ikaite (CaCO₃·6H₂O), and a basic calcium carbonate (BCC: Ca₃(CO₃)₂(OH)₂·H₂O; found in technical high alkaline settings; Ripken et al., 2018).

Further Ca-bearing carbonate minerals are numerous, like dolomite (CaMg(CO₃)₂), huntite (CaMg₃(CO₃)₄), ankerite (Ca(Fe^{II},Mg,Mn)(CO₃)₂), bütschliite (K₂Ca(CO₃)₂), sergeevite (Ca₂Mg₁₁(CO₃)₁₃·10H₂O), kutnohorite (Ca(Mn,Mg,Fe^{II})(CO₃)₂), barytocalcite (BaCa(CO₃)₂), shortite (Na₂Ca₂(CO₃)₃), gaylussite (Na₂Ca(CO₃)₂·5H₂O), kamphaugite

(CaY(CO₃)₂(OH)·H₂O), defernite (Ca₃(CO₃)(OH,Cl)₄·nH₂O), tilleyite (Ca₅Si₂O₇(CO₃)₂) and thaumasite (Ca₃Si(CO₃)(SO₄)(OH)₆·12(H₂O)) (e.g. Railbsack, 1999). Several of these minerals are rare in their occurrence and precipitate at highly diverse and specific environments; e.g. thaumasite as product of silicate alteration at alkaline conditions (e.g. Galan et al., 2019).

Besides minerals, amorphous calcium carbonate (ACC: CaCO₃·nH₂O) can be formed as a metastable and transition phase, e.g. temporarily stabilized by Mg ions to form amorphous calcium magnesium carbonate (ACMC: Ca_xMg_(1-x)CO₃·nH₂O; e.g. Purgstaller et al., 2019). It has to be noted that besides triangular CO₃²⁻ also tetrahedral CO₄⁴⁻ groups can be generated by reaction of CO₂ with CaCO₃ at Earth's Lower Mantle conditions (e.g. Ca₃CO₅ and Ca₂O₅; Yao et al., 2018; König et al., 2022), but are not in the focus herein.

In an aquatic environment the thermodynamic stability of a given solid phase is defined by its solubility constant (K_S) according to the equation.



for the *pure* Ca endmembers, where the value of K_S = (Ca²⁺) · (CO₃²⁻) · (H₂O)ⁿ depends on temperature (T) and pressure (P) (0 ≤ n ≤ 6; thermodynamic activity: (i)_i = γ_i [i]; γ_i: activity coefficient; [i]: molar concentration of component i; e.g. Appelo and Postma, 2005). Calcite has the lowest K_S value (10^{-8.5} at T = 25 °C; Plummer and Busenberg, 1982) of the solid CaCO₃ phases, thus being the thermodynamically stable modification at ambient conditions. In contrast, amorphous CaCO₃·0.45 H₂O has the highest K_S (10^{-6.5} at T = 25 °C), thus calcite is being ~100fold supersaturated in the presence of metastable ACC at 25 °C (e.g. Wedenig et al., 2021). The solubility of ACC is considered as the upper limit of apparent ion activity products (IAP = (Ca²⁺) · (CO₃²⁻) · (H₂O)ⁿ) to be reached in an aqueous medium.

ACC formation can be understood as a liquid-liquid segregation, thus ACC is acting as a liquid/gel-like phase rather than a solid (e.g. Brazier et al., 2024b; Gindale et al., 2024). The higher the temperature, the lower the solubility of solid CaCO₃·nH₂O (lower K_S). As an exception, the K_S of ikaite increases at elevated T (Bischoff et al., 1993). Ikaite's solubility behavior results in an interception with monohydrocalcite's solubility at about 7 °C, where above this T monohydrocalcite is stable over ikaite.

High pressure yields in elevated solubilities of CaCO₃ minerals, which causes deep-sea sediments below the so-called carbonate

compensation depth ($CCD = 3\text{--}5 \text{ km}$, e.g. Morse and Mackenzie, 1990) to be free of CaCO_3 . Considering carbonate-based rocks, pressure dissolution is a well-known phenomenon (Diao et al., 2020). However, the impact of total pressure on CaCO_3 solubility has to be distinguished from partial pressures of individual gases, in particular CO_2 , as discussed below.

Precipitation of CaCO_3 requires supersaturation to be reached, thus the saturation index ($SI = \log\{\Omega\} = \log\{(IAP \cdot K_S^{-1})\}$; Ω : saturation degree) in respect to a given solid phase being positive. For calcite, a spontaneous precipitation caused by instantaneous nucleation from a homogeneous solution is reached at about $SI_{\text{calcite}} > 0.8$ (about 6-fold supersaturation). Main driving forces to reach such a threshold are changes in T, P, pH, CO_2 degassing, evaporation, mixing of solution, etc. (see sections 3, 4 and 8.2.2) and can be quantified by hydrogeochemical modeling tools (e.g. Appelo and Postma, 2005; Parkhurst and Appelo, 2013). This includes aspects of the distribution of dissolved inorganic carbon (DIC) species (DIC: $\text{CO}_{2(\text{aq})}, \text{H}_2\text{CO}_3^\circ, \text{HCO}_3^-, \text{CO}_3^{2-}$, where $\text{CO}_{2(\text{aq})}$ is dominant over $\text{H}_2\text{CO}_3^\circ$ by a factor of 1000) and the occurrence of aquo-complexes such as $\text{CaCO}_3^\circ, \text{CaSO}_4^\circ$, and $\text{Ca}(\text{HPO}_4)^\circ$ (e.g. Usdowski, 1982; Tosca and Tutolo, 2023). Analogous relationships for carbonate based aquo-complexes are valid for e.g. Mg, Sr, Ba, and Na ions. In acidic solution the dissolution of CaCO_3 is favored by a high $\text{H}_2\text{CO}_3^\circ$ concentration ($[\text{H}_2\text{CO}_3^\circ] = [\text{CO}_{2(\text{aq})}] + [\text{H}_2\text{CO}_3]$) at low $[\text{CO}_3^{2-}] / [\text{DIC}]$ ratios, whereas at high pH the precipitation of CaCO_3 is stimulated.

In any case, DIC species re-distribution e.g. by change of pH needs time, where distinct equilibration times for a given pH scenario can be estimated by the kinetical approach developed by Sade et al. (2022a). It has to be noted that in extremely alkaline settings, not only precipitation, but also dissolution of (Mg-bearing) CaCO_3 can be initiated by the formation of sodium carbonate or magnesium hydroxide, e.g. observed for calcite and dolomite (Simoni et al., 2022 and Mittermayr et al., 2017, respectively).

An excellent example for the effect of strong aquo-complexes is $\text{Ca}(\text{HPO}_4)^\circ$, where Ca ions are nearly quantitatively bound by added phosphate ions according to its 1:1 stoichiometry, e.g. used to reduce water hardness and inhibit CaCO_3 precipitation. NaHCO_3° formation is relevant for alkaline solutions to reduce CO_3^- ion activities. CaSO_4° versus MgSO_4° aquo-complexes are discussed in the scope of the formation of Mg—Ca bearing carbonates, such as dolomite. Aufort et al. (2022) found Mg paired with CO_3^- in aqueous solution - besides reducing CO_3^- ion activities - to trigger the precipitation of Mg-bearing carbonates by accelerating water exchange around the aqueous Mg^{2+} ion. In this context, a comprehensive database of aqueous components to promote Mg-containing carbonate nucleation by Mg^{2+} dehydration is given in Toroz et al. (2022).

The distribution and activities of aqueous species can be strongly influenced by the exchange of compounds at the liquid-solid interface (e.g. dissolution, precipitation of solids) and/or liquid-gas interface. The latter effect comprises e.g. liberation or uptake of CO_2 and H_2O . The CO_2 exchange is assessed by the Henry constant ($K_H = (\text{CO}_{2(\text{aq})}) / P_{\text{CO}_2}$), where P_{CO_2} in atm can be calculated for a given solution as so-called internal partial pressure of CO_2 by considering thermodynamic equilibrium conditions. Assuming Earth's atmospheric conditions, the internal P_{CO_2} has to be higher ($P_{\text{CO}_2} > 10^{-3.4} \text{ atm}; \approx 400 \text{ ppm CO}_2$) to induce degassing of CO_2 from the solution to the atmosphere and vice versa. In the aspect of gaseous CO_2 exchange with an aqueous solution, carbon dioxide nanobubbles may increase the effective gas-transfer to solution and enhance buffering capacities (e.g. Antonio et al., 2022; Zarei et al., 2024).

3. Nucleation and precipitation pathways

The occurrence and formation of CaCO_3 in natural and man-made aqueous environments is based on inorganically and/or biogenically promoted precipitation (e.g. Morse and Mackenzie, 1990; Dove et al., 2003; Mpelwa and Tang, 2019). CaCO_3 formation of inorganic origin e.

g. in most speleothems or scale deposits can be followed by thermodynamic modeling approaches by considering chemical equilibria and reaction kinetics, surface speciation, solid structure characterization etc. (see also sections 2 and 4). Biogenically induced CaCO_3 precipitation is referred to much more complex settings, where internal fluids, micro/nano environments facilitating Ca and CO_3^- ionic bonding, organic templates and tissues, enzymes, ion pumping etc. have to be considered (see section 6).

The individual formation and assemblages of CaCO_3 bearing precipitates are highly kinetically controlled and depend on the individual formation pathways, which can be triggered by T and supersaturation degrees or might be inhibited by foreign aqueous ions, e.g. carboxylic/amino acids (Ma et al., 2019; Mpelwa and Tang, 2019; see also section 4). The classical theory of nucleation and growth of solid CaCO_3 considers homogenous or heterogeneous nucleation. In the first case, nucleation of CaCO_3 is described in a homogeneous solution as an ongoing formation and decomposition of CaCO_3 clusters as soon as a critical supersaturation degree is reached (e.g. Putnis, 2003). Avaro et al. (2023) applied *in-situ* small-angle X-ray scattering and found CaCO_3 prenucleation clusters of about 3.5 nm size, but even at undersaturation with respect to calcite, which hints at established nucleation concepts to be revised. However, as soon as a critical cluster size is reached - depending on the saturation state of the aqueous solution, reaction time etc. - these clusters do not dissolve, but keep on growing. The CaCO_3 nucleus obtained in this way grows at the expense of smaller clusters to yield seed crystals of e.g. calcite, aragonite, or ikaite. Heterogeneous CaCO_3 nucleation is based on the presence of surface sites and/or seeds, like crystalline CaCO_3 , where nucleation occurs by linking steps on Ca^{2+} and CO_3^{2-} ions at distinct surface sites and/or on attraction of aquo-complexes. For instance, Nehrk et al. (2007) have shown the control of CaCO_3° complex formation on the precipitation rate of calcite.

For such a **classical formation pathway** of calcite the rate of precipitation can be followed by the empirical and thermodynamic approaches of Wolthers et al. (2012) or Plummer et al. (1978), respectively. The latter rate equation is based on T depending reaction rate constants by considering the saturation degree, pH, and internal partial pressure of CO_2 . This concept was successfully used in numerous studies on both precipitation and dissolution of calcite (and dissolution of dolomite). It is in particular applicable being implemented in the computer code PhreeqC (Parkhurst and Appelo, 2013) and coupled with CO_2 exchange kinetics between solution and gas phase (e.g. simulating and assessing the impact of an inhibitor on nucleation and growth of CaCO_3 ; Wedenig et al., 2021).

Aragonite - the orthorhombic and thermodynamic stable CaCO_3 modification at high P - can be easily precipitated as metastable solid phase at near Earth's surface conditions within an aquatic medium at elevated Mg/Ca ratios due to poisoning of calcite nucleation and growth at its surface. The poisoning effect is based on the adsorption of Mg^{2+} ions onto the calcite nuclei or surfaces and the need to get rid of it's strongly bound hydration sphere to be incorporated as free Mg^{2+} ion into the crystal lattice. Thus, aragonite is often found in marine sediments, although it is metastable against (low-Mg) calcite (Berner, 1975). In analogy, calcite - the high T anhydrous CaCO_3 modification - is frequently formed at low temperatures in aquatic surroundings due to its low solubility.

For nucleation, growth and dissolution kinetics of CaCO_3 in aquatic surroundings the solid-liquid interface determines distribution and activities of solid surface sites and dissolved species have a main control on the direction, strength and specificity of CaCO_3 formation. In this context, the prominent so-called "dolomite problem" has to be addressed: Why is dolomite highly frequent in sedimentary rocks but rarely formed in modern natural environments and experimental settings? Contributions on this task are extremely voluminous and not in the main focus of this study, thus it is exemplarily referred to Hardie (1987), Land (1998), Meister et al. (2013), Gregg et al. (2015), Pina et al. (2020), and Immenhauser (2022). Briefly, it is concluded that

direct precipitation of dolomite and reaching its superstructure, which is based on an ideal alternation of separated Mg and Ca ion layers within the crystal lattice, is mainly inhibited by the high relative energy of dolomite (e.g. Pimentel et al., 2022) and by the above mentioned Mg poisoning effect, but can be overcome via progressive dissolution-(re) crystallization of precursor phases, such as ACMC and very high Mg-calcite, throughout extended (geological) time intervals (see Deelman, 1999; Kaczmarek et al., 2017; Kell-Duivestein et al., 2019; Meister and Frisia, 2019; Ryan et al., 2020; Pina et al., 2022; Kim et al., 2023a; Chen et al., 2023a). Very high Mg-calcite is denoted as VHMC or protodolomite, where the molar Mg/Ca ratio is close to unity with no or non-ideal Mg and Ca cation ordering in the crystal lattice. Early marine diagenetic formation of (proto)dolomite from reactive porewater is suggested to build up a main part of dolomitic rocks besides sabkha, playa, microbial, mixing-zone, and hydrothermal settings etc., but the formation kinetics and mechanisms of low temperature dolomite are still far from being completely understood (see section 8.1; Rieder et al., 2019; Chang et al., 2020; Meister et al., 2023; McCormack et al., 2024; Mueller et al., 2021; Immenhauser, 2022; Raudsepp et al., 2024; and references therein). In this context experimental approaches yield in protodolomite formation down to 40 °C (and 60 °C for dolomite) from highly concentrated solutions and crystalline/amorphous (Mg-bearing) CaCO_3 precursor phases (e.g. Usdowski, 1994; Kelleher and Redfern, 2002; Horita, 2014; Rodriguez-Blanco et al., 2015). In another setting, Zaquin et al. (2022) and Eichinger et al. (2023) documented the growth of high Mg-calcite (HMC) to act as aragonite nuclei in CaCO_3 overgrowth experiments and settings, respectively.

The presence of Mg ions may promote ikaite formation, both kinetically and thermodynamically, expanding the occurrence of ikaite in cold water (Chaka, 2019). Non-carbonate-bearing surfaces may also provide carbonate mineral nucleation sites: Fodor et al. (2020), Liu et al. (2019a, 2019b), and Strohm et al. (2022) hint on the role of clay surfaces for the heterogeneous nucleation of calcite and (proto)dolomite, and ikaite, respectively. Montmorillonite was found to be more efficient compared to kaolinite in capturing aqueous ion clusters, which are preferentially formed in the interlayer/liquid phase, to initiate nucleation and growth of calcium magnesium carbonate minerals.

The estimated CaCO_3 precipitation rates (R in $\text{mol/m}^2/\text{h}$) often disagree with values documented in nature, mostly caused by (i) inaccurately determined reactive mineral surfaces and (ii) inhibition effects by foreign ions or organic matter (e.g. Zaihua et al., 1995; Naviaux et al., 2019). For the latter aspect anions, like phosphate and polyaspartic acid, and in particular divalent ions such as Mg^{2+} , Fe^{2+} , Sr^{2+} , Ba^{2+} , Cs^{+} , and Li^{+} can significantly affect the precipitation behavior of CaCO_3 (Gutjahr et al., 1996; Marin-Troya et al., 2023; Strohm et al., 2023; see also section 4). Anyhow, CaCO_3 growth has to be understood as a coupled dissolution-precipitation process at the solid-water interface, which was recently *in-situ* monitored by Renard et al. (2019) using atomic force microscopy. Precipitation rates have to be considered as a positive net balance for precipitation versus dissolution, where $R = 0$ is referring to a dynamic chemical equilibrium. Thus, at chemical equilibrium uptake and liberation of Ca and CO_3 at the solid surface of e.g. calcite from/into the solution are ongoing depending on the rate constant of precipitation and dissolution reactions. These exchanges of ions at the solid-liquid interface can be verified and assessed by stable isotope distribution, where a couple of surface CaCO_3 layers are actively involved (e.g. Oelkers et al., 2019; Harrison et al., 2022; Harrison et al., 2023; see section 7.2).

In contrast, the so-called **non-classical crystallization pathway** is based on the formation precursors, in particular amorphous phases (e.g. Sawada, 1997; De Yoreo et al., 2015; De Yoreo, 2020). At this point, it should be noted that Nielsen et al. (2014) claimed both classical and non-classical pathways to be occurring simultaneously, and recently Zhang and Wang (2024) developed a surface kinetic model to evaluate the roles of classical and non-classical crystallization mechanisms in calcite precipitation by Ca and Sr isotope fractionation. However, such

metastable phases are formed at extremely high Ca^{2+} and CO_3^{2-} ion activity levels and are composed of ACC spherules of several tens to hundreds of nm (e.g. Gebauer and Cölfen, 2011; Brazier et al., 2023). Note, that in a different approach ACC can also be formed by heavy milling of calcite, where its mechanochemical amorphization was realized by Na ion incorporation into the amorphous phase for its stabilization (Leukel et al., 2018), which is not in the focus herein.

Precipitated ACC may contain different amounts of water molecules (n), where H_2O at $n = 0.45$ level is suggested to be bound within the inner ACC structure, whereas an outer H_2O layer is formed for n above this limit. At individual H_2O levels ($n > 0.9$ at ambient conditions) ACC instantaneously starts to transform towards crystalline CaCO_3 via dissolution and re-precipitation (e.g. Konrad et al., 2016; Koishi et al., 2019). In contrast, H_2O loss of ACC throughout heating in air induces solid state transformation at T of about 320 °C (e.g. Ihli et al., 2014). H_2O supply to ACC can be generated by condensation of gaseous H_2O at the ACC surface and/or from an interacting aqueous solution, where the atmospheric humidity can control the metastability of (Mg-bearing) ACC (Du and Amstad, 2020; Cheng et al., 2024; Patel et al., 2024). Gebauer et al. (2010) and Mergelsberg et al. (2020a) postulated pre-structured ACC to predict the final mineral phase or even local structures within ACC. In contrast, Gower and Odom (2000) and Wallace et al. (2013) suggested a liquid-liquid separation for amorphous CaCO_3 formation (see also section 2). A concept adapted by Gebauer et al. (2014) considering the formation of non-specific ACC involves the formation sequence in order of (i) pre-nucleation clusters, (ii) dense liquid nanodroplets, (iii) liquid/gel-like ACC, (iv) solid ACC, and (v) anhydrous crystalline polymorphs. This approach is in accordance with the general perception of Jensen et al. (2018), who concluded from neutron, X-ray total scattering and molecular modeling, local arrangement of the ions in ACC to be more similar to those of ions in aqueous solution than to any of a CaCO_3 mineral. Liu et al. (2019a, 2019b) and De Yoreo et al. (2022) further supported this view by considering crosslinking of ionic oligomers as conformable CaCO_3 precursors via TEM analyses and the formation of a CaCO_3 dense liquid phase by *in-situ* liquid-state NMR technique.

Recent developments in understanding ACC (trans)formation and non-classical CaCO_3 crystallization pathways are in particular gained by *in-situ* techniques, like X-ray, Raman and Infra Red Spectroscopy, where distinct and complex precipitation and dissolution mechanisms are traced highly time-resolved (Xto et al., 2019b; Purgstaller et al., 2021; Mehta et al., 2022). For instance, the early nucleation stage of CaCO_3 mineral formation has been studied by Avaro et al. (2019a) using mixing and freeze-quench-technique coupled to X-ray absorption spectroscopy. They concluded CaCO_3 prenucleation clusters to exist as highly hydrated with a short-range order - in the present case - similar to calcite in the first and second coordination shell, which supports the decisive role of non-classical nucleation.

Understanding and application of natural and man-made CaCO_3 formation via the non-classical ACC-based pathway requires advanced insight on the dynamics and limits of precipitation/dissolution of ACC, the effects initiating or inhibiting nucleation, and sequences of mineral (trans)formation. In this way, Brazier et al. (2024b) reviewed the formation and transformation behavior of ACC to be a liquid-like phase. This view implies highly dynamic ion exchange with the surrounding aqueous medium and thus a rapid elemental and also isotopic readjustment of its composition during transformation (e.g. Xto et al., 2019a). ACMC solubility and transformation experiments by Purgstaller et al. (2017a) and Purgstaller et al. (2019) support this rapid ion exchange phenomenon by finding an instantaneous adjustment of ACMC and aqueous Mg:Ca stoichiometry. Accordingly, a given ACMC educt may contain vaterite, calcite, monohydrocalcite, ikaite etc. and different crystal sizes and shapes depending on the environmental conditions during its transformation, which makes (Mg-bearing) ACC promising for the design of functional biomimetic and tailored materials (e.g. Asta et al., 2020). The formation and lifetime of ACC and its transformation

products are - besides T and P - affected by pH, Mg^{2+} , Cd^{2+} , PO_4^{3-} , SO_4^{2-} , silica, carboxylic acids, polysaccharides, amino acids, proteins etc., which occur in its structure, at its surface or in the transforming solution (e.g. Rodriguez-Navarro and Benning, 2013; Blue and Dove, 2015; Tobler et al., 2016; Blue et al., 2017; Konrad et al., 2018; Evans et al., 2019; Zou et al., 2020; Lam et al., 2007; Mergelsberg et al., 2021; Molnár et al., 2023).

Non-classical formation pathways indicate phase separation of liquid amorphous carbonates: a finding that should be taken into account in ongoing research on the use of environmental proxies. A hot topic for further research is the (trans)formation of amorphous $CaCO_3$ precursors in the fields of biomineralization, bionic, medicine and technical synthesis, as well as CO_2 capture and storage. For instance, (i) the formation of ACC buffers the dissolved Ba/Ca and Sr/Ca ratios (e.g. Segovia-Campos et al., 2022), (ii) changes in physicochemical conditions can be used to store/activate ACC and tailor its crystallization, shape etc. in biomineralization (e.g. Han and Eizenberger, et al., 2008; Evans et al., 2019), and (iii) even at low temperature ACMC formation provides a pathway to crystallize $Ca-Mg-CO_3$ minerals (e.g. high Mg-calcite, magnesite; Purgstaller et al., 2017a; Mergelsberg et al., 2020b; Liu et al., 2024a).

4. Driving and inhibiting forces

The overall driving force for the formation of $CaCO_3$ precipitates from an aqueous solution can be followed by an ongoing increase of saturation degree of a given $CaCO_3$ mineral to reach a distinct supersaturation state to induce nucleation and subsequently start growing e.g. calcite at a given rate (see sections 2 and 3). Increase of Ω can be reached by changing the physicochemical parameters of the solution, such as T, P, chemical composition (Oelkers and Schott, 2009). Temperature and P impact on $CaCO_3$ formation in aqueous media is mostly based on their effects on the stability constants, e.g. for solubilities, dissociation reactions and aquo-complex formation, and thus distribution of aqueous species (e.g. Stumm and Morgan, 1996).

For instance, an increase of T throughout burial of sedimentary carbonates can promote $CaCO_3$ cementation from the pore solution. In contrast, $CaCO_3$ pressure dissolution and associated re-crystallization forms stylolites (e.g. Tada and Siever, 1989; Rashid et al., 2020; see section 2). Modification of the chemical composition of the solution can be based on mixing of distinct solutions, evaporation, exchange of components at the liquid-solid and/or liquid-gas interface (see section 8.2.2). Mixing of solutions with different composition initiate redistribution of aqueous species, which induce for instance the formation of the hexahydrate of $CaCO_3$ building the ikaite tufa towers in Ikka Fjord (see section 8.1.8). Considering the solid phase interaction with an aqueous solution via dissolution, ion exchange and/or desorption effects can cause calcium, carbonate and/or hydroxide release into the aqueous solution, which supports $CaCO_3$ formation. The latter aspect is in particular valid for the dissolution of silicates and (hydr)oxides, like feldspar, pyroxene, periclase, portlandite, and based on an increase of pH, besides providing Ca ions. Prominent and extreme $CaCO_3$ precipitating environments comprise alteration of (ultra)mafic rocks (see section 8.1.9) and alteration of concrete and CO_2 sequestration (see section 8.2.6). An exchange of components between the liquid and gas phase can be referred to H_2O , CO_2 , NH_3 , H_2S , SO_2 etc., where evaporation of H_2O and degassing of CO_2 can induce $CaCO_3$ formation (e.g. sections 8.1.2, 8.1.4, 8.1.5, and 8.2.4).

Precipitation kinetics and mechanisms as well as polymorphism of $CaCO_3$ are influenced by the occurrence and concentration of specific chemical constituents in aqueous solution (see section 3). Laboratory experiments and empirical observations support effects of different molecules and functional groups acting as nucleation and crystal growth inhibitors (or stabilizers) of distinct mineral phases (e.g. Gebauer et al., 2009; Dobberschütz et al., 2018). Typically, moderate to very small concentrations of the inorganic or organic chemical agents are sufficient

to inhibit or alter the resulting mineral formation. Inhibition of $CaCO_3$ precipitation was observed from significant phosph(on)ate, nitrate and sulfate contents in natural as well as technical settings (e.g. Rodriguez-Navarro and Benning, 2013; Hu et al., 2015). Various organic molecular components from natural and biotechnical sources can also influence $CaCO_3$ crystal growth and mineralogy. Effects of variable significance have been reported for macromolecular humic and fulvic acids, citric and tartaric acid, EDTA, polyaspartic and other amino acids, polyacrylic acid, *aloe vera*, olive, fig and gambier extracts from leaves and other plant components, as well as from chitin derived constituents (e.g. Chaussemier et al., 2015; Lourteau et al., 2019).

Regarding (geo)technical and industrial applications, inorganic and organic additives play an increasing role as carbonate scale inhibitors, i.e. constituting a preventive measure against unwanted mineral deposits (loose sediments or hard crusts) during hydrogeothermal energy production, as well as petroleum and natural gas production from deep aquifers and reservoirs, drainage of waters in rail- and highway tunnels or drinking- and process water treatment (e.g. Li et al., 2015a; Mpela and Tang, 2019). Next to carbonate scaling evolving from chemical sedimentation and solidification in the context of dissolved solid and gas rich aqueous solutions, specific chemical additives (inhibitors) are also applied against various corrosion processes (e.g. antioxidants) and for suppression of problematic biofilms (biocides). The numerous agents being either commercially available or subject of research efforts support the labor and cost intense maintenance of (geo)technical infrastructure. More conventional (mostly phosphorus-based) additives can be discerned from a trend towards “green” agents, i.e. typically non-toxic, biodegradable, non-phosphorus and therefore eco-friendly green inhibitors.

Addressing the fundamental and distinct functional mechanisms related to the variable inhibition efficiency of $CaCO_3$ crystallization, the chemical additives affect critical interfaces and reaction steps during fluid-solid interaction in the atomic-molecular spatial range, e.g. the availability, stability and compatibility of dissolved ionic species being relevant with regard to crystal nucleation and growth. More specifically, the inhibitors can influence the prevalence of aqueous complexes, the hydration shell and dehydr(oxy)lation of dissolved ionic and molecular constituents, and the possible chelation of critical elements, e.g. keeping Ca in aqueous solution at higher total concentration levels.

Alternatively, inhibition effects are often based on distinct surface effects impacting further ion attachment and step propagation at crystal growth sites, i.e. poisoning and blockage of crystal growth based on surface entrapment and (ad)sorption processes (see section 3 for Mg ions). For example, $CaCO_3$ precipitation is restricted by the adsorption of soluble pre-nucleation clusters to various polycarboxylates in aqueous solution (e.g. Gebauer et al., 2009; Kumar et al., 2018). Next to specific functional groups (e.g. carboxyl-, amino-), the molecular weight and concentrations added strongly determine the inhibition process. In this context, a “threshold effect” might allow for non-stoichiometric concentrations of the inhibitor in aqueous solution still being favorable for the efficient suppression of crystallization (Ketrane et al., 2009). The necessary minimum inhibitor concentrations (MIC) might thus be (very) low and crystal nucleation might be inhibited even at high supersaturation conditions (e.g. Cooper et al., 1979; Sanni et al., 2019).

It is frequently observed that different inhibitors also modify crystal shapes and the resulting fabrics (e.g. Jones and Ogden, 2010; see section 5). For example, the edges and corners of calcite crystals might become less distinct, e.g. curved and rounded (Macedo, 2019). Also, the macroscopic calcium carbonate (scale) material consistencies can be affected significantly, i.e. resulting in compact and hard crusts or mud-grade carbonate (Zhang et al., 2016). Various inhibitors provided at relatively higher concentrations can also act as nutrient supply (e.g. NPK fertilizer) and hence can influence the occurrence of heterotrophic microbial communities (biofilms; Westphal et al., 2019).

The numerous available inhibitors and their inhibiting effects are the subject of an evolving spectrum of simple to complex testing procedures

in the experimental laboratory or site-specifically in the technical facilities (e.g. tunnels, wells). This concerns tests of different chemical agents, products and merchants, optimum (minimized) dosages and blended (combined) additives (e.g. Chaussemier et al., 2015; Li et al., 2019a). Further, it includes an assessment of inhibitor-specific retardation and reduction efficiencies, the occurrence of spontaneous homogeneous nucleation vs. heterogeneous nucleation on preexisting substrates and the variable CaCO_3 material consistencies. Established test procedures such as the more static jar (bottle) tests have to be distinguished from dynamic tube (capillary) blocking tests (e.g. Sanni et al., 2019). Further, new testing approaches involving automated data loggers based on distinct electrodes and optical sensors allow for high temporal and spatial resolution online and on-site monitoring of the crystallization processes vs. inhibitor effects (e.g. Ghosh and Lai, 2023). This includes the tracking of pH, electric conductivity, Ca concentration, alkalinity (HCO_3^-), dissolved organic carbon (DOC), CO_2 concentration and fluorescence of the investigated inhibitors interacting with typically CaCO_3 supersaturated aqueous solutions. Fluid and solid monitoring results are frequently combined with hydrogeochemical modeling (e.g. Dobberschütz et al., 2018; Li et al., 2019a; Wedenig et al., 2021; see section 9).

Apart from the interaction with specific chemical additives, CaCO_3 precipitation and different polymorphs can either be inhibited or promoted by physical triggers. Strong magnetic fields can influence crystal nucleation and material characteristics and are used against scaling in geothermal energy facilities, during crude oil production and the desalination of drinking or industrial process water (e.g. Gabrielli et al., 2001; Al et al., 2018). More specifically, during strong magnetic field exposure the hydration shell thickness around relevant ions (e.g. Ca^{2+}) can be manipulated by rearrangement of the polar water molecules, and magnetic treatment of carbonate supersaturated aqueous solutions was shown to affect the occurrence of the different CaCO_3 polymorphs mainly relying on the magnetic field strength, exposure time and fluid flow rate (Knez and Pohar, 2005; Zhou et al., 2018). The dominance of homogeneous versus heterogeneous nucleation, distinct crystal shapes and variable particle sizes, as well as the adhesion of carbonate to an underlying substrate are discussed in the context of magnetic effects by Fathi et al. (2006). Likewise, ultrasonic treatment was reported to modify CaCO_3 polymorphism and the average precipitation rates (e.g. Vasyliev et al., 2018).

Various substrate effects involving the precipitation of different CaCO_3 on different natural mineral and artificial substrates are also known for their inhibition or promotion potential (e.g. D'Souza et al., 1999; Chen et al., 2019). In principle, the availability and interaction of a substrate characterized by distinct physicochemical surface properties can control crystallization mechanisms, i.e. initial nucleation barriers, surface and crystal lattice energies (De Yoreo et al., 2015). This concerns CaCO_3 formation on specific materials and surfaces including (corroded) steels, glass and plastics (Wang et al., 2013a; Boch et al., 2017a).

Accordingly, the variation of distinct physicochemical parameters and/or the occurrence of specific (in)organic chemical constituents influence the saturation state and nucleation potential of minerals from aqueous solutions. Chemical agents possessing specific functional groups and molecular mechanisms can inhibit, stabilize or modify mineral formation and structures and result in preferential crystal shapes, particle sizes and material consistencies (e.g. polymorphism, fabrics). They typically affect critical interfaces and reaction steps such as aqueous species distribution, ion attachment and crystal growth propagation. Likewise, substrate effects relying on different materials and surfaces also show major inhibition versus promoted mineral precipitation potentials. Based on laboratory-, field- and modeling approaches the driving and inhibiting forces on mineralization are systematically investigated in the context of scaling and corrosion inhibitors, i.e. a preventive measure against unwanted mineral deposition and alteration in various technical environments.

5. Microstructure and fabrics

In view of the diverse forms of CaCO_3 precipitation in nature and in technology, there are clear differences in the appearance, consistency and properties of the material, which are related to its microstructure and fabrics. Macroscopic characteristics such as (an)isotropy, porosity, coloring (e.g. from light scattering), and durability are intimately related to crystal nucleation, individual crystal shapes and the resulting fabrics of CaCO_3 (Della Porta, 2015; Frisia et al., 2018; Bastianini et al., 2019). In this context, “fabric” has to be considered as an all-embracing term including properties such as size, shape and orientation of crystal aggregates (i.e., Dickson, 1993).

A rich variety of polymorph- and growth-specific textures and morphologies reflect the prevailing thermodynamic (energetic) and kinetic (reaction rate) conditions in close relation to variable fluid-solid interaction of the aqueous solution, gaseous constituents (atmosphere) and solid deposition (Jones, 2017; Mercedes-Martín et al., 2021). Importantly, underlying nano- to microscopic features affect the macroscopic visual expression and material characteristics following a hierarchical (taxonomic) principle of progressively ordered mineralization (Van Driessche et al., 2017; Mercedes-Martín et al., 2021). For example, a brittle consistency of the carbonate deposits or some forms of layering might result from specific crystallite nucleation, crystal orientation, associated pore spaces and spatiotemporally evolving growth (Fig. 3 A & B; Martín-Chivelet et al., 2017). In technical settings (e.g. unwanted carbonate deposits in tunnel drainages and geothermal wells) such textural and mechanical features affect the recurrent maintenance intervals and cleaning procedures applied (Boch et al., 2017a; Eichinger et al., 2020).

The analytical tools used in order to investigate the spatially diverse structures and fabrics hence cover a broad range from laboratory based light microscopy (transmitted and reflected light, UV, cathodoluminescence, etc.), different forms of scanning and transmission electron microscopy, atomic force microscopy, electron backscatter diffraction analysis, towards micro computer tomography and synchrotron-radiation based micro X-ray fluorescence, as well as computer software based evaluation of nucleation and crystal growth (e.g. Seaton et al., 2009; Ott and Oedai, 2015; Simonet et al., 2019; Németh et al., 2022).

Regarding different (an)hydrous CaCO_3 minerals and polymorphs, these are known for their diverse crystal symmetries and shapes, e.g. for calcite, over 400 different forms have been described (Aquilano et al., 2016; Mercedes-Martín et al., 2021) and a complex range of crystal shapes has also been described for aragonite (e.g. Jones, 2017; Ge et al., 2020; Immenhauser et al., 2023). The latter typically occurs as rhombohedral or prismatic-scalenohedral calcite crystals while aragonite mostly shows radiating-spherical, columnar-pseudohexagonal, acicular (needle), divergent (wheat-sheaf), and botryoidal forms (Fig. 3C). Vaterite crystals are rare in nature but typically show spherulitic, tabular and fibrous habits or might occur in the form of composite aggregates (e.g. spheres made of intersecting discs). These anhydrous CaCO_3 polymorphs are sometimes related to other carbonate minerals being indicative for specific environmental conditions, e.g. ikaite ($\text{CaCO}_3 \cdot 6\text{H}_2\text{O}$) reflecting low temperature and high pH conditions (Bischoff et al., 1993; Boch et al., 2015) or dypingite ($\text{Mg}_5(\text{CO}_3)_4(\text{OH})_2 \cdot 5\text{H}_2\text{O}$) forming in the course of prior CaCO_3 precipitation and desiccation (e.g. Eichinger et al., 2020).

Widespread fabric types related to these crystal shapes include columnar arrangements (Fig. 3B & C) characterized by the initial nucleation of numerous crystallites, competitive crystal growth with increasing orientation, and variable pore spaces and related fluid inclusions and hence more compact or porous carbonate fabrics (Frisia, 2015; Bastianini et al., 2019; Dickson, 2023). Likewise, more regular palisade-type fabrics evolve from strictly constrained competitive growth with little inter-crystalline porosity and sharp crystal boundaries. The columnar and palisade fabrics are promoted by relatively

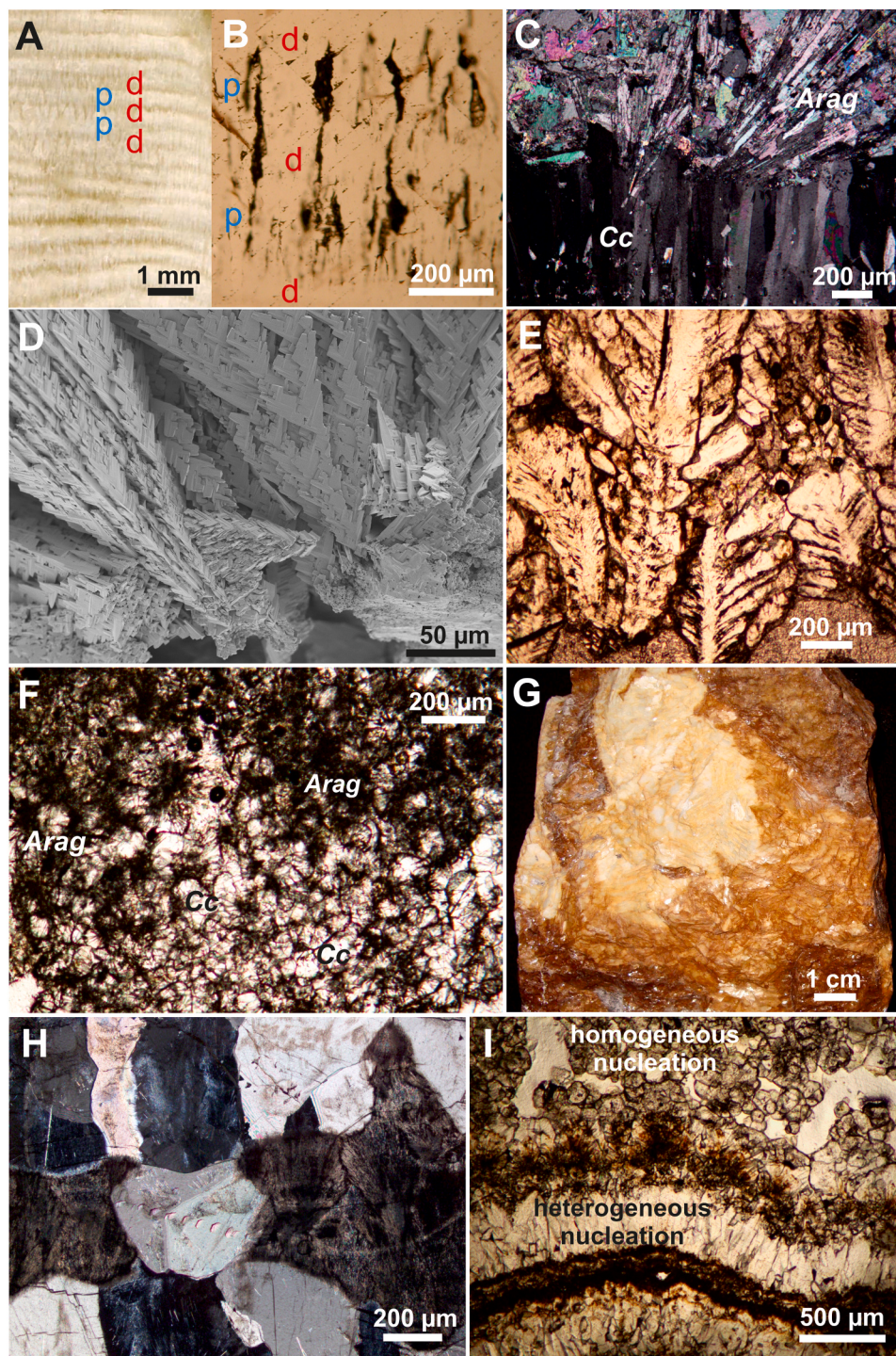


Fig. 3. Various fabrics in CaCO_3 precipitates. A) Layering of typically thicker white and porous (p) laminae alternating with thinner beige colored and dense (d) laminae in a stalagmite. B) Layers and coloring (light scattering) reflect a variable fabric based on the abundance of elongated pore spaces and fluid inclusions (transmitted light – TL). C) Competitively growing columnar calcite crystals (Cc) superimposed by radiating-spherical aragonite crystals (Arag; cross-polarized light – CPL) in a vein sealing a fracture. D) Scanning electron microscope and E) transmitted light images of dendritic (tree-like) calcite fabrics observed in hydrothermal precipitates. F) Micritic fabric (TL) consisting of individual calcite (light colored, rhombohedral) and aragonite (dark spheres, acicular) crystals of loose consistency and stochastic orientation deposited in a thermal water pipeline. G) Photograph showing the compact sparitic fabric of an iron-rich carbonate sample (siderite, ankerite). H) CPL image of mosaic calcite fabric recrystallizing from acicular bundles of prior (and partially remnant) aragonite crystals. I) TL image of well-oriented dense, compact calcite fabric resulting from heterogeneous nucleation on a substrate (wall crystallization) superimposed by loose, porous calcite from homogeneous nucleation (particles) in suspension in a thermal water pipeline.

constant (continuous or recurrent) precipitation conditions over extended time intervals. Rapid crystal growth from strongly supersaturated aqueous solutions is represented by dendritic fabrics (Fig. 3D & E). The tree-like crystal aggregates consisting of stems and branches typically evolving from some central trunk often display feather-like, skeletal or flaky forms depending on the crystallite sizes and complexity of branching. Micritic fabrics comprise of micro-crystalline agglomerations (e.g. mud-grade carbonate) with little orientation (c-axis) of the individual CaCO_3 crystals (Fig. 3F). These mostly porous fabrics typically originate from homogeneous crystal nucleation (high supersaturation) and subsequent sedimentation and accumulation from suspension (e.g. milky solution). Alternatively, calcareous micrite can derive from crystallization organic tissues (e.g. microbial mats) and later mobilization associated with decaying of the biofilms (remnants of biomineralization; e.g. Pedley, 2014; Eichinger et al., 2020) next to several other environmental settings of formation (e.g. cements in limestones). Sparitic fabrics are characterized by compact arrangements of variably oriented euhedral (sparry) crystals and macroscopically visible crystal faces that can either be of pristine origin (e.g. hydrothermal precipitation) or successively develop during recrystallization (e.g. metamorphism, meteoric diagenesis; Fig. 3G). This fabric might be encountered with marbles and carbonate-based ore deposits (e.g. siderite, magnesite). Another fabric type associated with some ripening process during diagenetic to metamorphic conditions is the mosaic texture (Fig. 3H). The mosaics often possess variable crystal orientations and indicative triple junctions and evolve in the course of carbonate dissolution-reprecipitation reactions involving remnant pore fluids (Hofmann et al., 2013; Frisia, 2015).

The occurrence and evolution of specific CaCO_3 fabrics mainly depends on the prevailing hydrochemistry (pH, saturation state, ion association), variable gradients (e.g. Pco_2), the flow rate and flow regime (e.g. stagnant vs. laminar vs. turbulent), and later-stage altering processes (e.g. recrystallization; Kile et al., 2000; Frisia et al., 2018; Shiraishi et al., 2019). Diagenetic and metamorphic alteration of pristine CaCO_3 structures and fabrics is also considered highly relevant with regard to the interpretation of different chemical and isotopic parameters ("proxies") used for (paleo)environmental reconstruction, i.e. these parameters could be modified/disturbed in the carbonate archives and might thus not be representative of the original depositional conditions (Gill et al., 2008; Mueller et al., 2021; see section 7).

In contrast, structural relicts (e.g. crystal shapes and fabrics) might occur in modern carbonate deposits and are often indicative of former formational and environmental conditions, e.g. remnants of ikaite crystals in cryogenic cave carbonates now consisting of calcite/glenodite (Németh et al., 2022), high-pressure aragonite relicts in exhumed marble sequences (Seaton et al., 2009) or marine biogenic calcite layers (tubes of serpulid worms) in speleothems being indicative of recurrent sea-level rise and flooding of the cave (Antonioli et al., 2004). Variable growth (precipitation) rates in association with variable fabrics further influence material consistencies from soft and porous mud-grade carbonate to hard and dense carbonate crusts next to the possible occurrence of layering (narrow lamination, broader zonation) or specific exterior shapes (morphology, topography) of the carbonate precipitates (Eichinger et al., 2020).

In a highly simplified view, CaCO_3 deposits can be placed into three major groups based on their dominant depositional mechanism: (i) inorganic formation, (ii) biologically mediated, and (iii) from particle/fragment mobilization and accumulation. Inorganic deposition can be separated into heterogeneous nucleation (nucleation and fabric development on preexisting substrate (e.g. mineral, plastic or metal surface)), which often results in dense and brittle crusts, and homogeneous nucleation (nucleation occurs spontaneously in highly supersaturated solution), which promotes loose crystalline mud-grade deposits (Fig. 3I; see section 3).

Biologically mediated CaCO_3 deposition involves microbial as well as macro-faunal biomineralization. The latter mainly concerns

metabolic processes and micro-environments regulating crystal growth and fabrics during hard part (exo- and endo-skeleton) formation (Simonet et al., 2019; see section 6). The spatial control (location, orientation) of CaCO_3 precipitation (e.g. via intermittent/amorphous mineral phases), however, is also widespread in microbial biofilms (Pedley, 2014; Shiraishi et al., 2019). Considering various microbial species and communities (bacteria, algae, fungi), passive and active contributions influence site-specific carbonate formation (Pedley, 2014; Eichinger et al., 2020). Passive functions of microbial presence include the availability of an attractive substrate for initial crystal nucleation or particle entrapment owed to the typically large specific surface area and sculptured topography of the filamentous and cross-linked biofilms. Active roles of microbes mainly address their ability to alter chemical gradients at the fluid-solid interface and to catalyze reactions relevant for CaCO_3 precipitation. This can be related to specific redox-reactions associated with the metabolism of chemoautotrophic microorganisms (Meister, 2015; Zhang et al., 2019b) or to the fundamental role of photosynthesis in the course of CaCO_3 precipitation (Shiraishi et al., 2019).

Microbial presence often results in porous fabrics and softer carbonate material consistencies, i.e. from the rapid decay and loss of the biomass (e.g. biofilm, extracellular polymeric substances) and the resulting high intercrystalline porosity (Pedley, 2014; Bastianini et al., 2019). The addition of diverse organic molecules or biopolymers (e.g. polyaspartate, alginate, polysaccharides, humic acids) constitutes another possibility to influence CaCO_3 precipitation, i.e. to inhibit or modify crystal growth and the related fabrics (Chaussemier et al., 2015; Karaseva et al., 2018). This concerns the occurrence of widespread dissolved organic matter in natural waters (e.g. Pearson et al., 2020), as well as the proactive addition of various crystallization inhibitors targeting the reduction of unwanted mineral deposits in various technical settings (e.g. thermal water and petroleum wells, drainages, industrial water circuits; e.g. Chhim et al., 2020; Leis et al., 2022).

Micrometer-range particle to centimeter-range fragment mobilization and accumulation and related carbonate fabrics depend on specific particle/fragment sources, variable fluid flow (e.g. turbulent, episodic) and geometries (e.g. sediment traps). Solid particulate components in natural and technical settings might originate from erosion, disintegration of biological components, corroding steel and concrete, from CaCO_3 rafts crystallizing at the surface of stagnant water bodies or from the exfoliation of scale-fragments in pipes (Boch et al., 2017a; Eichinger et al., 2020). The allochthonous and variably sized particulate components often undergo a chemical-sedimentary evolution involving their episodic mobilization and loose agglomeration (accumulation) in layers or in local traps (obstacles) followed by progressive cementation and alteration. The latter also includes the mineralogical transformation of pristine CaCO_3 precipitates, e.g. recrystallization of aragonite to calcite (Domínguez-Villar et al., 2017; Fig. 3H) or ikaite to calcite (Boch et al., 2015; Besseling et al., 2017), as well as petrographic changes during early diagenesis and meteoric alteration or burial diagenesis towards metamorphosis (De Boever et al., 2017; Mueller et al., 2021). Typically, the sequence of carbonate material alteration entails changing fabrics based on increasing and more homogeneous crystal sizes, overall decreasing intra- and inter-crystalline porosity, and a varying availability of water, e.g. fluid inclusions, fluids associated with organic matter or later-stage percolating waters (Frisia et al., 2018; Pederson et al., 2019).

Relying on the diverse but distinct relationships and processes CaCO_3 (micro)structures and fabrics are used in many ways for deciphering (paleo)environmental conditions in natural and technical settings. For example, specific growth patterns (e.g. annual or episodical lamination) are associated with recurrent climate conditions (Martín-Chivelet et al., 2017; Boch et al., 2019) or the fabric-related fluid inclusions (e.g. increased porosity and capture) in various CaCO_3 precipitates are analyzed for their physicochemical characteristics and isotopic compositions (Quandt et al., 2018; Demény et al., 2021). In the more technical

realm crystal morphologies, orientations and growth patterns might be used to infer flow conduits of geothermal fluids (e.g. from carbonate veins during deep geothermal exploitation, e.g. Lu et al., 2018) or for the reconstruction of variable hydrochemical and flow conditions in highway and railway tunnel drainage systems (Eichinger et al., 2020).

In conclusions, high-resolution spatial analytics comprising micro- to nano-structural, chemical or isotopic techniques are used to decipher the mechanisms of CaCO_3 formation. For this purpose, 3D imaging by computer tomography, (nano-)structural imaging and chemical/ isotopic mappings by different types of electron / X-ray microscopy approaches turned out to be highly valuable.

6. Biological influences

The presence and activity of biology and life of variable complexity are frequently related to CaCO_3 precipitation, sedimentation and alteration on different spatial and temporal scales. In fact, distinct biological habitats and calcifying organisms provide the worldwide most specific and largest volume of CaCO_3 precipitates from aquatic media. The role of organisms comprises of direct (metabolic) and indirect (substrate) effects on carbonate deposition and is often related to different forms of biominerization (Dove et al., 2003; see also section 8.2.8). Biological processes are known as major controls of physicochemical gradients and reaction pathways during carbonate nucleation and crystal growth in marine and continental environmental settings (Van Driessche et al., 2017; Middelburg, 2019). The relevance of micro-domains and the *in-situ* prevailing physicochemical conditions are increasingly recognized in the context of *exo-* and *endo-*skeletal hard part formation, e.g. in corals, mollusks, echinoderms and foraminifers (Sevilgen et al., 2019). Mineralogical and biogeochemical processes affect the progressive crystal growth and fabric development and consequently the carbonate material consistency and morphology (Pedley, 2014; Shiraishi et al., 2019; see section 5). The coupled fluid-solid interaction and alteration is further associated with elemental (re)cycling, enrichment or mobilization, as well as various isotope fractionation processes (Swart, 2015; Pederson et al., 2019; Saraswati, 2024). Exemplarily, a recent study of Schöne et al. (2023) showed the element incorporation of e.g. Sr/Ca, Mg/Ca and B/Ca of aragonitic shells of marine bivalves to be controlled by still insufficiently known vital effects, non-classical nucleation and growth, and/or kinetic mechanisms. A further challenge on the use and interpretation of elemental and isotope proxies is based on their potentially heterogeneous distribution in a precipitating CaCO_3 , which was impressively shown for Coccolithophores to produce Sr stripes in their CaCO_3 exoskeleton by high-resolution 3D synchrotron X-ray fluorescence mapping (Walker et al., 2024). Prosperous (multi)proxy approaches are numerous for a given task, such as (i) using $^{88}\text{Sr}/^{86}\text{Sr}$ ratios in calcite skeletons of precious corals (octocorals) to trace terrestrial and oceanic Sr cycling and biological processes (Yoshimura et al., 2022), (ii) Mg content of the urchin tooth structural elements to control calcite crystal orientation (Ma et al., 2009), (iii) fossil turtle eggshell to record the transformation from pristine aragonite to secondary calcite (e.g. Xu et al., 2022b), (iv) oxygen and carbon isotope distribution of fish otoliths to infer movement patterns (e.g. salmon: Nims et al., 2023; coral reef fish: Currey et al., 2014), and (v) combined $\delta^{44}/^{40}\text{Ca}$, Sr/Ca, and Δ_{47} values of fish otoliths to reconstruct paleotemperatures with a temperature resolution of $\sim \pm 0.9^\circ\text{C}$ (Mondal et al., 2022; see also section 7).

Biominerization also implies the formation of distinct features and functional components by organisms, i.e. shells and skeletons, spicules for protection, lenses for optics and floating crystals for gravity detection (Dove et al., 2003). These biogenic constituents are clearly more than mineral byproducts only. In this context distinct metabolic pathways of the organisms can either promote or retard CaCO_3 nucleation and crystal growth on small spatial scales (e.g. cell level). Also, processes such as photosynthesis or the oxidation of organic matter (e.g. microbial methane decay) have a variable effect on the carbonate-CO₂ chemical system (e.g. increase in pH and alkalinity) and hence on CaCO_3

precipitation (Morse et al., 2007; see sections 8.1.7 and 8.2.8.). Regarding the mineralogy of biogenic carbonate LMC and HMC as well as aragonite are most widespread while vaterite, monohydrocalcite and ACC are less abundant and/or metastable (Weiner and Dove, 2003). For example, the frequent occurrence of metastable aragonite next to Mg-calcite at ambient (e.g. shallow marine) environmental conditions constitutes a long-standing research subject involving vital effects and hydrochemical alteration in confined water volumes (e.g. in cells, biofilms, pores).

The initial nucleation of nano-sized and metastable precursor phases such as various forms of ACC are considered of major relevance during CaCO_3 biominerization and transformation (ripening) towards vaterite, aragonite or calcite (Bots et al., 2012; De Yoreo et al., 2015). The presence of organic macromolecules, predetermining templates and amorphous precursors might be decisive in the course of biominerization which is often expressed in distinct crystal sizes and shapes (see section 5), as well as elemental and isotopic fingerprints (see section 7). Likewise, the interrelation of CaCO_3 crystallization and polymorphism (calcite vs. aragonite vs. vaterite) were investigated based on different egg substrates (eggshell, egg membranes, egg white; Chen et al., 2019).

Considering the effects of organic molecules on CaCO_3 crystallization the presence or addition of functional polymers, proteins or organic acids (e.g. carboxylic acids) constitutes an emerging field of research and application (Wedenig et al., 2021; Adelnia et al., 2023). Even small amounts (few mg/l) of specific functional groups in the chemical agents (e.g. amino- and carboxylic groups) can inhibit or modify crystal nucleation and growth based on complexation of relevant ions (e.g. Ca^{2+}), adsorption on and blockage of crystal growth surfaces and/or dispersive effects amongst charged particles in suspension (Niedermayr et al., 2013; Li et al., 2022e; see section 4). These processes are widely accepted in the context of various scale (“encrustations” consisting of carbonates, sulfates, oxides, silicates) and corrosion inhibition of diverse water circuits such as geothermal and oilfield brines, groundwater drainage or industrial cooling water circulation (Chaussemier et al., 2015; Popov et al., 2016). Regarding the investigation and observation of biominerization mechanisms, relevant states and processes might be followed by *in-situ* and high spatiotemporal resolution analytical techniques including various forms of electron microscopy, fluorescence, Raman and infrared spectroscopy (Pederson et al., 2019; Carstea et al., 2020; Liu et al., 2021), as well as laboratory experiments tracing the transformation of relevant carbonate phases (e.g. Purgstaller et al., 2017a, 2017b).

Natural CaCO_3 precipitation is frequently related to the influence of highly specific microbial communities, e.g. stromatolites and microbialites, calcareous tufa and travertine, speleothems and ooids, as well as carbonate chimneys (Templeton and Benzerara, 2015; Diaz et al., 2017; Brasier et al., 2018). Mediated carbonate mineralization related to diverse bacterial, algal or fungal species strongly gained in recognition and interdisciplinary research efforts during recent years (Fig. 4). The microbial biomass associated with carbonate deposition is typically present as mats and biofilms made of interrelated species/communities and differentiated organic tissues and (indicative) mineralized components (Fig. 4A; Riding, 2000; Zhang et al., 2019b). Typical organic structures include micro- to millimeter-sized filamentous and dendritic, globular and rosette forms, as well as delicate strands of extracellular polymeric substances (EPS) connecting components of the habitat (Fig. 4B; Diaz et al., 2017; Jones, 2017; Eichinger et al., 2020). For example, based on EPS extracted from cyanobacterial biofilms/mats of a sabkha environment in Qatar, Paulo et al. (2020) highlighted the role of organic matter (carboxylated molecules in EPS) and temperature for the nucleation of (proto)dolomite. Several species of cyanobacteria were shown to regulate the intensity of calcium uptake (calcium sequestration) via the formation of intracellular ACC being beneficial to cell growth and buffering of favorable pH conditions (De Wever et al., 2019). Hohl et al. (2023) analyzed C, Cd, Ba, and Ni isotopes of microbial stromatolites to trace the long-term interplay of the biosphere,

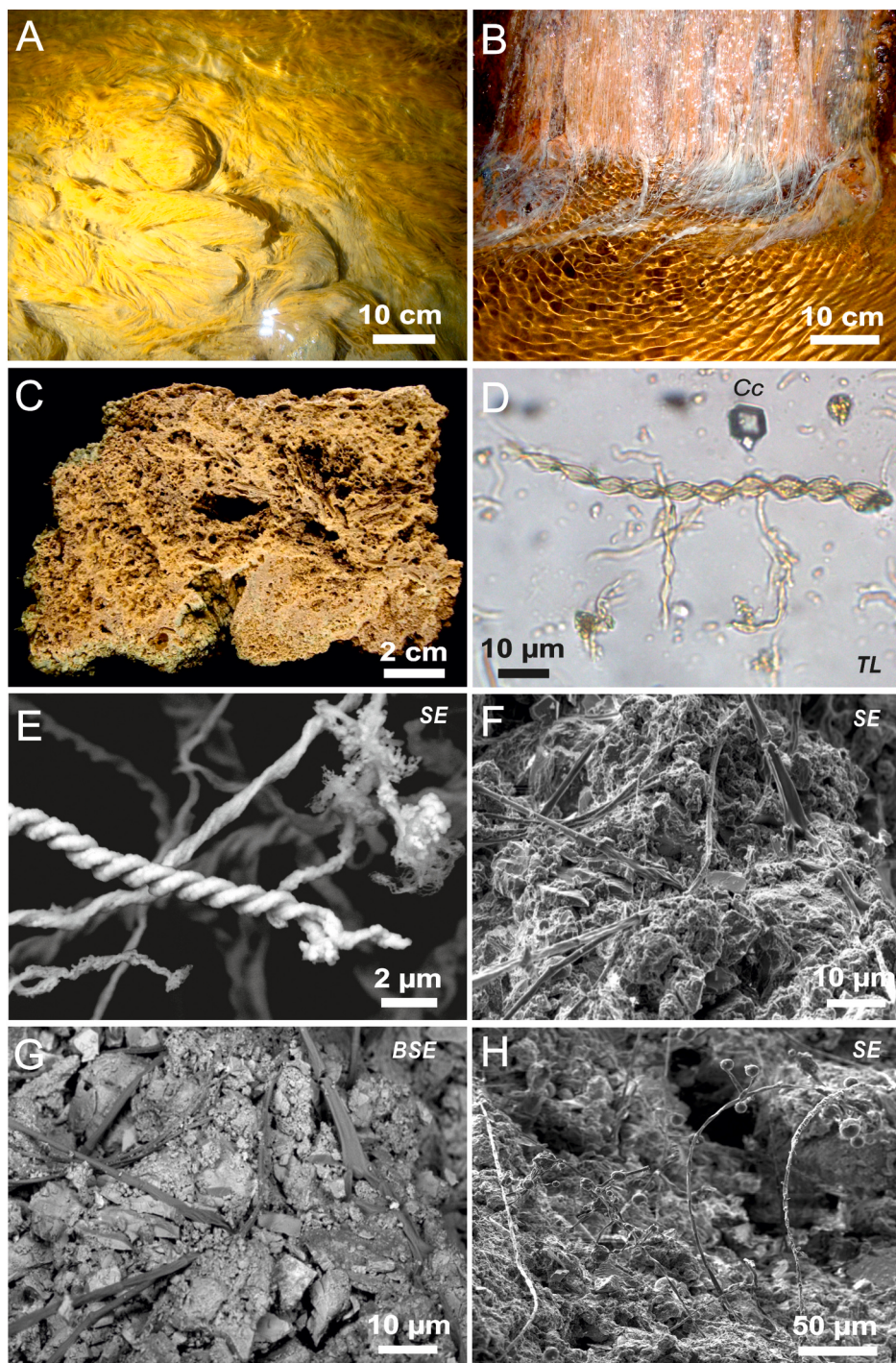


Fig. 4. Examples of microbial activity affecting CaCO_3 and related mineral deposition in different environmental settings. A) Hair-like bacterial mats in streaming drainage water of a railway tunnel. B) Filamentous whitish bacterial colonies growing in a thin water film flowing across a concrete wall. C) Calcareous tufa encrustation from a surface water flow supported by the presence of photosynthetic algae and mosses. D) Transmitted-light (TL) and E) secondary electron (SE) images showing prominent twisted stalks of the Fe-oxidizing bacterium *Gallionella ferruginea* encountered in iron- and CO_2 -rich groundwaters. F) Secondary electron (SE) and G) back-scattered electron (BSE) images of branched microbial tissues influencing mineral precipitation and material consistency of a CaCO_3 dominated scale deposit formed in a water pipeline of a geothermal district heating facility. Note the indicative colour contrast in BSE mode based on the relatively low density of the organic biomass (dark colour). H) Microbial tissue mainly consisting of fungi with branched mycelium and globular spores found in a calcareous scale deposit.

atmosphere, and hydrosphere and to assess early life environments and Earth's microbial metallome evolution. In particular, Cd and Ni isotopes were found to be promising and a novel isotope biomarker for early Earth's bio-chemical sedimentary records.

The properties of EPS also strongly affect the polymorphism and crystal morphologies of Ca/Mg-carbonates (Zhang et al., 2021). The

latter study investigated bacterial EPS and showed that common carbohydrates from the bacterium *Curvibacter* promoted aragonite formation and spherical aggregates while proteins in EPS from *Arthrobacter* favored the crystallization of HMC, vaterite and monohydrocalcite. Likewise, the importance of extracellular polymeric substances (proteins, polysaccharides, carbonic anhydrase), organic CaCO_3

complexes and bacterial cells utilized as a template is supported by the laboratory experiments of Liu et al. (2021), who focused on the transformation of biogenic amorphous phases towards organic-rich vaterite. In caves, bacteria-induced amorphous CaCO_3 formation was identified (i) to be caused by shielding lipids, proteins, carbohydrates and nucleic acids and (ii) to affect the geochemical records of the final CaCO_3 (Enyedi et al., 2020). Considering fungi, the cosmopolitan slime mold *Fuligo septica* was found by Garvie et al. (2022) to precipitate about 1-nm-sized ACC units, which are in a similar way stabilized by associated organic matter. In the Sonoran Desert ikaite is formed on infected plants (*Populus fremontii* tree) within a sulfur-rich jelly-like slime, which inhibits its transformation even at ambient temperature to yield microstructured ikaite-monohydrocalcite composites (Garvie, 2022). Further, the decay of the large columnar cactus *Carnegiea gigantea* is known to induce calcite formation via a monohydrocalcite precursor caused by the dissolution of Ca oxalate (Garvie, 2006).

Microbes exert either an active or passive contribution to carbonate crystallization and mineral deposition (Brasier et al., 2018; Shiraishi et al., 2019). The passive role mainly consists in substrate effects, e.g. providing a sculptured and typically high specific surface area for initial mineral nucleation and ongoing crystal growth or acting as a sedimentary trap for mineral particles (Fig. 4C). Frequent active roles of microbes comprise of their ability to alter physicochemical gradients in the reactive aqueous solution and thus the carbonate precipitation conditions based on different organism-specific and mostly catalytic (e.g. reduction of activation energies) processes (Fouke, 2011; Druschel and Kappler, 2015). This involves adjustments of pH gradients and carbonate alkalinity or the channeling and discarding of specific ionic constituents (e.g. Ca^{2+} , Fe^{2+} ; Vroom et al., 1999; Pedley, 2014; Brasier et al., 2018). Focusing on the carbonate chemical system, microbial communities possess a broad range of metabolic effects in order to sustain their autotrophic or heterotrophic nutrition amongst others involving photosynthesis and chemoautotroph energy transfers promoting carbonate mineral deposition or dissolution (Templeton and Benzerara, 2015).

Photosynthesis utilized by microbes such as algae and cyanobacteria existing in diversely lighted settings and described by the simplified reaction $\text{CO}_2 + \text{H}_2\text{O} \rightarrow \frac{1}{6} \text{C}_6\text{H}_{12}\text{O}_6 + \text{O}_2$ can actively influence the CO_2 budget and carbonate chemical equilibrium of their habitat and may trigger crystal nucleation and advance or reduce local mineral growth (Rogerson et al., 2008). Chemoautotroph life cycles based on organism-specific nutrition and energy gains from selected chemical constituents and reactions involving aqueous solutions and gases are often related to more or less extreme environmental conditions (e.g. thermophile, acidophile, halophile microbes; Takai et al., 2008). Frequently, the energy transfers are based on redox reactions involving redox-sensitive chemical constituents of common elements such as carbon, sulfur, nitrogen, manganese or iron being processed via the specialized microbial metabolism (Dhami et al., 2018). Examples are the oxidation of organic matter in sediments of the ocean floors or microbial methanogenesis in deep continental reservoirs which liberates CO_2 or CH_4 and thus affects dissolved carbon(ate) species in waters, gases and eventually minerals (Morse, 2004; Shuai et al., 2021). Other common microbial redox reactions include bacterial sulfate reduction (Baldermann et al., 2015), sulfide oxidation (Zammit et al., 2015) or iron ($\text{Fe}^{2+}/\text{Fe}^{3+}$) reduction and oxidation (Chan et al., 2016). Most of these aerobic (e.g. oxidic) or anaerobic (e.g. sulfidic) reactions exert a major influence on carbonate mineral precipitation or dissolution. In many natural settings, however, the roles and functions of specific bacteria are still poorly understood, e.g. a rich population of chemoautotrophic and heterotrophic bacteria (*Sphingomonadaceae*, *Oxalobacteraceae*, *Streptomycetaceae*, *Solirubrobacterales*, *Sphingomonadales*, *Rhizobiales*) associated with different carbonate formations in karst caves are compatible with the mediation of carbonate precipitation, as well as sulfur, iron and nitrogen cycling (Dhami et al., 2018).

Apart from natural environmental settings, microbial processes are

for a long time recognized in man-made (technical) settings (e.g. Lerm et al., 2013; Fig. 4D–H). Distinct microbial communities can enable or accelerate calcareous scale growth or corrosive and redox state related reactions in the course of deep geothermal energy utilization (Osvald et al., 2017; Westphal et al., 2019). Further, problematic and fugitive gas constituents (e.g. CH_4 , H_2S , CO_2 , H_2) might evolve from microbial presence and interaction in different constructional components (e.g. drainages, wells, filters) of technical settings such as sewage systems, geothermal energy and water treatment plants, oil and natural gas production facilities or rail- and highway tunnels.

Based on environmental scanning electron microscopy, epifluorescence imaging using specific DNA and RNA sensitive dyes and 16S rRNA gene sequencing scale samples and groundwaters from drainage systems were investigated with regard to biomeditated CaCO_3 and iron mineral (e.g. Fe(OH)_3) precipitation, as well as related biomass formation (Eichinger et al., 2020; Fig. 4D, E). Microbes such as the iron oxidizing bacteria *Gallionella ferruginea* (e.g. Chan et al., 2016; Koraïmann and Bischof, 2022) utilize dissolved iron (Fe^{2+}) contents and dissolved inorganic carbon (CO_2) as a carbon source (organic tissue) for the formation of major microbial mats and related iron (hydr)oxide precipitates (e.g. masses of spirally twisted stalks made of amorphous ferric hydroxide or ferrihydrate; Fig. 4D, E). In this way the bacteria affect the scale material consistency and are further represented by indicative minerals and fabrics. Moreover, the occurrence and relevant processes associated with these bacteria are redox- and pH-sensitive and determine both iron (hydr)oxide and CaCO_3 precipitation. More specifically, iron (hydr)oxide precipitation releases H^+ (decreases pH), the bacteria (e.g. *Gallionella*) consume (carbonic) acid (increases pH) and the iron content (mainly Fe^{3+}) further inhibits e.g. calcite crystallization. Wedenig et al. (2023) showed a strong interrelation of such microbial activity with the transport of relevant nutrients (elemental supply, e.g. Fe^{2+} and dissolved inorganic carbon), the exchange of CO_2 (assimilation vs. outgassing) and O_2 (uptake) with the water and biomass and consequently with a variable water flow rate and aeration.

The actual microbial activity and its effects on CaCO_3 deposition strongly depends on favorable vs. unfavorable natural (geogenic) and technical (operational) conditions including variable T and P, ionic speciation, as well as varying fluid flow and aeration conditions, for example during production cessations (Westphal et al., 2019). Moreover, organisms also hold some valuable potential for beneficial utilizations such as the enrichment of rare and precious metals (e.g. phytomining), the enhanced precipitation of specific minerals (e.g. during CO_2 sequestration) or the healing of material- and constructional defects (e.g. cracks; Zammit et al., 2015; Zhang et al., 2019b; see section 8.2).

In conclusions, biology and organic substances are known to influence or even control CaCO_3 formation. The omnipresence and relevance of microbiology is also increasingly recognized in the context of subsurface settings and processes and play a critical role in ongoing CaCO_3 - CO_2 research and for (engineered) environmental issues. Sorting out physiological effects from environmental signals is a challenge for further research and applications. On the other hand, organic molecules can be used to tailor properties and performances of products or to prevent their formation.

7. Elemental and isotope proxies

7.1. Elemental incorporation

In natural surroundings CaCO_3 precipitates are mostly far from being chemically pure caused by gas/fluid inclusions and/or incorporation of impurities such as isomorphic substitution of the Ca^{2+} or CO_3^{2-} ion by foreign ions or at enigmatic positions in the given crystal lattice (e.g. Rimstidt et al., 1998; Curti, 1999; Gaetani and Cohen, 2006; Prieto, 2011). Gas and fluid inclusions in CaCO_3 minerals have high variabilities of composition depending of the individual (trans)formation

environments. Accordingly, the chemical and isotope composition of gas and fluid inclusions can be used to trace the individual settings (e.g. Lécuyer and O’Neil, 1994; Xu et al., 2022a; Weissbach et al., 2023). Enigmatically incorporated foreign components in CaCO₃ minerals are alkalis, such as Li, Na, and K ions, which are trapped during precipitation into the solid at very low amounts (e.g. Kitano et al., 1975; Gabitov et al., 2011; Yoshimura et al., 2017; Flöter et al., 2022). The trapping mechanisms range from lattice defects to absorption phenomena. In analogy, anions, like SO₄²⁻, MoO₄²⁻ and Cl⁻, are known to be part of CaCO₃ precipitates at rather low concentrations, but according to their geometry, size and/or valence not easily to be localized and defined in its CaCO₃ lattice position (e.g. Midgley et al., 2021).

In contrast, isomorphic substitution of Ca in CaCO₃ minerals by divalent cations, such as Sr, Ba, Mg, and Zn, are mostly well-described by thermodynamic incorporation approaches, which may finally result in (ideal) solid solution formation (e.g. Prieto et al., 2016). For instance, the substitution of Ca by Sr ions in the calcite lattice is expressed by the elemental distribution coefficient

$$D_{Sr} = \frac{\left(\frac{n_{Sr}}{n_{Ca}} \right)_{calcite}}{\left(\frac{(Sr^{2+})}{(Ca^{2+})} \right)_{solution}} \quad (2)$$

where n denotes the molar concentration of Sr and Ca in the calcite crystal and round brackets denote the chemical activity of Sr and Ca ions of the reactive solution. The individual values of D depend on the foreign divalent versus Ca ion radius by considering the individual crystal structure, the solubility of the endmember minerals, temperature, pressure, precipitation rate etc. D values at thermodynamic equilibrium can be approached at very low precipitation rates (R: mol of CaCO₃ growth per m² reactive mineral surface and per reaction time), whereas at elevated R values significantly different apparent distribution coefficients are typically obtained. In the latter case, non-discrimination state conditions can be approached ($D_i \sim 1$; e.g. Brazier et al., 2024a for Zn incorporation into aragonite).

An overview about individual D values of CaCO₃ modifications and their changes as a function of physicochemical conditions is given in Böttcher and Dietzel (2010) and Gabitov et al. (2021a), where estimates are based on experiments and/or field observations (e.g. Wang et al., 2021a). Apparent elemental incorporation can be also significantly affected by diverse formation pathways, such as complex transformation reactions, environmental changes, close vs. open system in respect to the solid-liquid exchange, and individual crystal growth behavior of calcite: e.g. crystal lattice growth site specific incorporation of ions into calcite (Hodkin et al., 2018; Rezaei et al., 2024); Mg and pH dependent Sr incorporation into calcite (Jia et al., 2022; Knight et al., 2023); impact of aqueous carbonate complexes on REE uptake into calcite (Maskenskaya et al., 2015); Li, B, Mg, Sr, and Ba incorporation into Mg-calcite grown from seawater (Gabitov et al., 2019); incorporation of Li, B, Na, Mg, Mn, Sr, Ba, and U into inorganic ACMC precipitated from seawater (Evans et al., 2020); the impact of amorphous precursors on Mg and SO₄ ion uptake in the final calcite (Goetschl et al., 2021; see also section 3); Sr incorporation into calcite followed by a Rayleigh fractionation approach (e.g. Tang et al., 2008a); salinity effect on trace element incorporation based on cultured foraminifera (Hauzer et al., 2021); and impact of organic matter complexation on transition metal incorporation during cave-analogue calcite growth (Lindeman et al., 2022).

In case of biogenic CaCO₃ formation the so-called vital effects sum up complex and coupled metabolic and micro-environmental aspects, which results in species dependent apparent distribution coefficients for foreign ions between the precipitating solution and the solid CaCO₃, as e.g. documented for various metal ion incorporation into modern corals (e.g. Jiang et al., 2020; Ram and Erez, 2021) as well as for mollusks and brachiopods (see Immenhauser et al., 2016 and references therein).

In conclusion, the use of a single ion/component to be incorporated

into CaCO₃ as an environmental proxy is rather challenging, whereas an elemental multi-proxy approach is more promising to assess complex and coupled ion incorporation behaviors and to reconstruct the physicochemical conditions during its formation (e.g. past seawater temperature; Letulle et al., 2023). Recently, the strong need to consider temporal and spatial variability of elemental distribution in CaCO₃ and its potential to decipher dynamics of mineral formation and cyclic environmental changes is shown by high resolution analyses (e.g. Kusturica et al., 2022; Walker et al., 2024). In Fig. 5 an overview about the use of incorporated components into CaCO₃ precipitates are given as discussed in the following sections.

7.1.1. Cations

The incorporation of **monovalent ions**, such as K, Na, and Li into CaCO₃ occurs at a very low level and is not simply based on Ca ion lattice substitution, thus complex and still hotly debated to be used for (past) environmental reconstructions (e.g. Okumura and Kitano, 1986; Dellinger et al., 2018; Zhou et al., 2021). The uptake of K ions by calcite and aragonite is known from experimental findings by White (1977) and Ishikawa and Ichikuni (1984). Potassium has a high potential for tracing (bio)geochemical cycles, but (i) synchrotron data indicate e.g. K of foraminifera CaCO₃ to be hosted in different phases - such as amorphous K₂CO₃, within the calcite/aragonite lattice, or in intracrystalline organics - at different amounts and (ii) crystal growth rate is claimed to affect K incorporation into biogenic CaCO₃ (Li et al., 2021a; Li et al., 2022a; Nambiar et al., 2023). These findings obviously constitute K content of CaCO₃ precipitates to be challenging to be applied as an environmental proxy. Zhou et al. (2021) claimed Na/Ca ratio of foraminifera as a potential proxy for seawater calcium concentration. However, Kawabata et al. (2021) investigated Na incorporation into aragonite and calcite to be T dependent and Gray et al. (2023) showed Na to be incorporated into foraminiferal skeletons in calcite but also in residual metastable CaCO₃, fluid inclusions, and organics. The latter aspects have to be considered for Na/Ca in order to be used as proxy in particular in respect to pretreatments for analyses. Culture experiments indicate growth rate independent Li incorporation into benthic foraminifera (Charrieau et al., 2023), which supports Li to be used as environmental proxy and to discover past chemical weathering and carbon cycle conditions. Dellinger et al. (2018) found strong T dependent Li/Mg ratios in bivalve *Mytilus edulis* to be promising for paleo-temperature reconstructions. But inorganic co-precipitation experiments by Füger et al. (2019a) show Li incorporation into calcite to be regulated by pH and/or precipitation rate, which strongly hints on the above proxy approaches to be verified for a specific case. The Li incorporation mechanism seems to be valid to allow for more Li being incorporated into calcite at higher precipitation rates. Following this concept, fast calcite growth causes lattice defects acting for Li ions to be trapped, where incorporation of surface complexes like Li-HCO₃⁰ - keeping the charge balanced - are reasonably suggested at least during the initial step of Li adsorption onto the crystal surface (e.g. Füger et al., 2019a; Seyedali et al., 2021). Recently, Brazier et al. (2024c) verified a linear correlations between D_{Li} and D_{Na} for precipitated aragonite and saturation state, where the incorporation of both ions into aragonite is likely controlled by the density of defect sites.

In conclusion, the above monovalent cation incorporation behavior is not straight forward to trace the environmental conditions during CaCO₃ growth (e.g. Chen et al., 2023b: in the case of Li). On the other hand, the incorporation of monovalent ions into CaCO₃ in the context of multiproxy approaches offers great potential for determining the formation pathways and conditions of carbonates, e.g. with regard to aspects of biomineralization and diagenesis, in particular by considering the distribution of stable isotopes (see section 7.2.1).

In contrast to monovalent, **divalent cations** can be typically considered to substitute for Ca ions in a given CaCO₃ lattice. The general affinity of a divalent ion to be incorporated into CaCO₃ (see eq. (2)) can be followed by the endmember carbonate mineral solubilities to

K^+, Na^+, Li^+ <i>T, R, pH, com</i>	Cl^- , Br^- , F^- <i>R, com, deg</i>	IO_3^- <i>red, deg</i>	SO_4^{2-} (CAS) <i>pro, R</i>	$UO_2(CO_3)_2^{2-}$ <i>red, pH, T, com, sal, ads</i>
$Ba^{2+}, Sr^{2+}, Pb^{2+}$ <i>T, R, pH, com, deg</i>				
$Cd^{2+}, Ni^{2+}, Co^{2+}, Zn^{2+}$ <i>R, com, deg, ad</i>	CaCO₃·nH₂O			
Mn^{2+} <i>R, red, com, ad</i>			MoO_4^{2-} <i>red, com</i>	AsO_4^{3-}, AsO_3^{3-} <i>red</i>
Cr^{3+}, REE <i>red, com, ads</i>	Li^{+} <i>T, pH, R, com</i>	K^{+} <i>pro, deg</i>	Ni^{2+} <i>com, R, ads</i>	$CO_3: ^{18/16}O, ^{17/16}O, ^{13/13}C$ <i>T, pH, R, deg, CO₂, com, sal, red, eva</i>
$^{137/134}Ba$ <i>R, pro</i>	Ca^{2+} <i>T, R, dif, com</i>	Ca^{2+} <i>48/40</i>	Cd^{2+} <i>com, sal, ads</i>	$CO_3: \Delta_{47}, \Delta_{48}$ <i>T, R, pro, deg, CO₂</i>
$^{87/86}Sr$ <i>pro</i>	Mg^{2+} <i>T, R, com, dif, ads, deg</i>	Mg^{2+} <i>25/24</i>	Zn^{2+} <i>pH, R, com, ads</i>	Fe^{2+} <i>56/54</i>
			Cr^{2+} <i>11/10</i>	$Mo^{98/95}$ <i>red, com, ads</i>
			Cr^{2+} <i>red, pH, com, ads</i>	$H_2O: D/H, ^{18/16}O$ <i>eva, pro, sal</i>
				$B(OH)_3^{\circ}, B(OH)_4^-$ <i>pH, com, deg</i>

Fig. 5. Selected elemental and isotope ratios to be used or suggested to trace, reconstruct, and/or tailor anhydrous and hydrous CaCO₃ (trans)formation reactions and pathways. Exemplarily, main well-known, promising and/or challenging aspects on controlling parameters of individual elemental/isotope fractionation effects during CaCO₃ (trans)formation are given (see section 7): *T*: temperature; *R*: growth/precipitation rate; *dif*: ion diffusion; *deg*: amorphous to crystallization degree/pathway; *ads*: adsorption; *com*: aqueous / surface complex formation; *CO₂*: CO₂ degassing / absorption; *pH*: pH; *sal*: salinity; *eva*: evaporation; *red*: redox; *pro*: provenance. Blue and red colours denote cationic or anionic species, whereas black colour uncharged or both cationic and anionic species, to be involved in elemental/isotope uptake into CaCO₃·nH₂O phases (0 ≤ n ≤ 6). (For interpretation of the references to colour in this figure legend, the reader is referred to the web version of this article.)

crystallize isostructural to trigonal calcite (e.g. Fe²⁺, Mg²⁺, Mn²⁺, Cd²⁺, and Zn²⁺) or orthorhombic aragonite (e.g. Ba²⁺, Sr²⁺, and Pb²⁺), which depends on the individual ion radius (e.g. Speer, 1983; Morse and Bender, 1990; Antao and Hassan, 2009; Ruiz-Hernandez et al., 2010; Dietzel, 2011). For instance, Cd ions isomorphously substitute Ca ions in the calcite lattice, where the ideal solid-solution for the calcite-otavite system developed by Prieto (2011) shows a strong fractionation of Cd vs Ca caused by the very low solubility of otavite at ambient temperature (pK_S = 12.1; Stipp et al., 1993) versus that of calcite (pK_S = 8.5; Plummer and Busenberg, 1982).

In particular, divalent ion incorporation into CaCO₃ precipitates can provide decisive and quantitative information about the environmental physicochemical conditions during its formation (e.g. Böttcher and Dietzel, 2010; Gabitov et al., 2014). Based on individual distribution coefficients for Sr, Mg, Ba, Ra etc. in calcite and aragonite - which are the minerals of main focus in past studies due to their widespread occurrence - imprints of formation temperature (e.g. sea surface temperature estimation from Sr in aragonitic sponges; Rosenheim et al., 2004; Waite et al., 2018), solution chemistry (e.g. pH dependence on Sr ion distribution coefficients in calcite; Jia et al., 2022), discrete (trans)formation, e.g. from amorphous to crystalline state, and complex diagenetic alteration (e.g. Purton et al., 1999; He et al., 2021; Swart, 2015; Goetschl et al., 2021; Immenhauser, 2022), and precipitation rate (e.g. Sr and Mg in calcitic speleothems; Wassenburg et al., 2020) can be assessed. Obviously, the latter effect accounts for non-equilibrium conditions,

eq. (2)). This behavior is verified for D < 1 and D > 1 at thermodynamic equilibrium (e.g. Dromgoole and Walter, 1990; Lorens, 1981; Tesoriero and Pankow, 1996; Mavromatis et al., 2013).

Besides T and R, the D values may depend also on (i) additionally occurring foreign ions via competitive substitution, (ii) ionic strength, (iii) distinct Me distribution coefficients at nonequivalent crystallographic CaCO₃ faces, and (iv) aqueous and/or surface complexation (e.g. Böttcher and Dietzel, 2010). Therefore, different models for the incorporation of trace Me (and Me isotopes) in CaCO₃ have been developed such as the Surface Entrapment Model (Watson, 2004), the Surface Reaction Kinetic Model (DePaolo, 2011), the ion-by-ion crystal growth model, where ion attachment is confined to kink sites on the crystal surface (Nielsen et al., 2013), or extended approaches considering highly complex aqueous solid solutions (Thien et al., 2014) and ion diffusion (Watkins et al., 2017; see also section 3).

Magnesium substitutes the Ca ion well for 6-coordinated Ca vs. O ions structures, which can yield in the formation of Mg-calcite up to being close to the Ca:Mg stoichiometry of dolomite (Morse, 2004). The threshold of low vs. high Mg-calcite at 4 mol% MgCO₃ is determined by reaching a solubility minimum (Mucci and Morse, 1984). The higher T and R are, the more Mg ions can be incorporated into the calcite lattice (e.g. Oomori et al., 1987; Goetschl et al., 2019). D_{Mg} values of inorganically precipitated calcite were experimentally found to increase with growth rate (R) at 25 °C according to the equation.

$$\text{Log}(D_{\text{Mg}}) = 0.2517(\pm 0.0150) \cdot \text{log}(R) + 0.0944(\pm 0.0182) \quad (10^{-8.3} \leq R \leq 10^{-6.6} \text{ mol m}^{-2} \text{ s}^{-1}) \quad (3)$$

mostly based on strongly kinetically driven fractionation effects (e.g. Tesoriero and Pankow, 1996; Rimstidt et al., 1998). As a general rule apparent D values approach unity at fast precipitation rate, thus discrimination of aqueous divalent cations during very fast uptake into the CaCO₃ precipitate is comparatively low to negligible (see section 7.1;

but being limited to several mol % of Mg substituting Ca in the crystal lattice (Mavromatis et al., 2013)). In contrast, magnesium is incorporated into aragonite as impurities at an extremely low level due to 9-coordination of Ca to O; contrastingly, large Me²⁺ ions are preferentially trapped into aragonite (e.g. Dietzel et al., 2004; Gabitov et al.,

2008). For aragonite a Mg^{2+} site disordered structure model has been developed by Son et al. (2020), where substituted Mg^{2+} is five-fold coordinated and induces substantial disorder in the bond distances. Experimental results by Mavromatis et al. (2022) show a positive relationship between Mg incorporation into aragonite and the precipitation rate, which hint on Mg/Ca ratio of aragonite be used as a proxy for the saturation degree of the precipitating fluid. However, aragonite in natural deposits frequently contains coexisting Mg-rich phases such as calcite, clay minerals, organic matter, which can limit its use as an environmental proxy. Zhu et al. (2021) experimentally studied the incorporation behavior of Mg ions into vaterite, where the apparent D_{Mg} value was determined to increase as a function of temperature in a similar way as obtained for calcite (Oomori et al., 1987), but at a significantly higher level. Although literature dealing with Mg incorporation into $CaCO_3$ is multitudinous, controlling parameters for its incorporation comprising thermodynamic, kinetic and vital effects are still debated (e.g. freshwater microbial carbonate: Saunders et al., 2014). In this context, the inorganic transformation experiments of Purgstaller et al. (2016) indicate amorphous $CaCO_3$ to yield calcite up to 20 mol% $MgCO_3$ at ambient conditions, where at the given aqueous Mg/Ca ratio the formation of aragonite - the dominating $CaCO_3$ polymorph for non-amorphous formation pathway - was completely omitted.

Interestingly, the ACC precursor itself has a significantly lower Mg content than the final Mg-calcite, which also points on the great significance to consider closed vs. open system conditions during the transformation process for Mg to be used as proxy (e.g. Brazier et al., 2024b). Mesocrystals and spherulites of Mg-calcite can be formed via an amorphous reaction pathway, which is frequently documented in organic bearing surroundings, but also possible in inorganic systems (Yu et al., 2017; Tsao et al., 2020; Shang et al., 2021). By adjusting pH, cation-to-anion ratio, and solution concentration within the Ca - Mg - CO_2 - H_2O system the incorporation of Mg into the final calcite can be tuned up to about 45 mol% $MgCO_3$ via the amorphous reaction pathway (Xto et al., 2019a).

Incorporation of strontium into calcite and aragonite is experimentally investigated and assessed from a large number of designs and approaches (e.g. Lorens, 1981; Tesoriero and Pankow, 1996; Huang and Fairchild, 2001; Dietzel et al., 2004; Gabitov and Watson, 2006; Tang et al., 2008a; Terakado and Taniguchi, 2006; AlKhatib and Eisenhauer, 2017a/b; AlKhatib et al., 2022) to be used to infer paleoceanographic, speleothem and diagenetic histories as well as $CaCO_3$ growth rates, formation T and retention of heavy metal ions (e.g. Humphrey and Howell, 1999; Malone and Baker, 1999; Stoll et al., 2002; Mitchell and Ferris, 2005). In this context, Zhang and DePaolo (2020) provided D_{Sr} values for calcite from marine sediments and pore fluids at close to equilibrium conditions, which are consistent with former experimental results. Apparent D_{Sr} values for calcite are, besides temperature, in particular affected by the precipitation rate of calcite, thus provide a tool for assessing R if temperature is known and vice-versa (e.g. Tang et al., 2008a). Accordingly, Zhang and DePaolo (2020) developed a reaction rate model to follow and quantify the R dependence of Ca substitution by Sr in calcite by concerning former data sets. Gabitov et al. (2021a) developed a high-resolution approach to follow the spatially-resolved growth rate evolution by analysing sectoral Sr contents of calcite crystals.

In a recently developed ion-by-ion calcite growth modeling approach experimentally obtained data were used to assess and quantify pH as well as T dependence of D_{Sr} for calcite (Jia et al., 2022). This model indicates aqueous carbonate speciation to explain the pH dependence of D_{Sr} , but has to be verified by analysing bicarbonate to be directly involved in calcite growth in future studies. ACC precursors can result in an enhanced Sr uptake into the final calcite crystal (Littlewood et al., 2017), and coupled effects of Me and Sr ion incorporation during calcite precipitation have to be considered (e.g. high Mg content increases D_{Sr} values; Knight et al., 2023). In the case of Sr incorporation into aragonite, the temperature turned out to be a main controlling parameter (see

references above). Thus, Sr/Ca of aragonite has some valuable potential to estimate precipitation T (e.g. sclerosponge; Rosenheim et al., 2004), but can be restrictively influenced e.g. by Pco_2 (e.g. aragonitic corals; Cole et al., 2016a).

In analogy to Sr, barium substitutes Ca in aragonite more strongly compared to calcite (e.g. Böttcher and Dietzel, 2010 and references therein). In contrast to former experimental data (Dietzel et al., 2004; Gaetani and Cohen, 2006; Goncza et al., 2017) more recently obtained results of Mavromatis et al. (2018) indicate D_{Ba} of aragonite to be <1, which is suggested to be caused by partly witherite ($BaCO_3$) precipitation in the former approaches. The given typical relationships of precipitation rate on D_{Ba} values of aragonite and calcite have a high potential to trace growth rate regimes (for aragonite at low precipitation rates) and to provide information on the environmental conditions of the precipitating solutions. Yamazaki et al. (2021) found Ba distribution coefficients in an aragonitic coral (*Acropora*) to depend on light conditions, where at high-light conditions aragonite growth and thus Sr incorporation is stimulated, which mirrors the above R-effect on D_{Sr} .

Brazier and Mavromatis (2022) assessed the growth rate effect on nickel and cobalt incorporation into aragonite, where D values are below 1 and increase with increasing growth rate. In contrast, Lorens (1981) shows less incorporation of Co into calcite as a function of growth rate and D values for both Co and Ni are documented to be above unity (see also Kitano et al., 1980; Lakshtanov and Stipp, 2007). These different incorporation behaviors are reasonably expected as Ni and Co are structurally incompatible divalent cations for aragonite, but compatible for calcite (e.g. Pertlik, 1986). The incorporation of Co and Ni ions can be hindered by the competitive growth of hydroxide-cobalt/nickel carbonates on carbonate surfaces (e.g. for Co in calcite: Riechers et al., 2022) and apparent D values can be affected by surface-bound organic molecules (e.g. citrate and phthalate effect for Co in calcite: Lee and Reeder, 2006). Co and Ni incorporation/adsorption into/onto calcite are considered as paleoenvironmental reconstruction proxies, e.g. tracing $CaCO_3$ saturation state or mineral growth rate, but the coupled incorporation/adsorption phenomena can restrict these applications and also their Me ion mobility in aquatic settings (e.g. Lakshtanov and Stipp, 2007; Katsikopoulos et al., 2008). In this context, the availability of Ni and Co in terms of physiology and their toxicity at elevated concentrations have to be considered for biomineralization aspects (e.g. Sun et al., 2020).

Zinc has been experimentally studied to be incorporated into calcite and aragonite, where D values for calcite are typically found to be significantly higher compared to those for aragonite (e.g. Crocket and Winchester, 1966; Tsusue and Holland, 1966; Kitano et al., 1980; Mavromatis et al., 2019; Brazier et al., 2024a). The incorporation of Zn ions into calcite depends on the chemical composition of the solution, aqueous speciation, saturation degree / growth rate and surface adsorption, where the latter phenomena is also documented for the Zn ion precipitation behavior on calcite surfaces (e.g. Zachara et al., 1989). Recently, Brazier et al. (2024a) calculated from experimental data sets $D_{Zn} = 10^{-1.9}$ and $D_{Zn} = 10^{-1.6}$ at chemical equilibrium (25 °C) for calcite and aragonite, respectively. The typical inverse relationship of D_{Zn} values of calcite and aragonite as a function of precipitation rate ($10^{-8.6} < R < 10^{-7.3} \text{ mol m}^{-2} \text{ s}^{-1}$) can be quantified by the equations.

$$\text{Log}(D_{Zn}) = -0.331 (\pm 0.048) \text{ Log}(R) - 0.991 (\pm 0.375); \text{calcite} \quad (4)$$

$$\text{Log}(D_{Zn}) = +0.751 (\pm 0.089) \text{ Log}(R) + 5.160 (\pm 0.702); \text{aragonite} \quad (5)$$

Zn incorporation into calcite follows a dilute solid-solution (calcite-smithsonite), whereas for Zn uptake into aragonite defect sites at the growing mineral surface have to be taken into account (Brazier et al., 2024a). The incorporation of Zn into foraminiferal calcite was shown to be affected by pH and CO_3^{2-} concentration (van Dijk et al., 2017). Considering Zn ions in aspects of nutrient, adsorption phenomena (e.g. at clay minerals) and aqueous complex formation, the use of Zn uptake

in CaCO_3 as an environmental proxy might be most suitable within a multi-proxy approach.

Results from inorganic precipitation experiments show a decrease of manganese incorporation into calcite at higher precipitation rates and no significant T dependence (e.g. Lorens, 1981; Böttcher and Dietzel, 2010 and references therein). Mn adsorption is considered to be involved for its incorporating behavior into calcite at a high concentration level, which can result in significant Mn/Ca ratios of calcite (e.g. Franklin and Morse, 1983; Zachara et al., 1991). D_{Mn} values for aragonite are below unity, thus being (i) typically lower than those for calcite, (ii) characteristic for the aragonite structure in terms of Mn vs Ca ionic sizes, and (iii) mostly independent from T, but rather controlled by surface processes (Raiswell and Brimblecombe, 1977). Mn/Ca ratios of CaCO_3 precipitates are potential proxies for redox changes in aquatic media, e.g. seawater oxygenation (e.g. Davies et al., 2022). However, species specific differences in biomineralization strategies and aquatic speciation are found to be dominant factors for determining the Mn content in calcite, which results in individual calibrations for e.g. foraminifera species (e.g. Barras et al., 2018; Van Dijk et al., 2020).

Inorganic precipitation experiments indicate cadmium ions to be less incorporated into calcite at higher precipitation rates ($D_{\text{Cd}} > 1$; e.g. Lorens, 1981; Tesoriero and Pankow, 1996). Davis et al. (1987) found Cd ions to be adsorbed onto the calcite surface and subsequently to be trapped in a solid hydrated carbonate layer to yield finally in the formation of a solid solution. The latter was studied as a complete series of the calcite-otavite solid solution at 2 °C by Ma et al. (2022). However, experimental results showed both exposed calcite and aragonite material to trap Cd ions from the solution by forming a $(\text{Ca}, \text{Cd})\text{CO}_3$ solid-solution with calcite structure (e.g. Stipp et al., 1992; Prieto et al., 2003; Julia et al., 2023; see section 8.2.7). The potential formation of a short-range-ordered amorphous Cd-Ca carbonate phase - different from ACC - was verified by Mergelsberg et al. (2021), which has to be considered as a complex pathway for Cd incorporation into CaCO_3 precipitates.

Coprecipitation experiments by Fang et al. (2022) indicate chromium(III) not to be directly substituting Ca in the calcite structure, but in interstitial voids of the crystals or by occupying the position of Ca in the form of divalent $\text{Cr}(\text{OH})^{2+}$ both at low concentration levels.

Rare earth elements (REE) and actinide elements are also known for nonequivalent substitutions of Ca^{2+} ions caused by their trivalent state (e.g. Fernandez et al., 2008). REE distributions in inorganic and biogenic carbonate minerals are used as a proxy to reconstruct past seawater composition, redox state conditions and elemental cycling and provenance (e.g. Webb and Kamber, 2000; Azmy et al., 2011; Zhao

groundwater, where light REE are typically enriched compared to heavy REE in calcite formed at low temperature. D_{REE} values for calcite at high temperatures are experimentally derived at 200 °C by Perry and Gysi (2020).

The REE coprecipitation into CaCO_3 is still not fully understood and seems to be complex in particular by aqueous and surface complex formation depending on individual REE concentrations, Mg^{2+} exchange against Ca^{2+} ions at surface layer interfering with that of REE ions, and concurrent incorporation of monovalent ions such as Na^+ and OH^- or by exchange of 2Ca^{2+} to balance charge (e.g. Zhong and Mucci, 1995; Voigt et al., 2017; Perry and Gysi, 2020; Möller and De Lucia, 2020; Louvel et al., 2022).

7.1.2. Anions

In the scope of impurities in CaCO_3 phases, individual anions such as chloride, sulfate, chromate and borate were taken into account in addition to cations (e.g. Kitano et al., 1975; Kontrec et al., 2004). Anion substitution for CO_3^{2-} in the CaCO_3 lattice structure occurs mostly at low concentration levels caused by non-fitting charge (e.g. NO_3^- , CrO_4^{2-}) and/or geometry (e.g. SO_4^{2-} , $\text{B}(\text{OH})_4^-$). D values of anions and also uncharged species are defined analogically to eq. (2) by considering CO_3^{2-} instead of Ca^{2+} ion contents in CaCO_3 .

In a prominent case, sulfate ion incorporation into CaCO_3 precipitates is denoted as carbonate associated sulfate (CAS), where sulfate is decreasingly incorporated into CaCO_3 in the order of vaterite, calcite and aragonite (e.g. Kitano et al., 1975; Balan et al., 2014). Analysing the concentrations of CAS can be used to reconstruct the SO_4 content of the precipitating or diagenetic aqueous media, in particular for sea- or pore water reconstruction (e.g. Kampschulte and Strauss, 2004; Fichtner et al., 2018; Wynn et al., 2018; van Dijk et al., 2019). Sulfate incorporation behavior into CaCO_3 is related to unspecific incorporation sites in the crystal lattice caused by the non-fitting tetrahedral sulfate ion geometry (e.g. Kontrec et al., 2004). Accordingly, Wynn et al. (2018) experimentally found high precipitation rates to result in higher D_{SO_4} values caused by increasing defect sites at the growing calcite surfaces. Recently, a critical evaluation of the CAS proxy is given by Karancz et al. (2024) as sulfate complexation (CaSO_4°) seems to control sulfate uptake in inorganic calcite experiments.

Goetschl et al. (2019) assessed the incorporation of sulfate to affect that of Mg ions in calcite, where the incorporated SO_4 is expanding the c-axis dimension of the unit cell of the precipitating calcite. Consequently, a negative relationship between Mg and SO_4 incorporation into calcite is observed according to the equation.

$$D_{\text{Mg}} = 0.03726 - 0.02345 \cdot (-\log(R) - 7) - X_{\text{SO}_4} \cdot (-0.004607 + 0.002109 \cdot (-\log(R) - 7)) \quad (6)$$

et al., 2021; Mizuno et al., 2022; Zhang and Shields, 2023). The D_{REE} values for calcite and aragonite correlate to some degree with the solubility of their respective carbonate end member minerals and are significantly above unity; thus, REE ions are strongly incorporated into the precipitating CaCO_3 phases (e.g. Terakado and Masuda, 1988; Möller and De Lucia, 2020). Experiments in artificial seawater by Zhong and Mucci (1995) and in NaCl-bearing solutions by Voigt et al. (2017) indicated D_{REE} values for calcite to decrease systematically with the atomic number, thus being highest for La^{3+} and lowest for Yb^{3+} and to depend on saturation state conditions and on absolute REE concentration. Accordingly, Toyama and Terakado (2014) showed D_{REE} values for calcite at relatively low REE concentration in the fluid to be significantly smaller compared to e.g. Voigt et al. (2017). Maskenskaya et al. (2015) identified the decisive role of carbonate complexes and crystal habit on REE uptake into calcite precipitating from low mineralized

where X_{SO_4} is the SO_4 content of the calcite given in mol% and R the precipitation rate in $\text{mol m}^{-2} \text{s}^{-1}$ ($-8 \leq \log(R) \leq -7$; $0 \leq X_{\text{SO}_4} \leq 2.6$; $T = 25^\circ\text{C}$). This coupled negative correlation between Mg and SO_4 incorporation into calcite is promising to reconstruct precipitation rates or chemical compositions of the precipitating solutions. Assuming Mg-calcite to be formed through an ACC precursor phase, the long-lasting exchange of SO_4 and Mg ions between the obtained nanocrystalline Mg-calcite and the reactive solutions may limit (in this case) the use of Mg and SO_4 content of Mg-calcite as an environmental proxy (Goetschl et al., 2021).

Chloride, bromide, and fluoride are known to be incorporated into CaCO_3 as trace ions (e.g. Kitano and Okumura, 1973; Kitano et al., 1975; Okumura et al., 1986; Kontrec et al., 2004). These halogens are potential (marine) paleo-proxies, where their content in fluid inclusions, nanostructures (like chlorapatite), detrital and insoluble organic

particulates is challenging to be properly deduced (e.g. Roepert et al., 2020). However, these anions are preferentially incorporated into aragonite versus calcite, where e.g. coupled F_2^{2-} ions are suggested to substitute CO_3^{2-} (e.g. Kitano and Okumura, 1973; Kitano et al., 1975; Feng et al., 2021). Fluorine in biogenic $CaCO_3$ precipitates has to be considered as a main sink for F^- in the ocean (e.g. Carpenter, 1969; Tanaka and Ohde, 2010) and as a promising proxy for ocean Pco_2 level (e.g. Feng et al., 2021). Its use is limited for past seawater reconstruction as (i) fluoride co-precipitation with calcite and aragonite is known to be a function of the parent Mg concentration (Kitano and Okumura, 1973) and (ii) highly heterogeneous F content of foraminifera shells suggests F and also Cl to be governed by individual calcification pathways (Roepert et al., 2020).

Midgley et al. (2022) suggest from quantum mechanical calculations, the incorporation of **bromate** (BrO_3^-) into calcite and aragonite to be paired in nearest-neighbor configurations with compensating cations like Na, K, or Li. Bromate - together with sulfate and molybdate - incorporation into $CaCO_3$ speleothems constitutes a useful proxy of past volcanic activity (e.g. Badertscher et al., 2014).

Molybdate (MoO_4^{2-}) is also promising to trace paleo-redox conditions and ocean oxygenation. In this context, Chen et al. (2021a) experimentally assessed the molybdate incorporation into calcite to be extremely low ($D_{MoO_4} = 0.000015$; pH 8.3; 25 °C), where its incorporation behavior is suggested to depend on highly complex aqueous Mo speciation (e.g. Torres et al., 2016). Ab Initio Molecular Dynamics show molybdate to be favorable for surface substitution, but being less incorporated into calcite vs. the smaller sulfate (Midgley et al., 2021).

First-principles simulation indicates iodine to be best incorporated as **iodate** (IO_3^-) at the carbonate site in the order of vaterite > calcite > aragonite (Feng and Redfern, 2018). Interestingly, chromate and iodate in $CaCO_3$ is less competitive for the incorporation into $CaCO_3$ (e.g. Saslow et al., 2019; Katsenovich et al., 2021). I/Ca ratios of $CaCO_3$ precipitates are a promising (ocean) oxygenation proxy (e.g. Lu et al., 2021), where $CaCO_3$ precursors e.g. in the biocalcification process may affect the I/Ca ratio of the final calcite. This approach has in particular to be used with caution for (i) planktonic foraminifera as iodine in respective $CaCO_3$ deposits is reasonably considered to be gained post-mortem, either from the water column or during burial (Winkelbauer et al., 2023) and (ii) fish otoliths as iodine is related to organic matter and individual metabolisms (He et al., 2022). In addition, the incorporation of iodate into $CaCO_3$ precipitates was experimentally shown to be favored at lower pH and higher silicic acid concentration (Katsenovich et al., 2021).

Nitrate ions are known to be incorporated into $CaCO_3$ precipitates from experimental results (e.g. Kontrec et al., 2004). The concentration of aqueous nitrate is controlling its incorporation e.g. into cave carbonates, but the controlling mechanisms are still little explored (Wynn et al., 2021). Accordingly, the NO_3^- concentration of the precipitating solution can be traced by its content in the $CaCO_3$ precipitates, where the availability of NO_3^- has to be considered to be highly variable in most natural and anthropogenic environments caused by its redox sensitivity and biogenically mediated reactivity (e.g. Canfield et al., 2010).

Beside the poorly soluble Cr(III) (see section 7.1.1), chromium exists as oxidized and more soluble **chromate** (CrO_4^{2-}), where coprecipitated chromate and its isotopic composition in $CaCO_3$ may act as an archive to trace changes in Earth's surface redox levels (e.g. Wang et al., 2021b). Tang et al. (2007) verified by coprecipitation experiments and XANES spectra CrO_4^{2-} to be incorporated into calcite, where significant distortion/disruption is required to accommodate chromate in the calcite lattice. More recently, experimental data by Füger et al. (2019b) indicate CrO_4^{2-} incorporation into calcite to depend on pH and on aqueous chromate speciation. These dependences of D_{CrO_4} on the solution composition and the post-depositional overprinting of its pristine content (e.g. in foraminifera; Remmelzwaal et al., 2019) show this proxy to be demanding, which points on its application in terms of isotopic composition (see section 7.2.2).

Arsenic oxyanions can be trapped by surface adsorption and are subsequently incorporated into the $CaCO_3$ crystal lattice, where (i) the amount of **arsenate** (AsO_4^{4-}) retained in aragonite is higher compared to calcite and (ii) arsenate is preferentially incorporated into calcite compared to **arsenite** (AsO_3^{3-}) (e.g. Yokoyama et al., 2009; Khan et al., 2023 and references therein). Thus, the arsenic content of $CaCO_3$ precipitates acts as a promising (redox) archive in natural and anthropogenic sediments, where arsenate is known to be the dominant As species (Bia et al., 2021).

Coprecipitation experiments of Kitano and Oomori (1971) assessed the distribution of uranium in the form of **uranyl** (UO_2^{2+}) between solutions and $CaCO_3$ precipitates, where the uranyl coprecipitation is mainly controlled by the formation of $UO_2^{2+}-CO_3^{2-}-OH^-$ aqueous complexes. Chen et al. (2020a) addressed the aqueous species $UO_2(CO_3)_2^{2-}$ to be most likely incorporated into calcite. In contrast, the significantly higher U incorporation into aragonite is based on the more abundant $UO_2(CO_3)_3^{4-}$ species to be incorporated. The U content of coral skeletons have been explored as potential proxy for temperature, pH, carbonate concentration, and salinity (e.g. Wei et al., 2000; Gabitov et al., 2008; DeCarlo et al., 2015). However, U incorporation into aragonite is known to (i) depend on growth rate (Gabitov et al., 2008; for calcite: Were-mechik et al., 2017), (ii) decrease at elevated carbonate ion concentration, and (iii) be independent of pH and T from experiments in seawater (DeCarlo et al., 2015). Accordingly, Gothmann and Gagnon (2021) found in culturing experiments of cold-water corals the U/Ca ratio to be not a robust indicator of pH or aqueous carbonate ion concentration of the precipitation seawater, but to record the chemistry of the internal calcifying fluid and/or calcification strategies. The pristine U signals can be overprinted e.g. by $CaCO_3$ re-crystallization, where Gabitov et al. (2021b) showed under reduced conditions a potentially strong uptake of aqueous U in calcite by considering U^{4+} besides U^{6+} species.

The boron incorporation into $CaCO_3$ precipitates is used as tracer for pH and Earth's carbon chemistry, and is related to the dissociation of triangular **boric acid** to the tetrahedral **borate** ion according to the reaction.



where the monovalent borate is mainly incorporated into carbonate minerals substituting lattice CO_3^{2-} (e.g. Hemming and Hanson, 1992; Hobbs and Reardon, 1999; Holcomb et al., 2016; Uchikawa et al., 2017; Decarlo et al., 2018; Branson, 2018; Mavromatis et al., 2015). The pH dependent distribution of aqueous $B(OH)_3^\circ$ vs $B(OH)_4^-$ allows for pH reconstruction. Balan et al. (2016) showed by first-principles quantum mechanical modeling $B(OH)_4^-$ to be dominant in aragonite, whereas for calcite additionally deprotonated trigonal $BO_2(OH)^2-$ species have to be considered. The relative abundance of $B(OH)_3^\circ$ vs $B(OH)_4^-$ in calcite is shown to be independent of pH, but decreases at elevated precipitation rates. The detection of both triangular and tetrahedral coordination species in $CaCO_3$ precipitates has also been suggested to be reflected by an ACC precursor formation pathway (e.g. Rollion-Bard et al., 2011; Klochko et al., 2009).

Mavromatis et al. (2021) found the B distribution coefficient of Mg-calcite and aragonite formed via an ACC precursor to be about two orders of magnitude higher compared to the minerals formed via a classical pathway (see Mavromatis et al., 2015). Moreover, aragonite formed via ACC precursor contains higher $B(OH)_3^\circ/B(OH)_4^-$ ratios compared to classically grown aragonite. Farmer et al. (2019) used surface kinetic modeling and experimental data from Uchikawa et al. (2015) to assess the growth rate dependence of B incorporation into calcite by changing the contribution of aqueous boric acid vs. borate to be co-precipitated. Piazza et al. (2022) verified the B/Ca ratio in a calcareous red alga to be affected by growth rate. Hobbs and Reardon (1999) have evidence that even at very low growth rate the B partitioning into calcite does not approach a constant value, but depends

on the formation pathway; in their transformation approach vaterite or aragonite were used as precursors.

Recently, Uchikawa et al. (2023) claimed that crystallographic controls on B incorporation into calcite may outweigh kinetic effects, which was shown by deformation of the calcite lattice caused by sulfate and phosphate ions to substitute lattice carbonate. The B incorporation into CaCO_3 gets even more complex by consideration of aqueous deprotonated trigonal $\text{BO}_2(\text{OH})^{2-}$ (Balan, 2016) and polyborates (e.g. $\text{B}_3\text{O}_3(\text{OH})_4^-$, $\text{B}_4\text{O}_5(\text{OH})^{2-}$, and $\text{B}_5\text{O}_6(\text{OH})^-$) in brines; Gu et al., 2023) to be trapped into calcite. The application of boron as an environmental proxy seems to be most promising by coupled strategies e.g. measuring the triangular to tetrahedral B ratio in CaCO_3 together with B isotopes for an advanced pH estimation (e.g. Rollion-Bard et al., 2011; Hönnisch et al., 2018).

The incorporated dissolved or colloidal organic matter (DCOM) in CaCO_3 reflects the DCOM concentration in the precipitating solution, which was exemplarily shown by Pearson et al. (2020) in fresh water and by Kaushal et al. (2020) in marine to fresh water systems. DCOM in speleothems have the potential to record anthropogenic impacts, e.g. land-use (Pearson et al., 2020). Sub-annual band luminescence of aragonitic coral is applied to trace terrestrial DCOM, which was confirmed to be readily incorporated into aragonite, but not fluorescent DCOM from marine sources (Kaushal et al., 2020). However, DCOM comprises a highly diverse range of hydrocarbon structures with different functional groups (e.g. Leenheer and Croué, 2003), where its incorporation behavior into CaCO_3 has to be assessed individually. DCOM and transition metal ion (Me) incorporation into calcite can be coupled by complexation to significantly increase the Me uptake into calcite to pose as a quantitative paleo-hydrological proxy in speleothems (Me: Co^{2+} , Ni^{2+} and Cu^{2+} ; Hartland et al., 2014; Lindeman et al., 2022). In a similar way, anions, like I^- , Br^- and PO_4^{3-} , can be attached to DCOM and thus accordingly be trapped into growing CaCO_3 via DCOM incorporation as indicated by speleothems (Fairchild et al., 2010).

7.2. Isotope distribution

Following the complex aspects of element incorporation behavior into precipitating CaCO_3 and its use as environmental proxies, the respective isotope fractionation effects and individual isotope signatures open up an additional and highly sophisticated tool box to understand CaCO_3 mineral formation pathways and to reconstruct physicochemical (trans)formation conditions. Considering the main components, Ca^{2+} and CO_3^{2-} , the isotope fractionation between aqueous species and the precipitate were extensively used to decipher the origin of the components, environmental formation conditions, alteration effects etc. (e.g. Ripperdan, 2001; Gussone et al., 2016). For instance, Ca isotope distribution in CaCO_3 tracks precipitation rates, chemistry of the precipitating solution (e.g. seawater, interstitial solutions, speleothem drip water), mineralogy of the precipitate, climatic perturbations, global elemental cycles, diagenesis history etc. (e.g. Gussone et al., 2020). Ca ion - and more generally metal ion - isotope signatures are known to depend on kinetics of e.g. ion diffusion, growth rates, adsorption phenomena, besides approaching fractionation at isotopic equilibrium (e.g. Tang et al., 2008b; Gussone and Dietzel, 2016; Brazier et al., 2019; Griffith and Fantle, 2020; Li et al., 2024a).

Exemplarily, the $^{44}\text{Ca}/^{40}\text{Ca}$ fractionation between the mineral calcite and aqueous calcium is thermodynamically defined by the isotope fractionation factor.

$$\alpha^{44}\text{Ca}_{\text{calcite-aq}} = \left(\frac{^{44}\text{Ca}}{^{40}\text{Ca}} \right)_{\text{calcite}} / \left(\frac{^{44}\text{Ca}}{^{40}\text{Ca}} \right)_{\text{aq}} \\ = (\delta^{44}\text{Ca}_{\text{calcite}} + 1000) / (\delta^{44}\text{Ca}_{\text{aq}} + 1000) \quad (8)$$

where α can be related to fractionation at isotope equilibrium and by using other symbols to apparent values, e.g. depending on reaction kinetics. Herein α is used as a general term for an isotope fractionation

factor, where delta values are defined as $\delta^{44}\text{Ca} = (R_S/R_{\text{St}} - 1) \cdot 10^3$ with the isotope ratio $R = ^{44}\text{Ca}/^{40}\text{Ca}$ of the analyzed sample (R_S) and the standard material used for analyses (R_{St}). Analogous equations can be developed for isotope fractionation of components during their incorporation into CaCO_3 phases. Fundamentals and notation on isotope analyses, data and fractionation effects are well compiled by e.g. Hoefs (2021) and White (2023), where at this point only a brief remark is given on temperature and open to close system control on isotope discrimination during carbonate precipitation: (i) Isotope fractionation between a liquid and solid component has to increase with decreasing T considering isotope equilibrium conditions and (ii) in a closed system the control on isotope distributions can be described by the so-called Rayleigh (distillation) approach, which considers the enrichment/depletion of a given isotope during ongoing precipitation if the respective α value is unequal to 1.

In the case of the CO_3^{2-} molecule, the isotopic fractionation of stable carbon and oxygen between CaCO_3 and precipitating solutions has been widely and for a long time used to evaluate and assess elemental source, temperatures, reaction mechanisms, environmental changes etc. in many fundamental and applied disciplines (e.g. McCrea, 1950; Kim and O'Neil, 1997; Clark and Fritz, 1997; Kosednar-Legenstein et al., 2008; Carlson et al., 2020; Weidlich et al., 2023). In analogy to eq. (8) the respective isotope fractionation factors are defined by considering equilibrium and non-equilibrium conditions, where in particular α values considering H_2O , aqueous DIC species, distinct CaCO_3 phases and gaseous $\text{CO}_{2(g)}$ have to be taken into account (e.g. Zeebe and Wolf-Gladrow, 2005). Stable isotope fractionation and exchange behavior become increasingly interesting in respect to foreign cations, anions and uncharged molecules covering nearly all chemical elements with at least two stable isotopes within the periodic system (e.g. Valley and Cole, 2001; Johnson et al., 2004; Liu, 2015; Teng et al., 2017; Hoefs, 2021; White, 2023). Highly promising for a holistic understanding of complex mineral formation phenomena are multi-proxy approaches by coupling selected elemental / stable isotope distributions and their individual fractionation behaviors.

In the following the incorporation of individual (foreign) cations, anions and uncharged molecules are exemplarily discussed in its isotope fractionation behavior and potential applications. This comprises so-called traditional and non-traditional stable isotopes focused on equilibrium and kinetics during mass dependent stable isotope fractionation by considering classical and non-classical formation pathways. In the view of the enormous numbers of contributions and diversities on the above objectives and approaches, herein we provide a limited selection of prominent, successful and/or promising aspects including a couple of important radiogenic isotopes. In several cases individual isotope distributions in CaCO_3 are only briefly discussed with hint on more detailed references, textbooks and/or recent reviews.

Ongoing research on isotope distributions in CaCO_3 precipitates is used to trace and assess the (trans)formation conditions and surroundings, elemental origin, reaction rates, geochemical cycles, climate change etc. - like past seawater reconstruction (Hoefs and Harmon, 2023), hydrothermal overprint of marine carbonate archives (e.g. Mueller et al., 2024), terrestrial authigenic CaCO_3 (uranium isotopes: Rovan et al., 2021) or for tracking bound inorganic matter (nitrogen isotopes: Gillikin et al., 2017). The wide range of tasks and large number of contributions show the great need to trace and understand reactions in the $\text{CaCO}_3\text{-H}_2\text{O-CO}_2$ system. Fig. 5 gives a schematic overview about applications of (stable) isotopes as discussed in the following.

7.2.1. Cations

The fractionation of stable isotopes of the monovalent ions Li and K during incorporation into precipitating CaCO_3 depends on the physicochemical precipitation conditions and in particular on their entrapment mechanisms into the individual crystal lattice. As the latter reaction kinetics and mechanisms are still hotly debated, understanding and application of Li and K isotope signatures is challenging, but

indicate wide-ranging perspectives.

The **lithium** isotope distribution of marine CaCO_3 is of high interest to record and assess the evolution of $\delta^7\text{Li}$ values of seawater, the (reverse) silicate weathering reactivity, the global carbon, lithium and silicon cycle, and the Earth's climate history (e.g. Misra and Froelich, 2012; Lechner et al., 2015; Murphy et al., 2022; Wei et al., 2023a; Huber et al., 2024; Wei et al., 2023c). In a first step, the use of carbonate archives to reconstruct e.g. seawater Li isotope compositions requires the separation of potential other Li containing phases such as Mn (hydr) oxides and clays before analyses (Cao et al., 2023). However, ${}^7\text{Li}$ is well known to be discriminated vs. ${}^6\text{Li}$ during incorporation into growing calcite: According to the equation.

$$\Delta^7\text{Li}_{\text{calcite-aq}} = \delta^7\text{Li}_{\text{calcite}} - \delta^7\text{Li}_{\text{aq}} \sim 10^3 \ln(\alpha^7\text{Li}_{\text{calcite-aq}}) \quad (9)$$

negative $\Delta^7\text{Li}_{\text{calcite-aq}}$ values are evident (i.e., $\alpha^7\text{Li}_{\text{calcite-aq}} < 1$, see eq. (8); e.g. Marriott et al., 2004; Füger et al., 2022). Calcite precipitation experiments indicate individually observed $\Delta^7\text{Li}_{\text{calcite-aq}}$ values to be strongly controlled by precipitation kinetics and/or the physicochemical conditions of the precipitating fluid such as pH, DIC, T (e.g. Füger et al., 2022; Day et al., 2021; Seyedali et al., 2021). However, experimental data on lithium isotope fractionation during calcite formation show partly inconsistent trends, which hints on (i) the fractionation mechanisms to be complex and not completely understood yet and (ii) the need of future systematic studies on Li isotope distribution in CaCO_3 to be used as a robust environmental proxy (see Chen et al., 2023b and Branson et al., 2024 with references therein). The inconsistent trend is suggested to be related to different experimental setups/conditions and/or not identified controlling parameters. For instance, besides free Li^+ ions the entrapment of surface complexes like $\text{Li}-\text{HCO}_3^0$ (or $\text{Li}_2-\text{CO}_3^0$) are suggested to play a role for Li uptake into calcite. However, their occurrence and distribution as a function of solution chemistry (e.g. ionic strength) and/or temperature is an until now underestimated parameter on $\Delta^7\text{Li}_{\text{calcite-aq}}$ values.

The influence of CaCO_3 mineral type is insufficiently explored, but limited coprecipitation experiments indicate aragonite to discriminate ${}^7\text{Li}$ vs. ${}^6\text{Li}$ during its incorporation more strongly than calcite (mean $\Delta^7\text{Li}_{\text{aragonite-aq}} \sim -11\text{ ‰}$; Day et al., 2021; Gabitov et al., 2011; Marriott et al., 2004). *In-situ* $\delta^7\text{Li}_{\text{aragonite}}$ analyses of synthetic aragonites of Gabitov et al. (2011) verified the precipitation rate to be crucial for the use of Li isotopes as environmental proxy. The isotope fractionation of Li might be influenced by precursor phases. First data from inorganic precipitation experiments with artificial seawater indicate $\Delta^7\text{Li}_{\text{ACC-aq}}$ values being close to those of $\Delta^7\text{Li}_{\text{calcite-aq}}$ gained from its transformation (Schmidt et al., 2023).

In analogy to Li, the **potassium** isotope composition of (marine) CaCO_3 is suggested as a promising environmental proxy considering continental and reverse silicate weathering, fluid-mineral interactions and K as a nutrient e.g. for land plants (e.g. Li et al., 2021a; Li et al., 2022a). Accordingly, the K isotope record of seawater recovered by K isotope analysis of marine carbonates may help to understand coupled past changes in weathering, biosphere, and climate. Potassium isotope distribution can be influenced by structural incorporation into clays, surface adsorption of K^+ and early diagenesis reactions (Li et al., 2021b; Li et al., 2022c). A limiting aspect of $\delta^{41}\text{K}$ of marine carbonate to be used as paleoproxy is K to be hosted in amorphous K_2CO_3 and intracrystalline organic matrices of varying proportions with different $\delta^{41}\text{K}$ values (Li et al., 2021a). Interestingly, cultured scleractinian coral $\delta^{41}\text{K}$ values reflect this K phase partitioning, which traces the T-sensitive physiological modulation (Li et al., 2022a).

Stable **magnesium** isotope fractionation between carbonate precipitates and aqueous species is used for a long time as an environmental proxy, where the heavy Mg isotope is known to be discriminated vs. the light Mg isotope during CaCO_3 formation (e.g. Galy et al., 2002; Immenhauser et al., 2010; Yoshimura et al., 2011; Saenger and Wang, 2014; Shalev et al., 2020; Liu and Li, 2023). $\delta^{26}\text{Mg}_{\text{calcite}}$ values are used

as archives for past seawater composition, formation temperatures, elemental provenances, dolomitization, carbonate diagenesis etc. (e.g. Hu et al., 2017; Li et al., 2015b; Ning et al., 2019; Hu et al., 2021; Xie et al., 2022). Thus, the literature dealing with Mg isotope signatures of carbonates in the Mg-Ca-CO₂-H₂O system is voluminous (e.g. Hu et al., 2017; Guo et al., 2019; Shalev et al., 2019; Son et al., 2020), where in the following only selected and prominent relationships are introduced.

At first, Mg is a prominent example, where mass-dependent isotope fractionation behavior and analysis reliability check can be done by a three-isotope plot with a linear and a given positive correlation of $\delta^{26}\text{Mg}$ vs. $\delta^{25}\text{Mg}$ (e.g. Young and Galy, 2004). In general, the Mg—O bond strength plays an important role for distinct $\Delta^{26}\text{Mg}_{\text{mineral-aq}}$ values (e.g. Wang et al., 2019a; Son et al., 2020). The $\Delta^{26}\text{Mg}_{\text{calcite-aq}}$ values close to isotopic equilibrium can be followed by a distinct equation, which show less Mg isotope fractionation at elevated T as predicted from a thermodynamic view (e.g. aragonite-to-calcite conversion experiments between 98 and 170 °C: Liu and Li, 2023 and references therein). At ambient and low temperature conditions, apparent $\Delta^{26}\text{Mg}_{\text{calcite-aq}}$ values can be significantly different from isotope equilibrium, which is controlled e.g. by R and the Mg content in calcite (Wang et al., 2013b; Wang et al., 2019a), thus being related to (i) kinetic isotope fractionation effects caused by slow dehydration kinetics of aqueous Mg, ion diffusion, sorption/trapping phenomena and growth rates, (ii) aqueous speciation considering Mg aquo-complexes and free Mg^{2+} ions and (iii) the variabilities in calcite composition (e.g. Immenhauser et al., 2010; Mavromatis et al., 2013; Wang et al., 2019a). However, influence of apparent $\Delta^{26}\text{Mg}_{\text{calcite-aq}}$ on variabilities of calcite crystal texture and form seems to be insignificant (Chen et al., 2020b).

Coprecipitation experiments by Mavromatis et al. (2013) found Mg isotope fractionation to decrease at elevated precipitation rates according to the equation.

$$\Delta^{26}\text{Mg}_{\text{calcite-aq}} = 0.7918 (\pm 0.0452) \log(R) + 3.2366 (\pm 0.3360) \quad (10)$$

which linearly corresponds to eq. (3) for the Mg incorporation behavior into calcite as a function of R ($\text{mol m}^{-2} \text{s}^{-1}$). Interestingly, the isotopic trend in eq. (10) is opposite to the precipitation rate dependence of Ca, Ba and Sr isotope fractionation with respect to calcite, which is caused by the comparably high free energy of hydration of the aqueous Mg^{2+} ion vs. that of Ca, Ba and Sr. Although, an impact of aqueous complex formation of Mg^{2+} with organic ligands was shown to be not expected in most natural calcite precipitating environments, it cannot be completely ruled out as confirmed for citrate in experiments by Mavromatis et al. (2017a).

For biogenic calcite formation, Dämmer et al. (2021) showed a T impact on Mg isotope fractionation in cultured foraminifera, and Zhang and Li (2022) reported the Mg isotope fractionation during CaCO_3 precipitation to be associated with bacteria and extracellular polymeric substances. In contrast, Hu et al. (2023) reported no biological effects on $\Delta^{26}\text{Mg}_{\text{calcite-aq}}$ during stromatolite growth. Experimental studies have indicated aragonite to be enriched in ${}^{26}\text{Mg}$ relative to calcite, where obtained $\Delta^{26}\text{Mg}_{\text{aragonite-aq}}$ values are similar to biogenic aragonite (Saenger and Wang, 2014; Wang et al., 2013b). The experimental data of Wang et al. (2013b) show a noticeable decrease of Mg isotope fractionation between aragonite and the solution with increasing T. Son et al. (2020) attribute the range in Mg isotope fractionation data of aragonite to be caused to some extent to the variation in Mg—O distances, depending on the relative positions of Mg^{2+} sites within the aragonite crystal structure.

Mg isotope fractionation in precipitated Mg bearing CaCO_3 can also be used to trace amorphous phase transformation and thus to reconstruct reaction pathways (e.g. Mavromatis et al., 2017b; Ju et al., 2023; Brazier et al., 2024b; Liu et al., 2023a). Although, $\Delta^{26}\text{Mg}_{\text{ACC-aq}}$ is significantly less negative compared to the above observed $\Delta^{26}\text{Mg}_{\text{calcite-aq}}$ values, the finally formed Mg-calcite from this non-classical pathway approaches Mg isotopic equilibrium with the fluid (e.g. Mavromatis

et al., 2013; Mavromatis et al., 2017b). This re-isotope adjusting behavior reflects the highly dynamic exchange of Mg ions between ACC and the fluid as well as the ongoing Me (isotope) exchange between the final nano Mg-calcite crystals and the solution (Brazier et al., 2024b).

In conclusion, Mg isotope fractionation during CaCO_3 formation is extensively studied and individual relationships are quantified by well developed modeling concepts. Limitations of Mg isotope signatures of CaCO_3 to be used as environmental archives are due to complex formation kinetics and mechanisms, aqueous complexation, individual formation pathways and potential secondary re-adjustment and/or diagenetic overprints (e.g. Riechelmann et al., 2018; Liu and Li, 2023).

The fractionation of stable calcium isotopes during CaCO_3 formation has been intensively studied and applied to understand reaction kinetics and mechanisms, ion diffusion and adsorption, aqueous speciation as well as to reconstruct environmental conditions during (trans)formation, past seawater composition, elemental provenance, chemical weathering, (early) diagenesis etc. (e.g. Farkas et al., 2007a; Eisenhauer et al., 2009; Erhardt et al., 2020; Lammers et al., 2020; Riechelmann et al., 2020; Owen et al., 2016; Négre et al., 2021; Ahm et al., 2021; Druhan et al., 2020; Beaudoin et al., 2022). Knowledge on these aspects are compiled in a large number of contributions, where herein it is referred to the comprehensive overviews on calcium stable isotope geochemistry (Gussone et al., 2016), past lessons and future directions (Griffith and Fantle, 2020), and potentials and limitations of its use as environmental proxy (Gussone et al., 2020). In the following, key findings, important progress and recent challenges in the scope of stable Ca isotope distribution in CaCO_3 precipitates are highlighted.

Based on fundamental experimental results, such as Marriott et al. (2004), Gussone et al. (2005), Tang et al. (2008b), Gussone and Dietzel (2016), AlKhatib and Eisenhauer (2017a/b) and Harrison et al. (2023), calcium isotope fractionation during CaCO_3 precipitation from aqueous solution was found to strongly depend in particular on precipitation rates besides T, ion diffusion and aqueous/surface complex formation effects. Molecular simulations and precipitation models were developed to understand and quantify Ca isotope fractionation kinetics and at equilibrium (e.g. Tang et al., 2008b; DePaolo, 2011; Nielsen et al., 2012; Lammers et al., 2020; Druhan et al., 2020 and references therein). For instance, Mills et al. (2021) introduced process-based models of calcite growth to show the influence of Ca:CO_3 stoichiometry on Ca isotope fractionation (see also Nielsen and DePaolo, 2013).

Recently, the Ca isotope fractionation between CaCO_3 and aqueous Ca^{2+} at isotopic equilibrium was estimated by the three-isotope method with ^{42}Ca , ^{43}Ca and ^{44}Ca to be very small: $\Delta^{44/42}\text{Ca}_{\text{calcite-aq}} = -0.02 \pm 0.13 \text{ ‰}$ and $\Delta^{44/42}\text{Ca}_{\text{aragonite-aq}} = -0.80 \pm 0.10 \text{ ‰}$ (Harrison et al., 2023). Their data indicate Ca isotope exchange rates to be faster for aragonite compared to calcite, which is caused by larger extent of Ostwald ripening by dissolution and re-precipitation observed for aragonite. Even at ambient temperature, where bulk chemical equilibrium is reached with the coexisting fluid, a re-setting of Ca isotope distribution in respect to calcite and aragonite has to be considered (Oelkers et al., 2019; Harrison et al., 2023). Thus, pristine Ca isotope values of CaCO_3 in natural surroundings could be easily overprinted by recrystallization, which is controlled by reactive fluid-solid surface areas and volume ratios, reaction times, fluid flow rates, without considering any further diagenesis reactions (see also Chanda et al., 2019).

The use of Ca isotope distribution in CaCO_3 as (paleo)environmental proxy can be also hampered by the isotopic composition of aqueous free Ca^{2+} of the precipitating fluid to be changed by (i) formation of aqueous Ca-bearing complexes (e.g. Moynier and Fujii, 2017: caused by different Ca coordination numbers and Ca—O bond lengths), (ii) adsorption of Ca onto clay minerals (e.g. Brazier et al., 2019), (iii) precipitation of Ca-bearing solids besides CaCO_3 (e.g. Nelson et al., 2021: zeolites with strong Ca isotope fractionation during its uptake), (iv) distinct precipitation pathways through amorphous or crystalline precursors (e.g. Gussone et al., 2020 and references therein) and (v) coupled complex

reactions during microbially induced CaCO_3 formation (e.g. Bradbury et al., 2020). To summarize, Ca isotope distributions in CaCO_3 precipitates have been numerously investigated, assessed and quantified for decades, which frequently changes our view on the significance of specific isotope fractionation effects, but open up new and high potentials in its use as proxy for formation conditions, transformation pathways, diagenetic reaction etc.; in particular if the individual environments are well described and assessed by other geological and/or geochemical tools.

Stable strontium isotope distribution in CaCO_3 precipitates are widely used as paleoenvironmental and climate proxy signals using corals, cyanobacteria, cap and lagoon-estuarine carbonates etc. (e.g. Wang et al., 2019b; Shao et al., 2021; Wei et al., 2022; Yoshimura et al., 2022; Mehta et al., 2023; Wang et al., 2023b). The controlling parameters on the fractionation of stable Sr isotopes during CaCO_3 formation are partially similar as documented for Ca isotopes (e.g. Böhm et al., 2012; AlKhatib and Eisenhauer, 2017a/b; Knight et al., 2023; Brazier et al., 2023). Accordingly, equilibrium isotope fractionation of strontium at ambient T is considered to be very low ($\Delta^{88/86}\text{Sr}_{\text{calcite-aq}} = 0.01 \text{ ‰}$; $\Delta^{88/86}\text{Sr}_{\text{aragonite-aq}} = -0.01 \text{ to } -0.04 \text{ ‰}$; Böhm et al., 2012 and Brazier et al., 2023, respectively). Co-precipitation experiments by Böhm et al. (2012) reported a depletion of heavy isotopes of both Sr and Ca in the calcite crystal for increasing precipitation rates which yield in the expression.

$$\Delta^{88/86}\text{Sr}_{\text{calcite-aq}} = 0.18 \Delta^{44/40}\text{Ca}_{\text{calcite-aq}} - 0.01 \quad (25^\circ\text{C}) \quad (11)$$

Exemplarily, this linear relationship can be used as a simple multi-proxy approach, where the R effect can be ignored to interpret these coupled isotope fractionation effects. Recently, Brazier et al. (2023) showed through experiments and first-principles simulations that stable Sr isotope fractionation during incorporation into aragonite is higher at elevated growth rates. At isotope equilibrium $\Delta^{88/86}\text{Sr}_{\text{aragonite-aq}}$ is considered to be close to zero, whereas the kinetic isotope fractionation factor is about -0.6 ‰ (25°C ; Brazier et al., 2023).

Kinetic models for strontium (incl. calcium) isotope fractionation during CaCO_3 formation are numerous considering surface reactions, ion diffusion etc., but also non-classical crystallization pathways (e.g. Zhang and Wang, 2023). Besides stable Sr isotopes, radiogenic $^{87}\text{Sr}/^{86}\text{Sr}$ signatures have been used for a long time in CaCO_3 deposits to trace the isotopic composition of the precipitating solution, e.g. for assessing ocean history, silicate weathering/alteration, land-sea distribution, geochemical cycling, climate evolution, and/or secondary overprints, e.g. during (early) diagenesis (e.g. Palmer and Elderfield, 1985; Kovács et al., 2020). The latter proxy is not in the focus of the present contribution, but the main approach is based on $^{87}\text{Sr}/^{86}\text{Sr}$ values to be not fractionating during its uptake into CaCO_3 , but to depend on the radiogenic ^{87}Sr production due to beta-decay of ^{87}Rb .

In analogy to Sr, barium isotope signatures of CaCO_3 are used as proxy to reconstruct (paleo)environmental conditions, global Ba cycles etc. (e.g. Hsieh and Henderson, 2017; Bridgestock et al., 2018; Lin et al., 2022; Zhang et al., 2022a; Mehta et al., 2023; Hohl et al., 2024). Wang et al. (2021c) estimated from first-principles calculations $\Delta^{137/134}\text{Ba}_{\text{calcite-aq}} = 0.14 \text{ ‰}$ and $\Delta^{137/134}\text{Ba}_{\text{aragonite-aq}} = 0.36 \text{ ‰}$ at isotope equilibrium (25°C). Apparent Ba isotope fractionation values obtained for inorganically and biogenically precipitated CaCO_3 are mostly lower, which is suggested to be based on kinetic effects to play an important role (e.g. Wang et al., 2021c). For instance, experimental data of Mavromatis et al. (2020) show barium isotope fractionation between aragonite and aqueous Ba to decrease with increasing precipitation rate. In contrast, experimental data in respect to calcite ($\Delta^{137/134}\text{Ba}_{\text{calcite-aq}} = 0.003 \pm 0.040 \text{ ‰}$) do not exhibit a variation with precipitation rate. Mehta et al. (2023) claimed amorphous precursors, e.g. from bacteria forming intracellular CaCO_3 , could introduce Ba and Sr isotope variability in environmental records, but experimental $\Delta^{137/134}\text{Ba}_{\text{ACC-aq}}$ data are up to now missing.

Measuring the widespread stable **iron** isotopes of masses 54, 56, 57 and 58 constitutes a valuable application of the non-traditional isotope systematics (De Groot and e., 2009; Hoefs, 2021). The widely used $\delta^{56}\text{Fe}/\delta^{54}\text{Fe}$ isotope ratio ($\delta^{56}\text{Fe}$) reflecting variable mass-dependent isotope fractionation approximately ranging from -4 to $+2\text{\textperthousand}$ represents a proxy of iron sources and biogeochemical processes characterizing marine and continental rocks and sediments (Halverson et al., 2011; Hoefs, 2021). In this context, pronounced kinetic isotope effects as well as near-equilibrium fractionation are relevant. The most relevant fractionation processes include inorganic and biological (microbial) reactions such as various redox reactions ($\text{Fe}[\text{II}]$ vs. $\text{Fe}[\text{III}]$), mineral precipitation and dissolution, as well as microbially mediated iron cycling (Hoefs, 2021). Iron isotopic compositions of carbonate minerals (e.g. siderite), iron (hydr)oxides, iron sulfides and silicates (e.g. clay minerals) are frequently combined with other isotope tracers (S, Si, Mn, Cr, Cu isotopes).

Considering variable redox conditions, the equilibrium isotope effect between $\text{Fe}[\text{II}]$ and $\text{Fe}[\text{III}]$ typically shows a large fractionation of $\sim 3\text{\textperthousand}$ in $\delta^{56}\text{Fe}$ (Welch et al., 2003; Wiederhold, 2015). Redox-sensitive chemical reactions typically lead to light isotope ($\delta^{54}\text{Fe}$) depletion in the reduced ($\text{Fe}[\text{II}]$) species and heavy isotope ($\delta^{56}\text{Fe}$) increase in the oxidized ($\text{Fe}[\text{III}]$) species (Hoefs, 2021). Mineral formation can be associated with both kinetic and equilibrium Fe isotope fractionation, for example precipitation of carbonates (Wiesli et al., 2004) or iron (hydr)oxides (Saunier et al., 2011). Iron isotope fractionation further occurs during chemical weathering and nutrient release, i.e. preferential dissolution (faster removal) of lighter Fe isotopes from mineral surfaces leads to isotopically heavier surface layers (Chapman et al., 2009; Wiederhold, 2015). Likewise, significant Fe isotope fractionation was reported during liquid-gaseous phase separation, e.g. from hydrothermal fluids at mid-ocean ridges (Syverson et al., 2014). Kettler et al. (2022) studied Fe isotope fractionation in iron oxide concretions and ferroan carbonate cements related to the Navajo Sandstone (USA) in order to test different conceptual models of iron mineral formation. They found evidence for the mobilization of iron by reducing fluids, reprecipitation as siderite and subsequent oxidation by groundwaters.

Pronounced effects of Fe isotope fractionation are also related to organic processes and biological cycling. Heavy metals and their heavy isotopes are preferentially enriched in different functional groups of organic materials mainly relying on a stronger chemical bonding in organic aqueous complexes and solids (Dideriksen et al., 2008; Morgan et al., 2010). The stable iron isotope compositions are also of value with regard to distinct signatures ("fingerprints") of (micro)biological activity (Wiederhold, 2015; Hu et al., 2020). Typical metabolic reactions of chemoautotroph microbes are known to control differentiated iron isotope fractionation in organic tissues and related minerals, e.g. during bacterial iron reduction or oxidation (Beard and Johnson, 2004; Kappler et al., 2010; Tong et al., 2021). Biogeochemical processes based on redox transitions, sorption, complexation and enzymatic reactions often result in pronounced kinetic isotope variations, e.g. the enrichment of light metal isotopes in plant materials (von Blanckenburg et al., 2009). Hu et al. (2020) investigated $\delta^{56}\text{Fe}$ compositions of iron oxides, Fe-rich carbonates (siderite, ankerite) and Ca—Mg carbonates related to Neoproterozoic banded iron formations in China and found clear evidence for the role of microbial dissimilatory iron reduction.

The iron isotopic signatures can further be of value for discerning potential iron sources and for tracing geological iron cycling in the course of raw material exploitation and mining activities. For example, the iron carbonate ore occurrence of the prominent Austrian "Erzberg" mine is a long-standing subject of scientific debate with regard to genetic aspects of the iron ore formation (Prochaska, 2012). In this context, non-traditional isotope techniques (e.g. $\delta^{56}\text{Fe}/\delta^{54}\text{Fe}$, clumped isotopes) could shed light into the chemistry of paleofluids, processes of metasomatic or metamorphic alteration and the potential connection to other sites of Alpine ore mineralization (e.g. magnesite deposits). Considering the more applied geoscientific research efforts, stable Fe isotopes might be

measured in various (geo)technical settings involving iron-rich mineral precipitates such as carbonates (e.g. Fe-rich calcite), (hydr)oxides and sulfides from highly differentiated aqueous solutions.

Stable **nickel** isotope fractionation during its coprecipitation into calcite exhibits light isotopes to be preferentially incorporated and as the calcite precipitation rate slows down $\Delta^{60/58}\text{Ni}_{\text{calcite-aq}}$ changes from -0.3 to $-0.9\text{\textperthousand}$ (Alvarez et al., 2021). Thus, both Ni and Mg show less isotope fractionation at higher R values – an inverse trend compared to Sr and Ca isotope fractionation -, which is attributed to the stronger hydration of the aqueous Ni and Mg vs Sr and Ca. Light Ni isotopes are also preferentially adsorbed onto calcite surfaces with $\Delta^{60/58}\text{Ni}_{\text{calcite-aq}} \sim -0.5\text{\textperthousand}$ being pH independent (e.g. Alvarez et al., 2020). This value is indicative of the free Ni ion to be trapped at the surface and thus to be the driving mechanism for Ni isotope fractionation. Although, nickel isotope distribution in CaCO_3 has been less explored, the above relationship hints on Ni signatures to provide insight into the CaCO_3 saturation state and/or adsorption phenomena (Alvarez et al., 2021).

Little et al. (2021) reported stable **copper** and zinc isotope distributions in aragonitic cold-water corals with very low fractionation between the precipitating seawater, which addresses in particular the potential of $\delta^{66}\text{Zn}_{\text{coral}}$ as a seawater proxy.

Accordingly, **zinc** isotope composition in CaCO_3 precipitates is suggested as environmental proxy, e.g. for marine Zn cycling (e.g. Zhang et al., 2022b; Yuan et al., 2022). However, Müsing et al. (2022) showed $\delta^{66}\text{Zn}_{\text{CaCO}_3}$ records rather to reflect variations in Zn incorporation mechanism into CaCO_3 than directly tracing the isotopic composition of the precipitating solution. This rating matches with the observed pH dependence of the zinc isotope fractionation during inorganic calcite precipitation by Mavromatis et al. (2019), but open up $\Delta^{66}\text{Zn}_{\text{calcite-aq}}$ values to be used as a potential pH proxy (see also boron isotopes below). Mavromatis et al. (2019) identified the preferential enrichment of the heavier ^{66}Zn isotope in calcite relative to aqueous Zn, which is uncommon for Me^{2+} isotopes (see discussion above) and can be explained by the formation of a tetrahedral innersphere surface complex at the initial step of Zn incorporation vs. the aqueous $\text{Zn}(\text{H}_2\text{O})_6^{2+}$. ^{66}Zn was accordingly found to be preferentially adsorbed onto calcite surfaces compared to ^{64}Zn (Dong and Waslenki, 2016). The use of Zn isotope distribution in CaCO_3 in natural systems seems to be generally challenging due to complex Zn adsorption and isotope fractionation behavior considering e.g. organic matter and inorganic particles (see Junqueira et al., 2024; Li et al., 2024c and references therein).

Co-precipitation experiments by Xie et al. (2021) yield the light **cadmium** isotope to be preferentially enriched in the precipitating calcite, where ionic strength, Cd/Ca ratio, Mg concentrations and aquo-complex formation can cause different Cd isotope fractionation degrees. Analogous, a Cd isotope fractionation trend was found by adsorption of Cd onto calcite surfaces being insensitive to Cd/calcite ratio and pH, but being lowered in the presence of aqueous phosphate (Peng et al., 2023). The above results hint on the potential impact of solution chemistry on Cd isotope fractionation behavior, which has to be individually addressed in future studies. Due to the typically very low concentrations of the above heavy Me^{2+} ions in the CaCO_3 precipitates (being traces) and their affinity to be adsorbed/incorporated onto/into other solid phases, like Mn—Fe (hydr)oxides, preparation and pre-cleaning aspects seem to be highly important for these proxies to be applied properly (e.g. Druce et al., 2022; Yan et al., 2023).

In conclusion, the application of Ni, Cu, Zn and Cd isotope distribution in CaCO_3 as environmental proxies is highly promising, but still needs further investigations to assess and quantify specific and coupled isotope fractionation effects.

Selected **uranium** isotopic compositions including the two long-lived unstable parent isotopes ^{238}U (99.27 %; half-life ~ 4.47 Gyr) and ^{235}U (0.72 %; half-life ~ 704 Myr) and the naturally occurring but relatively rare and shorter-lived daughter isotope ^{234}U (half-life ~ 245.6 kyr) are increasingly measured in carbonate minerals and aqueous solutions (Paces et al., 2002; Shen et al., 2012; Cheng et al., 2013; Hoefs,

2021). The most widespread applications involve absolute age determination of CaCO_3 precipitates and various rocks based on constant radioactive decay of the different U isotopes, as well as their specific value as an environmental proxy of variable fluid-solid interaction (Stirling and Andersen, 2009). Amongst the different U isotope ratios measured, natural $^{238}\text{U}/^{235}\text{U}$ is traditionally assumed to be relatively constant over time, i.e. an average crustal value of ~ 137.88 (Hoefs, 2021). Hiess et al. (2012), however, reported $>5\%$ variation of measured $\delta^{238}\text{U}$ values based on a selection of minerals (e.g. zircon) and rocks. In contrast, measured as well as calculated (initial) $^{234}\text{U}/^{238}\text{U}$ ratios typically reported as $\delta^{234}\text{U}$ values ($\delta^{234}\text{U}_{\text{initial}} = \delta^{234}\text{U}_{\text{measured}} \times e^{\lambda^{234}\text{U}T}$; $^{234}\text{U}/^{238}\text{U}$ activity ratios in secular equilibrium) are known to vary extensively in space and time (Paces et al., 2002; Oster et al., 2023).

Considering typical environmental settings and scenarios of application, variable $^{234}\text{U}/^{238}\text{U}$ ratios in freshwaters and CaCO_3 are used as a tracer of hydrological processes in the course of water infiltration, groundwater flow and evolution in differentiated aquifers, as well as for aqueous solute provenance and rock weathering studies (Riotte and Chabaux, 1999; Imam, 2023). In this context, specific hydrogeochemical processes are of particular relevance, such as the alpha-recoil effect. The latter is based on radioactive decay of ^{238}U towards ^{234}U and related damage of the crystal lattice resulting in preferential mobilization (leaching) and enrichment of the ^{234}U isotope in natural aqueous solutions and hence in $^{234}\text{U}/^{238}\text{U}$ activity ratios ranging from 1 to 10 (Paces et al., 2002). Further, this ratio as well as variable U concentrations will also depend on pH and redox state, flow routes and mineral dissolution versus precipitation, e.g. during episodic water flow at the prospective nuclear waste repository site Yucca Mountain in Nevada (Cizdziel et al., 2005).

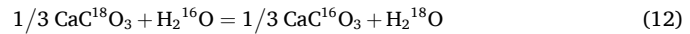
Likewise, Zhou et al. (2005) investigated $^{234}\text{U}/^{238}\text{U}$ variability in speleothems and cave drip waters and found an inverse correlation with U concentration and the calculated initial ratios varied with CaCO_3 precipitation rate substantiating a proxy for meteoric precipitation, flow rate and discharge over millennial timescales. Uranium isotope fractionation is also frequently related to organic or inorganic reduction of hexavalent uranium (U[VI]) to tetravalent U[IV]. This redox-reactive U fractionation might be controlled by microbial activity or by the prevailing aqueous speciation and redox state, e.g. during mobilization of the water-soluble uranyl cation (UO_2^{2+}) at oxidizing conditions (Paces et al., 2002; Hoefs, 2021). The latter uranium ion and its variable isotopic composition has stimulated some interest based on U incorporation into calcite and aragonite focusing on (paleo)hydrological processes, recrystallization (e.g. aragonite to calcite) and the accuracy of radiometric U-Th dating of the CaCO_3 (Reeder et al., 2000; Lachniet et al., 2012; Scholz et al., 2014; Bajo et al., 2016; see section 7.1.2).

Uranium isotopic compositions have been evaluated as a redox-sensitive tracer in the oceans, e.g. for understanding the evolution of oceanic anoxia in relation to the rise of life (Clarkson et al., 2023). The $\delta^{238}\text{U}$ signatures mainly rely on the water-soluble U(VI) form under oxidizing conditions or are related to either Fe/Mn (hydr)oxide formation (typically light $\delta^{238}\text{U}$) or organic-rich sediments (e.g. black shales; typically enriched $\delta^{238}\text{U}$) deposited under reducing conditions (Montoya-Pino et al., 2010; Rutledge et al., 2024). In this context potential diagenetic effects in the (marine) carbonates and other minerals influencing the $\delta^{238}\text{U}$ ratios and their paleoenvironmental interpretation are also critical (e.g. in coral CaCO_3 and shark tooth fluoroapatite; Yuan et al., 2023; Li et al., 2024b). Li et al. (2024b) investigated $\delta^{238}\text{U}$ and $\delta^{234}\text{U}$ compositions in shark teeth from diverse locations as a proxy for variable redox conditions in the ancient oceans and found a broad range of U concentrations and isotopic ratios being indicative of widespread postmortem (diagenetic) incorporation and fractionation. Uranium isotope signatures have further been used for distinction of major mantle and crustal sources and sinks of U (e.g. MORB, OIB), subduction, atmospheric oxygenation and weathering in the course of global uranium cycling (Andersen et al., 2015). The variable U isotope ratios are also of greater importance in their relation to other metal (e.g. Th, Pb) isotopic

compositions. More specifically, radiometric age determination of CaCO_3 minerals or zircons based on U-Th and U-Pb isotope systematics constitutes a widespread analytical approach for a diverse range of geological and paleoenvironmental investigations (Cheng et al., 2013; Hellstrom and Pickering, 2015; Spötl and Boch, 2019).

7.2.2. Anions

The main interest on isotope distribution of anions in CaCO_3 is obviously based on the **carbonate** ion in respect to the distribution of stable carbon and **oxygen** isotopes. The most prominent application of oxygen isotopes in CaCO_3 is based on the temperature dependence of the oxygen isotope fractionation between calcite and the precipitating solution according to the overall exchange reaction.



(e.g. Urey, 1947; McCrea, 1950; O'Neil et al., 1969; Kim and O'Neil, 1997). Accordingly, the oxygen isotope composition of CaCO_3 is classically used as (paleo)temperature proxy if the oxygen isotopic composition of the precipitating solution is known or can be reasonable estimated (e.g. Epstein et al., 1953; Hendy, 1971; Veizer et al., 1999; Adkins et al., 2003; Ison and Rauzi, 2024).

The studies on oxygen isotopes of CaCO_3 cover wide research areas comprising marine skeletons (e.g. brachiopod-based oxygen-isotope thermometer; Brand et al., 2019), fish otolith (e.g. fish movement patterns; Currey et al., 2014), eggs shells (e.g. dinosaur-bird transition; Tagliavento et al., 2023), methane derived carbonates (e.g. formation of seep carbonate; Savard et al., 2021), lacustrine deposits (e.g. paleoclimate reconstructions; Li et al., 2020), speleothems from karst caves (Boch et al., 2009), calcite veins (e.g. formation conditions and diagenetic overprint; Nooitgedacht et al., 2021), carbonate mortar (e.g. CO_2 origin; Kosednar-Legenstein et al., 2008), scaling (e.g. drainage sinter; Eichinger et al., 2020), travertine (e.g. alkaline spring water; Christensen et al., 2021) etc. In the following the focus is given on oxygen isotope distribution of calcite, where for e.g. aragonite almost analogous relationships have been found.

The oxygen isotope fractionation factor between calcite and H_2O is given by the expression

$$\alpha^{18}\text{O}_{\text{calcite-aq}} = \frac{^{18}\text{R}_{\text{calcite}}}{^{18}\text{R}_{\text{aq}}} = \frac{\frac{n_{\text{calcite}}(^{18}\text{O})}{n_{\text{calcite}}(^{16}\text{O})}}{\frac{n_{\text{aq}}(^{18}\text{O})}{n_{\text{aq}}(^{16}\text{O})}} = \frac{\delta^{18}\text{O}_{\text{calcite}} + 1000}{\delta^{18}\text{O}_{\text{aq}} + 1000} \quad (13)$$

and defined by n moles of ^{18}O and ^{16}O of the calcite precipitate divided by n moles of ^{18}O and ^{16}O of the precipitating aqueous solution (H_2O) (see alternative notation in eq. (8)). The $\alpha^{18}\text{O}_{\text{calcite-aq}}$ value at isotope equilibrium is approached in speleothem calcite grown at very low precipitation rates ($\alpha^{18}\text{O}_{\text{calcite-aq}} = 1.0302$; $\Delta^{18}\text{O}_{\text{calcite-aq}} \sim 10^3$ in $\alpha^{18}\text{O}_{\text{calcite-aq}} = 29.8\%$ at 25°C ; Coplen, 2007; Daëron et al., 2019; see eq. (9) for analogous definition), whereas most Earth-surface calcites precipitate out of isotopic equilibrium.

Kinetically driven oxygen isotope fractionation effects can be related to non-isotopically equilibrated DIC species, high precipitation rates, DIC species and CO_2 gas diffusion, biogenically mediated reactions etc. (e.g. Zeebe and Wolf-Gladrow, 2005; Dietzel et al., 2009; Geisler et al., 2012; Tripathi et al., 2015; Watkins et al., 2013; Watkins and Hunt, 2015; Zhang, 2024). For instance, from experimental studies precipitation rates are known to result in lower apparent $\Delta^{18}\text{O}_{\text{calcite-aq}}$ values compared to equilibrium conditions, which can be explained by kinetically driven isotope fractionation phenomena at the growing calcite surface (e.g. Dietzel et al., 2009; Gabitov et al., 2012). Moreover, isotopically non-equilibrated DIC can be trapped in the precipitated CaCO_3 . The reaction times to reach oxygen isotopic equilibration of DIC species with H_2O can be calculated from the expression developed by Weise and Kluge (2020) as a function of pH and T ($40\text{--}90^\circ\text{C}$), where in alkaline settings an increase of pH results in significantly longer

equilibration time spans. The latter effect is based on oxygen isotope exchange between DIC species and water to be kinetically controlled by the CO_2 hydration reaction ($\text{CO}_{2(\text{aq})} + \text{H}_2\text{O} = \text{H}_2\text{CO}_3$), where at high pH (i) very low $\text{CO}_{2(\text{aq})}$ concentrations, (ii) the isotope fractionation between OH^- and H_2O , and (iii) the $\text{CO}_{2(\text{aq})}$ hydroxylation to yield HCO_3^- have to be considered (e.g. Ustdowski and Hoefs, 1993; Dietzel et al., 1992; Beck et al., 2005; Lécuyer et al., 2009; Zeebe, 2009; Yumol et al., 2020; Zeebe, 2014; Zeebe, 2020; Bajnai and Herwartz, 2021).

Isotope fractionation is shown to be also affected by the formation pathways, where HMC formed via amorphous precursors was experimentally found to result in higher apparent $\Delta^{18}\text{O}_{\text{calcite-aq}}$ values compared to equilibrium conditions (Dietzel et al., 2020). Lucarelli et al. (2023) showed by O isotopically spiked transformation experiments a significant oxygen isotope (and $\Delta_{47}-\Delta_{48}$; see clumped isotopes below) variability of HMC from ACMC precursors depending on isotopically non-equilibrated DIC pools, reaction time and T (from 10 to 60 °C): analyzed $\delta^{18}\text{O}_{\text{calcite}}$ values do not represent HMC formation temperatures. Experimental results show, $\delta^{18}\text{O}_{\text{calcite}}$ values of carbonates formed via ACC transformation in air or at low water/solid ratios (e.g., valid for biominerals or cave carbonates) cannot be used as environmental proxy without assessing reaction kinetics and parameters like relative humidity, CO_2 , and H_2O sources (Asta et al., 2024). Scheller et al. (2023) reported $\delta^{18}\text{O}$ of calcite formed from transformation of monohydrocalcite to be partially isotopically re-equilibrated via oxygen exchange between the solid CO_3 and H_2O at a given T. Partial isotope re-equilibration during transformation steps was shown to depend on H_2O availability (open/closed conditions), pH and time for re-adjustment; parameters to be considered e.g. for vital effects of biogenic CaCO_3 formation (see Brazier et al., 2024b). An oxygen (and stable carbon) isotope exchange between calcite and an exposed solution can still occur if chemical equilibrium with calcite is reached, e.g. by rapid exchange of surface species and by ongoing dissolution-precipitation of pre-existing reactive surface sites (Harrison et al., 2022).

Accordingly, reaction kinetics and mechanisms in respect to O (and C) isotopes in the $\text{CaCO}_3-\text{CO}_2-\text{H}_2\text{O}$ system are highly diverse and complex, in particular by frequently occurring coupled reactions. Thus, advanced approaches, new techniques and higher resolutions of isotope analyses can act as important steps to increase our knowledge, like clumped isotope (see below), triple oxygen isotope (e.g. Sha et al., 2020) and real-time *in-situ* isotope analyses (e.g. Geisler et al., 2012; Wang et al., 2020). Examples for successful and promising applications of environmental proxies and analytic tools in the scope of O isotopes in CaCO_3 are (i) classical multi-proxy elemental and isotope approaches (e.g. brachiopod shell as archive of seawater T: Letulle et al., 2023), (ii) challenging fluid inclusion extraction and analyses (e.g. paleotemperature reconstructions from speleothems: Demény et al., 2021), (iii) combination of clumped (Δ_{47}) and oxygen isotope ratios (e.g. paleothermometer using planktonic foraminifera: Peral et al., 2022), (iv) dual clumped isotope ($\Delta_{47}-\Delta_{48}$) thermometry (e.g. paleotemperatures from coral and speleothem carbonate unraveled isotopic disequilibrium: Bajnai et al., 2020 and Davis et al., 2023), (v) dual clumped isotopes and fluid inclusions (e.g. formation temperature and diagenetic overprint: Staudigel et al., 2023), (vi) isotope equilibrium for DIC species by enzymatic power (e.g. carbonic anhydrase to stimulate isotope exchange kinetics via CO_2 hydration: Uchikawa et al., 2021; Olsen et al., 2022), and (vii) triple oxygen isotope ratios ($^{18/17/16}\text{O}$; e.g. tracing evaporation and hydroclimate dynamics: Passey and Ji, 2019; Sha et al., 2020; Wostbrock and Sharp, 2021).

The distribution of stable carbon isotopes in CaCO_3 precipitates is traditionally used to decipher the origin of the **carbonate** ion and to discover reaction kinetics, mechanisms, pathways etc. in the $\text{CaCO}_3-\text{CO}_2-\text{H}_2\text{O}$ system. The carbon isotope fractionation kinetics and at equilibrium between the DIC species, CaCO_3 minerals and gaseous CO_2 are mostly well known, where it is herein referred to text books (e.g. Clark and Fritz, 1997; Appelo and Postma, 2005; Zeebe and Wolf-Gladrow, 2005; White, 2023).

Exemplarily, $^{13/12}\text{C}$ distribution of CaCO_3 precipitates was applied to (i) seep carbonates to decipher carbon sources from seawater DIC, methane carbon and residual CO_2 from methanogenesis (Feng et al., 2023), (ii) speleothems as (paleo)climate proxy, where $\delta^{13}\text{C}_{\text{CaCO}_3}$ values are controlled by T dependent vegetation and soil processes, growth rate etc. (Fohlmeister et al., 2020), (iii) carbonate precipitating springs and alkaline man-made solutions (Dandurand et al., 1982; Galan et al., 2019), (iv) biotic CaCO_3 to trace the vital effects induced e.g. by microbial activity (Zhuang et al., 2018), (v) earthworm calcite to reconstruct (paleo) precipitation conditions (Prud'homme et al., 2018), (vi) coral skeletons to quantify the addition of anthropogenically derived atmospheric CO_2 (^{13}C Suess effect) to the DIC of seawater (Al-Rousan and Felis, 2013), and (vii) diagenetic alteration effects e.g. of benthic foraminifera (Schneider et al., 2017).

The incorporation of **sulfate** into CaCO_3 is used to trace the **sulfur** isotope composition of aqueous sulfate of the precipitating solution. The related $\delta^{34}\text{S}_{\text{CAS}}$ values were frequently applied to reconstruct past seawater by analysing calcifying marine skeletons, knowing different calcifying species to record both positive and negative S isotope fractionation between CAS and seawater sulfate within a range of close to 4 ‰ (e.g. Burdett et al., 1989; Kampschulte et al., 2001; Paris et al., 2014; Present et al., 2015; Rennie and Turchyn, 2014; Present et al., 2020). For instance, Richardson et al. (2019) found the vast majority of sulfate in investigated brachiopod shells to be inorganic and gained from seawater, where bulk $\delta^{34}\text{S}_{\text{CAS}}$ of modern brachiopods were about 1 ‰ more positive compared to seawater sulfate. Foraminifera from culturing experiments exhibit an almost constant positive sulfur isotope fractionation between CAS and seawater sulfate ($\Delta^{34}\text{S}_{\text{CAS-aq}} \sim 1.5\text{ ‰}$; Thaler et al., 2023), where organic matter in CaCO_3 had been oxidatively removed. Li et al. (2022b) reported $\delta^{34}\text{S}_{\text{CAS}}$ variation to be caused by varying proportions of calcifying organisms with species-dependent $\Delta^{34}\text{S}_{\text{CAS-aq}}$ values.

Sulfur isotope fractionation during sulfate incorporation into calcite was experimentally verified to discriminate ^{32}S depending on the CAS content (Barkan et al., 2020): CAS was found to be isotopically heavier from 1.3 to 3.1 ‰ than the aqueous sulfate. In accordance, first-principles quantum-mechanical calculations by Balan et al. (2014) of sulfate incorporation and $^{34}\text{S}/^{32}\text{S}$ isotopic fractionation in different CaCO_3 indicates the S isotopic fractionation between CAS in calcite and aqueous sulfate to be positive, but <4 ‰. $\delta^{34}\text{S}_{\text{CAS}}$ to be affected by diagenesis was verified for limestone deposits in reefs and slope facies largely incorporating sulfate from anoxic marine-phreatic interstitial solutions, which are isotopically modified from seawater by microbial sulfate reduction (Present et al., 2019). Fichtner et al. (2021) exposed aragonitic bivalves and corals to anaerobic microbial activity, where $\delta^{34}\text{S}_{\text{CAS}}$ values remained largely unaffected, which hint on less potential impact of microbial alteration during early diagenesis. Thus, challenges of the above applications of $\delta^{34}\text{S}_{\text{CAS}}$ are based on (i) sulfur to be occurring in biogenic calcite additionally in fluid inclusions, as adsorbed species, or within proteins, (ii) apparent fractionation of sulfur isotopes between CAS and SO_4 of the precipitating solution, and (iii) secondary alteration of S isotopes in CAS.

The **oxygen** isotope exchange between the aqueous **sulfate** ion and H_2O is known to be very slow (e.g. Zeebe, 2010), which is promising for $\delta^{18}\text{O}_{\text{CAS}}$ values to be used as $\delta^{18}\text{O}_{\text{SO}_4}$ record of the precipitating solution and to be a provenance proxy for the origin of CAS. The oxygen isotope fractionation of CAS vs. aqueous sulfate of the precipitating solutions is less explored, where $\delta^{18}\text{O}_{\text{CAS}}$ was found to be altered e.g. by reworking associated with sulfide oxidation (Rennie and Turchyn, 2014; Richardson et al., 2021). Although, the potential effects on the S (and O) isotope composition of CAS are numerous, both can be successfully used to reconstruct the precipitating solution conditions and to understand diagenetic processes if the individual settings are well-known and/or a multi-proxy approach is successfully developed (e.g. Borrelli et al., 2020; Smith et al., 2022).

Stable chromium isotope distribution in CaCO_3 is widely used as a

proxy for changes in the Earth's surface oxygen levels (e.g. Gilleaudeau et al., 2016; Bruggmann et al., 2020; Klaebe et al., 2021; Wang et al., 2021b). Cr occurs at two primary oxidation states, soluble **chromate** (Cr (VI)) and poorly soluble Cr(III) (see section 7.1). Once mobilized from Cr (III) sources on the continental crust by oxidative weathering it enters the ocean as aqueous chromate, CrO_4^{2-} and HCrO_4^- , depending on pH. In seawater, chromate can be reduced to Cr(III), thus being trapped in marine sediments, where a strong isotope fractionation between Cr(VI) and Cr(III) (coordination change) yields in $\delta^{53/52}\text{Cr}$ values of e.g. sediments to act as redox proxy (e.g. Frei et al., 2009; Cole et al., 2016b). In this context, CaCO_3 precipitates incorporate aqueous Cr(VI), thus may trace the isotope evolution of past seawater (e.g. Rodler et al., 2015).

Co-precipitation experiments by Füger et al. (2019b) revealed Cr isotope fractionation during Cr(IV) incorporation into calcite to be pH dependent, mirroring - besides redox conditions - the distribution of Cr aquo-complexes of the precipitating solution. Analyses of natural carbonates indicate Cr(III) to be the predominant species. Thus Cr(VI) reduction or preferentially direct Cr(III) uptake likely occurred during or after deposition (Fang et al., 2021). Recent experiments by Fang et al. (2022) show Cr(III) to be adsorbed onto the calcite surface or precipitated as amorphous Cr hydroxide. Only a very small fraction of Cr(III) is trapped into the calcite, likely in interstitial voids or substituting Ca^{2+} as Cr(OH)^{2+} for charge balance. It is concluded, that Cr(III) of CaCO_3 can be easily altered during (early) diagenesis due to Cr exchange with the later Cr sinks being incompatible with the crystal lattice of CaCO_3 minerals.

Thus, post-depositional overprinting of Cr and isotope distribution of CaCO_3 might be a challenging issue for paleoenvironment reconstruction (e.g. foraminifera: Remmelzwaal et al., 2019). In summary, the use of chromium isotope distribution in CaCO_3 as redox proxy has to be individually evaluated and assessed as the behavior of Cr species seems to be highly complex caused by Cr to be bound to different solid phases (e.g. clay minerals and ferromanganese oxides in natural sediments/soils) and/or to be remobilized/reprecipitated within a wide range of processes in the continental realms, in the ocean, during early and late diagenesis etc., where reactions are frequently accompanied with Cr isotopes to be fractionated (see Wang et al., 2021b and references therein; Yu et al., 2023; Fang et al., 2023).

Isotope signatures of **boron** incorporated into CaCO_3 precipitates are used to estimate its provenance, seawater history, climate changes etc., but in particular to unravel the pH of the precipitating solution (e.g. Hemming and Hanson, 1992; Legett et al., 2020; Chen et al., 2021b; Wei et al., 2021). The latter approach is based on a preferential incorporation of the isotopically lighter tetrahedral B(OH)_4^- species (vs. the planar B(OH)_3°) into CaCO_3 , where pH controls the distribution of both aqueous species (e.g. Balan et al., 2018; see section 7.1.2.). Recently, Yin et al. (2023) found from modeling, the theoretical B isotope fractionation between B(OH)_4^- and B(OH)_3° to be (i) similar to $\Delta^{11}\text{B}_{\text{B(OH)}_4-\text{B(OH)}_3}$ values obtained from isotope analyses of separated aqueous boron species (Nir et al., 2015), (ii) almost identical for seawater and pure water, and (iii) T dependent. Inorganic co-precipitating experiments indicated $\delta^{11}\text{B}$ of calcite to depend on growth rate (Mavromatis et al., 2015; Farmer et al., 2019; Uchikawa et al., 2023). Gu et al. (2023) reported that in brines the presence of polyborate ions can have an impact on the fractionation of B isotopes during calcite precipitation. Non-classical CaCO_3 formation via amorphous precursors indicates the B isotope fractionation between CaCO_3 and aqueous B to be controlled by dynamic exchange of aqueous species and nanoporous solid phases (Mavromatis et al., 2021), where the $\delta^{11}\text{B}$ value of the final Mg-calcite and aragonite approach B isotope equilibrium conditions estimated by Balan et al. (2018).

Thus, studies on the B content and its isotopic composition in CaCO_3 and the impact of precipitation rate, coordination of incorporated boron, formation pathway etc. (see also section 7.1.2.) reveal that the application of B isotope signatures as environmental proxy within the focus on pH estimation has to be individually evaluated, where contamination

by B bearing non-carbonate phases during sample preparation as well as (early) diagenetic overprints have to be additionally considered (e.g. Rollion-Bard et al., 2011; Hönsch et al., 2018; Farmer et al., 2019; Mavromatis et al., 2021; Hong et al., 2022).

Molybdenum isotope fractionation during coprecipitation of molybdate with CaCO_3 is proposed to be used for recording the redox conditions during its formation, thus e.g. tracking the Mo isotope composition and redox state of the ocean throughout time (e.g. Voegelin et al., 2010; Thoby et al., 2019; Hodgskiss et al., 2021; Li et al., 2022d; O'Sullivan et al., 2022; Jia et al., 2023). Chen et al. (2021a) found from inorganic co-precipitation experiments $\Delta^{98}\text{Mo}_{\text{calcite-aq}} = -0.15 \pm 0.06 \text{ ‰}$, where light Mo isotopes of the tetrahedral MoO_4^{2-} ion are preferentially incorporated into calcite. Higher Mo isotope fractionation observed for natural microbial calcite seems to be significantly affected by Mo bound to Fe and Mn (hydr)oxides. Mo isotope distribution of CaCO_3 to be properly used as elemental proxy requires consideration of Mo within organic matter, detrital particles, and Fe and Mn (hydr)oxides, and the potential alteration of Mo content and its isotopic signatures of pristine CaCO_3 deposits via (early) diagenesis (e.g. Romaniello et al., 2016; Chen et al., 2021a; Magette et al., 2023).

Recently, Johnston et al. (2024) assessed **cosmogenic** ^{36}Cl content of speleothem CaCO_3 to be challenging to be used as solar irradiance proxies because Cl occurs in highly diverse forms comprising crystal defect sites, fluid inclusions, detrital particles etc. Thus, future systematic studies on the ^{36}Cl behavior in CaCO_3 precipitates are required to justify its feasibility as proxy.

A major advance in stable isotope geochemistry concerns the measurement of rare multiply-substituted isotopologues (**clumped isotopes**) in carbonate minerals and other functional (molecular) groups (Eiler et al., 2014; Anderson et al., 2021). The clumped isotopic composition of carbonates relies on the analysis of relatively rare and heavy stable ^{13}C and ^{18}O isotopes bound together in the carbonate functional group ($^{13}\text{C}^{18}\text{O}^{16}\text{O}_2^-$). This quantity expressed as Δ_{47} value versus a stochastic isotopologue distribution depends on molecular bonding energy (thermodynamic) differences of the isotopes involved and therefore mainly on temperature during mineral (e.g. CaCO_3) crystallization. More specifically, ^{13}C and ^{18}O isotopes are preferentially clumped in the carbonate crystal lattice at lower temperature (Schauble et al., 2006; Eiler, 2013). The prevailing T is recorded in a single-phase isotope equilibrium in contrast to widely-used two-phase equilibria (e.g. oxygen isotope thermometers; Kim and O'Neil, 1997; Daëron et al., 2019). Consequently, mineral formation T can be reconstructed from measured clumped isotopic compositions without knowledge of the parental aqueous solution stable isotopic composition ($\delta^{18}\text{O}_{\text{aq}}$).

Different CO_2 isotopologues are measured simultaneously and the systematic deviation of the rare clumped $^{13}\text{C}^{18}\text{O}^{16}\text{O}$ molecule (m/z 47) in the carbonate versus the stochastic distribution in a $\sim 1000^\circ\text{C}$ CO_2 reference gas yields a Δ_{47} value decreasing with increasing T. From this mass spectrometric procedure the carbonate $\delta^{13}\text{C}$ and $\delta^{18}\text{O}$ values are also gained and in connection with Δ_{47} -based temperature estimates the mineral forming (parental) fluid $\delta^{18}\text{O}$ value can be calculated based on established T dependent O isotope fractionation factors. Isotopologue analyses therefore constitute a valuable tool regarding the source and evolution of (paleo)fluids next to their application as a (paleo)thermometer (Swanson et al., 2012; Boch et al., 2019; Clark et al., 2024). For example, clumped isotopes are increasingly used in paleoenvironmental (paleoclimate) studies (Eiler, 2011) based on various carbonate precipitates such as calcareous tufa and travertine (Kele et al., 2015), speleothems (Affek et al., 2008), soil nodules (Ghosh et al., 2006) and carbonate veins in fractures (Quandt et al., 2019). Other reconstructions include fault tectonics (Siman-Tov et al., 2016) and the uplift of mountain ranges (Xiong et al., 2019), thermal and fluid flow history of sedimentary basins and deep reservoirs (Mangenot et al., 2018; Lu et al., 2023a), diagenesis and metamorphic rocks (Shenton et al., 2015; Ryb et al., 2017), the variable energy consumption and body T of animals and humans (Eagle et al., 2010) or the verification of *in-situ* and rapid

CaCO_3 precipitation related to geological CO_2 sequestration (e.g. Carbfix on Iceland; Holdsworth et al., 2024).

Amongst the inherent preconditions of reliable clumped isotope measurements and signatures are the absence of altering effects such as later-stage isotope exchange and reordering of (clumped) isotopes, e.g. during diagenetic or metamorphic recrystallization processes and subsequent cooling below a specific closing (blocking) temperature (Shenton et al., 2015). The latter is distinct for different carbonate minerals, for example calcite (Henkes et al., 2014), siderite (Fernandez et al., 2014) and magnesite (Quesnel et al., 2016) or carbonate group containing minerals (e.g. apatite; Eagle et al., 2010). Further considering the accuracy and precision of the clumped isotope based estimates, the absolute crystallization T, the calibration of Δ_{47} vs. T applied, the laboratory protocols and number of replicate (sub)samples measurements are most relevant (Daëron et al., 2016; Petersen et al., 2019). In general, at elevated T ($>200^\circ\text{C}$) the precision of the temperature estimates decreases rapidly relying on the decreasing change in Δ_{47} versus T (Kluge et al., 2015).

Based on experimental, modeling and empirical studies, the numerical calibration functions of clumped isotope thermometry are a subject of critical evaluation (Winkelstern et al., 2016; Koltai et al., 2024). Universal and wide T range calibration functions being (in) dependent of the carbonate mineralogy and laboratory are targeted (Bonifacie et al., 2017; Kelson et al., 2017; Anderson et al., 2021). This motivates an international inter-laboratory comparison of the measurement protocols applied, i.e. critical analytical steps such as phosphoric acid digestion, correction terms and reference materials used (Bernasconi et al., 2018; Petersen et al., 2019). A reliable theoretical as well as practical implementation further involves the investigation of potentially relevant effects influencing equilibrium versus kinetic isotope fractionation during carbonate mineral precipitation (Tang et al., 2014; Levitt et al., 2018). In particular, potential kinetic fractionation effects have to be handled with caution for specific environmental settings and applications (Burgener et al., 2018; Guo, 2020), and empirical observations suggest that most calcites formed on the Earth's surface crystallize out of oxygen and clumped isotopic equilibrium to some degree (Daëron et al., 2019). Considering a representative T and fluid source determination specific effects such as pH and DIC speciation, highly saline hydrochemical compositions, polymorphism or mineral precipitation rates should also be evaluated in detail (Tripathi et al., 2015; Kluge et al., 2018). In this context, laboratory experiments have revealed valuable insights (Affek and Zaarur, 2014; Kluge and John, 2015; Lucarelli et al., 2023).

According to the current methodological developments, the measurement and applications of clumped isotopes are not restricted to the various carbonate minerals. Rather, multiply-substituted isotopologues also constitute common liquid and gaseous phases such as the numerous hydrocarbons (e.g. methane), nitrous oxide, molecular hydrogen and oxygen (Stolper et al., 2014; Eiler et al., 2014; Lalk et al., 2022). Fiebig et al. (2021) measured Δ_{48} signatures ($^{12}\text{C}^{18}\text{O}^{18}\text{O}$) next to the commonly used Δ_{47} values ($^{13}\text{C}^{18}\text{O}^{16}\text{O}$) in diverse CaCO_3 precipitates (e.g. corals, synthetic and vein calcites, geothermal pipeline CaCO_3) and for a broad temperature range (8 to 1100°C) and gained valuable new insights with regard to specific kinetic vs. temperature effects during clumping of C and O isotopes in the CaCO_3 minerals. Addressing clumped isotope calibration and specific (kinetic) effects, Lucarelli et al. (2023) analyzed dual clumped (Δ_{47} and Δ_{48}) isotope compositions of metastable carbonate phases (amorphous precursors; e.g. ACMC) (trans)formed in the laboratory and inferred that amorphous precursors could promote strongly localized environments and (clumped) isotope compositions in crystalline CaCO_3 , i.e. isotopic signatures may not be representative for the original formation T (e.g. during biomineralization). Recently, Bernecker et al. (2024) developed a methodology for triple (Δ_{47} , Δ_{48} , Δ_{49}) clumped isotope analysis of carbonates. Technical development introduces also an optical measurement of relevant CO_2 isotopologues (e.g. $^{13}\text{C}^{16}\text{O}^{18}\text{O}$) by laser-based infrared spectroscopy (e.g. Prokhorov

et al., 2019). In a foreseeable future this approach might outcompete IRMS measurements due to reduced instrumentation costs and space requirements, a simplified sample preparation, increased sample throughputs and advantages with regard to some critical isobaric interference.

Recently, the **triple oxygen isotope** composition of carbonates ($^{18}/^{17}/^{16}\text{O}$) is used to trace evaporation and hydroclimate dynamics, which is related to the evaporation-sensitive deviation from the $\delta^{17}\text{O}$ vs. $\delta^{18}\text{O}$ reference line (e.g. Sha et al., 2020; Wostrock and Sharp, 2021; Kelson et al., 2023).

In conclusions, isotope (and element) proxies for tracing, understanding and reconstructing CaCO_3 formation and alteration are extensive and increase in number and in their individual applications (Fig. 5). Traditionally used isotopes have been queried, adapted accordingly and renewed in their usability (case: T, R and formation pathway dependence of O isotopes). New promising tools were created to assess and quantify the conditions of CaCO_3 formation, e.g. dual clumped and triple oxygen isotopes for the reconstruction of T, evaporation and fluid origin and metal isotopes of Li, K, and Zn for tracing seawater composition, silicate weathering and (paleo)climate change.

8. Settings and archives

8.1. Natural environments

8.1.1. Overview

In nature, widespread CaCO_3 are represented by auto- and allochthonous chemical sedimentary deposition in the continental and marine realm as part of the global carbon cycle and can serve as valuable environmental archives (see Fig. 6). Different minerals and polymorphs of (an)hydrous CaCO_3 occur in diverse sedimentary, tectonic and climate settings (Morse and Mackenzie, 1990). In the oceans, CaCO_3 occurs as regionally extensive mud-grade carbonate in ocean basins and protected areas (low transport energy) or calcareous sands (e.g. arenites) in lagoons, platform carbonate and coral reefs of deep and shallow waters (Diaz et al., 2017; Cuny-Guiriec et al., 2019). The CaCO_3 secretion yields in the formation of skeletal carbonate in marine organisms such as foraminifera, coccolithophorida, red algae and mollusks in the course of biomineralization (Morse et al., 2007). Bivalves and brachiopods are investigated with regard to (in)organic CaCO_3 nucleation and polymorphism (Dettman et al., 1999; Simonet et al., 2019) and coral formation is tied to global sea-level variation and reconstruction in the coastal areas (Sevilgen et al., 2019). Stromatolites and microbial mats typically related to cyanobacteria and algae also form organically-mediated and often laminated carbonate deposits in shallow marine and freshwater sedimentary environments (Rogerson et al., 2008; Saunders et al., 2014). In these natural settings, skeletal hardparts, particulate components and sedimentary structures typically experience burial, hydrothermal and microbial diagenetic processes and depositional alteration including microbial decomposition, carbonate cementation of pore spaces or dolomitization (Baldermann et al., 2015; Swart, 2015; Pederson et al., 2019).

CaCO_3 is further of widespread occurrence in lake sediments of different regions and water chemistry and often display rhythmic (e.g. annual varves) micritic or more complex sedimentary successions (Della Porta, 2015). Other freshwater CaCO_3 such as compact and mostly laminated travertines or more porous and heterogeneous calcareous tufa deposits either form in thermal or ambient temperature fluvial streams or other specific sedimentary settings related to deep water circulation, (neo)tectonic or volcanic activity (Capezzuoli et al., 2014; Shiraishi et al., 2019). Considering natural settings, CaCO_3 dissolution (mobilization) and precipitation also characterize the widely distributed karst areas and caves involving hypo- and epigenetic karstification and speleothem formation (Fairchild and Baker, 2012). The latter CaCO_3 deposits provide another valuable chemical-sedimentary archive for multi-proxy paleoenvironmental reconstruction favored by precise

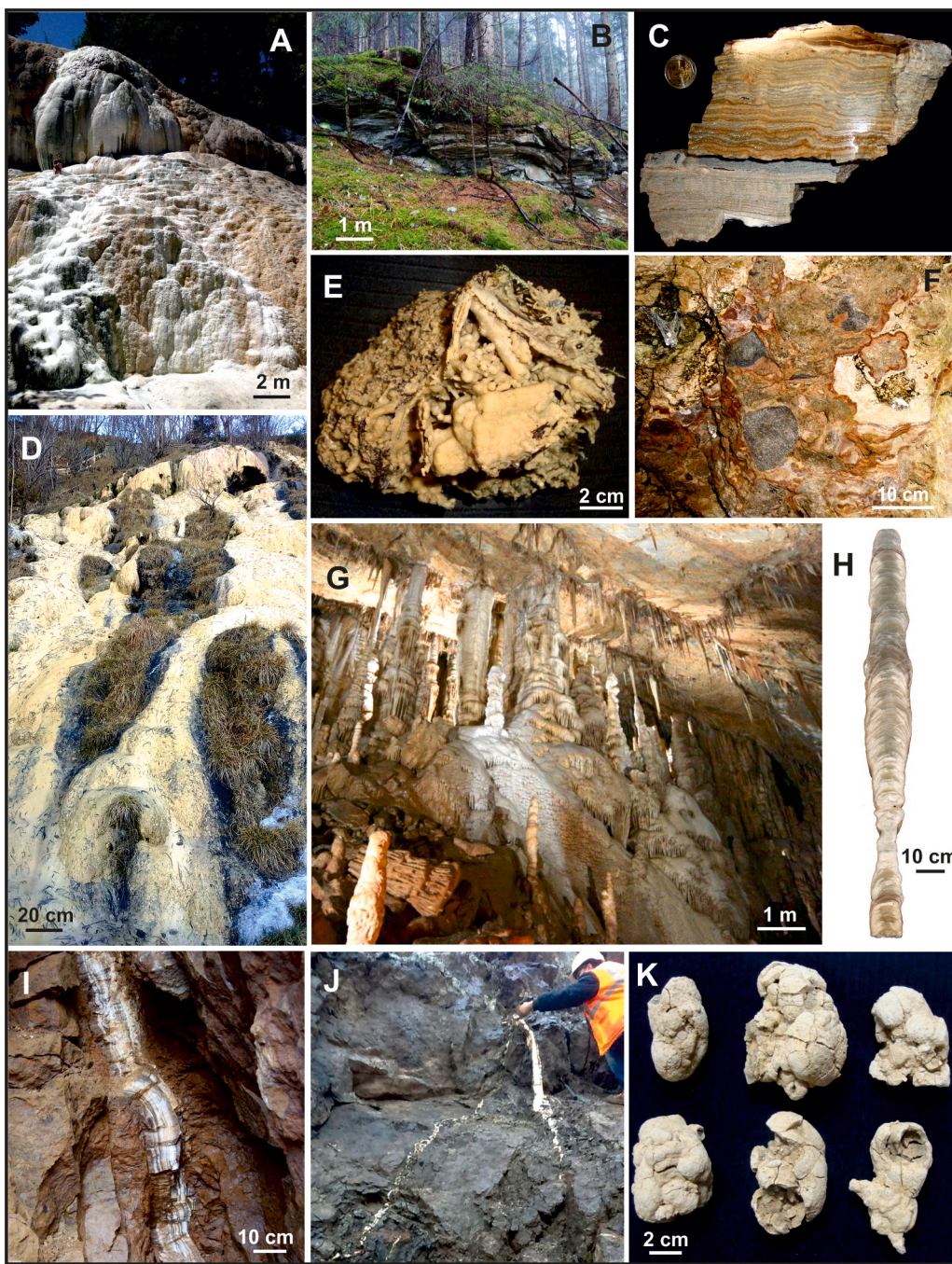


Fig. 6. CaCO_3 precipitation in a diverse range of natural settings. The selection displays A) slope of active travertine formation from thermal waters along cascades and pools in Bagni San Filippo (Italy); B) side view of a fossil travertine deposit near Ainetal (Austria) showing banded structures within successively precipitated CaCO_3 representing former cascades along flowing water; C) sample from the fossil travertine in B) consisting of compact and seasonally alternating aragonite (whitish) and calcite (brownish) layers (upper section is polished); D) active calcareous tufa formation at ambient temperature conditions encrusting vegetation and debris on a steep slope near Lingenau (Austria); E) sample from an active calcareous tufa deposit in Köttmannsdorf (Austria) showing typical features such as brownish stained calcite, a highly porous fabric, encrusted grass, moss, wooden fragments and pine needles; F) phreatic CaCO_3 cements encrusting rounded stones and fine grained matrix material and consequently compacting formerly loose multi-component glaciolacustrine sediments; G) rich speleothem decoration in Katerloch Cave (Austria) including different forms of stalagmites, stalactites along ruptures, stalagnates (columns), flowstones on slopes and drapery (curtains) on the ceiling; H) laminated calcitic stalagmite of variable fabric and diameter (e.g. discharge) from Katerloch; I) well-layered, vadose flow aragonite and calcite fracture filling and J) branched veins of variable thickness and age from Erzberg (Austria); K) selection of prominently shaped calcareous soil concretions ("Lösskindl") made of calcite and cementing fine-grained detrital material in periglacial sediments near Pottenbrunn (Austria).

radiometric (U—Th based) chronologies (Boch et al., 2011a; Regattieri et al., 2019).

Likewise, the environmental interpretation of chemical and petrographic proxy parameters in natural carbonate precipitates filling fractures and faults (e.g. meteoric veins) can capture interesting information

on paleoclimate conditions, as well as (neo)tectonic or gravitational mass movements (Quandt et al., 2019; Boch et al., 2019; Fig. 6I, J). Meteoric CaCO_3 precipitates cementing lime- or dolostone boulders of major mass movements have been analyzed for absolute radiometric age determination, i.e. minimum age constraints of the rock falls

(Ostermann et al., 2007). Nodules and concretions in (paleo)soils made of CaCO_3 (Fig. 6 K) were subject of (paleo)environmental studies targeting variable meteoric conditions or uplift rates of mountain ranges (Ghosh et al., 2006; Barta, 2014). The diverse settings of natural carbonate occurrence and its environmental dependencies further include cryogenic precipitates in freezing soil (Burgener et al., 2018), sea ice (e.g. ikaite; Fischer et al., 2013) or as coarse calcite crystals in cave ice (Colucci et al., 2017).

Magmatic rocks of specific formation conditions constitute another setting of natural CaCO_3 occurrence, for example alkaline or ultramafic igneous rocks such as carbonatites, kimberlites and even lava and explosive ejection materials (Weidendorfer et al., 2017). Related to magmatic processes and hot water circulation, diverse carbonates might precipitate as hydrothermal veins, i.e. mainly calcite or iron and magnesium carbonates (Quesnel et al., 2016; Quandt et al., 2019). Information on the fluid source, composition (e.g. brines) and evolution, as well as fluid-rock interaction and the vein formation T and age distribution can be inferred (Maskenskaya et al., 2014; Luetkemeyer et al., 2016). Carbonate concretions were even found in meteorites from Mars and the hydrous CaCO_3 minerals ikaite and monohydrocalcite represent phases of particular scientific focus during Mars exploration (Valley et al., 1997; Harner and Gilmore, 2015).

In the following, inventive studies on elemental, isotopic and/or microstructural characterization of CaCO_3 formation environments in aqueous media are selected to cover a wide range of applications to reconstruct formation conditions, to understand individual precipitation mechanisms and pathways and composite structures. It should be noted that marine environments are clearly the dominant carbonate factories on Earth compared to continental environments. In this review, CaCO_3 -forming environments are presented with jointly focus on the carbonate formation pathways and the use of proxies to trace the carbonate formation conditions. As excellent reviews and textbooks exist on topics like biogenic carbonate formation in marine environments, these contributions are referred to in the text and not repeatedly summarized herein. The present approach is therefore not encyclopedic, and the restriction of content to specific carbonate-forming environments does not reflect their importance in nature, but rather their description elsewhere. In consequence, the section 8.1 is more strongly - but not exclusively - focused on continental settings of carbonate formation compared to marine settings. However, marine environments are in particular discussed in section 6 in the scope of biologically influenced CaCO_3 formation and in subsections of 8.1 in aspects of e.g. evaporitic, cold seep, and hydrothermal carbonates. In Fig. 1 the main CaCO_3 precipitation settings are schematically shown in the natural context and referenced according to the following sections.

8.1.2. Evaporitic carbonates

Evaporitic CaCO_3 is typically initiated by the loss of the solvent (H_2O) to the atmosphere and formed in (past) marine and terrestrial settings (e.g. lagoons, sabkha, playa, caves; Warren, 2016). Thus, elemental and isotope proxies of carbonate precipitates can trace the progressing elemental and isotopic accumulation (e.g. stable Ca, Sr and O isotopes), diverse sources of solvent and aqueous species, T depending fractionation effects during CaCO_3 precipitation etc. For instance, in fresh to hypersaline lagoons (e.g. Coorong; South Australia) coupled $^{87}\text{Sr}/^{86}\text{Sr}$ and $\delta^{88/86}\text{Sr}$ values of Mg-Ca- CO_3 precipitates are used to constrain continental versus marine Sr sources and to assess local carbonate saturation states and salinities (Shao et al., 2021). In contrast, Chamberlayne et al. (2021) indicated incorporation of Sr/Ca, Mg/Ca and Ba/Ca in Arthritica helmsi aragonitic shells in these lagoon-estuarine environments to be not tracing aqueous elemental ratios, T, salinity or pH, but being more likely influenced by biological processes, which may limit their use as environmental proxies. Raudsepp et al. (2022) verified non-classical crystallization of Mg-calcite via an amorphous precursor in the Coorong Lakes during the late summer after extensive evaporation by their nanocrystal orientation and the very high

Mg content. Thus, the impact of distinct reaction pathways on elemental and isotope fractionation has to be considered to reconstruct their formation conditions (see section 7).

In the case of sabkha realms, Mg isotope distribution of precipitated dolomite is suggested as an archive for Mg isotope composition of seawater if the formation temperature is known (e.g. Shalev et al., 2020). However, Mg isotope signature of sabkha dolomites is accompanied with complex reaction kinetics, potential precursors, dissolution/precipitation reactions including microbiological effects and variable Mg sources and sinks in a temporally and spatially variable microenvironment, which have to be considered to reconstruct Mg isotope composition of seawater (e.g. Geske et al., 2015). Terrestrial evaporitic carbonates are highly divers, but most prominent is the formation of HMC and dolomite in alkaline lakes (e.g. Raudsepp et al., 2023).

Recently, Meister et al. (2023) identified by high-resolution transmission electron microscopy of HMC from a shallow alkaline lake (Lake Neusiedl, Austria) < 5-nm-sized domains with dolomitic ordering, which could be induced by oscillating dissolution and precipitation to overcome the kinetic barrier for dolomite formation (see also section 3). Martian paleolakes likely achieved precipitation of CaCO_3 by evaporation of high pH and DIC containing solutions, which are hotly debated for tracing the ancient atmosphere and climate, and in its role considering an origin of life beyond Earth (e.g. Horgan et al., 2020; Michalski et al., 2022; Burnie et al., 2023; Hurowitz et al., 2023).

8.1.3. Soil carbonates

Pedogenic CaCO_3 minerals are widespread in particular at mid latitudes, and their elemental as well as isotope signatures are used to understand Earth's terrestrial history. The highly divers formation conditions imply inorganic and biogenic processes, where warm and dry conditions generally favor soil carbonate growth (e.g. Zamanian et al., 2016; see also Fig. 6 K). Their element/isotope data are frequently applied to reconstruct CaCO_3 formation mechanisms and T, geochemical cycling, past climate, changes in topography and water cycle etc. (e.g. Zamanian et al., 2016; Diaz-Hernandez et al., 2018; Bayat et al., 2021; Licht et al., 2022).

For instance, Valera-Fernández et al. (2020) used the stable C and O isotope distribution in calcretes - pedogenic carbonate crusts formed by coupled dissolution and reprecipitation e.g. induced by evaporation - to trace past environmental trends, such as passing from arid to more humid conditions. A multi-isotope approach on rhizolith - roots encrusted with CaCO_3 - provides novel insight into the formation mechanisms (Brazier et al., 2020): $^{87}\text{Sr}/^{86}\text{Sr}$ signatures of the rhizoliths indicate dissolution of carbonate and non-carbonate minerals and the stable isotope distribution of Ca and Sr traces complex fractionation effects during their (i) uptake by the roots and (ii) incorporation into the CaCO_3 precipitates. CaCO_3 formation in soils, in particular in alkaline media, are known as a significant CO_2 sink and thus slowing global warming trends, where soil microorganisms can play an important role on managing its formation (e.g. Tibetan Plateau: Shao et al., 2023). Recently, Kelson et al. (2023) applied triple oxygen isotope compositions of soil carbonates to reveal evaporation trends of precipitating soil solutions, in particular valid for arid surroundings. This novel tool is based on the evaporation-sensitive deviation from the $\delta^{17}\text{O}$ vs. $\delta^{18}\text{O}$ reference line.

8.1.4. Cave carbonates

Cave carbonates such as stalagmites, flowstones and other more complex forms consist of CaCO_3 (mainly calcite, rarely aragonite) and precipitate from differentiated aqueous solutions (drip water) in various caves during different time intervals of the past and up to now (Fig. 6 G, H). Apart from other (clastic) cave sediments and cave ice, speleothems (cave decoration, dripstones) have emerged as an attractive and increasingly investigated chemical-sedimentary archive that records terrestrial and regional environmental (climate) information in multiple

ways (Fairchild and Baker, 2012; Spötl et al., 2024). Caves, karstification and speleothems, in principle, can be related to epigenetic or hypogenic sources and formation conditions, i.e. infiltration of meteoric waters (rain, snowmelt) and carbonic acid host rock dissolution from the surface (above the cave) versus hydrothermal and mostly sulfuric acid based cave and mineral formation originating from depth (White et al., 2019).

Geographically, carbonate host rock associated caves and their speleothem content are widespread and represent a (paleo)environmental archive available in populated areas, as well as in remote karst areas (e.g. Siberia, Greenland). This constitutes a spatial advantage compared to other established but locally restricted environmental (climate) archives, such as high-latitude ice cores or deep marine sediment cores (Barker et al., 2011; Lisiecki and Stern, 2016). Another spatial advantage is manifested in the favored preservation of speleothems underground, i.e. they are protected from destructive atmospheric, sedimentary and other alternating (diagenetic) processes. Furthermore, speleothem CaCO_3 material of variable age is typically well suited for reliable radiometric age determination based on uranium-series isotopes being incorporated and decaying in the CaCO_3 crystals (e.g. ^{238}U - ^{234}U - ^{230}Th , ^{238}U - ^{207}Pb - ^{206}Pb , ^{210}Pb ; Wang et al., 2017; Spötl and Boch, 2019). Consequently, precise and accurate chronologies and growth models can be established for individual speleothem samples and the specific environmental information recorded. This clearly constitutes the backbone of speleothem based (paleo)climate research. Further, caves and speleothems provide an environmental archive of the more recent geological past and variable climate conditions. Karst caves undergo more or less systematic maturity processes and distinct stages from initial porosity and dissolution enlarged fractures in the carbonate host rock towards a phreatic evolution of cave chambers, vadose water percolation and successive speleothem deposition, and finally their gravitational collapse or Earth's surface erosion (Ford and Williams, 2013).

Caves and the spatiotemporally evolving speleothems possess several connections to the prevailing climate and atmospheric conditions at the surface. The most important are chemical compositions and particle contents transferred by the percolating water (drip water), thermal assimilation of the cave interior versus exterior atmosphere, and the variable cave air exchange (ventilation) influencing air- and hydrochemical gradients. Importantly, during CaCO_3 precipitation from aqueous solution, the prevailing environmental parameters influence the chemical and structural (e.g. layering) speleothem composition, and this more or less continuously recorded variability can be reconstructed in a multi-proxy approach (Fairchild and Baker, 2012; Wassenburg et al., 2024). In this context, stalagmites and flowstones are most important as paleoclimate archives owing to their relatively simple growth geometry compared to stalactites, stalagnates, excentriques (helictites) and curtains (White et al., 2019; Fig. 6G, H).

Different speleothem samples from different regions and caves and even within a specific cave system provide different potential applications in terms of their depositional age, environmental sensitivity and temporal resolution. Onuk et al. (2014), for example, studied the formation and microstructure of helictites versus the more common stalactites and found distinct evidence for the role of secondary water channels, capillary hydrostatic forces and local clogging influencing the stacking and size of calcite crystals in the course of straight versus bended growth sections. Immenhauser et al. (2023) investigated the formation of “gravity-defying speleothems” (excentriques, helictites) consisting of calcite and aragonite using diverse optical analytical tools (macrophotography, SEM, EBSD, μ -CT), as well as elemental and isotope geochemistry. ^{234}U - ^{230}Th dating of selected helictite samples revealed ages from 347 kyr BP up to recent times. The authors also highlighted the relevance of fluid migration within an internal capillary network (channels of $\sim 150 \mu\text{m}$ diameter) in combination with enhanced CO_2 outgassing and further stressed that future work should also include microbiology. Specific speleothem formation conditions are also

associated with cryogenic cave minerals (CCM) representing an increasingly recognized chemical-sedimentary proxy for paleo-permafrost reconstruction (Németh et al., 2022; Donner et al., 2023; Spötl et al., 2023; see section 8.1.8).

Past T and past meteoric precipitation amounts, sources, trajectories and seasonal distributions as well as the composition of vegetation, soil and bedrock are the most relevant parameters addressed based on speleothem records (Luetscher et al., 2015; Railsback, 2018). Zhang et al. (2019a) studied the dominant forcing mechanisms and teleconnections with regard to the Asian Summer Monsoon (ASM) influencing the life of nearly one third of Earth's population and being recorded in Chinese speleothems of the past 640,000 years. They focused on the late Pleistocene, Holocene and the last two millennia and found a strong connection of the ASM to northern hemisphere summer insolation and to the North Atlantic climate and ocean currents. In many cases, the CaCO_3 oxygen isotopic composition constitutes a proxy of particular relevance, i.e. isotope curves across the speleothem growth axis reflect variable isotope fractionation between the dominant reservoirs (e.g. atmosphere, hydrosphere, pedosphere) and phases (drip water, CO_2 , calcite) involved. Baker et al. (2019) evaluated 39 caves on five continents with regard to meteoric precipitation amounts and seasonal distribution in relation to cave drip water oxygen isotope signatures, i.e. climatic and often recharge-weighted controls on the $\delta^{18}\text{O}$ of the drip water and consequently also on CaCO_3 . Considering the dependency of stalagmite growth rate on atmospheric precipitation and temperature Railsback (2018) investigated 80 stalagmites from the Holocene and found that the correlations are relatively low and not trivial, i.e. the growth rates do not increase monotonically with meteoric precipitation but reach maximum values within a specific range of precipitation (700–2300 mm/yr). So far, stalagmites have recorded variations of the El Niño Southern Oscillation (Wang et al., 2017), sea-level oscillations (Antonioli et al., 2004), tropical thunderstorms (Frappier et al., 2007), influences of Mediterranean cyclone activity (Demény et al., 2017), and the North Atlantic Oscillation and seasonal strength of the westerly winds (Fohlmeister et al., 2017).

High-resolution oxygen isotope analyses are typically combined with precise uranium-thorium age models in order to understand the influence of the North Atlantic marine and atmospheric conditions on Asian monsoon patterns (see above) and the speleothem isotope signals and absolute chronologies can further be used to improve the often floating chronology and timing of proxy signals from other archives, e.g. Greenland ice cores (Boch et al., 2011a; Cheng et al., 2016; Moseley et al., 2020). Campbell et al. (2023) used selected stalagmite samples from shallow caves (little rock overburden) from susceptible regions (e.g. Australia) to reconstruct wildfire activity. They evaluated promising paleofire proxies such as discrete horizons of highly enriched metals (iron, zinc) in stalagmites reflecting ash leaching and intermittent changes in drip water chemistry, as well as sulfur isotopes and mineral magnetism. The complex environmental signals, however, are also interfering with major meteoric precipitation events and flushing of soil organic matter. Further, the timing of speleothem deposition can be used to constrain the timing of rock fracturing and slope movements (Koltai et al., 2018; Baroň et al., 2022).

Next to the oxygen isotope ratios, the stable carbon isotopes in the speleothem CaCO_3 are simultaneously analyzed and discussed (Regattieri et al., 2019). More generally, equilibrium and kinetic effects of isotope fractionation between the aqueous solution, cave atmosphere and associated calcite or aragonite precipitate is a vivid subject of speleothem research (Daëron et al., 2019; Mickler et al., 2019; see also section 7.2.2). Based on cave-analogue laboratory experiments Hansen et al. (2019) studied stable carbon and oxygen isotope fractionation between water, DIC and CaCO_3 and found that both $\delta^{13}\text{C}$ and $\delta^{18}\text{O}$ depend on the water flow (residence time) and precipitation rate and consequently on kinetic conditions. The DIC reservoir has to be considered as a closed system leading to Rayleigh effects. This is also supported by the results of Sade et al. (2022b) who investigated the

effects of drip rate and speleothem geometry on the stable carbon and oxygen isotopic composition based on an advection-diffusion-reaction model. They found a strong dependence of calcite $\delta^{13}\text{C}$ and $\delta^{18}\text{O}$ on the drip rate and water flow distance and only a weak dependence on the slope of the speleothem surface. Importantly, changes in drip rate alone can account for major shifts in isotopic compositions (up to several ‰) when all other environmental parameters are kept constant, i.e. a critical conclusion with regard to the (paleo)environmental interpretation of these isotope proxies.

Considering the non-traditional isotopes analyzed in dripstones, Ca isotope signatures (Owen et al., 2016), magnesium isotopes (Immenhauser et al., 2010), clumped isotopes (Δ_{47} ; multiply-substituted isotopologues; Guo and Zhou, 2019; Hansen et al., 2022), as well as $\delta^{17}\text{O}$ in fluid inclusions (Affolter et al., 2015) are increasingly reported. Apart from radiometric dating uranium isotopes might also be used as a proxy for water-rock interaction: Wendt et al. (2019) sampled subaqueous calcite from the walls of Devils Hole 2 Cave (Nevada, USA) and the drillcores represent a 475,000 years long record of glacial and interglacial cycles. They used the initial $^{234}\text{U}/^{238}\text{U}$ ratios ($\delta^{234}\text{U}_0$) as a representative of groundwater recharge to the regional aquifer based on the assumption of significantly increased ^{234}U leaching during times of an elevated water table (increased meteoric water infiltration). Likewise, concentration and fractionation studies target specific minor and trace elements such as magnesium, strontium, barium and uranium (Drysdale et al., 2019). Sulfate contents and isotopic compositions in speleothem carbonate were addressed by Wynn et al. (2008) who discussed local and regional variations in the speleothem sulfur record depending on atmospheric (e.g. volcanic) sulfur loading or industrial emissions. They suggested sulfate $\delta^{34}\text{S}$ as a provenance tracer of atmospheric SO_2 while the $\delta^{18}\text{O}$ signature of sulfate is more complex relying on biogeochemical cycling in the ecosystem. Similarly, the contents and isotopic compositions of nitrate in karst aquifers, drip waters and speleothems depend on variable sources (e.g. agriculture) and dynamics (Wynn et al., 2021; see section 7.1.2).

Valuable information on the prevailing climate and vegetation can also be derived from various organic inclusions in speleothems, e.g. pollen and different (macro)molecules (Blyth et al., 2016; Frisia et al., 2018). Different detrital inclusions might either contribute indicative minerals or specific magnetic properties (Regattieri et al., 2019) and in rare cases speleothems have also encrusted and thus preserved human remains (Hellstrom and Pickering, 2015). Pearson et al. (2020) also showed that the precipitation of calcite is significantly reduced by high dissolved organic matter contents in ground- and drip waters and the CaCO_3 crystal structures and fabrics are further strongly influenced by the organic matter (see also DCOM in section 7.1.2). Ancient seepage water can be present in speleothem fluid inclusions of variable amount reflecting the composition of rainwater in the past (Johnston et al., 2018; Honiat et al., 2023). Uemura et al. (2020) measured δD and $\delta^{18}\text{O}$ signatures of fluid inclusions in speleothems based on laboratory experiments and using natural stalagmite material. They focused on the isotope exchange and potential bias (post depositional effects) between inclusion water and host calcite and found no trend in the hydrogen isotopes and only a small shift in the oxygen isotopes. This further implies a negligible effect on paleotemperature estimates derived from speleothem fluid inclusion based isotope signatures. In contrast, fluid inclusion analyses in speleothem samples from Hungary revealed unrealistic paleotemperatures based on calculations from measured δD and $\delta^{18}\text{O}$ values of calcite and fluid inclusion water (Demény et al., 2021). The authors attributed this observation to syn-formational isotope fractionation and diagenetic alteration and paleotemperature reconstructions from fluid inclusions should thus be handled with some caution. Considering fluid inclusions further analytical approaches including liquid-vapor homogenization and dissolved noble gas concentrations are used (Meckler et al., 2015; Wassenburg et al., 2021).

Regarding an advanced process understanding of the speleothem growth dynamics and proxy dependencies in relation to variable

environmental conditions, systematic and increasingly sophisticated, although highly site-specific, cave monitoring programs have shown great value (Mattey et al., 2008; Czuppon et al., 2018). The monitoring campaigns include periodical visits and sampling of drip waters, cave air compositions and eventually CaCO_3 precipitates on artificial substrates (Tremaine et al., 2011). Automated sensors and data loggers are also increasingly applied in order to gain *in-situ* and high-resolution data of relevant environmental parameters (Boch et al., 2011b). Major targets are the variable hydrochemistry, water discharge, cave air exchange (ventilation) and intimately related CaCO_3 precipitation dynamics. For example, intense monitoring work was conducted in Gibraltar where fluxes of water, air and carbon were studied over many years (Mattey et al., 2016 and Mattey et al., 2021). In some cases the monitoring data are compared to regional meteorological data in an attempt to establish quantitative transfer functions of the speleothem proxy versus (atmospheric) climate parameters (Lachniet, 2009).

Increasing evidence also promotes the scientific discussion on the potential role of metastable precursor phases such as ACC in relation to the more stable (anhydrous) CaCO_3 polymorphs, as well as the role of microorganisms (e.g. bacteria) for ACC nucleation and speleothem formation in general (Demény et al., 2016; Dhami et al., 2018). Enyedi et al. (2020) highlight the infiltration and concentration of organic and inorganic constituents from drip water on the surface of active speleothems, i.e. bacterial cells colonizing the wet habitat and creating a biofilm, thereby also influencing CaCO_3 precipitation. The study involved the collection of drip water, the in-vitro cultivation of microbial communities and the subsequent evaluation based on SEM, TEM, Raman- and infrared (FT-IR) spectroscopy, as well as 16S rRNA gene sequencing (Enyedi et al., 2020). The investigation showed the presence and relevance of dominantly heterotrophic (chemoorganotrophic) bacterial strains (e.g. *Stenotrophomonas maltophilia*, *Bacillus simplex*, *Rhodococcus degradans*) which liberate energy from organic compounds (carbon source) and are also widespread amongst soil microorganisms. Some of the bacterial strains are able to produce ammonia through ureolysis and further conduct dissimilatory nitrate reduction from organic nitrogen compounds (see section 8.2.8). Interestingly, several of the bacteria detected produce ACC being stable for at least half a year at room temperature in the humid environment, i.e. in contrast to the typically rapid decay of ACC observed for comparable laboratory conditions. This is attributed to the formation of EPS and more specifically relatively large amounts of long-chain fatty acids shielding the ACC phases from further crystallization. Thus, the occurrence of ACC in caves might typically be linked to the presence and metabolic activity of bacteria (Demény et al., 2016; Enyedi et al., 2020); see sections 3 and 6. The microbes (biofilms) also constitute a preferred nucleation site (substrate effect) and can affect (increase) the pH and saturation conditions in their microenvironment consequently influencing CaCO_3 precipitation, i.e. microbially influenced speleothem deposition. Considering that calcite/aragonite and ACC have a different stable isotope fractionation behavior the crystallization of the precursor ACC could significantly affect isotope signatures and the (paleo)environmental interpretation of the speleothem records (see section 7.2.2).

The intense research activities and rich (paleo)environmental data derived from speleothems on a global scale led to the development of specific databases such as the SISAL (Speleothem Isotopes Synthesis and Analysis) database (Atsawaranunt et al., 2018 – SISALv1; Kaushal et al., 2024 – SISALv3). This database comprises of speleothem isotope and other data from all over the world and allows for some detailed spatial and temporal evaluation and big data approach based on the freely available datasets. Comas-Bru et al. (2019) presented an updated version (SISALv1b) of this database including 456 globally distributed and well-documented stable oxygen isotope records. Amongst others the datasets are intended for proxy data versus climate model comparisons, e.g. speleothem based $\delta^{18}\text{O}$ data versus the isotope-enabled atmospheric circulation model. A newer version of the SISAL database (SISALv2; Comas-Bru et al., 2020) constitutes a global compilation of 691

speleothem isotope records from 294 cave sites and further improves the spatiotemporal coverage. In addition, multiple age-depth models (chronologies) of the speleothem records are integrated based on seven different approaches (e.g. linear interpolation, linear regression, OxCal, StalAge). This supports an evaluation of the temporal uncertainty in the paleoclimate records (e.g. specific climate events) and the identification of potential triggers. Campbell et al. (2023), for example, used the SISALv2 database and its filter functions in order to identify suitable speleothem samples for their paleo-wildfire research.

8.1.5. Travertine and calcareous tufa

Another form of chemical-sedimentary deposits is represented by travertine of diverse formation conditions (Fig. 6 A-C). These fossil or active freshwater CaCO_3 are typically compact and layered, consist of calcite as well as aragonite, and their successive precipitation is controlled by physicochemical and (micro)biological processes in relation to changing environmental conditions (Capezzuoli et al., 2014; Kano et al., 2019). The travertine successions of highly variable thickness (centimeter to hundreds of metres) are often associated with volcanic activity, thermal waters and fault zones. In principle, the travertine forming aqueous solutions can either be of epigenetic or hypogenetic source, i.e. surface meteoric or deep geothermal water infiltration towards discharge (Kele et al., 2008). In contrast to travertine, calcareous tufa deposits are typically more porous and dominantly consist of calcite precipitated from CO_2 outgassing and CaCO_3 supersaturated freshwaters at ambient atmospheric T conditions, i.e. they are not necessarily related to increased geothermal activity (Capezzuoli et al., 2014; Cantonati et al., 2016; Fig. 4C and Fig. 6D, E).

Microbes such as specific (cyanobacterial) communities (e.g. Rivularia) and algae (e.g. Oocardium) are involved in the formation process and photosynthetic activity (assimilation of CO_2) often promotes supersaturation of CaCO_3 and the associated biocalcification (Verrecchia et al., 1995; Cantonati et al., 2016). Calcareous tufa deposits are also characterized by increased moss (e.g. Palustriella, Eucladium) and other plant contents supporting a higher porosity of these encrusting CaCO_3 precipitates (Brogi et al., 2012; Tran et al., 2019). Microbially-mediated CaCO_3 precipitation is typically also associated with the formation of calcrete (or caliche), i.e. calcareous crusts near the surface (soil, shallow groundwaters) further being characterized by some lamination and/or spherulites (Verrecchia et al., 1995; Wright, 2007).

Travertine and tufa sequences involve depositional facies architectures of variable complexity and their material-specific characteristics are described using a differentiated nomenclature (Freytet and Verrecchia, 1998; De Filippis et al., 2013). The relevant depositional processes include various geological, tectonic and climatic settings determining critical atmospheric and hydrochemical parameters such as air and water T, discharge, CO_2 outgassing and evaporation, as well as the associated biology (biofilms) and consequently the travertine or tufa mineralogy, chemical composition and fabric (Della et al., 2017). Focusing on the organic (biotic) versus inorganic (abiotic) processes favoring CaCO_3 precipitation, a diverse range of redox-chemical and photosynthetic reactions affecting the pH, dissolved CO_2 and saturation states are determining (Fouke, 2011). For example, different microbes and plant metabolisms determine spatial pH and CO_2 gradients or might channel specific ionic constituents (e.g. Ca^{2+}) relevant for CaCO_3 precipitation (Shiraishi et al., 2019). Different forms of branched dendrite calcite crystals are typically indicative for hydrochemical conditions involving turbulent flow, rapid CO_2 outgassing and high CaCO_3 supersaturation (Jones and Renaut, 2008). Christensen et al. (2021) presented an interesting location at The Cedars (California) where serpentization of ultramafic rocks in the subsurface results in alkaline ($\text{pH} > 11$) spring emergence and related aragonite and calcite precipitation based on the uptake of atmospheric CO_2 and local mixing of spring water with surface waters. Next to travertine terraces and encrustations the differentiated depositional facies includes the occurrence of “flocs” (rafts) at the atmosphere-water interface and the nucleation of fine particles (“snow”,

mud-grade carbonate) at the bottom of local pools. A conceptual model explaining the recurrent formation of the rafts with regard to aragonite and calcite crystallization as well as water surface tension and pH is presented.

In-situ and *in-vitro* field studies as well as laboratory experimental approaches are increasingly recognized as being of high relevance (e.g. De Boever et al., 2017). Some studies have focused on the good access and spatiotemporal evolution of flowing waters forming the CaCO_3 deposits in variable facies sections, i.e. environmental monitoring of active travertines or tufas as natural laboratories of seasonal or daily variations in lamina formation or stable isotopes (Asta et al., 2017; Yan et al., 2017). Ritter et al. (2017), for example, monitored the role of biofilms/EPS of the microbial habitat in connection with the hydrogeochemistry of creek water and an active calcareous tufa in the Franconian Alb/Germany in a monthly rhythm and discussed systematics of Mg, Sr and Ba fractionation. Pedley (2014) conducted laboratory experiments facilitating near-natural and dynamic (flowing water) conditions over more than two years for observing calcite precipitating microbial biofilms. Importantly, externally derived major ions such as Ca^{2+} were channeled and redistributed in the organic tissue resulting in concentration and pH gradients and the precipitation of CaCO_3 as ACC at the outer surfaces of microbial filaments and EPS. These biogeochemical reactions enable the internal stabilization and well-being of the microbial community and the currently living filamentous bacteria always stay on the surface of the actively growing deposit. Finally, the arbitrarily induced end of the laboratory experiment and subsequent growth cessation, dying and decay of the biofilms resulted in a massive mobilization of micrite being disseminated in the organic tissue in the form of loose mud-grade carbonate. The typically open physicochemical system behavior and ongoing fluid exchange in travertine and tufa often leads to overprinting and material alteration of the carbonate fabrics and proxy signals (e.g. stable and clumped isotopes) based on the coarsening of fabrics (recrystallization) and successive homogenization of microstructures and compositions (De Boever et al., 2017).

Building on these formation conditions, the site-specific freshwater precipitates are increasingly investigated as a continental (paleo)environmental archive supporting a multi-proxy approach of parameters such as air/water temperature, water recharge and discharge or microbial and vegetation (palynological) changes (Bertini et al., 2008; Matera et al., 2021). The reconstruction of past environmental (climate) conditions is often related to fossil travertine and calcareous tufa sequences and their precise radiometric (U-Th) age determination (Boch et al., 2005; Sierralta et al., 2010; Brogi et al., 2012). Saunders et al. (2014) investigated Mg/Ca ratios in microbially-mediated freshwater CaCO_3 based on laboratory experiments including microbial biofilms and found no strong relation between Mg/Ca in calcite and the formation temperature, i.e. Mg/Ca not being a distinct (paleo)thermometer. Instead they recorded a dominant kinetic control (precipitation rate, vital effects) on major element partitioning. Likewise, Wang et al. (2021a) studied the incorporation of specific elements (Na, Mg, Sr, Ba, Li, Ni, Co, Mn, Zn, Cu) into calcite based on active travertine deposition in the main channel of the Baishuitai river system (Yunnan, China) and presented multiple environmental factors explaining the different distribution coefficients between solution and solids sampled during the field campaigns. REE and other trace elements (Sr, Ba, U) were researched in travertine precipitates related to low temperature serpentinization and hyperalkaline fluids (high pH, low DIC, absorption of CO_2) of the Ronda peridotite in Spain (Zwicker et al., 2022). The authors focused on reaction path modeling explaining the unusual distribution of the REE (e.g. enrichment of La and Ce in travertine) in the fluids versus travertine and discussed the role of hydroxide versus carbonate complexation. Importantly, CaCO_3 deposition was recognized as a sink of the REE as well as uranium.

Considering the investigation of isotope fractionation based on active and fossil travertine and tufa deposits an increasing number of sites and approaches emerged in recent years. Several studies discussed

the environmental dependency of stable carbon and oxygen isotope patterns. Osácar et al. (2016) conducted a multi-annual monitoring approach involving artificial substrates (carbonate tablets) placed in different sedimentary facies of three calcareous tufa precipitating river systems in Spain. They found distinct seasonal variations (warm vs. cold season modes) and the 13 years long Piedra River tufa record also archived ongoing global warming. The oxygen isotope signatures are clearly dependent on cyclic variability of air/water T while the carbon isotopes are obviously determined by more local processes and do not show distinct seasonal patterns.

Stable carbon and oxygen isotopic compositions were also monitored in active travertine precipitates of the Baishuitai river system (Yunnan, China; Yan et al., 2017). Based on *in-situ* travertine samples as well as artificial substrates (plexiglas) collected in the upstream, middle and downstream river section the study observed a regular biannual pattern involving the travertine fabric (thicker whitish layers and thinner darker layers) as well as the carbonate $\delta^{13}\text{C}$ and $\delta^{18}\text{O}$ values. Based on the same location of active travertine formation in China, Yan et al. (2020) focused on the (paleo)environmental interpretation of stable carbon isotope compositions of the travertine calcite and reported a large degree of carbon isotope disequilibrium related to the outgassing of CO_2 and dehydr(oxyl)ation of HCO_3^- in the course of CaCO_3 precipitation (see section 7.2.2). The environmental evolution of carbon and oxygen isotope fractionation was also examined in the alkaline spring waters at The Cedars (USA) and the authors found large ranges in the $\delta^{13}\text{C}$ (−9 to −28 ‰ VPDB) and $\delta^{18}\text{O}$ values (0 to −20 ‰ VPDB) related to kinetic isotope effects during CO_2 absorption and CO_2 hydroxylation (Christensen et al., 2021; see also section 8.1.6). In addition, the fractionation of stable Ca isotopes between CaCO_3 and the aqueous solution mostly depends on the prevailing CaCO_3 precipitation rate (travertine growth rate).

Kele et al. (2015) used calcite and aragonite in tufas and travertine of active settings in order to evaluate and calibrate the T dependence of oxygen and clumped isotope fractionation between aqueous solution and CaCO_3 . The latter environmental proxy was also the focus of Arnold et al. (2024) who evaluated clumped isotope composition versus T relationship and calibration based on lacustrine, fluvial and spring (freshwater) CaCO_3 (135 samples, 96 sites) including travertine, biologically-mediated carbonate (e.g. calcareous tufa), micrite and biological material (freshwater gastropods, bivalves). High-precision uranium-series dating (U-Th and U-Pb) gets increasingly relevant next to more conventional radiocarbon and optically stimulated luminescence dating (Hellstrom and Pickering, 2015; Spötl and Boch, 2019). Another focus of travertine research is centered around the coexistence with volcanic areas or major (neo)tectonic fault zones (Toker et al., 2015). Matera et al. (2021) studied laminated CaCO_3 veins within a major fissure ridge travertine near Larderello/Italy with a focus on chemical variations of the geothermal fluids and different phases of tectonic activity between 172 and 21 kyr BP.

8.1.6. Spring, lake and river carbonates

Tracing the formation of CaCO_3 in lacustrine and fluvial surroundings comprise of biogenically and inorganically induced mechanisms (e.g. Zeyen et al., 2021; Boussagol et al., 2023), which are partly discussed in sections 6, 8.1.2, and 8.1.5. Herein a couple of studies are presented to exemplarily show the broad and highly divers carbonate formation settings and the insights gained from environmental proxy signals. In Lake Kinneret (Israel) Sr/Ca, Mg/Ca, $^{87}\text{Sr}/^{86}\text{Sr}$, and $\delta^{18}\text{O}$ values of calcite precipitates and ostracods monitor the hydrological history by indicating distinct water influx from Jordan river, regional run off and brines (Lev et al., 2019). Katz and Nishri (2013) identified phytoplankton activity to rise pH and thus induce authigenic calcite in this lake during spring to early summer to be highly impact the elemental cycles. In Mexican and Spanish lakes, CaCO_3 from microbialites were identified to be formed through amorphous precursors, which can even result in the formation of protodolomite, both to be considered from

their proxy signals (Zeyen et al., 2021; del Buey and Sanz-Montero, 2023; see also sections 3 and 7).

Recently, McCormack et al. (2024) found from a combined microstructural, mineralogical and isotope-geochemical approach that early diagenetic dolomite in sediments of the alkaline Lake Van (Turkey) were formed via highly dynamic and fluctuating conditions caused by mixing glacial/stadial, high-alkalinity, oxic and interglacial/interstadial low-alkalinity anoxic deep fluids. In this context, Mg-Ca- CO_3 mineral formation in the shallow alkaline Lake Neusiedl (Austria) was found by saturation state modeling to occur in the water column and not in the sediment (Fussmann et al., 2020). At this site, very slow crystal growth rates of about 0.2 to 0.6 $\mu\text{m}/\text{ka}$ were estimated from radiocarbon analyses (Neuhuber et al., 2024).

A multi-proxy approach - including Sr/Ca ratios and $\delta^{13}\text{C}$ values of needle-like aragonites - in a Croatian lake sediment reveals past climate variations, e.g. T and hydrology records (Razum et al., 2021). Mg bearing CaCO_3 precipitation in rivers is well documented, e.g. for the Yangtze river (China), where Mg isotope signals can be used to assess the impact of carbonate precipitation on solution chemistry for the re-estimation of water and silicate weathering fluxes (Zhao et al., 2019a; Zhao et al., 2022a; Li et al., 2023a). From culturing experiments, Marchegiano et al. (2024) showed clumped isotope signatures of ostracods to excellently mirror their growth temperature, thus their Δ_{47} values to be used for T and hydrological reconstruction in lacustrine records.

8.1.7. Cold seep carbonates

Cold seep CaCO_3 occurs worldwide and most frequently at continental margins. Their formation is essentially based on the discharging of methane-rich solutions into the seawater, where the CaCO_3 precipitation is induced by anaerobic oxidation of CH_4 in the presence of sulfate to increase the carbonate alkalinity (e.g. Campbell, 2006; Feng et al., 2018; Thorsnes et al., 2019). Methane-derived authigenic CaCO_3 typically consists of Mg-calcite and aragonite - rarely also siderite or ikaite -, where these primary carbonate minerals can be subsequently transformed e.g. to (proto)dolomite (e.g. Phillips et al., 2018; Hiruta and Matsumoto, 2022; Lu et al., 2023b).

Elemental and isotope proxies of cold seep CaCO_3 are used to trace (past) element sources, redox and fluid dynamics and to assess the associated carbon sequestration within the global C cycle (e.g. Mg and Ca isotopes: Jin and Feng, 2023; C and Ca isotopes and RNA gene sequencing: Schroedl et al., 2024; Co and Zn isotopes: Zhang et al., 2024). In accordance with the latter aspect, $^{87}\text{Sr}/^{86}\text{Sr}$ and stable C and O isotope distribution of seep CaCO_3 can be used to quantify the contribution of carbonate from seawater and from deep fluid / meteoric origin (e.g. Phillips et al., 2018; Argentino et al., 2019; Zhu et al., 2019; Weidlich et al., 2023). Authigenic calcite precipitates of cold seeps yield in the incorporation of trace elements by co-precipitation, and fluctuating redox conditions can create characteristic fingerprints e.g. of U, Fe Mn, and REE (e.g. Lemaitre et al., 2014; Zhu et al., 2019; Smrzka et al., 2021).

In this context, individual Mo isotope distribution of methane-derived seep carbonates was shown to trace the complex biogeochemical cycling of carbon and sulfur in such settings (Lin et al., 2021). Gong et al. (2023) revealed Ca isotope signatures of methane-derived CaCO_3 seeps to depend on mineralogy (aragonite vs. Mg-calcite), where aragonite is found to be formed close to isotope equilibrium. Distinct disequilibrium conditions of clumped and oxygen isotopes in shell and cement carbonates can act as a proxy for cold seep carbonate archives (Savard et al., 2021). Dual-clumped isotope data (Δ_{47}/Δ_{48}) of methane-derived seep carbonates were successfully used to reconstruct paleotemperature and the oxygen isotopic composition of the seawater (Staudigel et al., 2024). Recently, Li isotope distribution of seep CaCO_3 was applied to trace the origin of Li from both seawater and a ^{6}Li enriched deep-seated fluid (Miyajima et al., 2023).

8.1.8. Cryogenic carbonates

CaCO_3 precipitation at T close or even below 0 °C occurs e.g. at the shelf-ocean floor, but also being prominent at the continent such as in caves, permafrost soils, and glacial settings (e.g. Lacelle, 2007; see also sections 8.1.2, 8.1.3, 8.1.4, 8.1.7). Herein focus is given on a couple of distinct cryogenic/cold continental settings in the scope of environmental proxies to understand, recover and trace (past) CaCO_3 formation conditions.

Precipitation of cryogenic carbonate in **caves** are based on ice formation to accumulate aqueous ions in the remaining solution, which may be forced by evaporation of H_2O and degassing of CO_2 (e.g. Lacelle, 2007; Žák et al., 2018). Cryo- CaCO_3 shows highly divers morphologies and structures, such as pseudo-biogenic crystal structures, and is characterized by light oxygen isotope signatures caused by ^{16}O isotope discrimination vs. ^{18}O during ice formation from the precipitating solution (e.g. Lacelle et al., 2009). Onac et al. (2023) recently found a new speleothem type consisting of cryogenic CaCO_3 ridges, where the $\delta^{18}\text{O}$ values indicate its formation to be induced by coupled evaporative cooling and freezing of the precipitating solution. Complexity of cryo- CaCO_3 formation was studied by experimental approaches (i) under controlled physicochemical conditions in the laboratory by Uwakwe et al. (2023) e.g. verifying $\delta^{13}\text{C}$ values to be affected by ongoing CO_2 degassing and (ii) within a natural (ice) cave by Spötl et al. (2023) assessing the formation mechanisms of cryo- CaCO_3 and its $\delta^{18}\text{O}$ isotope depletion. Burgener et al. (2018) indicated by Δ_{47} , $\delta^{18}\text{O}$, and $\delta^{13}\text{C}$ values of **soil** CaCO_3 from cold, arid settings fine-grained matrices to likely reach isotope equilibrium for suitable paleoclimate reconstructions, whereas isotope signatures of coarse-grained matrices are more affected by kinetics. Calcite lenses in alluvial fan deposits were identified by Bertran et al. (2023) by oxygen isotope signatures to be of cryogenic origin, where it is claimed that such settings may be unrecognized for environmental records.

In contrast, **subglacial** CaCO_3 deposits are well recognized as archives for (paleo) glacier presence and environmental conditions (e.g. Lipar et al., 2021). Their oxygen isotope data are tracing glacial ice as H_2O source of the precipitating solution at close to freezing conditions (e.g. Souchez and Lemmens, 1985; Faure and Mensing, 2010; Refsnider et al., 2012; Thomazo et al., 2017). The formation of subglacial CaCO_3 is initiated by glacier sliding over protuberances with pressure-melting on the stoss side and partial refreezing of meltwater on the lee side (e.g. Hanshaw and Hallet, 1978; Souchez and Lemmens, 1985). Calcite precipitates from subglacial fluids can act as an archive e.g. of maximum ice thickness and variations in sub-glacial draining, Pco_2 , and pH (e.g. Frisia et al., 2017).

Low T environmental conditions can be traced by the formation of the mineral ikaite and of the pseudomorphosis of calcite to ikaite (glendonite), and isotope compositions of both (e.g. Whiticar et al., 2022). Glendonite can be found throughout ancient sedimentary records (e.g. Whiticar et al., 2022; Mikhailova et al., 2019; Rogov et al., 2023). Rare occurrences of ikaite/glendonite comprise - besides marine settings - lakes (type locality: Ikka Fjord, Greenland), caves, calderas to early diagenesis settings (e.g. Schultz et al., 2022). However, the use of ikaite/glendonite as low T proxy is challenging by (i) its experimentally verified formation up to ambient T conditions (e.g. Purgstaller et al., 2017b) and (ii) amorphous precursor phases to be relevant for its formation in particular at elevated supersaturation stages, where notably ikaite can be also re-transformed to ACC (e.g. Zou et al., 2018; Strohm et al., 2022). Glendonite as environmental archive might be even more limited in its use if additional geochemical relicts and/or readjustments during ikaite-to-calcite transformation have to be considered (e.g. in cryogenic caves: Németh et al., 2022).

8.1.9. Hydrothermal carbonates

Precipitation of CaCO_3 from hydrothermal solutions occurs in a wide range of natural realms comprising submarine circulating fluids, blow out / discharging of geothermal solutions (e.g. hot springs and geysers),

and migration of interstitial solutions or fluid transport through fractures (e.g. Barnes, 1997; Campbell, 2006; Pirajno, 2012; Alçıçek et al., 2019; Pirajno, 2020; Luo et al., 2022; Silantyev et al., 2022; Dielforder et al., 2022; Wei et al., 2023b; see also sections 8.1.5 and 8.2.5). The CaCO_3 formation mechanisms are based on a change of the physico-chemical conditions, e.g. shift in T, mixing of solutions, exchange with gas phases (e.g. CO_2 degassing induced by reduced (partial CO_2) pressure), exposure to solids (e.g. dissolution of Ca or alkalinity bearing minerals) and impact of evaporation as well as (micro)organisms. The deposition of CaCO_3 yields in e.g. mud-grade carbonate, sinter basins, chimneys, cements or vein fillings (Fig. 6).

Modern and ancient hydrothermal fluids are well known to precipitate CaCO_3 in marine settings, in particular via leaching of (ultra)mafic rocks. For instance, Dubinina et al. (2020) showed submarine CaCO_3 to be hydrothermally precipitated by mixing alkaline fluids (pH up to 11) formed by serpentinization of locally occurring harzburgite with seawater (Lost City Hydrothermal Field: actively venting carbonate chimneys up to 60 m in height in the vicinity of the Mid-Atlantic Ridge; Ludwig et al., 2006). $\delta^{18}\text{O}$, $\delta^{13}\text{C}$ and $\delta^{88}\text{Sr}$ values were used to trace the CaCO_3 precipitation rates and $^{87}\text{Sr}/^{86}\text{Sr}$ ratios to value mixing proportions. Picazo et al. (2020) indicate low T serpentinite replacement by carbonates during seawater influx in the Newfoundland margin, where CaCO_3 deposits are associated with a sequential assimilation of manganese. $\delta^{13}\text{C}$, $\delta^{18}\text{O}$, $^{87}\text{Sr}/^{86}\text{Sr}$, and Δ_{47} values of vein calcites in pillow lavas were applied by Quandt et al. (2019) to discover timing and physicochemical conditions of postmagmatic fracturing, fluid circulation through the oceanic crust, and subsequent CaCO_3 precipitation.

Kaminskaite-Baranauskiene et al. (2023) found episodically introduced fluids into locally occurring Triassic rocks to precipitate fracture- and vug-filling calcite. Wang et al. (2023c) assessed fracture openings in a tectonically active, ultra-deep sandstone foreland basin (Kuqa depression in China) by $\delta^{13}\text{C}$, $\delta^{18}\text{O}$, and REE pattern of syntaxial calcite. Trace element and REE distribution of calcite in deep granitic fractures (Sweden) shows periodical coprecipitation (Kusturica et al., 2022). In analogous approaches, Drake et al. (2018) and Boch et al. (2019) used proxy data of recent CaCO_3 precipitates from solutions flowing in fractures of granite (Sweden) and of young CaCO_3 fracture fillings in a Fe-carbonate ore deposit (Austria) to study elemental uptake, flow behavior, fracture evolution and polymorph sequences. A prominent example of discharging geothermal solutions to yield CaCO_3 precipitation at the Earth's surface is the Pamukkale Geothermal Field (Turkey) including large sinter basins, where its origin is based on complex fluid mixing, water-rock interaction, input of mantle volatiles, and secondary CO_2 degassing (e.g. Alçıçek et al., 2019; Özgür and Uzun, 2022).

8.1.10. Carbonate diagenesis

Diagenesis of CaCO_3 deposits implies voluminous and complex aspects of dissolution, neoformation, re-crystallization of minerals as well as ion diffusion, fluid circulation and mixing, gas exchange etc., where besides physicochemical conditions and mineral structures, in particular pore volumes and conjunctures are driving forces for the diagenetic evolution/overprint (e.g. Engelhardt, 1960; Bathurst, 1975; Moore, 1989; Morse and Mackenzie, 1990; Morse, 2004; Moore and Wade, 2013; Immenhauser, 2022; Mehrabi and Tavakoli, 2024; see also section 8.1.1). Elemental, isotope and (micro/nano) structural proxies have been heavily used to understand diagenesis reaction kinetics, mechanisms and pathways and to reconstruct the evolution of CaCO_3 -bearing sediments, lime/dolostones, seawater and interstitial fluids (Martín-García et al., 2009; Pagel et al., 2018; Mueller et al., 2021; Chen et al., 2024; Holmden et al., 2024; Akhtar et al., 2024). Individual systems are characterized being rather fluid or rock buffered, where interstitial solutions may consist of marine solutions, meteoric water and brines (Pederson et al., 2019).

In this context, $\delta^{13}\text{C}$, $\delta^{18}\text{O}$, and $^{87}\text{Sr}/^{86}\text{Sr}$ isotope signals of (Mg) CaCO_3 were traditionally applied to distinguish elemental origins and formation temperatures (e.g. Veizer et al., 1999; Horita, 2014). Further

elemental ratios and stable isotope distributions such as of Ca, Sr, S, B, Mo etc. were applied to understand re-crystallization, aragonite-calcite transformation, redox change, ion diffusion and dolomitization process during (early) diagenesis (see also section 7). Herein we refer to the overviews given by Swart (2015), De Boever et al. (2017) and Immehauser (2022) on applications of individual proxies for diagenesis aspects.

Exemplarily, the following concepts are highlighted: Higgins et al. (2018) used coupled $\delta^{44}\text{Ca}$ and $\delta^{26}\text{Mg}$ values to understand the diagenetic history of shallow-water carbonate sediments (Bahamas and Australia), (ii) Müller et al. (2019) developed a dolomite specific $\Delta_{47}\text{T}$ relationship to calculate accurate T for its formation, (iii) Lv et al. (2018) used Zn—Sr isotope records combined with $^{87}\text{Sr}/^{86}\text{Sr}$, $\delta^{13}\text{C}$, $\delta^{18}\text{O}$ and Mn/Sr ratios of the Ediacaran Doushantuo Formation (China) to assess diagenesis effects, (iv) Fichtner et al. (2018) experimentally detected by the exposure of *Arctica islandica* shells to hydrothermal fluids that the sulfur isotope evolution of CAS and of the sulfate in the reactive fluid can act as proxy for diagenetic alteration of biogenic aragonite, (v) Casella et al. (2018) showed diagenetic alteration of modern and fossil brachiopod shell to be quantitatively assessed by micro-/nano-structural analysis, and (v) Staudigel et al. (2023) used fluid inclusion and dual-clumped isotopes to assess isotope kinetics, diagenetic exchange reactions and to reconstruct hydrothermal temperatures and $\delta^{18}\text{O}$ values of the reactive solutions.

8.2. Man-made environments

8.2.1. Overview

The man-made settings of CaCO_3 formation include differentiated environments influenced both by biogenic to geogenic and anthropogenic (e.g. operational) conditions. Widespread examples are the diverse scale deposits impairing (geo)technical water flows and circuits or energy (e.g. heat) transfers, i.e. unwanted mineral precipitates clogging channels, pipes and other technical components and making dedicated countermeasures and/or periodical maintenance (cleaning) procedures necessary. This includes preventive measures such as sensors operating in channels, water circuits or pipelines and the site-specific testing and application of chemical additives (inhibitors) against CaCO_3 scaling (Dietzel et al., 2013; Chaussemier et al., 2015). In contrast to natural settings of CaCO_3 precipitation, the man-made or technical settings mainly concern the actual and short-term state of typically undesired chemical sedimentation instead of long-term and mostly desired (paleo) environmental deposits. However, an advanced knowledge of fluid-solid interaction and the variable carbonate mineral growth dynamics elaborated from the study of natural environments (e.g. speleothems in caves) can be applied to carbonate mineralization in man-made settings such as geothermal power plants or infrastructure (Fig. 7). In principle, similar physicochemical processes and parameters determine the CaCO_3 crystallization and spatiotemporal progress of mineral growth and consequently the material characteristics like its consistency.

CaCO_3 is formed in various artificial channels and stream beds at ambient to elevated temperature conditions (Rinder et al., 2013). Scaling in tunnel drainages and travertine-like deposits in ancient or modern aqueducts constitutes widespread examples (Passchier et al., 2016b; Chen et al., 2019). Likewise, CaCO_3 precipitates from saline fluids - originating from deep reservoirs during geothermal energy or oil and natural gas production - constitute a major obstacle (Zarrouk and Moon, 2014; Kumar et al., 2018). This can result in narrowed inner diameters and blockage of boreholes and transport pipelines or reduced energy transfers in heat exchangers (Boch et al., 2017a; Fig. 7 A-C). CaCO_3 scaling and fouling processes further accompany water treatment, e.g. during desalination procedures of potable or industrial waters (Warsinger et al., 2015). CaCO_3 is also of major technical relevance in the concrete producing and processing industry, i.e. curing, cementation or weathering of construction materials (Galan et al., 2019).

Vein carbonates and trapped fluid inclusions are further investigated

in detail in the context of prospective nuclear waste disposal sites, e.g. Yucca Mountain (Dublyansky, 2014; Yardley et al., 2016). The technical settings also involve Ca- and Mg-carbonate formation in the course of CO_2 sequestration, i.e. carbon capture and storage (CCS) in deep sedimentary basins (Sanna et al., 2014; Khandozi et al., 2023). New concepts also combine CO_2 sequestration and carbonate crystallization with its utilization (CCUS), e.g. for deep geothermal CO_2 based energy production (Adams et al., 2015). In the laboratory, technical (synthetic) CaCO_3 formation targets fundamental, material scientific and industrial applications typically applying static steel autoclaves or dynamic flow reactors (e.g. Xu et al., 2019). Some laboratory experiments simulate specific environmental settings, e.g. biologically mediated calcareous tufa deposition or scaling in thermal water circuits (Pedley, 2014; Zotzmann et al., 2018).

Considering the variable mineralogy, fabrics and porosity, the diagenetic alteration of such CaCO_3 deposits with time is another aspect of high relevance, e.g. regarding the interpretation of acoustic properties (sonic velocity) of hydrocarbon bearing carbonate reservoirs, the utilization of travertine and tufa as a decoration and construction material of various ancient and modern buildings, as well as the paleoenvironmental interpretation of such chemical-sedimentary archives (Soete et al., 2015).

Experiments and analyses further focus on historic building materials and archeological artefacts involving CaCO_3 mineralization, e.g. lime mortar, plaster or concrete of ancient Greek, Roman or Medieval times (Kosednar-Legenstein et al., 2008). In principle, the development and application of experimental approaches and setups (see Fig. 8) provides a deeper insight into the main carbonate precipitation strategies not only for advanced techniques in artificial environments, but also for basic reaction kinetics and mechanisms in natural environments by transferring and adapting the individual experimental results from more controlled physico-chemical conditions to the complex specifications of nature. In Fig. 2 individual man-made CaCO_3 precipitation settings are schematically shown and referenced in the following sections.

8.2.2. Synthesis of carbonates

The synthesis of CaCO_3 from aqueous media can be induced by single and coupled reaction mechanisms and pathways, where in any case proper supersaturation levels and environmental control on individual precipitates have to be achieved (see also sections 2 and 4; e.g. Liendo et al., 2022; Zhong et al., 2024). In Fig. 8 eight typical concepts of experimental setups to precipitate CaCO_3 from aqueous media are schematically viewed: #1: mixing of two solutions with different chemical composition, mostly based on a Ca^{2+} and a DIC containing solution, #2: change in T, for instance, an increase in T by taking advantage on the retrograde solubility of CaCO_3 , #3: CO_2 exchange by pressure gradients induced $\text{CO}_{2(\text{g})}$ uptake into a commonly alkaline Ca^{2+} bearing solution or $\text{CO}_{2(\text{aq})}$ degassing from a $\text{Ca}-\text{HCO}_3$ rich solution into the atmosphere, #4: continuous addition (e.g. titration) of a stock solution usually containing Ca^{2+} HCO_3^- , CO_3^{2-} and/or OH^- into a $\text{Ca}-\text{HCO}_3$ rich solution, #5: decrease in volume of the solvent H_2O by (a) evaporation or (b) freezing, #6: double Ca^{2+} and (bi)carbonate ion diffusion through a hydrogel, #7: CO_2 gas diffusion through a membrane into a Ca^{2+} bearing solution, and #8: liberation of Ca and/or (bi)carbonate ions from solids into a reactive solution (including re-crystallization). These straightforward experimental concepts can yield in the development of highly complex individual CaCO_3 synthesis designs depending on the specific expectations and needs.

Exemplarily, the following techniques were designed to evaluate and quantify elemental and isotopic fractionation behavior during CaCO_3 formation and conditions for (trans)formation of individual solid CaCO_3 phases: #1: microfluidic injections into microchannels to trigger, monitor and tailor ongoing CaCO_3 precipitation (e.g. Xu and Balhoff, 2023). #2: Local heating by near-infrared laser light controls spatio-temporal CaCO_3 crystallization, where single crystals of vaterite, calcite, and aragonite can be positioned (Bistervels et al., 2023). #3a:



Fig. 7. CaCO_3 precipitation affecting various technical settings. A) Layered calcite dominated mineral deposit from thermal water in a horizontal steel pipeline of a geothermal facility for heat extraction (Kakasszék, Hungary). The morphology of the compact scale deposit results from a two-phase (liquid and gas) flow in the pipe. B) Scale-fragments exfoliating inside a steel pipe from a deep geothermal well (Kirchstocach, Germany). The rapidly formed scales consist of well developed rhombohedral calcite crystals and accessory metal sulfides and hydrocarbons (dark coloring). C) Massive block of cemented scale-fragments (see B) accumulated within few weeks only at the front end of a heat exchanger (obstacle) consequently impairing thermal fluid flow and electric power generation. D) Calcite and aragonite crystallization blocking water drainage in a highway tunnel (Semmering, Austria). E) Calcite rafts floating on the surface of stagnant water in a plastic pipe draining CaCO_3 supersaturated solutions in a railway tunnel (Koralm, Austria). F) CaCO_3 dominated and relatively porous scaling interrupted by detrital siliciclastic (sandy) layers (red arrows) from episodic water discharge and G) laminated (yellow arrow) and reddish (Fe) stained hard CaCO_3 scale both deposited in the same highway tunnel (Spital, Austria). Note the ripple structures and lateral bending of the latter channel deposit. H) Beige colored calcareous tufa like precipitation at the outflow of a plastic pipe towards a natural creek (Steinhaus, Austria). I) Different forms (stalactites, stalagmites, flowstones) of CaCO_3 and partially iron-stained mineralization in a railway tunnel (Koralm, Austria). J) Rapidly deposited carbonates encrusting boulders in a man-made concrete river bed (Longsgraben, Austria). K) The soft crusts consist of millimeter-sized and rarely documented ikaite ($\text{CaCO}_3 \cdot 6\text{H}_2\text{O}$) crystals indicative of strongly restricted, mostly low temperature formation conditions. L) Calcitic concretion ('lime pop'; blue arrow) crystallized in multi-component mortar cementing a historic Roman wall fragment (Ybbs, Austria). (For interpretation of the references to colour in this figure legend, the reader is referred to the web version of this article.)

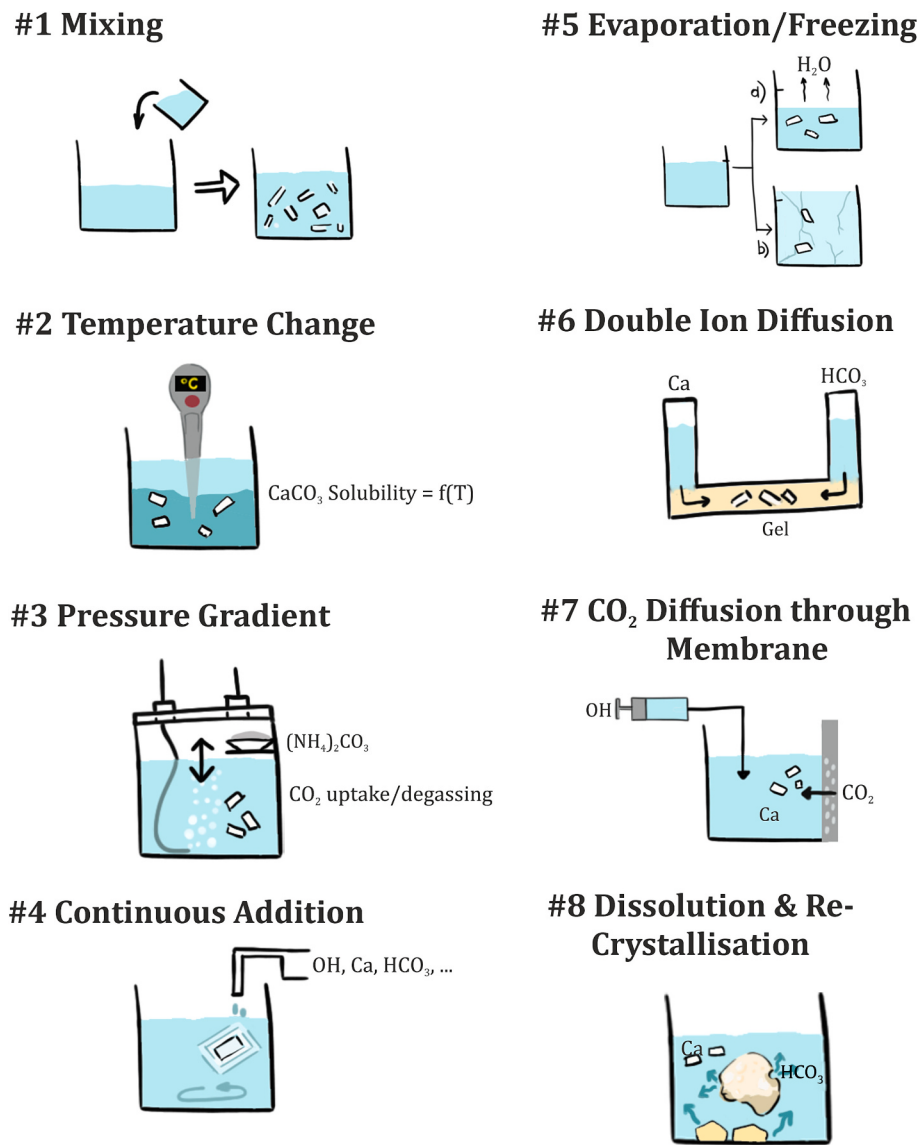


Fig. 8. Concepts of experimental setups to precipitate CaCO₃ from aqueous media.

Decomposition of ammonium carbonate ((NH₄)₂CO₃) releases ammonia and carbon dioxide to the atmosphere, where the uptake of both gases in the reactive solution results in an increase of pH and DIC, respectively (Gruzensky, 1967; Alkhatab et al., 2022); continuous CaCO₃ precipitation by CO₂ uptake into an alkaline Ca²⁺-bearing solution (e.g. Tiefenthaler and Mazzotti, 2022). #3b: Degassing of CO₂ regulates CaCO₃ formation by an increase of pH e.g. to quantify inhibition effects (Wedenig et al., 2021). #4: Continuous pumping of a Ca²⁺ and a CO₃²⁻ containing solution in a reactive solution, where ongoing bubbling of CO₂ keeps the pH constant (Tesoriero and Pankow, 1996; Mavromatis et al., 2018). #5: Calcite precipitation induced by evaporation of H₂O using a dehumidifier and ongoing refilling of the precipitating solution (Terakado and Taniguchi, 2006). #6: Double-ion-diffusion through a hydrogel, e.g. based on silica, agarose or sulfonic acid, allows ion diffusion controlled CaCO₃ crystallization (Katsikopoulos et al., 2009; Grassmann and Löbmann, 2003), where e.g. precipitation of ACC in agarose hydrogel was found to control CaCO₃ formation (Lopez-Berganza et al., 2019). #7: CO₂ gas diffusion though a membrane (e.g. polyethylene) into the reactive solution determines nucleation time and growth rate of CaCO₃ by membrane thickness and material density, where OH titration keeps the pH constant and traces carbonate nucleation and growth (Dietzel et al., 2004; Tang et al., 2014). #8: Providing

Ca and carbonate from dissolution (or transformation) of solids, such as dissolution of anhydrite in a carbonate-rich solution (Cuesta et al., 2018), carbonate liberation from decomposition of organics or classical dissolution-precipitation controlled re-crystallization of e.g. aragonite to calcite (Jacobson and Usdowski, 1976). The latter is in particular used to precipitate CaCO₃ at very low precipitation rates, thus approaching equilibrium elemental/isotope fractionation.

It has to be noted, that studying the controlling parameters for elemental and isotopic incorporation into CaCO₃, e.g. to calibrate individual environmental proxies, requires well-known physicochemical conditions during the experiment. This is commonly the case providing constant T, whereas keeping pH, precipitation rate, saturation stage, and/or solution composition constant is rather challenging or even impossible based on the concept of the experimental design (e.g. pH shift in #3 and ion concentration gradient in #6). Thus, experimental setups in the laboratory (and in the field) are essential to assess and verify individual (trans)formation sequences and the behavior of proxy signatures. Besides a large number of successfully used approaches, special sophisticated techniques are e.g. the use of micro-fluid cells and laser light control to follow and control local CaCO₃ precipitation.

8.2.3. Industrial and tailored products

Industrial approaches for processing and using of CaCO_3 are of high value for many disciplines (e.g. Tegethoff, 2001; Hashizume, 2022; see also section 1). Classically, fragments or grinded limestone/dolostone are used as bricks, aggregates, pigments, educts of cement and soda production etc. For instance, the so-called ground CaCO_3 (GCC) and precipitated CaCO_3 (PCC) are used for plastics, paints, pharmaceuticals, food, decolorization, cosmetics, cements etc. (e.g. Ghiasi and Abdollahy, 2022; Zhao et al., 2023). PCC as well as carbonate binders are produced by calcination of lime(dolo)stone at temperatures around 900 °C, which yields in the release of CO_2 and the formation of CaO (MgO), called (quick)lime. Lime and water exothermically react via “slaking” to form the mineral portlandite ($\text{Ca}(\text{OH})_2$). Portlandite creates upon its high solubility a Ca^{2+} -rich and strongly alkaline medium, wherein CO_2 is absorbed to precipitate interconnected CaCO_3 crystals, e.g. in a paste in conjunction with aggregates (lime mortar; see review on carbonation mechanisms of lime-based binders by Rodriguez-Navarro et al., 2023). Essential for the curing kinetics is - besides T, reactive surface area, H_2O content and additives (e.g. Mohd Darus et al., 2015; additive: chitosan to catalyze carbonation; Carmona-Carmona et al., 2023) - the availability of CO_2 , where the diffusion coefficients of CO_2 in air have to be about 10,000 times higher than in water (Van Balen, 2005).

In a similar approach tailored micro/nano-sized CaCO_3 crystals (PPC) are synthesized in large-scale reactors by trapping gaseous CO_2 in a “milk of lime” (aqueous suspension of lime) or other alkaline Ca^{2+} -bearing solutions such as Solvay wastewater (e.g. Jung et al., 2010; Farrag et al., 2022). The CaCO_3 precipitation kinetics, polymorphisms and shapes of precipitated CaCO_3 minerals can be adjusted by the kind of mixing, CO_2 uptake rates, concentrations of aqueous Mg, Sr, B, carbonic and amino acids etc. (see also sections 3 and 4; Isopescu et al., 2010; Liendo et al., 2022; Yan et al., 2024). However, during the ongoing CaCO_3 formation in alkaline media, besides common and distinct $\text{Me}-\text{CO}_3-\text{OH}-\text{H}_2\text{O}$ minerals, the so-called basic calcium carbonate ($\text{Ca}_3(\text{CO}_3)_2(\text{OH})_2\cdot\text{H}_2\text{O}$) was identified to be formed as a relevant metastable mineral throughout the carbonation process (e.g. Ripken et al., 2018; see section 2). Kobayashi et al. (2020) showed boron incorporation into PPC to be affected by aqueous pH, reaching a maximum at pH 10, thus the B content of PCC and its isotopic composition might be used as proxies for processing conditions (see sections 7.1.2 and 7.2.2).

Many exceptional approaches were realized to produce tailored and customized CaCO_3 such as its precipitation in the presence of electric and magnetic fields. The latter approaches have been developed in aspects of delayed CaCO_3 formation as well as change in polymorphism and morphology of the precipitates (e.g. Chen et al., 2019; Gao et al., 2020; Huang and Lin, 2023; see also section 4). The addition of sticky rice was used to regulate calcite growth and to create a denser microstructure and hydrophobic properties of lime mortar (e.g. Otero et al., 2019). Forjanes et al. (2022) suggested CaCO_3 building stones to be protected from weathering by micrometric-thick mineral cohesive layers of e.g. SrCO_3 / BaCO_3 ; both minerals, strontianite and whiterite, exhibit very low solubilities. Kandirmaz et al. (2020) assessed the addition of micro-sized CaCO_3 and cationic starch in paper coatings to optimize printability parameters. Gindele et al. (2023) claimed a liquid-like ACC precursor technique to be used for advanced material synthesis up to industrial scales in the scope of restoration, soil-stabilization, biomedical application etc. In a different amorphous precursor approach, Mg-stabilized ACC paste was used for 3D printing to develop new bio-inspired routes of low-temperature printing (Shaked et al., 2021). In this context, Jiang et al. (2022) successfully prepared stabilized ACC in water-free ethylene glycol without the addition of a stabilizer.

8.2.4. Water draining and supply

Most important purposes for draining of water are related to the supply of drinking water and process solution for cleaning, temperature

control, suspensions, reactive fluids, etc. as well as to drain off solutions from tunnel buildings, waste deposits, mining areas etc. (e.g. Bürgmayr et al., 2023; Li et al., 2023b; Galan et al., 2019 and references therein; see also section 8.2.5). In such systems, precipitation of CaCO_3 is mostly unwanted and frequently induced by (i) leaching of a given local natural or man-made material, thus liberating Ca, DIC and OH into the water, (ii) exchange of CO_2 between a gas phase and a $\text{Ca}-\text{HCO}_3$ -bearing solution, thus changing the distribution of DIC species, or (iii) a change of T (e.g. Rinder et al., 2013; Ye et al., 2021; see also section 4). Typical materials to be leached comprise lime-/dolostone, concrete/shotcrete and tailings, like lime kiln waste (e.g. Shen et al., 2022; Eichinger et al., 2020). Unwanted calcium carbonate deposits were already formed and cleaned in ancient water supply systems (e.g. Roman Empire; Sürmeli-hindi and Passchier, 2024).

Strategies to avoid these CaCO_3 scales are based on developing less leachable materials or its sealing from water, minimizing CO_2 degassing and/or evaporation, adjusting T and/or the chemical composition of the water. Technologies of water treatment to reduce CaCO_3 formation are based on adding scale inhibitors and/or pH controlling agents, desalination, mixing with water of low Ca and DIC content, applying magnetic fields etc. (e.g. Al et al., 2018; Sakoparnig et al., 2021; see section 4). It has to be noticed that the latter approach is known to change precipitation dynamics, structure and shape of CaCO_3 precipitates, but is less approved in large scale settings (e.g. Esmailnezhad et al., 2017). The pathway, mode and rate of CaCO_3 precipitation can be traced by *in-situ* monitoring of pH and electric conductivity, the evolution of content and ratios of the relevant dissolved species (e.g. DIC, Mg/Ca, Sr/Ca) and the composition of the precipitate, as well as the stable carbon and oxygen isotopic composition of the DIC and the precipitated CaCO_3 (e.g. Dietzel et al., 1992; Wedenig et al., 2023; see section 9).

8.2.5. Geothermal power plants

Geothermal heat and electricity productions are based on the extraction of thermal water from deep reservoirs (e.g. sedimentary basins) and frequently entails processes of unwanted mineral deposition (scaling), blockage of pore spaces (plugging) and material alteration (e.g. corrosion) affecting technical components (pipelines, pumps, filters, valves, heat exchangers) of the power plants (Fig. 7 A-C and Fig. 9). The hydrogeochemically differentiated aqueous fluids equilibrated with the regional aquifer host rocks and T and P conditions at depth typically feature elevated dissolved gas and aqueous species contents (brines). Under natural conditions (no technical intervention) the geothermal reservoirs reside near physicochemical equilibrium, i.e. water-soluble minerals reach a saturated state (Cosmo et al., 2022; Bu et al., 2022). Deep wells (e.g. production and reinjection wells of hydrothermal circuits), however, tapping the target aquifer and waters of long residence times always entail P, T and chemical gradient changes (disequilibrium) promoting outgassing, cooling, mineral formation and material alteration reactions. For example, most of the unwanted CaCO_3 precipitation (e.g. 60 to 90%; Cosmo et al., 2022) is typically related to the rapid release (flashing) of dissolved CO_2 in the course of hydrostatic pressure decrease. Common scale mineral deposits include various carbonates, besides sulfates, sulfides, (hydr)oxides, chlorides or silica phases (Finster et al., 2015). The scales possess more wanted or unwanted material characteristics, e.g. their variable material consistency and durability with regard to maintenance intervals and mechanical or chemical cleaning procedures (Candido and Zarrouk, 2017). Compact and brittle carbonate crusts strongly adhering to the underlying substrate material (e.g. pipe, valve) are more difficult to remove compared to soft mud-grade carbonate from nucleation in suspension being locally deposited at filters and heat exchangers (Fig. 7 A-C).

Corrosive constituents such as dissolved chloride, H_2S , CO_2 , O_2 , H_2 , as well as elevated T and flow rate favor sulfidic or oxidic steel corrosion (Valdez et al., 2009). The scaling and corrosion processes lead to dynamic and problematic reduction of inner diameters, disturbed flow regimes, local blockage, motion malfunctions, material deterioration

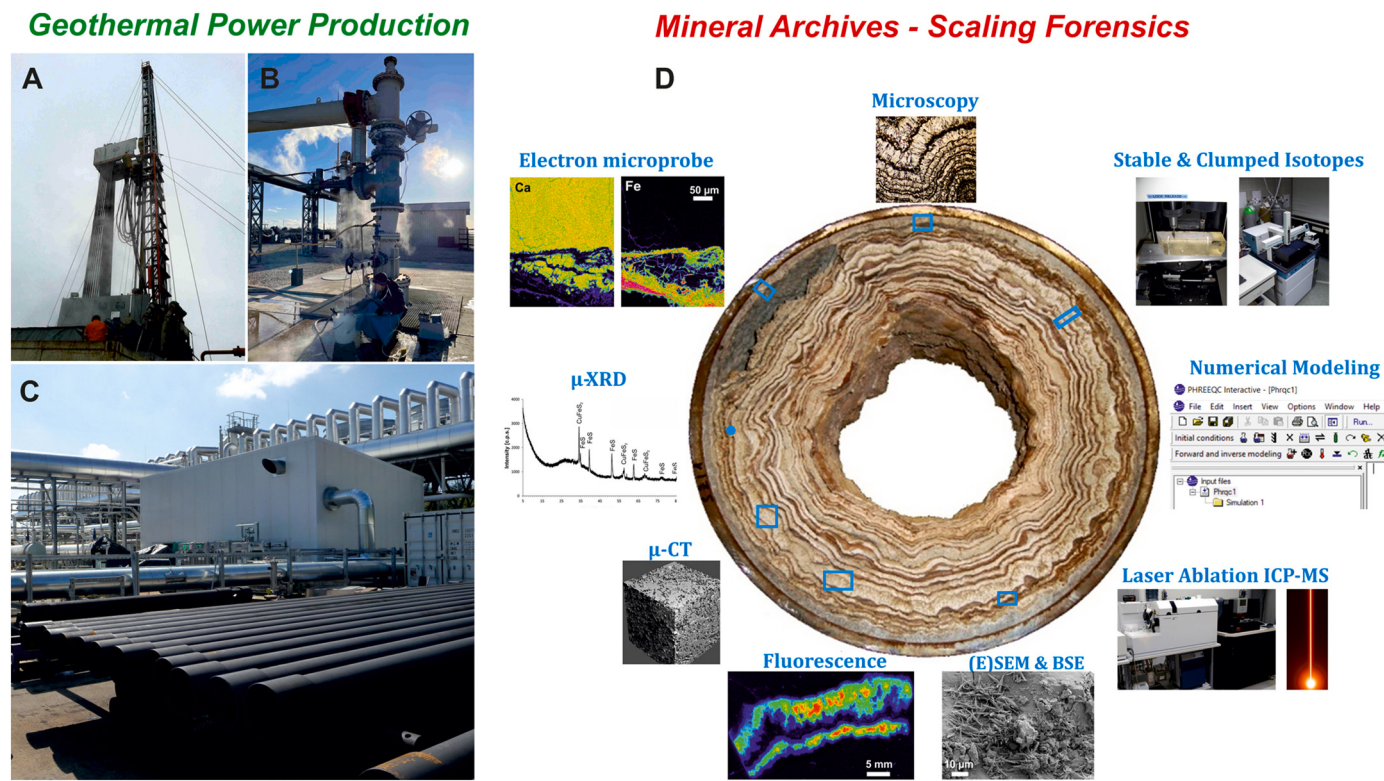


Fig. 9. A) Geothermal energy exploitation based on deep (production and injection) wells. B) Monitoring of thermal waters, gases and mineral precipitates at the wellhead. C) Scaling and corrosion in steel pipelines and various technical components (e.g. heat exchangers, filters, valves) of geothermal power plants. D) Concept of “Scaling Forensics” based on a multi-parameter approach involving high-resolution imaging, phase analytical, (trace) elemental and isotopic techniques. The mineral deposits constitute a spatiotemporally evolving chemical-sedimentary archive of site-specific natural and technical (operational) thermal fluid production conditions. A reconstruction and process understanding of (un)favorable conditions determining the variable scaling and corrosion progress are targeted.

and overall reduced heat and energy transfers. Their progress depends on natural (geogenic) as well as technical (anthropogenic) environmental conditions in the fluid circuit and this is highly installation- and even section-specific. Adjustable and operational parameters such as the prevailing physicochemical gradients, flow geometries and flow volumes and the construction materials used are of importance. Conditions such as two-phase fluid flows (water plus gas) in the pipelines and heat exchangers or recurrent production cessations can be of high relevance (Boch et al., 2017a; Bu et al., 2022). Natural preconditions encountered, however, are often decisive with respect to the initial scaling, plugging and/or corrosion potential and unwanted CaCO_3 deposits are mostly related to aquifers including lime- and dolostones, marls or calcareous sandstones. In Hungary, for example, geothermal exploitation has a longstanding tradition based on hydrocarbon exploration, thermal water and heat production for agriculture (greenhouses), balneology (medical recreation) and district heating (Szanyi et al., 2021). Most of the disturbing processes, such as scaling, corrosion and problems with water reinjection (plugging), are of relevance in the Hungarian Pannonian Basin. Likewise, in Belgium Pauwels et al. (2021) reported the unwanted occurrence of galena (PbS) and carbonate (witherite, siderite, rhodocrosite) scaling in heat exchangers and filters in combination with the co-precipitation of radionuclides (^{226}Ra , ^{210}Pb , ^{210}Po) constituting some problematic waste material (Eggeling et al., 2013).

The individual visual and chemical appearance of CaCO_3 dominated scale deposits encountered in the different geothermal facilities is an expression of the site-specific character of the scaling and corrosion processes (Boch et al., 2016; Haas-Nüesch et al., 2018). Thus, the unique chemical-sedimentary deposits capture (un)favorable thermal water production conditions in their chemical and fabric compositions, which can be evaluated in a scaling forensic approach (Boch et al., 2017b). In essence, “Scaling Forensics” is based on a multi-proxy laboratory

analytical approach involving state-of-the-art and mostly high-resolution mineralogical, geochemical and imaging techniques (Fig. 9). The detailed reconstruction of variable site-specific (long- vs. short-term) carbonate scale growth dynamics is envisaged, i.e. a qualitative and quantitative investigation of favorable (reduced scale deposition) and unfavorable (increased scaling) environmental and operational conditions. This involves parameters and processes such as varying T and P, fluid flow rate, CO_2 and H_2O (steam) separation, pH and pe (redox) changes, the mobilization of particles and elements (leaching), incompatible fluid mixing, effects from production cessations and the construction materials used (steels, plastics). Sustained or intermittent effects on the scaling and corrosion dynamics can result from these interrelated variables (e.g. Bowman et al., 2023).

Based on density contrasts, back-scattered electron imaging can be of value for the detection of organic tissues in the scales (Boch et al., 2017b), and microbes (e.g. bacteria, fungi) can also be visualized by fluorescence staining and microscopic imaging of fresh scale material surfaces using mixed dyes sensitive to nucleic acids (DNA, RNA) being present (e.g. Grengg et al., 2017). Further methods include micro-computer tomography (μ -CT) for resolving scale material contrasts such as variations in porosity at high spatial resolution (Ott et al., 2012), elemental distribution mapping ($\mu\text{-range}$) using electron probe microanalysis or by spot analyses of energy-dispersive X-ray spectra (Mittermayr et al., 2017). Minor and trace elemental concentrations of the solid scale materials might also be quantified applying different pointwise or continuous sampling strategies of laser ablation coupled to mass spectrometry, i.e. for high-resolution (10s of μm spot size) and sensitive (ppb range) chemical information (Almirall and Trejos, 2016). Spatially resolved analysis of $\delta^{13}\text{C}$ and $\delta^{18}\text{O}$ isotope signatures are sensitive with respect to outgassing of CO_2 and H_2O from the upflowing thermal fluid. This process is intimately coupled to the amount and rate

of CaCO_3 precipitation and consequently to the overall progress of scale deposition.

The diversified scale deposits in geothermal infrastructure also reveal a large set of indicative minerals and fabrics next to specific element and isotopic compositions (Fig. 7 A-C). Different minerals either form *in situ* (authigenic/autochthonous) or deposit after (detrital) mobilization (allochthonous) and their formation processes involve specific crystallization and depositional mechanisms, redox conditions or microbial contributions. For example, the occurrence of aragonite instead of calcite is often related to increased aqueous Mg/Ca ratios favored by dolomite aquifers or pronounced prior CaCO_3 precipitation along the water flow path (see sections 3 and 4). Dendritic (tree- or feather-like) calcite crystals are mostly indicative of high CaCO_3 supersaturation and rapid crystal growth, while micritic calcite (mud-grade carbonate) is found to be rather derived either from spontaneous particle nucleation in suspension favored by turbulent flow, or might originate from decaying biofilms (e.g. Pedley, 2014). In the CaCO_3 dominated scales, mineral layers (e.g. Fe-sulfides/Fe-(hydr)oxides) can form from (temporary) microbial activity associated with flowing or stagnant (production cessations) thermal water (Würdemann et al., 2016). These layers acting as distinct substrates have a significant effect on the progressing crystal nucleation and growth and thus on the scale material consistency and durability. The latter is also determined by different crystallization mechanisms such as homogeneous suspended particulate nucleation or heterogeneous crystal growth on some (in) organic substrate provided consequently favoring either loose crystal agglomerations or hard mineral crusts.

The forensic investigations of variable geothermal production conditions also support the role of distinct interfaces with regard to CaCO_3 scale initiation, progress and the resulting material characteristics. These interfaces include the layer between the scale deposit and the underlying substrate material, where the initial CaCO_3 crystallization and ongoing crystal growth is influenced by the substrate material, e.g. conventional or alloyed steel or different plastics used for pipes and other technical components (Bowman et al., 2023). For example, initial CaCO_3 nucleation can be enhanced on basal corrosion layers (Boch et al., 2017a). The attractive substrate mostly relies on a low degree of crystallinity, defect sites, high specific surface area and possible electric charges of corroded steel surfaces and its characteristic iron- and other metal (Cu, Zn, Ni) sulfide or (hydr)oxide minerals. A variable carbonate scaling progress is further affected by the scale growth surface versus streaming thermal fluid flow. Some scales show rough growth surfaces resulting from relatively large idiomorphic (e.g. rhombohedral) and oriented crystal terminations which favor an increased flow resistance, as well as the occurrence of (micro)turbulences at the fluid-solid interface and consequently enhanced CO_2 and H_2O outgassing (bubble formation) directly related to enhanced CaCO_3 precipitation (*in-situ* self-reinforcing mechanism; e.g. Boch et al., 2017a; Wanner et al., 2017). In some geothermal wells and pipelines delivering a high gas to water ratio, a two-phase fluid flow consisting of thermal water and gases (CO_2 , H_2O , CH_4 , N_2) as separate streams might persist (Jamero et al., 2018; Bu et al., 2022; Fig. 7 A). This often results in ascending bubbles, pulsating flow, enhanced turbulences and therefore in intensified scale deposition in some sections.

An advanced process understanding of diverse scale mineral deposition in combination with efficient problem-solving strategies and countermeasures constitute a lively subject of current research activities within the growing geothermal community. Key elements might be an increased working P and adjusted flow geometries in the geothermal water circuit, as well as more elaborate approaches of resolving fluid-solid interaction in the technical installations and thermal fluid producing reservoir (Wen et al., 2018; Stefánsson et al., 2019). Considering an enhanced understanding of scaling and corrosion processes numerical modeling constitutes another approach of increasing relevance (Cosmo et al., 2022; Cao et al., 2024; Bonto and Andreassen, 2024). For example, Ahmad et al. (2015) applied numerical modeling for the

prediction of dissolved carbonate versus carbonate scaling and Khasani and Itoi (2021) investigated effects of variable CO_2 contents in thermal waters and carbonate scale deposition on the fluid flow and power output. Different hydrogeochemical modeling approaches were used by Ma et al. (2023) for the prediction of CaCO_3 and silica scaling related to sandstone reservoir in the Xi-an Basin (China) and Markó et al. (2021) analyzed widespread problems related to scaling and plugging during thermal water reinjection into sandstone reservoirs of the Hungarian Pannonian Basin based on numerical modeling of aqueous speciation and variable operational parameters.

Unwanted CaCO_3 precipitation in the context of geothermal energy exploitation is further investigated by laboratory experiments - in combination with computer-based numerical modeling (Zacherl and Baumann, 2023). Schäffer et al. (2022) used autoclave experiments in combination with hydrogeochemical modeling for an investigation of subsurface conditions and unwanted chemical reactions at different T (30, 90, 150 °C) related to scaling, leaching (dissolution) and plugging in Permian and Triassic sandstones of the North German Basin and Upper Rhine Graben. Laboratory and field-based tests are also used in order to evaluate the performance and optimized application (e.g. selected agent, product and dosage) of scaling and corrosion inhibitors, i.e. a directly intervening countermeasure against unwanted mineral precipitation from thermal waters (Huttenloch et al., 2019; Rangel et al., 2019; Spinthaki et al., 2021). Bu et al. (2022) conducted a field experiment in China targeting the evaluation of three different inhibitors (acrylic copolymer, sulfonated ionic polymer, sodium polyacrylate) with diverse effects (complexation, dispersion, electrostatic repulsion, crystal distortion) against CaCO_3 scaling. They found a high inhibitor efficiency at dosages between 20 and 40 ppm and also emphasized the high relevance of flashing point determination and the location of inhibitor addition (e.g. Khasani and Itoi, 2021).

The technical injection and partial circulation of CO_2 is currently under critical evaluation as an alternative working fluid for combined geothermal energy extraction and CO_2 storage underground (Garapati et al., 2017; Esteves et al., 2019). CPG (CO_2 Plume Geothermal) systems as a form of CCUS (Carbon Capture Utilization and Storage) use CO_2 in its supercritical state as the subsurface working fluid in sedimentary reservoirs overlain by impervious caprocks and these geothermal systems are considered to produce more baseload capable electricity at moderate T and permeability conditions than hydrothermal systems (Fleming et al., 2020; Adams et al., 2021). Geothermal energy production is further being evaluated in connection with compressed air energy storage (CAES) which uses the injection and discharge of air in order to balance excess electricity supply (vs. demand) from clean energy technologies (Li et al., 2020). CPG and CAES are increasingly studied with regard to geogenic versus technical (pre)conditions of fluid-solid interaction (e.g. carbonate dissolution and precipitation) in the target reservoirs and aquifers applying a broad range of methodological approaches.

8.2.6. CO_2 sequestration

As a consequence of ongoing global climate change and increasing atmospheric CO_2 concentrations, carbon capture and storage (CCS) is considered a promising geoengineering approach for the retroactive reduction of significant CO_2 volumes emitted from major industrial sources (refineries, power plants, chemical and concrete factories) or being absorbed from the Earth's atmosphere (Lackner, 2003; Sanna et al., 2014; Oelkers and Gislason, 2023). In principal, CO_2 sequestration can be based on direct air capture with synthetic sorbents (DACCSS) involving enrichment/purification and (sub)surficial carbon mineralization (Kelemen et al., 2020). Surficial carbon dioxide removal (CDR) from air typically entails the reaction of CO_2 -enriched air and surface waters with highly reactive (e.g. crushed, increased surface area) mine tailings, industrial waste or sedimentary rock fragments, while *in-situ* CDR typically means the circulation of CO_2 -enriched water in rocks and reservoirs. Geologic carbon sequestration is essentially based on the

natural and technically enhanced potential of rock formations underground being far from chemical equilibrium with principal atmospheric and hydrospheric constituents, i.e. having a potential energy ready for rapid reaction and eventually (permanent) mineralization (Kelemen et al., 2020).

CCS typically implies large CO₂ volumes (mega- to gigatons) being stored underground in order to have a significant effect on the atmospheric greenhouse gas contents. Industry-sized CO₂ sequestration is typically associated with the injection of compressed CO₂ into depleted oil and gas fields (Enhanced Oil Recovery; Enhanced Gas Recovery) or the dissolution and mineralization of CO₂ in deep sedimentary basin formation waters/brines (DePaolo et al., 2013). In most cases purified CO₂ or mixed gas (e.g. CO₂/H₂S) is injected into various reservoir host rocks, such as different basalts, ultramafic rocks (e.g. peridotite) or sandstones (Matter et al., 2016; Raza et al., 2019; Rasool and Ahmad, 2023). Importantly, the CO₂ must remain in the subsurface, i.e. dense ("gas-tight") cap rocks (e.g. shales) overly the storage reservoir and protect other horizons (e.g. potable water aquifers) from leakage and related unwanted effects. In this context, the spatiotemporal evolution and reactions involving the CO₂-carbonate chemical system are also critically evaluated with respect to regional sedimentary and tectonic structures (e.g. storage vs. cap rocks), specific well configurations, near well versus distal reservoir alteration, potential leakage to nearby aquifers or the atmosphere and the appropriate sampling and monitoring and hence verification strategies (Wolff-Boenisch and Evans, 2014; Matter et al., 2016).

The mineralogy and geochemistry of intimately interrelated CO₂ versus groundwater versus reservoir rocks versus secondary mineral precipitation, dissolution or mobilization play a crucial role and implies a process understanding on broad spatial (nanometer to kilometer) and temporal (seconds to millennia) scales (Kharaka et al., 2006; Ott and Oedai, 2015; Oelkers and Gislason, 2023). The purified and compressed CO₂ is typically injected and flowing in its supercritical state (scCO₂; T_c = 31 °C, P_c = 7.4 MPa) in the porous and/or fractured rock formations. At the relevant T and P conditions scCO₂ is not easily soluble in water and brine, i.e. the scCO₂ and water/brine possess a significantly different density and viscosity (CO₂ both lower) and therefore behave like two separate phases and flow regimes (DePaolo et al., 2013). Water and brine show a stronger adherence (wetting) to mineral surfaces (thin coatings on mineral grains) while scCO₂ behaves more like a non-wetting phase promoting bubble formation in the pore spaces. This might lead to an incomplete water/brine displacement in the reservoir rocks and the injected CO₂ further tends to move upwards (necessity of impermeable cap rock). In this context, it is a challenge to predict the spatiotemporal behavior of scCO₂ in the subsurface (e.g. in flow and reactive transport models) and problems such as mineral scaling and plugging (e.g. closing of pore throats) near the injection well(s), corrosion of components (steel, concrete) and a successive reduction in the reservoir permeability have to be considered. In general, the solubility of CO₂ mostly depends on P, T and ionic strength/speciation (salinity) and a maximum conversion of scCO₂ to (bi)carbonate ions dissolved in water/brine or enhanced carbonate mineral formation are critical steps for CO₂ removal (Kelemen et al., 2020). Thus, different CO₂ trapping mechanisms exist, i.e. physical trapping of CO₂ in pore spaces, CO₂ dissolution in water/brine and mineral trapping (Khandozzi et al., 2023). Dissolved CO₂ entails a pronounced acidification of the water/brine and consequently leads to enhanced reaction with silicate (and other) minerals of the reservoir rocks (Berndsen et al., 2024).

In principal, technical CO₂ sequestration might therefore be considered as a form of induced and enhanced silicate weathering involving CO₂ removal at elevated T and P. Silicates of major relevance include pyroxenes, feldspars (e.g. anorthite), olivine, amphiboles, wollastonite, chlorite and serpentine, which facilitate the release of divalent cations (Ca²⁺, Mg²⁺, Fe²⁺) reacting with (bi)carbonate to form solid carbonate minerals and alteration products (e.g. calcite, (hydro) magnesite; Oelkers and Gislason, 2010). The preferential formation of

hydrated magnesium carbonates over magnesite and dolomite and their potential relevance for CCUS was investigated by Santos et al. (2023) and their results support a slow dehydration of hydrated Mg cations which impairs the overall carbonation process (kinetic restriction). The progressive solid-phase carbonation might also involve precursor and amorphous mineral phases and the process of carbonate nucleation and crystal growth is typically considered rapid in comparison to silicate dissolution and in some cases only a minor proportion of the injected CO₂ is mineralized (e.g. Kelemen and Matter, 2008; DePaolo et al., 2013). An understanding of the spatial distribution of reaction products and their quantities, the evolution of porosity and permeability, pressure build-up and unwanted effects such as induced seismicity and contamination of freshwater is therefore critical (Kelemen et al., 2019; Khandozzi et al., 2023).

An increased process understanding related to CO₂ sequestration is pursued in laboratory experiments based on representative physico-chemical conditions in different types of reactors combined with appropriate monitoring and analytical strategies (e.g. Gysi and Stefansson, 2011, 2012 and 2012; Tutolo et al., 2015; Berndsen et al., 2024), field testing (Matter et al., 2016), as well as computer-based numerical simulations facilitating reactive transport modeling (Harrison et al., 2019; Raza et al., 2019; Bonto and Andreassen, 2024). Examples of recent projects conducted in the field of CCS are the injection of major CO₂ volumes into depleted oil and gas reservoirs such as the off-shore Snøhvit and Sleipner gas fields (Barents Sea, Norway), the Quest CCS facility run by Shell (Alberta, Canada) or the In Salah CCS project run by BP and Statoil in Algeria (Mathieson et al., 2011; Kelemen et al., 2019). A promising study was reported by Matter et al. (2016) who investigated the permanent disposal of CO₂ at the CarbFix test site near the Hellisheiði geothermal power plant on Iceland. In less than two years, 95 % of the pressurized CO₂ injected into highly reactive basalts was fixed in carbonate minerals (Matter et al., 2016).

An advanced concept of Carbon Capture Utilization and Storage (CCUS) consists in storing and circulating CO₂ as a geothermal working fluid for heat and enthalpy extraction in the context of renewable, sustainable and baseload-capable energy production (Esteves et al., 2019; Adams et al., 2021). This can further be distinguished in CO₂-enhanced geothermal systems (EGS) typically exploiting different rock and reservoir types in 4 to 7 km depth (Pruess, 2006), as well as CO₂-plume geothermal systems (CPG) targeting porous sedimentary aquifers in 1 to 4 km depth covered by some impermeable cap rock (Randolph and Saar, 2011; Adams et al., 2015). The major CO₂ volumes again derive from industrial producers or eventually the atmosphere and deep saline aquifers as well as depleted oil and gas fields are the potential reservoirs of primary relevance. Importantly, the compressed and supercritical-state CO₂ holds some interesting thermodynamic properties, for example carrying a total exergy (amount of mechanical work a fluid at specific temperature and pressure can provide) 4 to 16 times higher than water for geothermal heat and electric power production (Esteves et al., 2019). At moderate temperature and permeability CPG systems can therefore generate more heat and/or electricity than hydrothermal (brine) systems (Adams et al., 2021). In comparison to thermal water, the supercritical CO₂ at elevated pressure and temperature reservoir conditions offers a lower kinematic viscosity (higher mobility) resulting in increased flow-through and energy extraction rates (Garapati et al., 2015). The significantly higher thermal expansion coefficient of CO₂ also results in a buoyancy related and pronounced thermosiphon effect enhancing the circulation and energy recovery from this working fluid while reducing parasitic electric power consumption (pumps). Unwanted scaling processes often involving calcium carbonate mineral precipitation from saline thermal waters and affecting different technical components of the geothermal installations are largely avoided when CO₂ is exploited as the geothermal working fluid (see section 8.2.5).

An interesting research direction further represents the interaction of CO₂ sequestration with organic constituents and (micro)biological

activity. Regarding the typical depth zonation of CC(U)S some interaction with biomass and microbial (bacterial) populations is anticipated (DePaolo et al., 2013). Khandozzi et al. (2023) discussed an increase of CO₂ solubility and enhancement of CO₂ mineral trapping by co-injection of CO₂ with water plus additives (e.g. bio-generated carbonic anhydrase) or selected microbes (carbonate-forming bacteria, urea bacteria; see section 8.2.8). An interesting study was further reported by Peck et al. (2023) who studied carbon sequestration in the context of wollastonite mining in the Adirondack Mountains (NY, USA). In crushed ore the cementation of wollastonite by calcite and opal was observed ($\text{CaSiO}_3 + \text{CO}_2 \rightarrow \text{CaCO}_3 + \text{SiO}_2$), i.e. a form of silicate weathering and carbonation. Based on the observation of distinct biofilms and indicative isotope signatures a major role of microbes in the mineralization process and for CO₂ sequestration were inferred.

8.2.7. Ion removal and recovery

The application of CaCO₃ to remove dissolved ions from an aqueous medium is well established and covers a wide range of man-made environments, in particular for environmental heavy metal ion mitigation, remediation and/or recovery. Typical examples are based on (i) sorption of Zn, Cd and Cr on calcite to purify industrial wastewater in a continuous flow system (García-Sánchez and Álvarez-Ayuso, 2002), (ii) removing of Cd from water by calcite-otavite solid solution formation induced by aragonitic freshwater mussel shells (Van et al., 2019), (iii) coprecipitation of Cd and Zn with CaCO₃ for durable sequestration of toxic metals (Kim et al., 2023b), (iv) fixation of heavy metal ions from coal fly ash leachate by coprecipitation (metastable) CaCO₃ phases induced by CO₂ uptake (Hunter et al., 2021), and (v) immobilization of arsenic oxyanions by carbonation of CaO (Khan et al., 2023).

CaCO₃ is also used to remove phosphate from solutions, where for instance Mg-stabilized ACC (ACMC) have been proven to incorporate significant higher PO₄ concentrations compared to calcite (Xu et al., 2014). Monovalent cation recovery from solutions is mainly based on Li by liming (CaO/Ca(OH)₂ addition) or by adding a DIC source (e.g. Na₂CO₃), where ultrasound can accelerate the nucleation of Li₂CO₃ (e.g. Li et al., 2019b; Zhao et al., 2019b). Zeng et al. (2020) found the efficiency of Pb ion removal from wastewater to be increased by activating solid CaCO₃ via milling, where PbCO₃ is finally formed. Pb ion removal experiments conducted by Roza-Llera et al. (2024) indicate (i) biogenic CaCO₃ to be more active than inorganic counterparts caused by higher reactive surface areas and (ii) biogenic calcite to perform better than biogenic aragonite in a long-term. The latter feature is due to randomly oriented growth of cerussite (PbCO₃; aragonite type; see section 2) onto calcite to prevent surface passivation, whereas its orientated growth on aragonite is passivating its surface.

Boosted techniques to remove and/or recover metal ions from a solution are based on microbially/enzymatically induced carbonate precipitation (e.g. Wang et al., 2023d; see also section 8.2.8). Exemplarily, for microbial-induced carbonate formation the ureolytic bacterium *Ochrobactrum* is applied to reduce phytotoxicity effects of Cd in soils (Zakrzewska et al., 2023), *Sporosarcina luteola* is used for bioimmobilization of toxic metals (Cuaxinque-Flores et al., 2020), *Enterobacter* yields in bioremediation of ⁹⁰Sr (Su et al., 2023).

8.2.8. Microbial-induced carbonate precipitation

Microorganisms can have a decisive role in the formation of CaCO₃, which results in a wide range of environmental and engineering implications and applications to reduce resources and energy-intensive manufacturing (e.g. for constructions, soil stabilization, sealings, biotechnology and medical fields: Akyel et al., 2022 and Zhang et al., 2023; see also section 8.2.7). Robles-Fernández et al. (2022) summarized the current knowledge on the implications of microbial cells and metabolic products - such as EPS, proteins and amino acids - on adsorption of ionic species, nucleation phenomena, as well as structure, size, and morphology of CaCO₃ precipitates.

The major processes involved in microbial-induced carbonate

precipitation (MICP) are (i) urea hydrolysis, (ii) ammonification of amino acids, (iii) denitrification, (iv) dissimilatory sulfate reduction, (v) nitrate reduction, (vi) photosynthesis, and (vii) oxidation of methane or organic salts (e.g. Castro-Alonso et al., 2019; Akyel et al., 2022). MICP pathways have been explored for potential engineering applications such as building stones and self-healing concrete (e.g. De Belie and Wang, 2016; Chetty et al., 2021). For the latter purpose MICP techniques can seal micro-cracks in concrete or other artificial rocks by precipitation of calcite and rarely aragonite or vaterite (Vijay et al., 2017; Zhang et al., 2019b; Jafarnia et al., 2020). Zehner et al. (2021a) assessed the impact of calcite seeds during MICP by monitoring pH and optical density evolution to be indicative of complex CaCO₃ (trans)formation pathways, including ACC formation.

Enzyme-induced carbonate precipitation (EICP) catalyzes the hydrolysis of urea into ammonium and carbonate ions by the enzyme urease (e.g. Ahenkorah et al., 2021). In addition, the enzyme carbonic anhydrase can fasten the formation of CaCO₃ by catalyzing CO₂ hydration (e.g. Rosewitz et al., 2021; see sections 6 and 7.2.2). MICP and EICP techniques are also used for soils and sediments - like sands, beach rocks and loess - for stabilization, reinforcement, remediation of contaminants, enhancement of oil recovery through bio-plugging etc. (e.g. Liu et al., 2022a; Cheng et al., 2021). However, both techniques yield in the formation of ammonia, where its gaseous emission in the environment can be reduced by stimulating pH and/or by adsorption onto or intercalation into clay minerals, activated carbon, zeolite etc. (e.g. Lee et al., 2019; Jafarnia et al., 2020; Yan et al., 2022). Zehner et al. (2021b) and Shu et al. (2022) monitored in real-time the MICP/EICP process in microfluidic porous chips, which is simulating quasi-2-dimensional pore structures etched and sealed in a transparent material.

In particular, *in-situ* monitoring of local pH combined with non-destructive Raman micro-spectroscopy were found to be a promising approach for unravelling reaction kinetics and mechanisms at the pore scale to understand the MICP/EICP controlling parameters (Zehner et al., 2021b).

8.2.9. Archeometry

Archeometric studies on the composition and the formation of CaCO₃ in aquatic media are voluminous comprising forensic tasks from historical processing/application of binders and pigments to aspects of provenance, trade and migration routes, and environmental changes (e.g. Válek et al., 2013; Lindroos et al., 2018; Falkenberg et al., 2023; Oriols et al., 2022; Petchey et al., 2022; Barrett et al., 2023). Herein a couple of archeometric approaches to trace and assess the origin and/or the formation conditions of CaCO₃ are exemplarily introduced.

A highly prominent man-made CaCO₃ formation setting is referred to historical carbonate binder, e.g. lime mortar or plaster, where its composition can hint on the provenance of the raw materials, processing technology, age of constructions etc. (e.g. Fort et al., 2023). Boese et al. (2023) identified from mineralogical and micro-chemical and -structural analyses of historical mortar/plaster of a building in Solunto (Italy) individual processing concepts and distinct raw materials for their production, thus shedding light on trade routes and divers building technologies. Falkenberg et al. (2023) used calcareous nannofossils - relics of shells of marine algae - in various historical binders to reconstruct the provenance of the raw materials, but also to reveal information on the processing of a given historic mortar, like the degree of burning temperature. Kosednar-Legenstein et al. (2008) applied stable carbon and oxygen isotope signatures of Roman, medieval and early modern carbonate binders to identify and quantify the setting pathways within the matrix by their linear correlation. Different deviations from this isotopic correlation line can trace different sources of H₂O used for slaking, evaporation effects, origin of carbonate (e.g. from atmospheric/biogenic CO₂; relicts of the primary limestone), and secondary effects (e.g. recrystallization of CaCO₃). Even ancient hydraulic lime mortar of a Punic-Roman cistern (Pantelleria Island, Italy), which was in contact with fresh water for about two millennia, preserved chemical

and isotopic signatures to trace ancient formation strategies and processing periods (Dietzel et al., 2016).

Although being far from routine applications, radiocarbon dating of historical lime binder - besides optically stimulated luminescence dating of quartz aggregates - was frequently and successfully used to get reliable information about construction and repair histories (e.g. Labeyrie and Delibrias, 1964; Urbanová et al., 2020). In the “pure lime lumps” strategy for ^{14}C dating the main challenge is based on providing exclusively pristine isotope signals from the ancient atmospheric CO_2 used for carbonation, which can be valued by complex pre-analyses of the chemical, mineralogical and in particular of the stable C and O isotopic composition on extracted binder samples (e.g. Kosednar-Legenstein et al., 2008; Dietzel and Boch, 2019; Fig. 7 L). In the “chemical separation” technique the time-resolved ^{14}C data of liberated CO_2 throughout acidification with phosphoric acid was used to distinguish between fast and slow reacting lime binder and limestone, respectively (e.g. Van Strydonck, 2016). In the “thermal decomposition” approach separation of the ^{14}C signals of the (pristine) lime mortar from e.g. charcoal or coke from lime production, limestone (or incompletely burnt limestone) or secondary re-crystallized calcite is obtained by sequential heating (e.g. Barrett et al., 2021).

Special foci are given on organic additives to historical lime binders (see Hwang et al., 2022). Sticky rice additions in ancient Chinese mortar significantly increase adhesive strength, toughness, and watertightness by interconnections of rice membranes and calcite crystals and slower carbonation (Yang et al., 2009; see section 8.2.3). George and Jayasingh (2021) reported plants, fruits and parts of vegetables to be added in lime mortar in India to fasten setting and to promote sustainable and eco-friendly repair mortar. In Pre-Columbian civilizations in Mesoamerica highly plastic lime mortar with enhanced properties were prepared by adding nopal juice into lime slurries to stimulate the formation of nanosized $\text{Ca}(\text{OH})_2$ crystals, which act as a nucleation inhibitor and crystal shape modifier via specific adsorption of polysaccharides.

Moreover, MICP is applied for the restauration of historic monuments, e.g. surfaces of ornamental stones (e.g. Adolphe et al., 1990; Castanier et al., 2000; see section 8.2.8). Carbonation of lime was recently shown to follow the sequence of hydrated ACC, anhydrous ACC and the formation of crystalline polymorphs of CaCO_3 (finally calcite), which is essential to be understood to design proper strategies for conservation of respective fresco paintings (Oriols et al., 2020).

Archeological assemblages of CaCO_3 of food shells, fish otoliths etc. are heavily applied to record seasonal (paleo)environmental changes and resources using proxies like isotopes (e.g. $^{87}\text{Sr}/^{86}\text{Sr}$, $\delta^{18}\text{O}$, $\delta^{13}\text{C}$) and trace elements (e.g. Mg/Ca, Sr/Ca) (Cook et al., 2016; Disspain et al., 2016; Prendergast et al., 2018; see section 7). In this context, age determination, such as ^{14}C dating, is essential to recover past environments, societal and/or climate dynamics, where potential alteration of the CaCO_3 has to be considered (e.g. Petchey et al., 2022).

Recently, Sürmelihindi and Passchier (2024) provided a comprehensive overview about the use of ancient CaCO_3 precipitates in historical water supply/draining systems as hidden archives for archeology and environmental sciences (see also section 8.2.4). Such carbonate scaling, most prominent in ancient aqueducts, can indirectly mirror urban development, population- and socioeconomic dynamics, paleoclimate changes, and environmental pollution, which is based on changes in water composition, T, biological content, and water supply management (e.g. Sürmelihindi et al., 2013; Passchier et al., 2016a; Sürmelihindi et al., 2023). Calibration of proxy information of the commonly annually laminated carbonate deposits in aqueducts by $^{230}\text{Th}/\text{U}$ -dating requires the consideration of frequently large amounts of initial detrital Th (e.g. Wenz et al., 2016; see section 7.2.1).

In some cases, the travertine and tufa precipitates are also associated with archeological artefacts or hominid remains of ancient civilizations, e.g. during the Neolithic evolution in Slovakia (Šolcová et al., 2018). Meyer et al. (2017) studied a fossil travertine occurrence of hydrothermal origin on the Tibetan Plateau (4270 m a.s.l.) exhibiting well

preserved hand- and footprints of six human individuals. $^{234}\text{U}-^{230}\text{Th}$ dating supports human occupation of the remote area at ~ 7.4 kyr BP (minimum age) and potentially older up to 12.7 kyr BP.

8.2.10. Healthcare and medical applications

CaCO_3 solids are used for healthcare and medical applications in many ways comprising concealer, toothpaste, body scrub, and face wash as well as products for biosensing, diagnostics, targeted delivery of (oncology) drugs, immunomodulation, tumor imaging, tissue engineering, and Ca supplementation (e.g. Shan et al., 2007; Qi et al., 2018; Baldassarre et al., 2020; Fadia et al., 2021; Zhao et al., 2022b; Liu, 2024b). For such an extremely divers application range of CaCO_3 grinded and in particular precipitated CaCO_3 is used, where advanced products are mostly referred to CaCO_3 micro- and nanoparticles (e.g. Won et al., 2010; Fadia et al., 2021; Galotta et al., 2023). Herein, the focus is given on the potential of ACC as “a star ascending in the realm of biomedical application” (see Liu et al., 2024b). ACC can be synthesized as highly porous CaCO_3 to act as a carrier in life science, pharmaceutical and medical applications, where impurity-free or individually stimulated ACC is preferred (e.g. Ihli et al., 2014; Lundin et al., 2017; Avaro et al., 2019b; see sections 3 and 6).

For instance, porous ACMC acts as a carrier for hydrophobic drugs (Liu et al., 2022b). Göçtü et al. (2023) developed selenite-containing ACMC nanoparticles, where the release of selenite ions can inhibit bacterial growth. Gadolinium-containing ACC was synthesized as a highly hydrated paramagnetic material to be used as Magnetic Resonance Imaging contrast agent (Dong et al., 2022). Besides Mg ions, highly diverse components, including silica, phosphate and organics, can be added to stabilize and/or tailor ACC depending on the individual application (Kellermeier et al., 2010; Liu et al., 2024b). In this way, ACC is applied for bone tissue engineering due to its excellent biocompatibility and ability to release bone mineral constitutive ions, where Merle et al. (2022) studied pyrophosphate-stabilized ACC to design novel tunable amorphous and bioinspired inorganic bone substitute materials.

ACC is also studied in its usability as nutrient for humans, e.g. to decrease inflammatory and muscle damage response for trained individuals (Hoffman et al., 2022). Future research on nanosized ACC is highly encouraged and promising to develop innovative and novel medical products for a wide range of use and applications with the advantages of CaCO_3 being non-toxic, biodegradable, responsive, and highly abundant (Liu et al., 2024b and references therein).

9. Environmental monitoring

Monitoring campaigns in various natural and technical settings - involving a broad range of environmental parameters - constitute an attempt of increased process understanding of modern and past CaCO_3 formation and alteration. The determining mechanisms of spatiotemporally variable fluid-solid interaction, environmental proxy dependencies and the monitoring approaches applied are strongly site-specific. The natural places and technical installations being the subjects of differentiated observational programs include springs and streams, soil and permafrost, karst and cave systems, geothermal and hydrocarbon wells and reservoirs or the drainage systems (e.g. Schölderle et al., 2021; Eichinger et al., 2023).

In-situ time-resolved analysing of CaCO_3 precipitation is further relevant for biominerization or in the industrial material sciences based on Raman spectroscopy and other techniques (e.g. Purgstaller et al., 2016; Sevilgen et al., 2019). Monitoring of specific parameters and processes is always tied to data acquisition based on analytical techniques and instrumentation being restricted by its sensitivity and (limited) spatial and temporal resolution of the geogenic or anthropogenic (operational) conditions. The measurements (e.g. flow rate, pH, concentration) can be done in regular or irregular time intervals at one or multiple sampling points of the system being monitored. The distribution and density (spacing) of the sampling sites (e.g. different

sections) and the frequency of sampling intervals (e.g. seconds to annual) has to be arranged in compliance with the parameters and processes (e.g. CaCO_3 precipitation) of interest, i.e. the timing, duration, progress of the relevant environmental variables should be captured. For example, effects of the prevailing weather conditions (e.g. storm event) on a karst spring or the air exchange (atmosphere) in a tunnel affecting the hydrochemical or air composition should be based on a high temporal (e.g. 5 min) resolution monitoring approach (Celle-Jeanton et al., 2001; Ozyurt et al., 2014), in contrast to the long-term evolution of water recharge and discharge of aquifers or inter-annual environmental trends such as global warming (e.g. Mechal et al., 2017; IPCC, 2023). Considering the differentiation of causes and effects, the spatiotemporal strategy has to be well-balanced, i.e. low-resolution monitoring runs the risk of an oversimplification while a high resolution approach might suffer from unfavorable signal to noise detection and overwhelming data acquisition. Moreover, the resolution and duration of an environmental monitoring campaign is often restricted by the available time, human resources, costs and other restrictions of the setting (e.g. Boch et al., 2015; Wedenig et al., 2023).

Monitoring campaigns typically involve the one-time or repeated sampling at selected spots during visits of a particular setting (e.g. cave, stream, power plant) applying different sampling procedures and preparation techniques in combination with field based analytical instruments (Tremaine et al., 2011). Analytical phases of interest include aqueous solutions (freshwater, brines), gases of different partial pressure (free atmosphere, soil air, deep wells), as well as various solid phases such as (un)wanted CaCO_3 and accessory minerals (e.g. speleothems, scale deposits, corrosion products). In this context, different sample vessels are used and play a critical role with regard to sample transport, storage and alteration. The latter concerns altering mineral precipitation, element specific leaching or adsorption effects in the vessel. Sample preparation includes filtering (e.g. 0.45 μm), acidification for conservation or cooling during sample transport and an immediate sample analysis is typically recommended.

The rapidly advancing field of environmental monitoring is an analytical technology driven endeavor within the geosciences increasingly involving automated data acquisition. The mostly electronic instruments consist of specific sensors connected to a data processing and data storage unit and some power supply. Sensors rely on electrochemical reactions, optical or acoustic signals (Boch et al., 2011b; Töchterle et al., 2017). Power supplies benefit from reduced energy consumption of the sensors and new types of (lithium) batteries related to the public interest in mobile electronics. Many data loggers, however, still need a higher voltage energy source and their spatial flexibility is thus restricted. Wireless and mostly online data transfer from local monitoring stations to the user via telecommunication networks is increasingly utilized (Eichinger et al., 2020). Future developments of sensor-based monitoring could also implement mobile platforms such as flying drones or humanoid robots, e.g. conducting sampling campaigns independently or being a companion.

Considering automated sensors and data loggers different air- and water-T loggers are applied in various settings and allow for a long-term (e.g. multi-annual) autonomous measurement of subtle T variations, e.g. distinct warm versus cold season modes of air exchange (ventilation) or changes associated with the prevailing weather conditions affecting natural (e.g. caves) or technical (e.g. tunnels) settings. Ongoing developments further comprise of different gas analyzers, e.g. for measuring CO_2 , CH_4 and H_2S concentrations. Most of these instruments are based on non-dispersive infrared absorption of the gases but differ with regard to the measurement range, sensitivity, resolution, accuracy and applicability to rough environmental conditions (Luetscher and Ziegler, 2012). Considering the carbonate system, variable CO_2 fluxes in the atmosphere or the variable gradient between atmosphere and aqueous solution are critical constituents affecting major processes of fluid-solid interaction (Liu et al., 2015; Boch et al., 2022; see sections 3 and 4). Monitoring water discharge is based on mechanical

measurements (e.g. propeller, tipping buckets), radar, ultrasound or acoustic detection and typically depends on the amounts and variability of water discharge. Vadose (drip) water supply, for example, can be measured by acoustic counting (Collister and Matthey, 2008; Boch et al., 2011b). Modern developments of *in-situ* and continuous environmental monitoring also involve the measurement of stable isotopes of gases and aqueous solutions participating in the major water, carbon and nitrogen cycles, e.g. stable C isotope ratios of carbon dioxide and methane or stable H and O in water and vapor (Maher et al., 2014; Erler et al., 2015). Mid-infrared or laser light absorption based gas analyzers, i.e. isotope ratio infrared spectrometry, laser-light interactive cavity ring-down spectroscopy or off-axis integrated cavity output spectroscopy are continuously improved.

The increasingly sensitive techniques facilitate an on-site and time-resolved tracing of isotope signals associated with their reduced size requirement and weight compared to mass spectrometers and the portable and robust construction scheme for field application. Typical applications include spatiotemporally variable greenhouse gas fluxes from natural gas vents and wells to the atmosphere or high-resolution carbon and oxygen isotope ratio and concentration variations of CO_2 in cave systems (Maher et al., 2014; Töchterle et al., 2017). Apart from liquid and gaseous phases, solid materials such as mineral precipitates can be monitored by exposing artificial substrates to natural or technical fluid flows (Eichinger et al., 2023). Active speleothem growth dynamics can be studied by mounting different glass or other substrates on the top of different stalagmites and drip sites distributed in a cave and these solids are then recovered after some definite time interval for laboratory analysis (Tremaine et al., 2011).

Living corals and their calcification mechanisms are observed using microsensors and fluorescent dyes (Sevilgen et al., 2019) and varying photosynthesis related to aqueous CO_2 and O_2 was detected using a CO_2 -flux monitoring chamber (Liu et al., 2015). Microbial metabolic and often catalytic processes related to biofilm formation, scaling and corrosion affecting geothermal energy and oil production wells or water treatment infrastructure are also monitored increasingly (Würdemann et al., 2014; Regenspurg et al., 2020). Monitoring approaches in (geo) technical settings further target scaling or corrosion and material alteration processes being monitored by exposing coupons made of carbon steel, alloys or different plastics in the fluid flow (Nogara and Zarrouk, 2018). Okazaki et al. (2021) monitored thermal waters from hot springs and geothermal wells continuously and remotely and investigated the efficiency of various scale inhibitors (organic polymers) against scaling based on fiber optic sensors and Schölderle et al. (2021) used permanent fiber optic cables to trace water injection and heat transport in a geothermal well based on spatially highly resolved T, P, and acoustic sensing. Carbonate precipitates in drainages often being related to concrete leaching can be monitored continuously by *in-situ* sensor-based measurements of principal parameters (e.g. pH, electric conductivity, Pco_2) being representative of the scaling potential (e.g. Dietzel et al., 2013; Grengg et al., 2019; see section 8.2.4).

For example, Boch et al. (2022) conducted a field test in the major Alpine Koralmtunnel (~33 km length) comprising of three different test fields involving different sensors/data loggers (water and air parameters) in order to optimize the constructive solution of the drainage system suffering from critical groundwaters, i.e. promoting substantial mineral (calcareous scale, iron ochre) and biological (bacterial mats) deposits. Likewise, Wedenig et al. (2023) implemented a drainage test-track at an active railway construction site and a combination of *in-situ*/time-resolved sensor-based measurements, recurrent sampling of fluids and solids and computer-based hydrogeochemical modeling revealed the dominant relevance of variable drainage water flow conditions and air exchange (CO_2 , O_2) with regard to the unwanted CaCO_3 deposits.

In this context, **multiproxy approaches** are known for their ability to reveal distinct and coupled reaction mechanisms and pathways, and they are key to illustrate and develop advanced research strategies in favor or against CaCO_3 formation. This goal is best achieved by

considering the composition of involved solid, liquid and gaseous phases and coupled mineralogical and structural changes of the CaCO_3 precipitates. Materials from man-made settings such as CaCO_3 precipitates at well constrained formation conditions (e.g. from geothermal and drainage pipelines) can be of major value with regard to fundamental insights (e.g. element and isotope fractionation). *In-situ* analyses and monitoring of the mineralogy and shapes of CaCO_3 precipitates or transformation products (e.g. Raman, electron, X-Ray spectroscopy), concentration of aqueous species (including pH / redox / Ca / CO_2 sensors), and (isotopic) composition of interacting gaseous phases such as CO_2 , NH_3 , and H_2O (e.g. laser-light spectroscopy) are available at a highly time-resolved level. Tracked data can be used to decipher complex reaction kinetics in particular with coupled thermodynamic modeling concepts to identify conceptual pathways and to develop on-demand strategies for promoting/prohibiting CaCO_3 formation.

10. Concluding remarks

The diversity of $\text{CaCO}_3 \cdot n\text{H}_2\text{O}$ precipitates and their formation environments that have been documented in recent decades has increased enormously. The concept developed herein to illustrate CaCO_3 precipitation in aquatic media aims to provide an overview of our knowledge about formation mechanisms, analogous settings and tracing of CaCO_3 (trans)formation by elemental, isotopic and structural proxies in natural (Fig. 1) and man-made environments (Fig. 2). Current and comprehensive insights into the $\text{CaCO}_3\text{-CO}_2\text{-H}_2\text{O}$ system are provided in aspects of (i) nucleation, growth, stimulation, and inhibition of CaCO_3 , (ii) (micro-nano) structuring and biological manipulation, (iii) tracking, monitoring and tailoring, and (iv) function as (un)wanted product and environmental archive. However, the more we know in applying promising analytical techniques and environmental signals, the more limitations and challenges arise. But this often opens up new and advanced concepts, especially when using the extensive analysis and modeling tools developed for the carbonate system.

CRediT authorship contribution statement

Martin Dietzel: Writing – original draft, Conceptualization. **Ronny Boch:** Writing – original draft, Conceptualization.

Declaration of competing interest

The authors declare that they have no known competing financial interests or personal relationships that could have appeared to influence the work reported in this paper.

Acknowledgements

The authors would like to thank the editor in chief Astrid Holzheid and the former editorial board member Klaus Keil (†) for their invitation to write this review and for their encouragement and support in its preparation and printing as well as Adrian Immenhauser and one anonymous reviewer for their constructive comments on a previous version of the contribution. Special gratitude is addressed to Hans-Eberhard Usdowski, Adrian Immenhauser, Albrecht Leis, Vasileios Mavromatis, Anton Eisenhauer, Christoph Spötl, Jan Kramers, Michael Böttcher, Andre Baldermann, Bettina Purgstaller, Jean-Michel Brazier, Michael Pettauer, Katja Götschl, Attila Demény, Jens Fiebig, Stephan Köhler, Jiangwu Tang, Nikolaus Gussone, Xianfeng Wang, János Szanyi, Stefanie Eichinger, and Tobias Kluge for inspiring discussions and cooperations on many aspects of above CaCO_3 formations and to Iris Zögl for the schematic illustrations.

References

- Adams, B.M., Kuehn, T.H., Bielicki, J.M., Randolph, J.B., Saar, M.O., 2015. A comparison of electric power output of CO_2 Plume Geothermal (CPG) and brine geothermal systems for varying reservoir conditions. *Appl. Energy* 140, 365–377.
- Adams, B.M., Vogler, D., Kuehn, T.H., Bielicki, J.M., Garapati, N., Saar, M.O., 2021. Heat depletion in sedimentary basins and its effect on the design and electric power output of CO_2 Plume Geothermal (CPG) systems. *Renew. Energy* 172, 1393–1403.
- Adelia, H., Sirous, F., Blakey, I., Ta, H.T., 2023. Metal ion chelation of poly(aspartic acid): From scale inhibition to therapeutic potentials. *Int. J. Biol. Macromol.* 229, 974–993.
- Adkins, J.F., Boyle, E.A., Curry, W.B., Lutringer, A., 2003. Stable isotopes in deep-sea corals and a new mechanism for "vital effects". *Geochim. Cosmochim. Acta* 67, 1129–1143.
- Adolphe J., Loubière J., Paradas J. and Soleilhavoup F. (1990) Procédé de traitement biologique d'une surface artificielle. European patent 90400G97. 0 1989.
- Affek, H.P., Bar-Matthews, M., Ayalon, A., Matthews, A., Eiler, J.M., 2008. Glacial/interglacial temperature variations in Soreq cave speleothems as recorded by 'clumped isotope' thermometry. *Geochim. Cosmochim. Acta* 72, 5351–5360.
- Affek, H.P., Zaarur, S., 2014. Kinetic isotope effect in CO_2 degassing: Insight from clumped and oxygen isotopes in laboratory precipitation experiments. *Geochim. Cosmochim. Acta* 143, 319–330.
- Affolter, S., Häuselmann, A.D., Fleitmann, D., Häuselmann, P., Leuenberger, M., 2015. Triple isotope (8D, $\delta^{17}\text{O}$, $\delta^{18}\text{O}$) study on precipitation, drip water and speleothem fluid inclusions for a Western Central European cave (NW Switzerland). *Quat. Sci. Rev.* 127, 73–89.
- Ahenkorah, I., Rahman, M.M., Karim, M.R., Beecham, S., Saint, C., 2021. A Review of Enzyme Induced Carbonate Precipitation (EICP): The Role of Enzyme Kinetics. *Sustainable Chemistry* 2, 92–114.
- Ahm, A.S.C., Bjerrum, C.J., Hoffman, P.F., Macdonald, F.A., Maloof, A.C., Rose, C.V., Strauss, J.V., Higgins, J.A., 2021. The Ca and Mg isotope record of the Cryogenian Trezona carbon isotope excursion. *Earth Planet. Sci. Lett.* 568.
- Ahmadi, M.-A., Bahadori, A., Shadizadeh, S.R., 2015. A rigorous model to predict the amount of Dissolved Calcium Concentration throughout oil field brines: Side effect of pressure and temperature. *Fuel* 139, 154–159.
- Akhtar, A.A., Cruger Ahm, A.-S., Higgins, J.A., 2024. Geochemical fingerprints of early diagenesis in shallow-water marine carbonates: insights from paired $\delta^{44/40}\text{Ca}$ and $\delta^{26}\text{Mg}$ values. *Geochim. Cosmochim. Acta* 383, 57–69.
- Akyel, A., Coburn, M., Phillips, A.J., Gerlach, R., 2022. Key Applications of Biomineralization. In: Berenjian, A., Seifan, M. (Eds.), *Mineral Formation by Microorganisms: Concepts and Applications*. Springer International Publishing, Cham, pp. 347–387.
- Al, Helal A., Soames, A., Gubner, R., Iglaer, S., Barifcane, A., 2018. Influence of magnetic fields on calcium carbonate scaling in aqueous solutions at 150°C and 1bar. *J. Colloid Interface Sci.* 509, 472–484.
- Alçığek, H., Bülbül, A., Yavuzer, İ., Çihat, Alçığek M., 2019. Origin and evolution of the thermal waters from the Pamukkale Geothermal Field (Denizli Basin, SW Anatolia, Turkey): Insights from hydrogeochemistry and geothermometry. *J. Volcanol. Geotherm. Res.* 372, 48–70.
- AlKhatib, M., Eisenhauer, A., 2017a. Calcium and strontium isotope fractionation in aqueous solutions as a function of temperature and reaction rate; I. Calcite. *Geochimica et Cosmochimica Acta* 209, 296–319.
- AlKhatib, M., Eisenhauer, A., 2017b. Calcium and strontium isotope fractionation during precipitation from aqueous solutions as a function of temperature and reaction rate; II. Aragonite. *Geochimica et Cosmochimica Acta* 209, 320–342.
- Alkhatib, M., Qutob, M., Alkhatab, S., Eisenhauer, A., 2022. Influence of precipitation rate and temperature on the partitioning of magnesium and strontium in calcite overgrowths. *Chem. Geol.* 599.
- Almirall, J.R., Trejos, T., 2016. Application of LA-ICP-MS to forensic science. *Elements* 12, 335–340.
- Alonso-Zarza, A.M., Tanner, L.H., 2010. Carbonates in Continental Settings: Geochemistry. In: *Developments in Sedimentology*. Elsevier. p. iii, Diagenesis and Applications.
- Al-Rousan, S., Felis, T., 2013. Long-term variability in the stable carbon isotopic composition of Porites corals at the northern Gulf of Aqaba, Red Sea. *Palaeogeogr. Palaeoclimatol. Palaeoecol.* 381–382, 1–14.
- Alvarez, C.C., Quitté, G., Schott, J., Oelkers, E.H., 2020. Experimental determination of Ni isotope fractionation during Ni adsorption from an aqueous fluid onto calcite surfaces. *Geochim. Cosmochim. Acta* 273, 26–36.
- Alvarez, C.C., Quitté, G., Schott, J., Oelkers, E.H., 2021. Nickel isotope fractionation as a function of carbonate growth rate during Ni coprecipitation with calcite. *Geochim. Cosmochim. Acta* 299, 184–198.
- Andersen, M.B., Elliott, T., Freymuth, H., Sims, K.W.W., Niu, Y., Kelley, K.A., 2015. The terrestrial uranium isotope cycle. *Nature* 517, 356–359.
- Anderson, N.T., Kelson, J.R., Kele, S., Daéron, M., Bonifacie, M., Horita, J., Mackey, T.J., John, C.M., Kluge, T., Petschnig, P., Jost, A.B., Huntington, K.W., Bernasconi, S.M., Bergmann, K.D., 2021. A Unified Clumped Isotope Thermometer Calibration (0.5–1,100°C) Using Carbonate-Based Standardization. *Geophys. Res. Lett.* 48 e2020GL092069.
- Antao, S.M., Hassan, I., 2009. The orthorhombic structure of CaCO_3 , SrCO_3 , PbCO_3 and BaCO_3 : Linear structural trends. *Can. Mineral.* 47, 1245–1255.
- Antonio, Cerrón-Calle G., Luna, Magdaleno A., Graf, J.C., Apul, O.G., Garcia-Segura, S., 2022. Elucidating CO_2 nanobubble interfacial reactivity and impacts on water chemistry. *J. Colloid Interface Sci.* 607, 720–728.

- Antonioli, F., Bard, E., Potter, E.-K., Silenzi, S., Impronta, S., 2004. 215-ka History of sea-level oscillations from marine and continental layers in Argentilarola Cave speleothems (Italy). *Glob. Planet. Chang.* 43, 57–78.
- Appelo, C.A.J., Postma, D., 2005. Geochemistry, Groundwater and Pollution, 2nd edition. A.A. Balkema Publishers, Amsterdam. 634 pp.
- Aquilano, D., Otálora, F., Pastero, L., García-Ruiz, J.M., 2016. Three study cases of growth morphology in minerals: halite, calcite and gypsum. *Prog. Cryst. Growth Charact. Mater.* 62, 227–251.
- Argentino, C., Lugli, F., Cipriani, A., Conti, S., Fontana, D., 2019. A deep fluid source of radiogenic Sr and highly dynamic seepage conditions recorded in Miocene seep carbonates of the northern Apennines (Italy). *Chem. Geol.* 522, 135–147.
- Armenteros I. (2010) Chapter 2 Diagenesis of Carbonates in Continental Settings, Developments in Sedimentology, pp. 61–151.
- Arnold A., Mering J., Santi L., Román-Palacios C., Li H., Petryshyn V., Mitsunaga B., Elliott B., Wilson J., Lucarelli J., Boch R., Ibarra D., Li L., Fan M., Kaufman D., Cohen A., Dunbar R., Russell J., Lalonde S., Roy P. D., Dietzel M., Liu X., Chang F., Eagle R. A. and Tripathi A. (2024) Comparative clumped isotope temperature relationships in freshwater carbonates. *The Depositional Record* (in press).
- Arvidson R. S. and Morse J. W. (2014) 9.3 - Formation and Diagenesis of Carbonate Sediments. In Treatise on Geochemistry (Second Edition) (eds. H. D. Holland and K. K. Turekian). Elsevier, Oxford. pp. 61–101.
- Asta, M.P., Auqué, L.F., Sanz, F.J., Gimeno, M.J., Acero, P., Blasco, M., García-Alix, A., Gómez, J., Delgado-Huertas, A., Mandado, J., 2017. Travertines associated with the Alhama-Jaraba thermal waters (NE, Spain): Genesis and geochemistry. *Sediment. Geol.* 347, 100–116.
- Asta, M.P., Bonilla-Correa, S., Pace, A., Dietzel, M., García-Alix, A., Vennemann, T., Meibom, A., Adams, A., 2024. Oxygen isotope fractionation during amorphous to crystalline calcium carbonate transformation at varying relative humidity and temperature. *Geochim. Cosmochim. Acta* (in press).
- Asta, M.P., Fernandez-Martinez, A., Alonso, J., Charlet, L., Findling, N., Magnin, V., Ruta, B., Sprung, M., Westermeier, F., 2020. Nanoscale Ion Dynamics Control on Amorphous Calcium Carbonate Crystallization: Precise Control of Calcite Crystal Sizes. *J. Phys. Chem. C* 124, 25645–25656.
- Atsawaranunt, K., Comas-Bru, L., Amirnezhad, Mozhdehi S., Deininger, M., Harrison, S.P., Baker, A., Boyd, M., Kaushal, N., Ahmad, S.M., Ait, Brahim Y., Arienzio, M., Bajío, P., Braun, K., Burstyn, Y., Chawchai, S., Duan, W., Hatvani, I.G., Hu, J., Kern, Z., Labuhn, I., Lachniet, M., Lechleitner, F.A., Lorrey, A., Pérez-Mejías, C., Pickering, R., Scroxton, N., Members, S.W.G., 2018. The SISAL database: a global resource to document oxygen and carbon isotope records from speleothems. *Earth Syst. Sci. Data* 10, 1687–1713.
- Aufort, J., Raiteri, P., Gale, J.D., 2022. Computational insights into Mg²⁺ dehydration in the presence of carbonate. *ACS Earth Space Chem.* 6, 733–745.
- Avaro, J., Moon, E.M., Rose, J., Rose, A.L., 2019a. Calcium coordination environment in precursor species to calcium carbonate mineral formation. *Geochim. Cosmochim. Acta* 259, 344–357.
- Avaro, J., Moon, E.M., Schulz, K.G., Rose, A.L., 2023. Calcium carbonate prenucleation cluster pathway observed via in situ small-angle X-ray scattering. *J. Phys. Chem. Lett.* 14, 4517–4523.
- Avaro, J.T., Ruiz-Agudo, C., Landwehr, E., Hauser, K., Gebauer, D., 2019b. Impurity-free amorphous calcium carbonate, a preferential material for pharmaceutical and medical applications. *Eur. J. Mineral.* 31, 231–236.
- Azmy, K., Brand, U., Sylvester, P., Gleeson, S.A., Logan, A., Bitner, M.A., 2011. Biogenic and abiogenic low-Mg calcite (bLMC and aLMC): Evaluation of seawater-REE composition, water masses and carbonate diagenesis. *Chem. Geol.* 280, 180–190.
- Badertscher, S., Borsato, A., Frisia, S., Cheng, H., Edwards, R.L., Tüysüz, O., Fleitmann, D., 2014. Speleothems as sensitive recorders of volcanic eruptions – the Bronze Age Minoan eruption recorded in a stalagmite from Turkey. *Earth Planet. Sci. Lett.* 392, 58–66.
- Bajnai, D., Guo, W., Spötl, C., Coplen, T.B., Methner, K., Löffler, N., Kršnik, E., Gischler, E., Hansen, M., Henkel, D., Price, G.D., Raddatz, J., Scholz, D., Fiebig, J., 2020. Dual clumped isotope thermometry resolves kinetic biases in carbonate formation temperatures. *Nat. Commun.* 11, 4005.
- Bajnai, D., Herwartz, D., 2021. Kinetic Oxygen Isotope Fractionation between Water and Aqueous OH⁻ during Hydroxylation of CO₂. *ACS Earth and Space Chemistry* 5, 3375–3384.
- Bajo, P., Hellstrom, J., Frisia, S., Drysdale, R., Black, J., Woodhead, J., Borsato, A., Zanchetta, G., Wallace, M.W., Regattieri, E., Haese, R., 2016. “Cryptic” diagenesis and its implications for speleothem geochronologies. *Quat. Sci. Rev.* 148, 17–28.
- Baker, A., Hartmann, A., Duan, W., Hankin, S., Comas-Bru, L., Cuthbert, M.O., Treble, P. C., Banner, J., Genty, D., Baldini, L.M., Bartolomé, M., Moreno, A., Pérez-Mejías, C., Werner, M., 2019. Global analysis reveals climatic controls on the oxygen isotope composition of cave drip water. *Nat. Commun.* 10, 2984.
- Balan, E., Blanchard, M., Pinilla, C., Lazzeri, M., 2014. First-principles modeling of sulfate incorporation and ³⁴S/³²S isotopic fractionation in different calcium carbonates. *Chem. Geol.* 374–375, 84–91.
- Balan, E., Noireaux, J., Mavromatis, V., Saldi, G.D., Montouillout, V., Blanchard, M., Pietrucci, F., Gervais, C., Rustad, J.R., Schott, J., Gaillardet, J., 2018. Theoretical isotopic fractionation between structural boron in carbonates and aqueous boric acid and borate ion. *Geochim. Cosmochim. Acta* 222, 117–129.
- Balan, E., Pietrucci, F., Gervais, C., Blanchard, M., Schott, J., Gaillardet, J., 2016. First-principles study of boron speciation in calcite and aragonite. *Geochim. Cosmochim. Acta* 193, 119–131.
- Baldassarre, F., Stradis, A.D., Altamura, G., Vergaro, V., Citti, C., Cannazza, G., Capodilupo, A.L., Dini, L., Ciccarella, G., 2020. Application of calcium carbonate nanocarriers for controlled release of phytodrugs against *Xylella fastidiosa* pathogen. *Pure Appl. Chem.* 92, 429–444.
- Baldermann, A., Deditius, A.P., Dietzel, M., Fichtner, V., Fischer, C., Hippler, D., Leis, A., Baldermann, C., Mavromatis, V., Stickler, C.P., Strauss, H., 2015. The role of bacterial sulfate reduction during dolomite precipitation: Implications from Upper Jurassic platform carbonates. *Chem. Geol.* 412, 1–14.
- Barkan, Y., Paris, G., Webb, S.M., Adkins, J.F., Halevy, I., 2020. Sulfur isotope fractionation between aqueous and carbonate-associated sulfate in abiotic calcite and aragonite. *Geochim. Cosmochim. Acta* 280, 317–339.
- Barker, S., Knorr, G., Edwards, R.L., Parrenin, F., Putnam, A.E., Skinner, L.C., Wolff, E., Ziegler, M., 2011. 800,000 Years of Abrupt Climate Variability. *Science* 334, 347–351.
- Barnes, H.L., 1997. Geochemistry of hydrothermal ore deposits. John Wiley & Sons.
- Baroni, I., Plan, L., Grasemann, B., Melichar, R., Mitrović-Woodell, I., Rowberry, M., Scholz, D., 2022. Three large prehistoric earthquakes in the Eastern Alps evidenced by cave rupture and speleothem damage. *Geomorphology* 408, 108242.
- Barras, C., Mouret, A., Nardelli, M.P., Metzger, E., Petersen, J., La, C., Filipsson, H.L., Jorissen, F., 2018. Experimental calibration of manganese incorporation in foraminiferal calcite. *Geochim. Cosmochim. Acta* 237, 49–64.
- Barrett, G.T., Allen, K., Reimer, P.J., Ringbom, Å., Olsen, J., Lindroos, A., 2023. Ramped pyrolysis radiocarbon dating of lime lumps: Establishing the earliest mortar-based construction phase of Turku cathedral, Finland. *J. Cult. Herit.* 61, 201–210.
- Barrett, G.T., Keaveney, E., Lindroos, A., Donnelly, C., Daugbjerg, T.S., Ringbom, Å., Olsen, J., Reimer, P.J., 2021. Ramped pyrooxidation: A new approach for radiocarbon dating of lime mortars. *J. Archaeol. Sci.* 129, 105366.
- Barta, G., 2014. Paleoenvironmental reconstruction based on the morphology and distribution of secondary carbonates of the loess-paleosol sequence at Sütő, Hungary. *Quat. Int.* 319, 64–75.
- Bastianini, L., Rogerson, M., Mercedes-Martín, R., Prior, T.J., Cesar, E.A., Mayes, W.M., 2019. What Causes Carbonates to Form “Shrubby” Morphologies? An Anthropocene Limestone Case Study. *Frontiers. Earth Sci.* 7.
- Bathurst R. G. C. (1971) Carbonate sediments and their diagenesis. *Dev. Sedimentol.* 12, 658pp.
- Bathurst, R.G.C., 1975. Carbonate Sediments and Their Diagenesis. Elsevier.
- Bayat, O., Karimi, A., Amundson, R., 2021. Stable isotope geochemistry of pedogenic carbonates in calcareous materials, iran: A review and synthesis. *Geol. Soc. Spec. Publ.* 507, 255–272.
- Beard, B.L., Johnson, C.M., 2004. Fe isotope variations in the modern and ancient earth and other planetary bodies. *Rev. Mineral. Geochem.* 55, 319–357.
- Beaudoin, N.E., Lacombe, O., Hoareau, G., Callot, J.P., 2022. How the geochemistry of syn-kinematic calcite cement depicts past fluid flow and assists structural interpretations: a review of concepts and applications in orogenic forelands. *Geol. Mag.* 159, 2157–2190.
- Beck, W.C., Grossman, E.L., Morse, J.W., 2005. Experimental studies of oxygen isotope fractionation in the carbonic acid system at 15°, 25°, and 40°C. *Geochim. Cosmochim. Acta* 69, 3493–3503.
- Bernasconi, S.M., Müller, I.A., Bergmann, K.D., Breitenbach, S.F.M., Fernandez, A., Hodell, D.A., Jaggi, M., Meckler, A.N., Millan, I., Ziegler, M., 2018. Reducing Uncertainties in Carbonate Clumped Isotope Analysis Through Consistent Carbonate-Based Standardization. *Geochem. Geophys. Geosyst.* 19, 2895–2914.
- Berndsen, M., Erol, S., Akin, T., Akin, S., Nardini, I., Immehausser, A., Nehler, M., 2024. Experimental study and kinetic modeling of high temperature and pressure CO₂ mineralization. *International Journal of Greenhouse Gas Control* 132, 104044.
- Bernecker, M., Hofmann, S., Staudigel, P.T., Davies, A.J., Tagliavento, M., Meijer, N., Ballian, A., Fiebig, J., 2024. A robust methodology for triple (Δ_{47} , Δ_{48} , Δ_{49}) clumped isotope analysis of carbonates. *Chem. Geol.* 642, 121803.
- Berner, R.A., 1975. The role of magnesium in the crystal growth of calcite and aragonite from sea water. *Geochim. Cosmochim. Acta* 39, 489–504.
- Bertini, A., Minissale, A., Ricci, M., 2008. Use of Quaternary travertines of central-southern Italy as archives of paleoclimate, paleohydrology and neotectonics. *Italian Journal of Quaternary Sciences* 21, 99–112.
- Bertran, P., Couchoud, I., Charlier, K., Hatté, C., Lefrais, Y., Limondin-Lozouet, N., Queffelec, A., 2023. Last Glacial Maximum cryogenic calcite deposits in an alluvial fan at Villetteoreix, southwest France. *Permafrost. Periglac. Process.* 34, 244–258.
- Besseling, R., Rodriguez-Blanco, J.D., Stawski, T.M., Benning, L.G., Tobler, D.J., 2017. How Short-Lived Ikaite Affects Calcite Crystallization. *Cryst. Growth Des.* 17, 6224–6230.
- Bia, G., García, M.G., Rueda, E.S., Mors, R.A., Mlewski, E.G., Gomez, F.J., Borgnino, L., 2021. Arsenic in natural carbonates: The role of the biogeochemical conditions in its solid speciation. *Chem. Geol.* 583, 120477.
- Bischoff, J.L., Fitzpatrick, J.A., Rosenbauer, R.J., 1993. The Solubility and Stabilization of Ikaite (CaCO₃·6H₂O) from 0° to 25°C: Environmental and Paleoclimatic Implications for Thinolite Tufa. *The Journal of Geology* 101, 21–33.
- Bissell H. J. and Chilingar G. V. (1967) Chapter 4 Classification of Sedimentary Carbonate Rocks. *Developments in Sedimentology* 9, 87–168.
- Bistervels, M.H., Antalícz, B., Kamp, M., Schoenmaker, H., Noorduin, W.L., 2023. Light-driven nucleation, growth, and patterning of biorelevant crystals using resonant near-infrared laser heating. *Nat. Commun.* 14, 6350.
- Blue, C.R., Dove, P.M., 2015. Chemical controls on the magnesium content of amorphous calcium carbonate. *Geochim. Cosmochim. Acta* 148, 23–33.
- Blue, C.R., Giuffre, A., Mergelsberg, S., Han, N., De Yoreo, J.J., Dove, P.M., 2017. Chemical and physical controls on the transformation of amorphous calcium carbonate into crystalline CaCO₃ polymorphs. *Geochim. Cosmochim. Acta* 196, 179–196.
- Blyth, A.J., Hartland, A., Baker, A., 2016. Organic proxies in speleothems – New developments, advantages and limitations. *Quat. Sci. Rev.* 149, 1–17.

- Boese, B., Amicone, S., Cantisi, E., Schön, F., Berthold, C., 2023. Mortars in context: an integrated study of mortars and plasters from the so-called Ginnasio in Solunto (Sicily, Italy). *Archaeometry* 65, 702–720.
- Boch, R., Cheng, H., Spötl, C., Edwards, R.L., Wang, X., Häuselmann, P., 2011a. NALPS: a precisely dated European climate record 120–60 ka. *Clim. Past* 7, 1247–1259.
- Boch, R., Dietzel, M., Reichl, P., Leis, A., Baldermann, A., Mittermayr, F., Pölt, P., 2015. Rapid ikaite ($\text{CaCO}_3 \cdot 6\text{H}_2\text{O}$) crystallization in a man-made river bed: Hydrogeochemical monitoring of a rarely documented mineral formation. *Appl. Geochem.* 63, 366–379.
- Boch, R., Leis, A., Haslinger, E., Goldbrunner, J.E., Mittermayr, F., Fröschl, H., Hippler, D., Dietzel, M., 2017a. Scale-fragment formation impairing geothermal energy production: interacting H_2S corrosion and CaCO_3 crystal growth. *Geothermal Energy* 5.
- Boch, R., Leis, A., Mindszenty, A., Goldbrunner, J.E., Szanyi, J., Deák, J., Haslinger, E., Virág, M., Mittermayr, F., Dietzel, M. (2017b) Scaling Forensics: Evaluating geothermal production conditions from scales as chemical-sedimentary archives. *Proceedings of the German Geothermal Congress 2017 paper #P6*, 1–12.
- Boch, R., Pilgerstorfer, T., Moritz, B., 2022. Reduction of scale formation by optimized drainage conditions – Insights from field testing. *Geomechanics and Tunnelling* 15, 371–391.
- Boch, R., Spötl, C., Frisia, S., 2011b. Origin and palaeoenvironmental significance of lamination in stalagmites from Katerloch Cave, Austria. *Sedimentology* 58, 508–531.
- Boch, R., Spötl, C., Kramers, J., 2009. High-resolution isotope records of early Holocene rapid climate change from two coeval stalagmites of Katerloch Cave, Austria. *Quat. Sci. Rev.* 28, 2527–2538.
- Boch, R., Spötl, C., Reitner, J.M., Kramers, J., 2005. A Lateglacial travertine deposit in Eastern Tyrol (Austria). *Austrian J Earth Sci* 98, 78–91.
- Boch, R., Szanyi, J., Leis, A., Mindszenty, A., Deák, J., Kluge, T., Hippler, D., Demény, A., Dietzel, M., 2016. Geothermal Carbonate Scaling: Forensic Studies Applying High-Resolution Geochemical Methods. *Proceedings of the European Geothermal Congress Paper #111*, 1–10.
- Boch, R., Wang, X., Kluge, T., Leis, A., Lin, K., Pluch, H., Mittermayr, F., Baldermann, A., Böttcher, Michael E., Dietzel, M., 2019. Aragonite–calcite veins of the ‘Erzberg’ iron ore deposit (Austria): Environmental implications from young fractures. *Sedimentology* 0.
- Böhm, F., Eisenhauer, A., Tang, J., Dietzel, M., Krabbenhöft, A., Kisakürek, B., Horn, C., 2012. Strontium isotope fractionation of planktic foraminifera and inorganic calcite. *Geochim. Cosmochim. Acta* 93, 300–314.
- Bonifacie, M., Calmels, D., Eiler, J.M., Horita, J., Chaduteau, C., Vasconcelos, C., Agrinier, P., Katz, A., Passey, B.H., Ferry, J.M., Bourrand, J.-J., 2017. Calibration of the dolomite clumped isotope thermometer from 25 to 350°C, and implications for a universal calibration for all (Ca, Mg, Fe) CO_3 carbonates. *Geochim. Cosmochim. Acta* 200, 255–279.
- Bonto, M., Andreasen, A., 2024. Modelling the solubility of gases in aqueous solutions with a focus on geothermal applications– assessment and benchmarking of two free software packages. *Unconventional Resources* 4, 100088.
- Borrelli, C., Gabitol, R.I., Liu, M.C., Hertwig, A.T., Panieri, G., 2020. The benthic foraminiferal 834S records flux and timing of paleo methane emissions. *Sci. Rep.* 10.
- Bots, P., Benning, L.G., Rodriguez-Blanco, J.-D., Roncal-Herrero, T., Shaw, S., 2012. Mechanistic Insights into the Crystallization of Amorphous Calcium Carbonate (ACC). *Cryst. Growth Des.* 12, 3806–3814.
- Böttcher, M.E., Dietzel, M., 2010. Metal-ion partitioning during low-temperature precipitation and dissolution of anhydrous carbonates and sulphates. *European Mineralogical Union Notes in Mineralogy* 10, 139–187.
- Boussagol, P., Vennin, E., Bouton, A., Roche, A., Thomazo, C., Kolodka, C., Buoncristiani, J.F., Monna, F., Musset, O., Visscher, P.T., 2023. Quaternary lacustrine carbonate deposits of the Great Basin, USA: Impact of climate, tectonics and substrate. *Sedimentology* 70, 969–1007.
- Bowman, S., Agrawal, V., Sharma, S., 2023. Role of pH and Eh in geothermal systems: Thermodynamic examples and impacts on scaling and corrosion. *Geothermics* 111.
- Bradbury, H.J., Halloran, K.H., Lin, C.Y., Turchyn, A.V., 2020. Calcium isotope fractionation during microbially induced carbonate mineral precipitation. *Geochim. Cosmochim. Acta* 277, 37–51.
- Brand, U., Bitner, M.A., Logan, A., Azmy, K., Crippa, G., Angiolini, L., Colin, P., Griesshaber, E., Harper, E.M., Ruggiero, E.T., Häussermann, V., 2019. Brachiopod-based oxygen-isotope thermometer: Update and review. *Riv. Ital. Paleontol. Stratigr.* 125, 775–787.
- Branson, O., 2018. Boron Incorporation into Marine CaCO_3 . In: Marschall, H., Foster, G. (Eds.), *Boron Isotopes: The Fifth Element*. Springer International Publishing, Cham, pp. 71–105.
- Branson, O., Uchikawa, J., Bohlin, M.S., Misra, S., 2024. Controls on Li partitioning and isotopic fractionation in inorganic calcite. *Geochim. Cosmochim. Acta* 382, 91–102.
- Brasier, A., Wacey, D., Rogerson, M., Guagliardo, P., Saunders, M., Kellner, S., Mercedes-Martin, R., Prior, T., Taylor, C., Matthews, A., Reijmer, J., 2018. A microbial role in the construction of Mono Lake carbonate chimneys? *Geobiology* 16, 540–555.
- Brazier, J.-M., Blanchard, M., McHeut, M., Schmitt, A.-D., Schott, J., Mavromatis, V., 2023. Experimental and theoretical investigations of stable Sr isotope fractionation during its incorporation in aragonite. *Geochim. Cosmochim. Acta* 358, 134–147.
- Brazier, J.-M., Goetschl, K.E., Dietzel, M., Mavromatis, V., 2024a. Effect of mineral growth rate on Zinc incorporation into calcite and aragonite. *Chem. Geol.* 643, 121821.
- Brazier, J.-M., Harrison, A.L., Rollion-Bard, C., Mavromatis, V., 2024c. Controls of temperature and mineral growth rate on lithium and sodium incorporation in abiotic aragonite. *Chem. Geol.* 654, 122057.
- Brazier, J.-M., Mavromatis, V., 2022. Effect of growth rate on nickel and cobalt incorporation in aragonite. *Chem. Geol.* 600, 120863.
- Brazier, J.-M., Pettauer, M., Goetschl, K., Dietzel, M., 2024b. Review on the formation and transformation behaviour of amorphous calcium carbonate and its control on environmental proxies. *Sedimentology* (accepted).
- Brazier, J.-M., Schmitt, A.-D., Gangloff, S., Pelt, E., Chabaux, F., Tertre, E., 2019. Calcium isotopic fractionation during adsorption onto and desorption from soil phyllosilicates (kaolinite, montmorillonite and muscovite). *Geochim. Cosmochim. Acta* 250, 324–347.
- Brazier, J.M., Schmitt, A.D., Gangloff, S., Pelt, E., Gocke, M.I., Wiesenberg, G.L.B., 2020. Multi-isotope approach ($\delta^{44/40}\text{Ca}$, $\delta^{88/86}\text{Sr}$ and $\delta^{87}\text{Sr}/\delta^{86}\text{Sr}$) provides insights into rhizolith formation mechanisms in terrestrial sediments of Nussloch (Germany). *Chem. Geol.* 545.
- Bridgestock, L., Hsieh, Y.-T., Porcelli, D., Homoky, W.B., Bryan, A., Henderson, G.M., 2018. Controls on the barium isotope compositions of marine sediments. *Earth Planet. Sci. Lett.* 481, 101–110.
- Brogi, A., Capezzuoli, E., Buracchi, E., Branca, M., 2012. Tectonic control on travertine and calcareous tufa deposition in a low-temperature geothermal system (Sarteano, Central Italy). *J. Geol. Soc. Lond.* 169, 461–476.
- Bruce, Railsback L., 1999. Patterns in the compositions, properties, and geochemistry of carbonate minerals. *Carbonates Evaporites* 14, 1–20.
- Bruggmann, S., Rodler, A.S., Klaebe, R.M., Goderis, S., Frei, R., 2020. Chromium isotope systematics in modern and ancient microbialites. *Minerals* 10, 1–25.
- Bu, X., Jiang, K., Wang, X., Liu, X., Tan, X., Kong, Y., Wang, L., 2022. Analysis of calcium carbonate scaling and antiscalant field experiment. *Geothermics* 104, 102433.
- Burdett, W.J., Arthur, A.M., Richardson, M., 1989. A Neogene seawater sulfur isotope age curve from calcareous pelagic microfossils. *Earth Planet. Sci. Lett.* 94, 189–198.
- Burgener, L.K., Huntington, K.W., Sletten, R., Watkins, J.M., Quade, J., Hallet, B., 2018. Clumped isotope constraints on equilibrium carbonate formation and kinetic isotope effects in freezing soils. *Geochim. Cosmochim. Acta* 235, 402–430.
- Burgess, K.M.N., Bryce, D.L., 2015. On the crystal structure of the vaterite polymorph of CaCO_3 : A calcium-43 solid-state NMR and computational assessment. *Solid State Nucl. Magn. Reson.* 65, 75–83.
- Bürgmair, S., Tanner, J., Batchelor, W., Hoadley, A.F.A., 2023. CaCO_3 solubility in the process water of recycled containerboard mills. *Nordic Pulp and Paper Research Journal* 38, 181–195.
- Burnie, T.M., Power, I.M., Paulo, C., Alçıçek, H., Falcón, L.I., Lin, Y., Wilson, S.A., 2023. Environmental and Mineralogical Controls on Biosignature Preservation in Magnesium Carbonate Systems Analogous to Jezero Crater, Mars. *Astrobiology* 23, 513–535.
- Campbell, K.A., 2006. Hydrocarbon seep and hydrothermal vent paleoenvironments and paleontology: Past developments and future research directions. *Palaeogeogr. Palaeoclimatol. Palaeoecol.* 232, 362–407.
- Campbell, M., McDonough, L., Treble, P.C., Baker, A., Kosarac, N., Coleborn, K., Wynn, P.M., Schmitt, A.K., 2023. A Review of Speleothems as Archives for Paleofire Proxies, With Australian Case Studies. *Rev. Geophys.* 61 e2022RG000790.
- Candido C. A. S., Zarrouk, S.J. (2017) Scaling Mitigations for the Binary Plant Vaporizer: Upper Mahiao, the Philippines. *Proceedings 39th New Zealand Geothermal Workshop, 22–24 November 2017, Rotorua, New Zealand*, 1–8.
- Canfield, D.E., Glazer, A.N., Falkowski, P.G., 2010. The Evolution and Future of Earth’s Nitrogen Cycle. *Science* 330, 192–196.
- Cantonati, M., Segadelli, S., Ogata, K., Tran, H., Sanders, D., Gerecke, R., Rott, E., Filippini, M., Gargini, A., Celico, F., 2016. A global review on ambient Limestone-Precipitating Springs (LPS): Hydrogeological setting, ecology, and conservation. *Sci. Total Environ.* 568, 624–637.
- Cao, B., Ma, Y., Liu, M., Li, S., Tian, H., Feng, G., 2024. Predictions of locations of flash point and calcite scaling of geothermal fluids in wellbore by chemical and thermodynamic simulations. *Geothermics* 121, 103057.
- Cao, C., Liu, X.-M., Wang, X.-K., Chen, J., 2023. Effective use of limestones to reconstruct seawater Li isotope compositions - A community standard proposal. *Chem. Geol.* 626, 121441.
- Capezzuoli, E., Gandin, A., Pedley, M., 2014. Decoding tufa and travertine (fresh water carbonates) in the sedimentary record: The state of the art. *Sedimentology* 61, 1–21.
- Carlson, P.E., Noronha, A.L., Banner, J.L., Jenson, J.W., Moore, M.W., Partin, J.W., Deininger, M., Breecker, D.O., Bautista, K.K., 2020. Constraining speleothem oxygen isotope disequilibrium driven by rapid CO_2 degassing and calcite precipitation: Insights from monitoring and modeling. *Geochim. Cosmochim. Acta* 284, 222–238.
- Carmona-Carmona, M., Acedo-Fuentes, P., Romero-Casado, A., Meneses-Rodríguez, J.M., Trujillo-Gómez, M., Tejado-Ramos, J.J., 2023. Chitosan as a carbonation catalyst in lime mortars. *Results. Engineering* 17.
- Carpenter, R., 1969. Factors controlling the marine geochemistry of fluorine. *Geochim. Cosmochim. Acta* 33, 1153–1167.
- Carstea, E.M., Popa, C.L., Baker, A., Bridgeman, J., 2020. In situ fluorescence measurements of dissolved organic matter: A review. *Sci. Total Environ.* 699, 134361.
- Casella, L.A., Griesshaber, E., Simonet, Roda M., Ziegler, A., Mavromatis, V., Henkel, D., Laudien, J., Häussermann, V., Neuser, R.D., Angiolini, L., Dietzel, M., Eisenhauer, A., Immenhauser, A., Brand, U., Schmahl, W.W., 2018. Micro- and nanostructures reflect the degree of diagenetic alteration in modern and fossil brachiopod shell calcite: A multi-analytical screening approach (CL, FE-SEM, AFM, EBSD). *Palaeogeogr. Palaeoclimatol. Palaeoecol.* 502, 13–30.
- Castanier, S., Le Métayer-Levrel, G., Oriol, G., Loupière, J.-F., Perthuisot, J.-P., 2000. Bacterial Carbonatogenesis and Applications to Preservation and Restoration of Historic Property. In: Ciferri, O., Tiano, P., Mastromei, G. (Eds.), *Of Microbes and Art: The Role of Microbial Communities in the Degradation and Protection of Cultural Heritage*. Springer, US, Boston, MA, pp. 203–218.
- Castro-Alonso M. J., Montañez-Hernandez L. E., Sanchez-Muñoz M. A., Macias Franco M. R., Narayanasamy R. and Balagurusamy N. (2019) Microbially Induced Calcium

- Carbonate Precipitation (MICP) and Its Potential in Bioconcrete: Microbiological and Molecular Concepts. *Frontiers in Materials*. 6.
- Celle-Jeanton, H., Travi, Y., Blavoux, B., 2001. Isotopic typology of the precipitation in the Western Mediterranean Region at three different time scales. *Geophys. Res. Lett.* 28, 1215–1218.
- Chaka, A.M., 2019. Quantifying the impact of magnesium on the stability and water binding energy of hydrated calcium carbonates by ab initio thermodynamics. *J. Phys. Chem. A* 123, 2908–2923.
- Chamberlayne, B.K., Tyler, J.J., Gillanders, B.M., 2021. Elemental concentrations of waters and bivalves in the fresh to hypersaline Coorong Lagoons, South Australia: Implications for palaeoenvironmental studies. *Estuar. Coast. Shelf Sci.* 255, 107354.
- Chan, C.S., McAllister, S.M., Leavitt, A.H., Glazer, B.T., Krepški, S.T., Emerson, D., 2016. The Architecture of Iron Microbial Mats Reflects the Adaptation of Chemolithotrophic Iron Oxidation in Freshwater and Marine Environments. *Front. Microbiol.* 7, 18.
- Chanda, P., Gorski, C.A., Oakes, R.L., Fantle, M.S., 2019. Low temperature stable mineral recrystallization of foraminiferal tests and implications for the fidelity of geochemical proxies. *Earth Planet. Sci. Lett.* 506, 428–440.
- Chang, B., Chang, B., Li, C., Liu, D., Foster, I., Tripati, A., Lloyd, M.K., Maradiaga, I., Luo, G., An, Z., She, Z., Xie, S., Tong, J., Huang, J., Algeo, T.J., Lyons, T.W., Immenhauser, A., 2020. Massive formation of early diagenetic dolomite in the Ediacaran ocean: Constraints on the "dolomite problem". *Proc. Natl. Acad. Sci. USA* 117, 14005–14014.
- Chapman, J.B., Weiss, D.J., Shan, Y., Lemberger, M., 2009. Iron isotope fractionation during leaching of granite and basalt by hydrochloric and oxalic acids. *Geochim. Cosmochim. Acta* 73, 1312–1324.
- Charrieau, L.M., Rollion-Bard, C., Terbrueggen, A., Wilson, D.J., Pogge von Strandmann, P.A.E., Misra, S., Bijma, J., 2023. Controls on lithium incorporation and isotopic fractionation in large benthic foraminifera. *Minerals* 13, 127.
- Chaussemer, M., Pourmohtasham, E., Gelus, D., Pécul, N., Perrot, H., Lédition, J., Cheap-Charpentier, H., Horner, O., 2015. State of art of natural inhibitors of calcium carbonate scaling. A review article. *Desalination* 356, 47–55.
- Chen, C., Zhong, H., Wang, X., Ning, M., Wang, X., Ge, Y., Wang, H., Tang, R., Hou, M., 2023a. Thermodynamic and Kinetic Studies of Dolomite Formation: A Review. *Minerals* 13, 1479.
- Chen, D., Thibon, F., Felbacq, A., Weppe, L., Metian, M., Vigier, N., 2023b. Coupled survey of lithium isotopes and Li/Ca in biogenic and inorganic carbonates. *Earth Sci. Rev.* 244, 104500.
- Chen, J., Jiang, M., Su, M., Han, J., Li, S., Wu, Q., 2019. Mineralization of Calcium Carbonate Induced by Egg Substrate and an Electric Field. *Chem. Eng. Technol.* 42, 1525–1532.
- Chen X., Cao M., Algeo T. J., Li N., Wei G.-y., Lin Y.-b., Zhang H., Xiang L., Zhu Y., Xu C., Fan C., Shen S. and Zhang F. (2024) Diagenetic effects on strontium isotopes in shallow-water carbonate sediments from Middle Miocene to Recent. *Chem. Geol.* 646, 121882.
- Chen, X., Deng, W., Wang, H., Zeng, T., Zhang, L., Zhao, J.X., Wei, G., 2021b. A Replication Study on Coral δ11B and B/Ca and Their Variation in Modern and Fossil Porites: Implications for Coral Calcifying Fluid Chemistry and Seawater pH Changes Over the Last Millennium. *Paleoceanography and Paleoclimatology* 36.
- Chen, X., Romaniello, S.J., Anbar, A.D., 2021a. Preliminary exploration of molybdenum isotope fractionation during coprecipitation of molybdate with abiotic and microbial calcite. *Chem. Geol.* 566, 120102.
- Chen, X.-Y., Teng, F.-Z., Sanchez, W.R., Romanek, C.S., Sanchez-Navas, A., Sánchez-Román, M., 2020b. Experimental constraints on magnesium isotope fractionation during abiogenic calcite precipitation at room temperature. *Geochim. Cosmochim. Acta* 281, 102–117.
- Cheng, H., Edwards, R.L., Sinha, A., Spötl, C., Yi, L., Chen, S., Kelly, M., Kathayat, G., Wang, X., Li, X., Kong, X., Wang, Y., Ning, Y., Zhang, H., 2016. The Asian monsoon over the past 640,000 years and ice age terminations. *Nature* 534, 640–646.
- Cheng H., Lawrence Edwards R., Shen C.-C., Polyak V. J., Asmerom Y., Woodhead J., Hellstrom J., Wang Y., Kong X., Spötl C., Wang X. and Calvin Alexander Jr E. (2013) Improvements in ^{230}Th dating, ^{230}Th and ^{234}U half-life values, and U-Th isotopic measurements by multi-collector inductively coupled plasma mass spectrometry. *Earth Planet. Sci. Lett.* 371–372, 82–91.
- Cheng, J., Raudsepp, M.J., Wilson, S., Alessi, D.S., 2024. Amorphous-to-crystalline transition of Ca-Mg-carbonates as a function of composition, time, and temperature. *Cryst. Growth Des.* 24, 2349–2361.
- Cheng, Y.-J., Tang, C.-S., Pan, X.-H., Liu, B., Xie, Y.-H., Cheng, Q., Shi, B., 2021. Application of microbial induced carbonate precipitation for loess surface erosion control. *Eng. Geol.* 294, 106387.
- Chetty, K., Xie, S., Song, Y., McCarthy, T., Garbe, U., Li, X., Jiang, G., 2021. Self-healing bioconcrete based on non-axenic granules: A potential solution for concrete wastewater infrastructure. *Journal of Water Process Engineering* 42, 102139.
- Chhimi, N., Haddad, E., Neveux, T., Bouteleux, C., Teychené, S., Biscans, B., 2020. Performance of green antiscalants and their mixtures in controlled calcium carbonate precipitation conditions reproducing industrial cooling circuits. *Water Res.* 186, 116334.
- Christensen, J.N., Watkins, J.M., Devriendt, L.S., DePaolo, D.J., Conrad, M.E., Voltolini, M., Yang, W., Dong, W., 2021. Isotopic fractionation accompanying CO₂ hydroxylation and carbonate precipitation from high pH waters at The Cedars, California, USA. *Geochim. Cosmochim. Acta* 301, 91–115.
- Christy, A.G., 2017. A Review of the Structures of Vaterite: The Impossible, the Possible, and the Likely. *Cryst. Growth Des.* 17, 3567–3578.
- Gizdziel, J., Farmer, D., Hodge, V., Lindley, K., Stetzenbach, K., 2005. $^{234}\text{U}/^{238}\text{U}$ isotope ratios in groundwater from Southern Nevada: a comparison of alpha counting and magnetic sector ICP-MS. *Sci. Total Environ.* 350, 248–260.
- Clark, A.J., Torres-Romero, I., Jaggi, M., Bernasconi, S.M., Stoll, H.M., 2024. A clumped isotope calibration of coccoliths at well-constrained culture temperatures for marine temperature reconstructions. *Clim. Past* 20, 2081–2101.
- Clark I. D. and Fritz P. (1997) Environmental Isotopes in Hydrology. CRC Press, 352pp.
- Clarkson, M.O., Sweere, T.C., Chiu, C.F., Hennekam, R., Bowyer, F., Wood, R.A., 2023. Environmental controls on very high $\delta^{238}\text{U}$ values in reducing sediments: Implications for Neoproterozoic seawater records. *Earth Sci. Rev.* 237, 104306.
- Cole, C., Finch, A., Hintz, C., Hintz, K., Allison, N., 2016a. Understanding cold bias: variable response of skeletal Sr/Ca to seawater pCO₂ in acclimated massive Porites corals. *Sci. Rep.* 6, 26888.
- Cole, D.B., Reinhard, C.T., Wang, X., Gueguen, B., Halverson, G.P., Gibson, T., Hodgkiss, M.S.W., Ryan, McKenzie N., Lyons, T.W., 2016b. A shale-hosted Cr isotope record of low atmospheric oxygen during the Proterozoic. *Geology* 44, 555–558.
- Collister, C., Mattey, D., 2008. Controls on water drop volume and speleothem drip sites: an experimental study. *J. Hydrol.* 358, 259–267.
- Colucci, R.R., Luetscher, M., Forte, E., Guglielmin, M., Lenaz, D., Princivalle, F., Vita, F., 2017. First alpine evidence of in situ coarse cryogenic cave carbonates (CCCoarse). *Geog. Fis. Dinam. Quat.* 40, 53–59.
- Comas-Bru, L., Harrison, S.P., Werner, M., Rehfeld, K., Scroxton, N., Veiga-Pires, C., members S. w. g., 2019. Evaluating model outputs using integrated global speleothem records of climate change since the last glacial. *Clim. Past* 15, 1557–1579.
- Comas-Bru, L., Rehfeld, K., Roesch, C., Amirnezhad-Mozhdehi, S., Harrison, S.P., Atsawaranunt, K., Ahmad, S.M., Brahim, Y.A., Baker, A., Bosomworth, M., Breitenbach, S.F.M., Burstyn, Y., Columbu, A., Deininger, M., Demény, A., Dixon, B., Fohlemeister, J., Hatvani, I.G., Hu, J., Kaushal, N., Kern, Z., Labuhn, I., Lechleitner, F. A., Lorrey, A., Martrat, B., Novello, V.F., Oster, J., Pérez-Mejías, C., Scholz, D., Scroxton, N., Sinha, N., Ward, B.M., Warken, S., Zhang, H., members S. W. G., 2020. SISALV2: a comprehensive speleothem isotope database with multiple age-depth models. *Earth Syst. Sci. Data* 12, 2579–2606.
- Cook, P.K., Dufour, E., Langlione, M.A., Mocuta, C., Réguer, S., Bertrand, L., 2016. Strontium speciation in archaeological ooliths. *J. Anal. At. Spectrom.* 31, 700–711.
- Cooper, K.G., Hanlon, L.G., Smart, G.M., Talbot, R.E., 1979. The threshold scale inhibition phenomenon. *Desalination* 31, 257–266.
- Coplen, T.B., 2007. Calibration of the calcite–water oxygen-isotope geothermometer at Devils Hole, Nevada, a natural laboratory. *Geochim. Cosmochim. Acta* 71, 3948–3957.
- Cosmo, R.d.P., Pereira, F.d.A.R., Soares, E.J., Ferreira, E.G., 2022. Addressing the root cause of calcite precipitation that leads to energy loss in geothermal systems. *Geothermics* 98, 102272.
- Crocket, J.H., Winchester, J.W., 1966. Coprecipitation of zinc with calcium carbonate. *Geochim. Cosmochim. Acta* 30, 1093–1109.
- Cuauquique-Flores, G., Aguirre-Noyola, J.L., Hernández-Flores, G., Martínez-Romero, E., Romero-Ramírez, Y., Talavera-Mendoza, O., 2020. Bioimmobilization of toxic metals by precipitation of carbonates using Sporosarcina luteola: An in vitro study and application to sulfide-bearing tailings. *Sci. Total Environ.* 724, 138124.
- Cuesta, Mayorga I., Astilleros, J.M., Fernández-Díaz, L., Morales, J., Prieto, M., Roncal-Herrero, T., Benning, L.G., 2018. Epitactic Overgrowths of Calcite (CaCO_3) on Anhydrite (CaSO_4) Cleavage Surfaces. *Crystal Growth and Design* 18, 1666–1675.
- Cuny-Guirriec, K., Douville, E., Reynaud, S., Allemand, D., Bordier, L., Canesi, M., Mazzoli, C., Taviani, M., Canese, S., McCulloch, M., Trotter, J., Rico-Esenero, S.D., Sanchez-Cabeza, J.-A., Ruiz-Fernández, A.C., Carricart-Ganivet, J.P., Scott, P.M., Sadekov, A., Montagna, P., 2019. Coral Li/Mg thermometry: Caveats and constraints. *Chem. Geol.* 523, 162–178.
- Currey, L.M., Heupel, M.R., Simpfendorfer, C.A., Williams, A.J., 2014. Inferring movement patterns of a coral reef fish using oxygen and carbon isotopes in otolith carbonate. *J. Exp. Mar. Biol. Ecol.* 456, 18–25.
- Curti, E., 1999. Coprecipitation of radionuclides with calcite: Estimation of partition coefficients based on a review of laboratory investigations and geochemical data. *Appl. Geochem.* 14, 433–445.
- Czuppon, G., Bočić, N., Buzjak, N., Óvári, M., Molnár, M., 2018. Monitoring in the Barać and Lower Cerovacka caves (Croatia) as a basis for the characterization of the climatological and hydrological processes that control speleothem formation. *Quat. Int.* 494, 52–65.
- Daëron, M., Blamart, D., Peral, M., Affek, H.P., 2016. Absolute isotopic abundance ratios and the accuracy of Δ_{47} measurements. *Chem. Geol.* 442, 83–96.
- Daëron, M., Drysdale, R.N., Peral, M., Huyghe, D., Blamart, D., Coplen, T.B., Lartaud, F., Zanchetta, G., 2019. Most Earth-surface calcites precipitate out of isotopic equilibrium. *Nat. Commun.* 10, 429.
- Dämmer L. K., van Dijk I., de Nooijer L., van der Wagt B., Wilckens F. K., Zoetemelk B. and Reichart G.-J. (2021) Temperature Impact on Magnesium Isotope Fractionation in Cultured Foraminifera. *Frontiers in Earth Science* 9.
- Dandurand, J.L., Gout, R., Hoefs, J., Menschel, G., Schott, J., Usdowski, E., 1982. Kinetically controlled variations of major components and carbon and oxygen isotopes in a calcite-precipitating spring. *Chem. Geol.* 36, 299–315.
- Davies, A.J., Guo, W., Bernecker, M., Tagliavento, M., Raddatz, J., Gischler, E., Flögel, S., Fiebig, J., 2022. Dual clumped isotope thermometry of coral carbonate. *Geochim. Cosmochim. Acta* 338, 66–78.
- Davis, C.V., Doherty, S., Fehrenbacher, J., Wishner, K., 2023. Trace element composition of modern planktic foraminifera from an oxygen minimum zone: Potential proxies for an enigmatic environment. *Frontiers in Marine Science* 10.
- Davis, J.A., Fuller, C.C., Cook, A.D., 1987. A model for trace metal sorption processes at the calcite surface: Adsorption of Cd²⁺ and subsequent solid solution formation. *Geochim. Cosmochim. Acta* 51, 1477–1490.

- Day, C.C., Pogge von Strandmann, P.A.E., Mason, A.J., 2021. Lithium isotopes and partition coefficients in inorganic carbonates: Proxy calibration for weathering reconstruction. *Geochim. Cosmochim. Acta* 305, 243–262.
- De Belie, N., Wang, J., 2016. Bacteria-based repair and self-healing of concrete. *J. Sustain. Cem.-Based Mater.* 5, 35–56.
- De Boever, E., Brasier, A.T., Fouquet, A., Kele, S., 2017. What do we really know about early diagenesis of non-marine carbonates? *Sediment. Geol.* 361, 25–51.
- De Filippis, L., Faccenna, C., Billi, A., Anzalone, E., Brilli, M., Soligo, M., Tuccimei, P., 2013. Plateau versus fissure ridge travertines from Quaternary geothermal springs of Italy and Turkey: Interactions and feedbacks between fluid discharge, paleoclimate, and tectonics. *Earth Sci. Rev.* 123, 35–52.
- De Groot, P.A., e., 2009. *Handbook of Stable Isotope Analytical Techniques*. Elsevier, Amsterdam, The Netherlands.
- De Wever, A., Benzerara, K., Coutaud, M., Caumes, G., Poinsot, M., Skouri-Panet, F., Laurent, T., Duprat, E., Gugger, M., 2019. Evidence of high Ca uptake by cyanobacteria forming intracellular CaCO_3 and impact on their growth. *Geobiology* 17, 676–690.
- De Yoreo, J., 2020. A Perspective on Multistep Pathways of Nucleation. In: *Crystallization via Nonclassical Pathways Volume 1: Nucleation. Observation & Application*. American Chemical Society, Assembly, pp. 1–17.
- De Yoreo, J., Jin, B., Chen, Y., Pyles, H., Baer, M., Legg, B., Wang, Z., Washton, N., Mueller, K., Baker, D., Schenter, G., Mundy, C., 2022. Formation, Chemical Evolution, and Solidification of the Calcium Carbonate Dense Liquid Phase. Research Square.
- De Yoreo, J.J., Gilbert, P.U.P.A., Sommerdijk, N.A.J.M., Penn, R.L., Whitelam, S., Joester, D., Zhang, H., Rimer, J.D., Navrotsky, A., Banfield, J.F., Wallace, A.F., Michel, F.M., Meldrum, F.C., Cölfen, H., Dove, P.M., 2015. Crystallization by particle attachment in synthetic, biogenic, and geologic environments. *Science* 349.
- DeCarlo, T.M., Gaetani, G.A., Holcomb, M., Cohen, A.L., 2015. Experimental determination of factors controlling U/Ca of aragonite precipitated from seawater: Implications for interpreting coral skeleton. *Geochim. Cosmochim. Acta* 162, 151–165.
- DeCarlo, T.M., Holcomb, M., McCulloch, M.T., 2018. Reviews and syntheses: Revisiting the boron systematics of aragonite and their application to coral calcification. *Biogeosciences* 15, 2819–2834.
- Deelman, B.J.C., 1999. Low-temperature nucleation of magnesite and dolomite. *N. Jahrb. Mineral. MH*, 7, 289–302.
- del Buey, P., Sanz-Montero, M.E., 2023. Biomineralization of ordered dolomite and magnesian calcite by the green alga Spirogyra. *Sedimentology* 70, 685–704.
- Della Porta, G. (2015) Carbonate build-ups in lacustrine, hydrothermal and fluvial settings: comparing depositional geometry, fabric types and geochemical signature. *Bosence, D. W. J., Gibbons, K. A., Le Heron, D. P., Morgan, W. A., Pritchard, T., Vining, B. A. (eds) 2015. Microbial Carbonates in Space and Time: Implications for Global Exploration and Production. Geological Society London, Special Publications* 418, 17–68.
- Della Porta, G., Croci, A., Marini, M., Kele, S., 2017. Depositional architecture, facies character and geochemical signature of the Tivoli travertines (Pleistocene, Acque Albule Basin, Central Italy). *Riv. Ital. Paleontol. Stratigr.* 123, 487–540.
- Dellinger, M., West, A.J., Paris, G., Adkins, J.F., Pogge von Strandmann, P.A.E., Ullmann, C.V., Eagle, R.A., Freitas, P., Bagard, M.-L., Ries, J.B., Corsetti, F.A., Perez-Huerta, A., Kampf, A.R., 2018. The Li isotope composition of marine biogenic carbonates: Patterns and mechanisms. *Geochim. Cosmochim. Acta* 236, 315–335.
- Demény, A., Kern, Z., Czuppon, G., Németh, A., Leél-Össy, S., Siklósy, Z., Lin, K., Hu, H.-M., Shen, C.-C., Vennemann, T.W., Haszprá, L., 2017. Stable isotope compositions of speleothems from the last interglacial – Spatial patterns of climate fluctuations in Europe. *Quat. Sci. Rev.* 161, 68–80.
- Demény, A., Németh, P., Czuppon, G., Leél-Össy, S., Szabó, M., Judik, K., Németh, T., Stieber, J., 2016. Formation of amorphous calcium carbonate in caves and its implications for speleothem research. *Sci. Rep.* 6, 39602.
- Demény, A., Rinyu, L., Kern, Z., Hatvani, I.G., Czuppon, G., Surányi, G., Leél-Össy, S., Shen, C.-C., Koltai, G., 2021. Paleotemperature reconstructions using speleothem fluid inclusion analyses from Hungary. *Chem. Geol.* 563, 120051.
- Deocampo D. M. (2010) Chapter 1 The Geochemistry of Continental Carbonates, Developments in Sedimentology, pp. 1–59.
- DePaolo, D.J., 2011. Surface kinetic model for isotopic and trace element fractionation during precipitation of calcite from aqueous solutions. *Geochim. Cosmochim. Acta* 75, 1039–1056.
- DePaolo, D.J., Cole, D.R., Navrotsky, A., Bourg, I.C., 2013. Geochemistry of Geologic Carbon Sequestration: An Overview. *Rev. Mineral. Geochem.* 77, 1–14.
- Dettman, D.L., Reische, A.K., Lohmann, K.C., 1999. Controls on the stable isotope composition of seasonal growth bands in aragonitic fresh-water bivalves (unionidae). *Geochim. Cosmochim. Acta* 63, 1049–1057.
- Dhami, N.K., Mukherjee, A., Watkin, E.L.J., 2018. Microbial Diversity and Mineralogical-Mechanical Properties of Calcitic Cave Speleothems in Natural and in Vitro Biominerization Conditions. *Front. Microbiol.* 9.
- Diao, Y., Li, A., Espinosa-Marzal, R.M., 2020. Ion specific effects on the pressure solution of calcite single crystals. *Geochim. Cosmochim. Acta* 280, 116–129.
- Diaz, M.R., Eberli, G.P., Blackwelder, P., Phillips, B., Swart, P.K., 2017. Microbially mediated organomineralization in the formation of ooids. *Geology* 45, 771–774.
- Diaz-Hernandez, J.L., Sánchez-Nava, A., Delgado, A., Yepes, J., García-Casco, A., 2018. Textural and isotopic evidence for Ca-Mg carbonate pedogenesis. *Geochim. Cosmochim. Acta* 222, 485–507.
- Dickson, J.A.D., 1993. Crystal growth diagrams as an aid to interpreting the fabrics of calcite aggregates. *J. Sediment. Petrol.* 63, 1–17.
- Dickson, J.A.D., 2023. Insights into the growth morphology of calcite cement. *Depositional Rec.* 9, 457–481.
- Dideriksen, K., Baker, J.A., Stipp, S.L.S., 2008. Equilibrium Fe isotope fractionation between inorganic aqueous Fe(III) and the siderophore complex, Fe(III)-desferrioxamine B. *Earth Planet. Sci. Lett.* 269, 280–290.
- Dielforder, A., Villa, I.M., Berger, A., Herwegh, M., 2022. Tracing wedge-internal deformation by means of strontium isotope systematics of vein carbonates. *Geol. Mag.* 159, 2191–2205.
- Dietzel, M. (2011) Carbonates. *Encyclopaedia of Geobiology (eds: J. Reitner, V. Thiel): Part 3 Springer Verlag* 261–266.
- Dietzel, M., Boch, R. (2019) Radiometrische Altersdatierung von historischem Kalkmörtel. In *St. Johann im Mauerthal und Ybbs an der Donau - Zwei neu entdeckte römische Militäranlagen am norischen Limes und ihre Nachfolgebauten* (ed. B. Hebert). Fokus Denkmal - Bundesdenkmalamt, Vienna, pp. 229–233.
- Dietzel, M., Gussone, N., Eisenhauer, A., 2004. Co-precipitation of Sr²⁺ and Ba²⁺ with aragonite by membrane diffusion of CO₂ between 10 and 50 °C. *Chem. Geol.* 203, 139–151.
- Dietzel, M., Purgstaller, B., Kluge, T., Leis, A., Mavromatis, V., 2020. Oxygen and clumped isotope fractionation during the formation of Mg calcite via an amorphous precursor. *Geochim. Cosmochim. Acta* 276, 258–273.
- Dietzel, M., Purgstaller, B., Leis, A., Reichl, P., Stadler, H., Niedermayr, A., Rinder, Th., Wagner, H., 2013. Current challenges for scaling of tunnel drainage systems - Modelling approaches, monitoring tools and prevention strategies. *Geomechanics and Tunnelling* 6, 743–753.
- Dietzel, M., Schön, F., Heinrichs, J., Deditius, A.P., and Leis, A. (2016) Tracing formation and durability of calcite in a Punic-Roman cistern mortar (Pantelleria Island, Italy). *Isot. Environ. Health Stud.* 52, 112–127.
- Dietzel, M., Tang, J., Leis, A. and Köhler, S.J. (2009) Oxygen isotopic fractionation during inorganic calcite precipitation - Effects of temperature, precipitation rate and pH. *Chem. Geol.* 268, 107–115.
- Dietzel, M., Usdowski, E., Hoefs, J., 1992. Chemical and ¹³C/¹²C- and ¹⁸O/¹⁶O-isotope evolution of alkaline drainage waters and the precipitation of calcite. *Appl. Geochem.* 7, 177–184.
- Disspain, M.C.F., Ulm, S., Gillanders, B.M., 2016. Otoliths in archaeology: Methods, applications and future prospects. *J. Archaeol. Sci. Rep.* 6, 623–632.
- Dobberschütz, S., Nielsen, M.R., Sand, K.K., Civio, R., Bovet, N., Stipp, S.L.S., Andersson, M.P., 2018. The mechanisms of crystal growth inhibition by organic and inorganic inhibitors. *Nat. Commun.* 9, 1578.
- Domínguez-Villar, D., Krklec, K., Pelicon, P., Fairchild, I.J., Cheng, H., Edwards, L.R., 2017. Geochemistry of speleothems affected by aragonite to calcite recrystallization – Potential inheritance from the precursor mineral. *Geochim. Cosmochim. Acta* 200, 310–329.
- Dong, L., Xu, Y.-J., Sui, C., Zhao, Y., Mao, L.-B., Gebauer, D., Rosenberg, R., Avaro, J., Wu, Y.-D., Gao, H.-L., Pan, Z., Wen, H.-Q., Yan, X., Li, F., Lu, Y., Cölfen, H., Yu, S.-H., 2022. Highly hydrated paramagnetic amorphous calcium carbonate nanoclusters as an MRI contrast agent. *Nat. Commun.* 13, 5088.
- Dong, S., Wasylkeni, L.E., 2016. Zinc isotope fractionation during adsorption to calcite at high and low ionic strength. *Chem. Geol.* 447, 70–78.
- Donner, A., Töchterle, P., Spötl, C., Hajdas, I., Li, X., Edwards, R.L., Moseley, G.E., 2023. Cryogenic cave minerals recorded the 1889 CE melt event in northeastern Greenland. *Clim. Past* 19, 1607–1621.
- Dove, P.M., De Yoreo, J.J., Weiner, S. (Eds.), 2003. *Biomineralization*: Washington, Mineralogical Society of America and the Geochemical Society, Reviews in Mineralogy and Geochemistry, 54, 381 pp.
- Drake, H., Mathurin, F.A., Zack, T., Schäfer, T., Roberts, N.M.W., Whitehouse, M., Karlsson, A., Broman, C., Åström, M.E., 2018. Incorporation of Metals into Calcite in a Deep Anoxic Granite Aquifer. *Environ. Sci. Technol.* 52, 493–502.
- Dromgoole, E.L., Walter, L.M., 1990. Iron and manganese incorporation into calcite: Effects of growth kinetics, temperature and solution chemistry. *Chem. Geol.* 81, 311–336.
- Druce, M., Stirling, C.H., Bostock, H.C., Rolison, J.M., 2022. Examining the effects of chemical cleaning, leaching, and partial dissolution on zinc and cadmium isotope fractionation in marine carbonates. *Chem. Geol.* 592.
- Druhan, J.L., Lammers, L., Fantle, M.S., 2020. On the utility of quantitative modeling to the interpretation of Ca isotopes. *Chem. Geol.* 537, 119469.
- Druschel, G.K., Kappler, A., 2015. *Geomicrobiology and Microbial Geochemistry*. Elements 11, 389–394.
- Drysdale, R.N., Zanchetta, G., Baneschi, I., Guidi, M., Isola, I., Couchoud, I., Piccini, L., Greig, A., Wong, H., Woodhead, J.D., Regattieri, E., Corrick, E., Paul, B., Spötl, C., Denison, E., Gordon, J., Jaitlet, S., Dux, F., Hellstrom, J.C., 2019. Partitioning of Mg, Sr, Ba and U into a subaqueous calcite speleothem. *Geochim. Cosmochim. Acta* 264, 67–91.
- D'Souza, S.M., Alexander, C., Carr, S.W., Waller, A.M., Whitcombe, M.J., Vulson, E.N., 1999. Directed nucleation of calcite at a crystal-imprinted polymer surface. *Nature* 398, 312–316.
- Du, H., Amstad, E., 2020. Water: How Does It Influence the CaCO_3 Formation? *Angew. Chem. Int. Ed. Eng.* 59, 1798–1816.
- Dubinin, E.O., Kramchaninov, A.Y., Silantyev, S.A., Bortnikov, N.S., 2020. Influence of the Precipitation Rate on the Isotope ($\delta^{18}\text{O}$, $\delta^{13}\text{C}$ and $\delta^{88}\text{Sr}$) Composition of Carbonate Chimneys of the Lost City Hydrothermal Field (30° N, Mid-Atlantic Ridge). *Petrology* 28, 374–388.
- Dublyansky, Y.V., 2014. Evaluation of the US DOE's conceptual model of hydrothermal activity at Yucca Mountain. Nevada. *Geosci. Model Dev.* 7, 1583–1607.
- Eagle, R.A., Schauble, E.A., Tripathi, A.K., Tütken, T., Hulbert, R.C., Eiler, J.M., 2010. Body temperatures of modern and extinct vertebrates from ¹³C-¹⁸O bond abundances in biapatite. *Proc. Natl. Acad. Sci.* 107, 10377–10382.
- Eggeling, L., Genter, A., Köbel, T., Münnich, W., 2013. Impact of natural radionuclides on geothermal exploitation in the Upper Rhine Graben. *Geothermics* 47, 80–88.

- Eichinger, S., Boch, R., Baldermann, A., Goetschl, K., Wenighofer, R., Hoffmann, R., Stamm, F., Hippel, D., Grengg, C., Immenhauser, A., Dietzel, M., 2023. Unravelling calcite-to-aragonite evolution from a subsurface fluid - Formation pathway, interfacial reactions and nucleation effects. *Chem. Geol.* 641.
- Eichinger, S., Boch, R., Leis, A., Koraimann, G., Grengg, C., Domberger, G., Nachtnebel, M., Schwab, C., Dietzel, M., 2020. Scale deposits in tunnel drainage systems - A study on fabrics and formation mechanisms. *Sci. Total Environ.* 718.
- Eiler, J.M., 2011. Paleoclimate reconstruction using carbonate clumped isotope thermometry. *Quat. Sci. Rev.* 30, 3575–3588.
- Eiler, J.M., 2013. The Isotopic Anatomies of Molecules and Minerals. *Annu. Rev. Earth Planet. Sci.* 41, 411–441.
- Eiler, J.M., Bergquist, B., Bourg, I., Cartigny, P., Farquhar, J., Gagnon, A., Guo, W., Halevy, I., Hofmann, A., Larson, T.E., Levin, N., Schauble, E.A., Stolper, D., 2014. Frontiers of stable isotope geoscience. *Chem. Geol.* 372, 119–143.
- Eisenhauer, A., Kisakürek, B., Böhm, F., 2009. Marine calcification: An alkali earth metal isotope perspective. *Elements* 5, 365–368.
- Engelhardt, W., 1960. Der Porenraum der Sedimente. Springer, Berlin, Heidelberg.
- Enyedi, N.T., Makk, J., Kótai, L., Berényi, B., Klébert, S., Sebestyén, Z., Molnár, Z., Borsodi, A.K., Leél-Ossy, S., Demény, Á., Németh, P., 2020. Cave bacteria-induced amorphous calcium carbonate formation. *Sci. Rep.* 10, 8696.
- Epstein, S., Buchsbaum, R., Lowenstein, H.A., Urey, H.C., 1953. Revised carbonate-water isotopic temperature scale. *Geol. Soc. Am. Bull.* 64, 1315–1326.
- Erhardt, A.M., Turchyn, A.V., Bradbury, H.J., Dickson, J.A.D., 2020. The calcium isotopic composition of carbonate hardground cements: a new record of changes in ocean chemistry? *Chem. Geol.* 540, 119490.
- Erler, D.V., Duncan, T.M., Murray, R., Maher, D.T., Santos, I.R., Gatland, J.R., Mangion, P., Eyre, B.D., 2015. Applying cavity ring-down spectroscopy for the measurement of dissolved nitrous oxide concentrations and bulk nitrogen isotopic composition in aquatic systems: Correcting for interferences and field application. *Limnol. Oceanogr. Methods* 13, 391–401.
- Esmaeilnezhad, E., Choi, H.J., Schaffie, M., Gholizadeh, M., Ranjbar, M., 2017. Characteristics and applications of magnetized water as a green technology. *J. Clean. Prod.* 161, 908–921.
- Esteves, A.F., Santos, F.M., Magalhães, Pires J., C., 2019. Carbon dioxide as geothermal working fluid: An overview. *Renew. Sust. Energ. Rev.* 114, 109331.
- Evans, D., Webb, P.B., Penkman, K., Kröger, R., Allison, N., 2019. The Characteristics and Biological Relevance of Inorganic Amorphous Calcium Carbonate (ACC) Precipitated from Seawater. *Cryst. Growth Des.* 19, 4300–4313.
- Evans, D., Gray, W.R., Rae, J.W.B., Greenop, R., Webb, P.B., Penkman, K., Kröger, R., Allison, N., 2020. Trace and major element incorporation into amorphous calcium carbonate (ACC) precipitated from seawater. *Geochim. Cosmochim. Acta* 290, 293–311.
- Fadia, P., Tyagi, S., Bhagat, S., Nair, A., Panchal, P., Dave, H., Dang, S., Singh, S., 2021. Calcium carbonate nano- and microparticles: synthesis methods and biological applications. *3 Biotech* 11, 457.
- Fairchild, I.J., Baker, A., 2012. Speleothem Science - From Process to Past Environments. Wiley-Blackwell, Chichester, UK.
- Fairchild, I.J., Spötl, C., Frisia, S., Borsato, A., Susini, J., Wynn, P.M., Cauzid, J., 2010. Petrology and geochemistry of annually laminated stalagmites from an Alpine cave (Obir, Austria): Seasonal cave physiology. *Geol. Soc. Spec. Publ.* 336, 295–321.
- Falkenberg, J., Kaplan, U., Mutterlose, J., 2023. Understanding the provenance and production process of historic mortars—a novel approach employing calcareous nanofossils. *Archaeol. Anthropol. Sci.* 15.
- Fang, Z., He, X., Yu, X., Qin, L., 2023. Chromium isotope fractionation during adsorption of chromium(III) by soils and river sediments. *Journal of University of Science and Technology of China* 53.
- Fang, Z., Liu, W., Yao, T., Zhou, G., Wei, S., Qin, L., 2022. Experimental study of chromium (III) coprecipitation with calcium carbonate. *Geochim. Cosmochim. Acta* 322, 94–108.
- Fang, Z., Qin, L., Liu, W., Yao, T., Chen, X., Wei, S., 2021. Absence of hexavalent chromium in marine carbonates: Implications for chromium isotopes as paleoenvironment proxy. *Natl. Sci. Rev.* 8.
- Fantle, M.S., Barnes, B.D., Lau, K.V., 2020. The Role of Diagenesis in Shaping the Geochemistry of the Marine Carbonate Record. *Annu. Rev. Earth Planet. Sci.* 48, 549–583.
- Farkas, J., Böhm, F., Wallmann, K., Blenkinsop, J., Eisenhauer, A., van Geldern, R., Munnecke, A., Voigt, S., Veizer, J., 2007. Calcium isotope record of Phanerozoic oceans: Implications for chemical evolution of seawater and its causative mechanisms. *Geochim. Cosmochim. Acta* 71, 5117–5134.
- Farmer, J.R., Branson, O., Uchikawa, J., Penman, D.E., Hönnisch, B., Zeebe, R.E., 2019. Boric acid and borate incorporation in organic calcite inferred from B/Ca, boron isotopes and surface kinetic modeling. *Geochim. Cosmochim. Acta* 244, 229–247.
- Farrag, N.M., Bayoumi, R.A., Mohamed, T.A., 2022. Factorial analysis of nano-precipitated calcium carbonate via a carbonation route using Solvay wastewater. Case Studies in Chemical and Environmental Engineering 6, 100236.
- Fathi, A., Mohamed, T., Claude, G., Maurin, G., Mohamed, B.A., 2006. Effect of a magnetic water treatment on homogeneous and heterogeneous precipitation of calcium carbonate. *Water Res.* 40, 1941–1950.
- Faure, G., Mensing, T.M., 2010. The Transantarctic Mountains: rocks, ice, meteorites and water. Springer Science & Business Media, 600pp.
- Feng, D., Qiu, J.-W., Hu, Y., Peckmann, J., Guan, H., Tong, H., Chen, C., Chen, J., Gong, S., Li, N., Chen, D., 2018. Cold seep systems in the South China Sea: An overview. *J. Asian Earth Sci.* 168, 3–16.
- Feng, X., Jia, Z., Wang, X., 2023. Uncovering the temporal carbon isotope ($\delta^{13}\text{C}$) heterogeneity in seep carbonates: a case study from Green Canyon, northern Gulf of Mexico. *Frontiers in Marine. Science* 10.
- Feng, X., Redfern, S.A.T., 2018. Iodate in calcite, aragonite and vaterite CaCO_3 : Insights from first-principles calculations and implications for the I/Ca geochemical proxy. *Geochim. Cosmochim. Acta* 236, 351–360.
- Feng, X., Steiner, Z., Redfern, S.A.T., 2021. Fluorine incorporation into calcite, aragonite and vaterite CaCO_3 : Computational chemistry insights and geochemistry implications. *Geochim. Cosmochim. Acta* 308, 384–392.
- Fernandes, M.M., Stumpf, T., Rabung, T., Bosbach, D., Fanghänel, T., 2008. Incorporation of trivalent actinides into calcite: A time resolved laser fluorescence spectroscopy (TRLFS) study. *Geochim. Cosmochim. Acta* 72, 464–474.
- Fernandez, A., Tang, J., Rosenheim, B.E., 2014. Siderite ‘clumped’ isotope thermometry: A new paleoclimate proxy for humid continental environments. *Geochim. Cosmochim. Acta* 126, 411–421.
- Fichtner, V., Lange, S.M., Krause, S., Huthwelker, T., Borca, C.N., Schurr, S.L., Immenhauser, A., Pederson, C.L., Treude, T., Erhardt, A.M., Strauss, H., 2021. Microbial activity affects sulphur in biogenic aragonite. *Depositional Rec.* 7, 500–519.
- Fichtner, V., Strauss, H., Mavromatis, V., Dietzel, M., Huthwelker, T., Borca, C.N., Guagliardo, P., Kilburn, M.R., Göttlicher, J., Pederson, C.L., Griesshaber, E., Schmalz, W.W., Immenhauser, A., 2018. Incorporation and subsequent diagenetic alteration of sulfur in Arctica islandica. *Chem. Geol.* 482, 72–90.
- Fiebig, J., Daérón, M., Bernecker, M., Guo, W., Schneider, G., Boch, R., Bernasconi, S.M., Jautzy, J., Dietzel, M., 2021. Calibration of the dual clumped isotope thermometer for carbonates. *Geochim. Cosmochim. Acta* 312, 235–256.
- Finster, M., Clark, C., Schroeder, J., Martino, L., 2015. Geothermal produced fluids: Characteristics, treatment technologies, and management options. *Renew. Sust. Energ. Rev.* 50, 952–966.
- Fischer, M., Thomas, D.N., Krell, A., Nehrke, G., Göttlicher, J., Norman, L., Meiners, K., M., Riaux-Gobin, C., Dieckmann, G.S., 2013. Quantification of ikaite in Antarctic sea ice. *Antarct. Sci.* 25, 421–432.
- Fleming, M.R., Adams, B.M., Kuehn, T.H., Bielicki, J.M., Saar, M.O., 2020. Increased Power Generation due to Exothermic Water Exsolution in CO_2 Plume Geothermal (CPG) Power Plants. *Geothermics* 88, 101865.
- Flöter, S., Fietzke, J., Gutjahr, M., Nehrk, G., Eisenhauer, A., 2022. Incorporation of Na and S in bamboo coral skeletons. *Chem. Geol.* 597, 120795.
- Flügel E. (2010) Microfacies of Carbonate Rocks: Analysis, Interpretation and Application. Springer Berlin Heidelberg, 984pp.
- Fodor, M.A., Ható, Z., Kristóf, T., Pósfai, M., 2020. The role of clay surfaces in the heterogeneous nucleation of calcite: Molecular dynamics simulations of cluster formation and attachment. *Chem. Geol.* 538, 119497.
- Fohlmeister, J., Plessen, B., Dudashvili, A.S., Tjallingii, R., Wolff, C., Gafurov, A., Cheng, H., 2017. Winter precipitation changes during the Medieval Climate Anomaly and the Little Ice Age in arid Central Asia. *Quat. Sci. Rev.* 178, 24–36.
- Fohlmeister, J., Voarintsoa, N.R.G., Lechleitner, F.A., Boyd, M., Brandstätter, S., Jacobson, M.J., Oster, J.L., 2020. Main controls on the stable carbon isotope composition of speleothems. *Geochim. Cosmochim. Acta* 279, 67–87.
- Ford, D., Williams, P., 2013. Karst Hydrogeology and Geomorphology. John Wiley & Sons.
- Forjanés, P., Pérez-Garrido, C., Álvarez-Lloret, P., Astilleros, J.M., Fernández-Díaz, L., 2022. Formation of strontianite and witherite cohesive layers on calcite surfaces for building stone conservation. *Cryst. Growth Des.* 22, 6418–6428.
- Fort, R., Varas-Muriel, M.J., Ergenç, D., Cassar, J., Anastasi, M., Vella, N.C., 2023. The technology of ancient lime mortars from the Żejtun Roman Villa (Malta). *Archaeol. Anthropol. Sci.* 15, 15.
- Fouke, B.W., 2011. Hot-spring Systems Geobiology: abiotic and biotic influences on travertine formation at Mammoth Hot Springs, Yellowstone National Park, USA. *Sedimentology* 58, 170–219.
- Franklin, M.L., Morse, J.W., 1983. The interaction of manganese(II) with the surface of calcite in dilute solutions and seawater. *Mar. Chem.* 12, 241–254.
- Frappier, A.B., Sahagian, D., Carpenter, S.J., González, L.A., Frappier, B.R., 2007. Stalagmite stable isotope record of recent tropical cyclone events. *Geology* 35, 111–114.
- Frei, R., Gaucher, C., Poulton, S.W., Canfield, D.E., 2009. Fluctuations in Precambrian atmospheric oxygenation recorded by chromium isotopes. *Nature* 461, 250–253.
- Freytet, P., Verrecchia, E.P., 1998. Freshwater organisms that build stromatolites: a synopsis of biocrystallization by prokaryotic and eukaryotic algae. *Sedimentology* 45, 535–563.
- Frisia, S., 2015. Microstratigraphic logging of calcite fabrics in speleothems as tool for palaeoclimate studies. *Int. J. Speleol.* 44, 1–16.
- Frisia, S., Borsato, A., Hellstrom, J., 2018. High spatial resolution investigation of nucleation, growth and early diagenesis in speleothems as exemplar for sedimentary carbonates. *Earth Sci. Rev.* 178, 68–91.
- Frisia, S., Weyrich, L.S., Hellstrom, J., Borsato, A., Golledge, N.R., Anesio, A.M., Bajo, P., Drysdale, R.N., Augustinus, P.C., Rivard, C., Cooper, A., 2017. The influence of Antarctic subglacial volcanism on the global iron cycle during the Last Glacial Maximum. *Nat. Commun.* 8, 15425.
- Füger, A., Bruggmann, S., Frei, R., Leis, A., Dietzel, M., Mavromatis, V., 2019b. The role of pH on Cr(VI) partitioning and isotopic fractionation during its incorporation in calcite. *Geochim. Cosmochim. Acta* 265, 520–532.
- Füger, A., Konrad, F., Leis, A., Dietzel, M., Mavromatis, V., 2019a. Effect of growth rate and pH on lithium incorporation in calcite. *Geochim. Cosmochim. Acta* 248, 14–24.
- Füger, A., Kuessner, M., Rollion-Bard, C., Leis, A., Magna, T., Dietzel, M., Mavromatis, V., 2022. Effect of growth rate and pH on Li isotope fractionation during its incorporation in calcite. *Geochim. Cosmochim. Acta* 323, 276–290.
- Fujihara, M., Shiokawa, K., Araki, M., Ashitaka, N., Morigaki, K., Kubota, T., Nakahara, Y., 2010. Encapsulation of Proteins into CaCO_3 by Phase Transition from Vaterite to Calcite. *Cryst. Growth Des.* 10, 4030–4037.

- Fussmann, D., Von Hoyningen-Huene, Jean Elisabeth, A., Reimer A., Schneider D., Babková H., Peticzka R., Maier A., Arp G., Daniel R. and Meister P., 2020. Authigenic formation of Ca-Mg carbonates in the shallow alkaline Lake Neusiedl, Austria. *Biogeosciences* 17, 2085–2106.
- Gabitov, R., Migdisov, A., Nguyen, A., Van Hartesveldt, N., Perez-Huerta, A., Sadekov, A., Sauer, K.B., Baker, J., Paul, V., Caporuscio, F., Xu, H., Roback, R., 2021b. Uptake of uranium by carbonate crystallization from reduced and oxidized hydrothermal fluids. *Chem. Geol.* 564, 12054.
- Gabitov, R., Sadekov, A., Yapaskurt, V., Borrelli, C., Bychkov, A., Sabourin, K., Perez-Huerta, A., 2019. Elemental Uptake by Calcite Slowly Grown From Seawater Solution: An in-situ Study via Depth Profiling. *Frontiers. Earth Sci.* 7.
- Gabitov, R.I., Gaetani, G.A., Watson, E.B., Cohen, A.L., Ehrlich, H.L., 2008. Experimental determination of growth rate effect on U^{6+} and Mg^{2+} partitioning between aragonite and fluid at elevated U^{6+} concentration. *Geochim. Cosmochim. Acta* 72, 4058–4068.
- Gabitov, R.I., Sadekov, A., Dyer, J., Perez-Huerta, A., Xu, H., Migdisov, A., 2021a. Sectoral and growth rate control on elemental uptake by individual calcite crystals. *Chem. Geol.* 585.
- Gabitov, R.I., Sadekov, A., Leinweber, A., 2014. Crystal growth rate effect on Mg/Ca and Sr/Ca partitioning between calcite and fluid: An in situ approach. *Chem. Geol.* 367, 70–82.
- Gabitov, R.I., Schmitt, A.K., Rosner, M., McKeegan, K.D., Gaetani, G.A., Cohen, A.L., Watson, E.B., Harrison, T.M., 2011. In situ 7Li , Li/Ca, and Mg/Ca analyses of synthetic aragonites. *Geochemistry, Geophysics, Geosystems*, p. 12.
- Gabitov, R.I., Watson, E.B., 2006. Partitioning of strontium between calcite and fluid. *Geochim. Geophys. Geosyst.* 7 (11).
- Gabitov, R.I., Watson, E.B., Sadekov, A., 2012. Oxygen isotope fractionation between calcite and fluid as a function of growth rate and temperature: An in situ study. *Chem. Geol.* 306–307, 92–102.
- Gabrielli, C., Jaouhari, R., Maurin, G., Keddam, M., 2001. Magnetic water treatment for scale prevention. *Water Res.* 35, 3249–3259.
- Gaetani, G.A., Cohen, A.L., 2006. Element partitioning during precipitation of aragonite from seawater: A framework for understanding paleoproxies. *Geochim. Cosmochim. Acta* 70, 4617–4634.
- Galan, I., Baldermann, A., Kusterle, W., Dietzel, M., Mittermayr, F., 2019. Durability of shotcrete for underground support– Review and update. *Constr. Build. Mater.* 202, 465–493.
- Galotta, A., Rubenis, K., Locs, J., Sglavo, V.M., 2023. Dissolution-precipitation synthesis and cold sintering of mussel shells-derived hydroxyapatite and hydroxyapatite/chitosan composites for bone tissue engineering. *Open Ceramics* 15, 100418.
- Galy, A., Bar-Matthews, M., Halicz, L., O’Nions, R.K., 2002. Mg isotopic composition of carbonate: insight from speleothem formation. *Earth Planet. Sci. Lett.* 211, 105–115.
- Gao, Y., Zhao, J., Zhao, E., Liu, X., Jia, Y., Ying, C., Lin, L., 2020. Effect of electric field and Mg^{2+} doping on calcium carbonate scaling shown in experiments and first principle calculations. *Water Sci. Technol. Water Supply* 20, 3251–3265.
- Garapati, N., Adams, B.M., Bielićki, J.M., Schaedle, P., Randolph, J.B., Kuehn, T.H., Saar, M.O., 2017. A Hybrid Geothermal Energy Conversion Technology - A Potential Solution for Production of Electricity from Shallow Geothermal Resources. *Energy Procedia* 114, 7107–7117.
- Garapati, N., Randolph, J.B., Saar, M.O., 2015. Brine displacement by CO_2 , energy extraction rates, and lifespan of a CO_2 -limited CO_2 -Plume Geothermal (CPG) system with a horizontal production well. *Geothermics* 55, 182–194.
- García-Sánchez, A., Álvarez-Ayuso, E., 2002. Sorption of Zn, Cd and Cr on calcite. Application to purification of industrial wastewaters. *Miner. Eng.* 15, 539–547.
- Garrels, R.M., Christ, C.L., 1965. Solutions. New York, Verlag Harper International, Minerals and Equilibria, p. 450.
- Garvie, L.A.J., 2006. Decay of cacti and carbon cycling. *Naturwissenschaften* 93, 114–118.
- Garvie, L.A.J., 2022. Seasonal formation of ikaite in slime flux jelly on an infected tree (*Populus fremontii*) wound from the Sonoran Desert. *The Science of Nature* 109, 48.
- Garvie, L.A.J., Németh, P., Trif, L., 2022. An exceptionally stable and widespread hydrated amorphous calcium carbonate precipitated by the dog vomit slime mold *Fuligo septica* (*Myxogastria*). *Sci. Rep.* 12, 3642.
- Ge, Y., Pederson, C.L., Lokier, S.W., Traas, J.P., Nehrk, G., Neuser, R.D., Goetschl, K.E., Immenhauser, A., 2020. Late Holocene to Recent aragonite-cemented transgressive lag deposits in the Abu Dhabi lagoon and intertidal sabkha. *Sedimentology* 67, 2426–2454.
- Gebauer, D., Cölfen, H., 2011. Prenucleation clusters and non-classical nucleation. *Nano Today* 6, 564–584.
- Gebauer, D., Cölfen, H., Verch, A., Antonietti, M., 2009. The Multiple Roles of Additives in $CaCO_3$ Crystallization: A Quantitative Case Study. *Adv. Mater.* 21, 435–439.
- Gebauer, D., Gunawidjaja, P.N., Ko, J.Y.P., Bacsk, Z., Aziz, B., Liu, L., Hu, Y., Bergström, L., Tai, C.-W., Sham, T.-K., Edén, M., Hedin, N., 2010. Proto-Calcite and Proto-Vaterite in Amorphous Calcium Carbonates. *Angew. Chem. Int. Ed.* 49, 8889–8891.
- Gebauer, D., Kellermeier, M., Gale, J.D., Bergström, L., Cölfen, H., 2014. Pre-nucleation clusters as solute precursors in crystallisation. *Chem. Soc. Rev.* 43, 2348–2371.
- Geisler, T., Perdikouri, C., Kasiopatis, A., Dietzel, M., 2012. Real-time monitoring of the overall exchange of oxygen isotopes between aqueous CO_2 and H_2O by Raman spectroscopy. *Geochim. Cosmochim. Acta* 90, 1–11.
- George, R.S., Jayasingh, S., 2021. Experimental Investigation on Organic Water Slaked Lime Mortar. In: Sena-Cruz, J., Correia, L., Azenha, M. (Eds.), Proceedings of the 3rd RILEM Spring Convention and Conference (RSCC 2020). Springer International Publishing, Cham, pp. 245–257.
- Geske, A., Lokier, S., Dietzel, M., Richter, D.K., Buhl, D., Immenhauser, A., 2015. Magnesium isotope composition of sabkha porewater and related (Sub-)Recent stoichiometric dolomites, Abu Dhabi (UAE). *Chem. Geol.* 393–394, 112–124.
- Ghiasi, M., Abdollahy, M., 2022. Precipitated Calcium Carbonate (PCC). In *The Chemistry of Calcium Carbonate*. 1–197.
- Ghosh, S., Lai, J.-Y., 2023. Recent advances in the design of intracellular pH sensing nanoprobes based on organic and inorganic materials. *Environ. Res.* 237, 117089.
- Ghosh, P., Garzione, C.N., Eiler, J.M., 2006. Rapid Uplift of the Altiplano Revealed Through ^{13}C - ^{18}O Bonds in Paleosol Carbonates. *Science* 311, 511–515.
- Gilbert, P.U.P.A., Porter, S.M., Sun, C.-Y., Xiao, S., Gibson, B.M., Shenkar, N., Knoll, A.H., 2019. Biomineralization by particle attachment in early animals. *Proc. Natl. Acad. Sci.* 116, 17659–17665.
- Gill, B.C., Lyons, T.W., Frank, T.D., 2008. Behavior of carbonate-associated sulfate during meteoric diagenesis and implications for the sulfur isotope paleoproxy. *Geochim. Cosmochim. Acta* 72, 4699–4711.
- Gilleadeau, G.J., Frei, R., Kaufman, A.J., Kah, L.C., Azmy, K., Bartley, J.K., Chernyavskiy, P., Knoll, A.H., 2016. Oxygenation of the mid-Proterozoic atmosphere: clues from chromium isotopes in carbonates. *Geochim. Perspect. Lett.* 2, 178–187.
- Gillikin, D.P., Lorrain, A., Jolivet, A., Kelemen, Z., Chauvaud, L., Bouillon, S., 2017. High-resolution nitrogen stable isotope sclerochronology of bivalve shell carbonate-bound organics. *Geochim. Cosmochim. Acta* 200, 55–66.
- Gindele, M.B., Nolte, S., Stock, K.M., Kebel, K., Gebauer, D., 2023. Bottling Liquid-Like Minerals for Advanced Materials Synthesis. *Adv. Mater.* 35, 2300702.
- Gindele, M.B., Vinod-Kumar, S., Rochau, J., Boemke, D., Groß, E., Redrouth, V.S., Gebauer, D., Mathies, G., 2024. Colloidal pathways of amorphous calcium carbonate formation lead to distinct water environments and conductivity. *Nat. Commun.* 15, 80.
- Göçüttü, Y., Oral C. M. and Ercan B. (2023) Selenite-Incorporated Amorphous Calcium–Magnesium Carbonate Nanoparticles Reduce Bacterial Growth. *ACS Applied Nano Materials* 6, 16286–16296.
- Goetschl, K. E., Dietzel M., Purgstaller, B., Greeng C. and Μωροπούτης (2021) Control of $MgSO_4^{(aq)}$ on the transformation of amorphous calcium carbonate to high-Mg calcite and long-term reactivity of the crystalline solid. *Geochim. Cosmochim. Acta* 312, 357–374.
- Goetschl, K.E., Purgstaller, B., Dietzel, M., Mavromatis, V., 2019. Effect of sulfate on magnesium incorporation in low-magnesium calcite. *Geochim. Cosmochim. Acta* 265, 505–519.
- Gong, S., Luo, M., Griffith, E.M., Peckmann, J., Liang, Q., Feng, D., 2023. Calcium isotopic fractionation during aragonite and high-Mg calcite precipitation at methane seeps. *Earth Planet. Sci. Lett.* 622, 118419.
- Gonneea, M.E., Cohen, A.L., DeCarlo, T.M., Charette, M.A., 2017. Relationship between water and aragonite barium concentrations in aquaria reared juvenile corals. *Geochim. Cosmochim. Acta* 209, 123–134.
- Gothmann, A.M., Gagnon, A.C., 2021. The primary controls on U/Ca and minor element proxies in a cold-water coral cultured under decoupled carbonate chemistry conditions. *Geochim. Cosmochim. Acta* 315, 38–60.
- Gower, L.B., Odom, D.J., 2000. Deposition of calcium carbonate films by a polymer-induced liquid-precursor (PILP) process. *J. Cryst. Growth* 210, 719–734.
- Grassmann, O., Löbmann, P., 2003. Morphogenetic control of calcite crystal growth in sulfonic acid based hydrogels. *Chem. Eur. J.* 9, 1310–1316.
- Gray, W.R., Evans, D., Hennehan, M., Weldeab, S., Lea, D.W., Müller, W., Rosenthal, Y., 2023. Sodium incorporation in foraminiferal calcite: An evaluation of the Na/Ca salinity proxy and evidence for multiple Na-bearing phases. *Geochim. Cosmochim. Acta* 348, 152–164.
- Gregg, J.M., Bish, D.L., Kaczmarek, S.E., Machel, H.G., 2015. Mineralogy, nucleation and growth of dolomite in the laboratory and sedimentary environment: A review. *Sedimentology* 62, 1749–1769.
- Greeng, C., Mittermayr, F., Koraimann, G., Konrad, F., Szabó, M., Demeny, A., Dietzel, M., 2017. The decisive role of acidophilic bacteria in concrete sewer networks: A new model for fast progressing microbial concrete corrosion. *Cem. Concr. Res.* 101, 93–101.
- Greeng, C., Müller, B., Staudinger, C., Mittermayr, F., Breininger, J., Ungerböck, B., Borisov, S.M., Mayr, T., Dietzel, M., 2019. High-resolution optical pH imaging of concrete exposed to chemically corrosive environments. *Cem. Concr. Res.* 116, 231–237.
- Griffith, E.M., Fantle, M.S., 2020. Introduction to calcium isotope geochemistry: Past lessons and future directions. *Chem. Geol.* 537, 119470.
- Gruzensky P. M. (1967) Growth of calcite crystals. In *Crystal Growth, Conference Proceedings of the International Conference on Crystal Growth (1966: Boston MA) (ed. H. Steffen Peiser)*, Supplement to *Journal of Physics and Chemistry of Solids S: 365 Suppl. 1*. Pergamon Press, New York.
- Gu, H., Ma, Y., Peng, Z., Zhu, F., Ma, X., 2023. Influence of polyborate ions on the fractionation of B isotopes during calcite deposition. *Chem. Geol.* 622.
- Guo, B., Zhu, X., Dong, A., Yan, B., Shi, G., Zhao, Z., 2019. Mg isotopic systematics and geochemical applications: A critical review. *J. Asian Earth Sci.* 176, 368–385.
- Guo, W., 2020. Kinetic clumped isotope fractionation in the $DIC-H_2O-CO_2$ system: Patterns, controls, and implications. *Geochim. Cosmochim. Acta* 268, 230–257.
- Guo, W., Zhou, C., 2019. Patterns and controls of disequilibrium isotope effects in speleothems: Insights from an isotope-enabled diffusion-reaction model and implications for quantitative thermometry. *Geochim. Cosmochim. Acta* 267, 196–226.
- Gussone, N., Ahm, A.-S.C., Lau, K.V., Bradbury, H.J., 2020. Calcium isotopes in deep time: Potential and limitations. *Chem. Geol.* 544, 119601.
- Gussone, N., Böhm, F., Eisenhauer, A., Dietzel, M., Heuser, A., Teichert, B.M.A., Reitner, J., Wörheide, G., Dullo, W.-C., 2005. Calcium isotope fractionation in calcite and aragonite. *Geochim. Cosmochim. Acta* 69, 4485–4494.
- Gussone, N., Dietzel, M., 2016. Calcium isotope fractionation during mineral precipitation from aqueous solution. *Advances in Isotope Geochemistry* 75–110.

- Gussone, N., Schmitt, A.-D., Heuser, A., Wombacher, F., Dietzel, M., Tipper, E., Schiller, M., Bohm, F., 2016. Calcium stable isotope geochemistry. Springer-Verlag, Berlin Heidelberg.
- Gutjahr, A., Dabringhaus, H., Lacmann, R., 1996. Studies of the growth and dissolution kinetics of the CaCO_3 polymorphs calcite and aragonite II. The influence of divalent cation additives on the growth and dissolution rates. *J. Cryst. Growth* 158, 310–315.
- Gysi, A.P., Stefansson, A., 2011. CO_2 -water-basalt interaction. Low temperature experiments and implications for CO_2 sequestration into basalts. *Geochemica et Cosmochimica Acta* 81, 129–152.
- Gysi, A.P., Stefansson, A., 2012. Mineralogical aspects of CO_2 sequestration during hydrothermal basalt alteration - An experimental study at 75 to 250 °C and elevated pCO_2 . *Chem. Geol.* 306–307, 146–159.
- Haas-Nüesch, R., Heberling, F., Schild, D., Rothe, J., Dardenne, K., Jähnichen, S., Eiche, E., Marquardt, C., Metz, V., Schäfer, T., 2018. Mineralogical characterization of scalings formed in geothermal sites in the Upper Rhine Graben before and after the application of sulfate inhibitors. *Geothermics* 71, 264–273.
- Halverson, G.P., Poitrasson, F., Hoffman, P.E., Nedelec, A., Montel, J.M., Kirby, J., 2011. Fe isotope and trace element geochemistry of the Neoproterozoic syn-glacial Rapitan iron formation. *Earth Planet. Sci. Lett.* 309, 100–112.
- Hansen, M., Kluge, T., Scholz, D., 2022. Investigation of disequilibrium clumped isotope fractionation in (speleothem) CaCO_3 with cave analogous laboratory experiments using thin films of flowing solution. *Geochim. Cosmochim. Acta* 321, 244–264.
- Hansen, M., Scholz, D., Schöne, B.R., Spötl, C., 2019. Simulating speleothem growth in the laboratory: Determination of the stable isotope fractionation ($\delta^{13}\text{C}$ and $\delta^{18}\text{O}$) between H_2O , DIC and CaCO_3 . *Chem. Geol.* 509, 20–44.
- Hanshaw, B.B., Hallet, B., 1978. Oxygen Isotope Composition of Subglacially Precipitated Calcite: Possible Paleoclimatic Implications. *Science* 200, 1267–1270.
- Hardie, L.A., 1987. Dolomitization; a critical view of some current views. *J. Sediment. Res.* 57, 166–183.
- Harrison, P.L., Gilmore, M.S., 2015. Visible–near infrared spectra of hydrous carbonates, with implications for the detection of carbonates in hyperspectral data of Mars. *Icarus* 250 (0), 204–214.
- Harrison, A.L., Heuser, A., Liebtrau, V., Eisenhauer, A., Schott, J., Mavromatis, V., 2023. Equilibrium Ca isotope fractionation and the rates of isotope exchange in the calcite-fluid and aragonite-fluid systems at 25 °C. *Earth Planet. Sci. Lett.* 603, 117985.
- Harrison, A.L., Schott, J., Oelkers, E.H., Maher, K., Mavromatis, V., 2022. Rates of carbon and oxygen isotope exchange between calcite and fluid at chemical equilibrium. *Geochim. Cosmochim. Acta* 335, 369–382.
- Harrison, A.L., Tutolo, B.M., DePaolo, D.J., 2019. The Role of Reactive Transport Modeling in Geologic Carbon Storage. *Elements* 15, 93–98.
- Hartland, A., Fairchild, I.J., Müller, W., Dominguez-Villar, D., 2014. Preservation of NOM-metal complexes in a modern hyperalkaline stalagmite: Implications for speleothem trace element geochemistry. *Geochim. Cosmochim. Acta* 128, 29–43.
- Hashizume, H., 2022. Carbonate Minerals. In: Hashizume, H. (Ed.), *Natural Mineral Materials*. Springer Japan, Tokyo, pp. 85–102.
- Hauer, H., Evans, D., Müller, W., Rosenthal, Y., Erez, J., 2021. Salinity Effect on Trace Element Incorporation in Cultured Shells of the Large Benthic Foraminifer *Oculinaria ammonoides*. *Paleoceanography and Paleoclimatology* 36 e2021PA004218.
- He, M., Cai, Y., Zhang, H., Xue, G., Cheng, X., Lu, Y., Wang, G., Qin, X., Ma, L., Wei, Y., Huang, S., Chang, H., Yan, H., 2021. The impact and implications of aragonite-to-calcite transformation on speleothem trace element composition. *Sediment. Geol.* 425.
- He, R., Limburg, K.E., Walther, B.D., Samson, M.A., Lu, Z., 2022. Iodine content of fish otoliths in species found in diverse habitats. *Environ. Biol. Fish.* 105, 351–367.
- Hellstrom J. and Pickering R. (2015) Recent advances and future prospects of the U-Th and U-Pb chronometers applicable to archaeology. *J. Archaeol. Sci.* 56, 32–40.
- Henning, N.G., Hanson, G.N., 1992. Boron isotopic composition and concentration in modern marine carbonates. *Geochim. Cosmochim. Acta* 56, 537–543.
- Henderson, G.M., 2002. New oceanic proxies for paleoclimate. *Earth Planet. Sci. Lett.* 203, 1–13.
- Hendy, C.H., 1971. The isotopic geochemistry of speleothems-I. The calculation of the effects of different modes of formation on the isotopic composition of speleothems and their applicability as palaeoclimatic indicators. *Geochim. Cosmochim. Acta* 35, 801–824.
- Henkes, G.A., Passey, B.H., Grossman, E.L., Shenton, B.J., Pérez-Huerta, A., Yancey, T.E., 2014. Temperature limits for preservation of primary calcite clumped isotope paleotemperatures. *Geochim. Cosmochim. Acta* 139, 362–382.
- Hickman, G.J., Belton, D.J., Newick, R., Perry, C.C., 2019. Barriers to adoption of biogenic carbonates in the food, pharmaceutical & supplement sectors. *NFS Journal* 16, 1–8.
- Hiess, J., Condon, D.J., McLean, N., Noble, S.R., 2012. $^{238}\text{U}/^{235}\text{U}$ Systematics in Terrestrial Uranium-Bearing Minerals. *Science* 335, 1610–1614.
- Higgins, J.A., Blättler, C.L., Lundstrom, E.A., Santiago-Ramos, D.P., Akhtar, A.A., Crüger, Ahm A., S., Bialik O., Holmen C., Bradbury H., Murray S. T. and Swart P. K., 2018. Mineralogy, early marine diagenesis, and the chemistry of shallow-water carbonate sediments. *Geochim. Cosmochim. Acta* 220, 512–534.
- Hiruta, A., Matsumoto, R., 2022. Geochemical comparison of ikaite and methane-derived authigenic carbonates recovered from Echigo Bank in the Sea of Japan. *Mar. Geol.* 443, 106672.
- Hobbs, M.Y., Reardon, E.J., 1999. Effect of pH on boron coprecipitation by calcite: further evidence for nonequilibrium partitioning of trace elements. *Geochim. Cosmochim. Acta* 63, 1013–1021.
- Hodgkiss, M.S.W., Lalonde, S.V., Crockford, P.W., Hutchings, A.M., 2021. A carbonate molybdenum isotope and cerium anomaly record across the end-GOE: Local records of global oxygenation. *Geochim. Cosmochim. Acta* 313, 313–339.
- Hodkin, D.J., Stewart, D.I., Graham, J.T., Cibin, G., Burke, I.T., 2018. Enhanced Crystallographic Incorporation of Strontium(II) Ions into Calcite via Preferential Adsorption at Obtuse Growth Steps. *Cryst. Growth Des.* 18, 2836–2843.
- Hoefs, J., 2021. *Stable Isotope Geochemistry*. Springer Nature Switzerland, 504 p.
- Hoefs, J., Harmon, R.S., 2023. Isotopic history of seawater: the stable isotope character of the global ocean at present and in the geological past. *Isot. Environ. Health Stud.* 59, 349–411.
- Hoffman, J.R., Ben-Zeev, T., Zamir, A., Levi, C., Ostfeld, I., 2022. Examination of Amorphous Calcium Carbonate on the Inflammatory and Muscle Damage Response in Experienced Resistance Trained Individuals. *Nutrients* 14, 1894.
- Hofmann, P., Marschallinger, R., Unterwurzacher, M., Zobl, F., 2013. Marble provenance designation with object based image analysis: state-of-the-art rock fabric characterization from petrographic micrographs. *Austrian Journal of Earth Sciences* 106, 40–49.
- Hohl, S., Lv, Y., Viehmann, S., Lin, Y.-B., Jiang, Y., Zhang, Y., 2023. Early Earth Microbial Metallome: Insights From Cd, Ba, and Ni Isotopes in Stromatolites. <https://doi.org/10.21203/rs.3.rs-2923288/v1>.
- Hohl, S.V., Lin, Y.-B., Wei, H.-Z., Wei, G.-Y., Viehmann, S., 2024. Barium isotopes in stromatolites through deep-time: A novel tracer for metal cycling in the photic zone. *Earth Planet. Sci. Lett.* 632, 118639.
- Holcomb, M., DeCarlo, T.M., Gaetani, G.A., McCulloch, M., 2016. Factors affecting B/Ca ratios in synthetic aragonite. *Chem. Geol.* 437, 67–76.
- Holdsworth, C.M., John, C.M., Snæbjörnsdóttir, S.Ó., Johnson, G., Sigfusson, B., Leslie, R., Haszeldine, R.S., Gilfillan, S.M.V., 2024. Reconstructing the temperature and origin of CO_2 mineralisation in CarbFix calcite using clumped, carbon and oxygen isotopes. *Appl. Geochem.* 162, 105925.
- Holmden, C., Kimmig, S.R., Nadeau, M.D., 2024. Ca isotopic gradients in epeiric marine carbonates: diagenetic origins and significance for Ca cycle reconstructions. *Geochim. Cosmochim. Acta* 373, 151–168.
- Hong, W.L., Lepland, A., Kirsimäe, K., Crémère, A., Rae, J.W.B., 2022. Boron concentrations and isotopic compositions in methane-derived authigenic carbonates: Constraints and limitations in reconstructing formation conditions. *Earth Planet. Sci. Lett.* 579.
- Honiati, C., Kolta, G., Dublyansky, Y., Edwards, R.L., Zhang, H., Cheng, H., Spötl, C., 2023. A paleoprecipitation and paleotemperature reconstruction of the Last Interglacial in the southeastern Alps. *Clim. Past* 19, 1177–1199.
- Hönisch, B., Egging, S.M., Haynes, L.L., Allen, K.A., Holland, K.D., Lorbacher, K., 2018. Boron Proxies in Paleoceanography and Paleoclimatology, 231p.
- Horgan, B.H.N., Anderson, R.B., Dromart, G., Amador, E.S., Rice, M.S., 2020. The mineral diversity of Jezero crater: Evidence for possible lacustrine carbonates on Mars. *Icarus* 339, 113526.
- Horita, J., 2014. Oxygen and carbon isotope fractionation in the system dolomite-water- CO_2 to elevated temperatures. *Geochim. Cosmochim. Acta* 129, 111–124.
- Hsieh, Y.-T., Henderson, G.M., 2017. Barium stable isotopes in the global ocean: Tracer of Ba inputs and utilization. *Earth Planet. Sci. Lett.* 473, 269–278.
- Hu, J., Wang, H., Tan, J., 2020. Fe and C isotopes constrain the pathways of hematite and Fe-rich carbonates formation in the Late Neoproterozoic Dahongliutan BIF. NW China. *Ore Geology Reviews* 121, 103485.
- Hu, Y.-B., Wolthers, M., Wolf-Gladrow, D.A., Nehrke, G., 2015. Effect of pH and Phosphate on Calcium Carbonate Polymorphs Precipitated at near-Freezing Temperature. *Cryst. Growth Des.* 15, 1596–1601.
- Hu, Z., Bialik, O.M., Hohl, S.V., Xia, Z., Waldmann, N.D., Liu, C., Li, W., 2021. Response of Mg isotopes to dolomitization during fluctuations in sea level: Constraints on the hydrological conditions of massive dolomitization systems. *Sediment. Geol.* 420, 105922.
- Hu, Z., Hohl, S.V., Viehmann, S., Meister, P., Tepe, N., 2023. No biological effect on magnesium isotope fractionation during stromatolite growth. *Geochim. Cosmochim. Acta* 358, 1–11.
- Hu, Z., Hu, W., Wang, X., Lu, Y., Wang, L., Liao, Z., Li, W., 2017. Resetting of Mg isotopes between calcite and dolomite during burial metamorphism: Outlook of Mg isotopes as geothermometer and seawater proxy. *Geochim. Cosmochim. Acta* 208, 24–40.
- Huang, C.Y., Lin, C.H., 2023. Influence on the magnetic field on the scale formation in a microfluidic channel under a low Reynolds number flow. *Microfluid. Nanofluid.* 27.
- Huang, Y., Fairchild, I., 2001. Partitioning of Sr^{2+} and Mg^{2+} into calcite in karst-analogue experimental solutions. *Geochim. Cosmochim. Acta* 65, 47–62.
- Huber, S.J., Schlüdt, V., Seitz, H.-M., Kniest, J.F., Raddatz, J., Marschall, H.R., Voigt, S., 2024. Assessment of Chalk as an Archive for the Lithium Isotope Composition of Seawater. *Geochem. Geophys. Geosyst.* 25 e2023GC011150.
- Humphrey, J.D., Howell, R.P., 1999. Effect of differential stress on strontium partitioning in calcite. *J. Sediment. Res.* 69, 208–215.
- Hunter, H.A., Ling, F.T., Peters, C.A., 2021. Coprecipitation of Heavy Metals in Calcium Carbonate from Coal Fly Ash Leachate. *ACS ES&T Water* 1, 339–345.
- Hurowitz, J.A., Catling, D.C., Fischer, W.W., 2023. High Carbonate Alkalinity Lakes on Mars and their Potential Role in an Origin of Life Beyond Earth. *Elements* 19, 37–44.
- Huttenloch, P., Zorn, R., Makni, L., Steger, H., Schilling, F., Hater, W., 2019. Inhibitor performance on carbon steel in the geothermal environment of the Upper Rhine graben (Central Europe) – A laboratory study. *Geothermics* 81, 198–208.
- Hwang, H.Y., Kwon, Y.H., Hong, S.G., Kang, S.H., 2022. Comparative study of effects of natural organic additives and cellulose ether on properties of lime-clay mortars. *Journal of Building Engineering* 48.
- Ihli, J., Wong, W.C., Noel, E.H., Kim, Y.-Y., Kulak, A.N., Christenson, H.K., Duer, M.J., Meldrum, F.C., 2014. Dehydration and crystallization of amorphous calcium carbonate in solution and in air. *Nat. Commun.* 5, 3169.
- Imam, N., 2023. Dating of groundwater using uranium isotopes disequilibrium in Siwa Oasis, Western Desert, Egypt. *Scientific Reports* 13, 12406.

- Immenhauser, A., 2022. On the delimitation of the carbonate burial realm. *Depositional Rec.* 8, 524–574.
- Immenhauser, A., Buhl, D., Richter, D., Niedermayr, A., Riechelmann, D., Dietzel, M., Schulte, U., 2010. Magnesium-isotope fractionation during low-Mg calcite precipitation in a limestone cave – Field study and experiments. *Geochim. Cosmochim. Acta* 74, 4346–4364.
- Immenhauser, A., Hoffmann, R., Riechelmann, S., Mueller, M., Scholz, D., Voigt, S., Niggemann, S., Buhl, D., Dornseif, M., Platte, A., 2023. Petrographic and geochemical constraints on the formation of gravity-defying speleothems. *Depositional Rec.* 9, 413–436.
- Immenhauser, A., Schöne, B.R., Hoffmann, R., Niedermayr, A., 2016. Mollusc and brachiopod skeletal hard parts: Intricate archives of their marine environment. *Sedimentology* 63, 1–59.
- Intergovernmental Panel on Climate C, 2023. *Climate Change 2021 – The Physical Science Basis: Working Group I Contribution to the Sixth Assessment Report of the Intergovernmental Panel on Climate Change*. Cambridge University Press, Cambridge.
- Ishikawa, M., Ichikuni, M., 1984. Uptake of sodium and potassium by calcite. *Chem. Geol.* 42, 137–146.
- Ispescu, R., Mateescu, C., Mihai, M., Dabija, G., 2010. The effects of organic additives on induction time and characteristics of precipitated calcium carbonate. *Chem. Eng. Res. Des.* 88, 1450–1454.
- Isson, T., Rauzi, S., 2024. Oxygen isotope ensemble reveals Earth's seawater, temperature, and carbon cycle history. *Science* 383, 666–670.
- Jacobson, R.L., Usdowski, H.E., 1976. Partitioning of strontium between calcite, dolomite and liquids: An experimental study under higher temperature diagenetic conditions, and a model for the prediction of mineral pairs for geothermometry. *Contrib. Mineral. Petrol.* 59, 171–185.
- Jafarnia, M.S., Khodadad, Saryazdi M., Moshtaghioun, S.M., 2020. Use of bacteria for repairing cracks and improving properties of concrete containing limestone powder and natural zeolite. *Constr. Build. Mater.* 242, 118059.
- Jamero, J., Zarrouk, S.J., Mroczek, E., 2018. Mineral scaling in two-phase geothermal pipelines: Two case studies. *Geothermics* 72, 1–14.
- James, N.P., Jones, B., 2015. *Origin of Carbonate Sedimentary Rocks*. Wiley, 446pp.
- Jensen, A.C.S., Imberti, S., Parker, S.F., Schneck, E., Polit, Y., Fratzl, P., Bertinetti, L., Habraken, W.J.E.M., 2018. Hydrogen Bonding in Amorphous Calcium Carbonate and Molecular Reorientation Induced by Dehydration. *J. Phys. Chem. C* 122, 3591–3598.
- Jia, Q., Zhang, S., Lammers, L., Huang, Y., Wang, G., 2022. A model for pH dependent strontium partitioning during calcite precipitation from aqueous solutions. *Chem. Geol.* 608, 121042.
- Jia, Z., Hu, Y., Bayon, G., Peckmann, J., Wang, X., Gong, S., Li, J., Roberts, H.H., Chen, D., Feng, D., 2023. Seawater-Fluid Composition Records From Molybdenum Isotopes of Sequentially Extracted Phases of Deep Carbonate Rocks. *Geochemistry, Geophysics, Geosystems*, p. 24.
- Jiang, J., Xu, S., Xiao, H., Tao, C., Chen, C., Li, Q., Shi, R., 2022. The synthesis of long-term stable amorphous calcium carbonate in water-free ethylene glycol system without any phase stabilizer. *Adv. Powder Technol.* 33.
- Jiang, W., Yu, K., Wang, N., Yang, H., Yang, H., Xu, S., Wei, C., Wang, S., Wang, Y., 2020. Distribution coefficients of trace metals between modern coral-lattices and seawater in the northern South China Sea: Species and SST dependencies. *J. Asian Earth Sci.* 187, 104082.
- Jimoh, O.A., Ariffin, K.S., Hussin, H.B., Temitope, A.E., 2018. Synthesis of precipitated calcium carbonate: a review. *Carbonates Evaporites* 33, 331–346.
- Jin, M., Feng, D., 2023. Non-traditional Stable Isotope Geochemistry of Seep Deposits. In: *South China Sea Seeps*. 171–187.
- Johnson, C.J., Brian, L.B., F.A., 2004. Geochemistry of non-traditional stable isotopes. *Rev. Mineral. Geochim.* 55, 454.
- Johnston, V.E., Borsato, A., Frisia, S., Spötl, C., Dublyansky, Y., Töchterle, P., Hellstrom, J.C., Bajo, P., Edwards, R.L., Cheng, H., 2018. Evidence of thermophilisation and elevation-dependent warming during the Last Interglacial in the Italian Alps. *Sci. Rep.* 8, 2680.
- Johnston, V.E., Frisia, S., Borsato, A., Woodhead, J.D., McDermott, F., 2024. The incorporation of chlorine and cosmogenic ^{36}Cl into speleothem carbonate. *Quat. Res.* 118, 2–19.
- Jones, B., 2017. Review of aragonite and calcite crystal morphogenesis in thermal spring systems. *Sediment. Geol.* 354, 9–23.
- Jones, B., Renaut, R.W., 2008. Cyclic development of large, complex, calcite dendrite crystals in the Clinton travertine, Interior British Columbia, Canada. *Sediment. Geol.* 203, 17–35.
- Jones, F., Ogden, M.I., 2010. Controlling crystal growth with modifiers. *Cryst. Eng. Comm.* 12, 1016–1023.
- Ju, Y.-M., Huang, F., Ding, X., Mao, L.-B., Yu, S.-H., 2023. Phase transformation-induced Mg isotope fractionation in Mg-mediated CaCO_3 mineralization. *Nano Res.* 16, 3597–3602.
- Julia, M., Putnis, C.V., King, H.E., Renard, F., 2023. Coupled dissolution-precipitation and growth processes on calcite, aragonite, and Carrara marble exposed to cadmium-rich aqueous solutions. *Chem. Geol.* 621, 121364.
- Jung, W.-M., Hoon, Kang S., Kim, K.-S., Kim, W.-S., Kyun, Choi C., 2010. Precipitation of calcium carbonate particles by gas-liquid reaction: Morphology and size distribution of particles in Couette-Taylor and stirred tank reactors. *J. Cryst. Growth* 312, 3331–3339.
- Junqueira, T.P., Vriens, B., Leybourne, M.I., Harrison, A.L., Sullivan, K.V., Jeong, H., Araújo, D.F., 2024. Applications of zinc stable isotope analysis in environmental and biological systems: a review. *Geochem.: Explor., Environ., Anal.* 24 (3).
- Kaczmarek, S.E., Gregg, J.M., Bish, D.L., Machel, H.G., Fouke, B.W., 2017. Dolomite, very high-magnesium calcite, and microbes— implications for the microbial model of dolomitization. *SEPM Special Publications* 109, 7–20.
- Kaminskaite-Baranauskienė, I., Wang, H., Liu, Z., Li, H., 2023. Geothermal carbonate reservoirs and their sustainability: what can natural hydrothermal systems tell us? *Geothermics* 114.
- Kampschulte, A., Bruckschen, P., Strauss, H., 2001. The sulphur isotopic composition of trace sulphates in Carboniferous brachiopods: implications for coeval seawater, correlation with other geochemical cycles and isotope stratigraphy. *Chem. Geol.* 175, 149–173.
- Kampschulte, A., Strauss, H., 2004. The sulfur isotopic evolution of Phanerozoic seawater based on the analysis of structurally substituted sulfate in carbonates. *Chem. Geol.* 204, 255–286.
- Kandirmaz, E.A., Yenidogân, S., Aydemir, C., Karademir, A., 2020. Effect of using calcium carbonate (CaCO_3) in surface coating on liquid absorption of paper and some printability parameters. *Cellul. Chem. Technol.* 54, 485–493.
- Kano, A., Okumura, T., Takashima, C., Shiraishi, F., 2019. *Sedimentology of Travertine. In: Kano, A., Okumura, T., Takashima, C., Shiraishi, F. (Eds.), Geomicrobiological Properties and Processes of Travertine: With a Focus on Japanese Sites*. Springer Singapore, Singapore, pp. 43–66.
- Kappler, A., Johnson, C.M., Crosby, H.A., Beard, B.L., Newman, D.K., 2010. Evidence for equilibrium iron isotope fractionation by nitrate-reducing iron(II)-oxidizing bacteria. *Geochim. Cosmochim. Acta* 74, 2826–2842.
- Karancz, S., Uchikawa, J., de Nooijer, L.J., Wolthers, M., Conner, K.A., Hite, C.G., Zeebe, R.E., Sharma, S.K., Reichart, G.-J., 2024. Constraining sulfur incorporation in calcite using inorganic precipitation experiments. *Geochim. Cosmochim. Acta* 381, 116–130.
- Karaseva, O.N., Lakshtanov, L.Z., Okhrimenko, D.V., Belova, D.A., Generosi, J., Stipp, S. L.S., 2018. Biopolymer Control on Calcite Precipitation. *Cryst. Growth Des.* 18, 2972–2985.
- Katsenovich, Y.P., Gort, R.T., Gudavalli, R., Szecsody, J., Freedman, V.L., Qafoku, N.P., 2021. Silicon concentration and pH controls over competitive or simultaneous incorporation of iodate and chromate into calcium carbonate phases. *Appl. Geochim.* 128, 104941.
- Katsikopoulos D., Fernández-González Á. and Priet M. (2009) Crystallization behaviour of the $(\text{Mn},\text{Ca})\text{CO}_3$ solid solution in silica gel: Nucleation, growth and zoning phenomena. *Mineral. Mag.* 73, 269–284.
- Katsikopoulos, D., Fernández-González, A., Prieto, A.C., Prieto, M., 2008. Co-crystallization of Co(II) with calcite: Implications for the mobility of cobalt in aqueous environments. *Chem. Geol.* 254, 87–100.
- Katz, A., Nishri, A., 2013. Calcium, magnesium and strontium cycling in stratified, hardwater lakes: Lake Kinneret (Sea of Galilee), Israel. *Geochim. Cosmochim. Acta* 105, 372–394.
- Kaushal, N., Lechleitner, F.A., Wilhelm, M., Azenoud, K., Bühl, J.C., Braun, K., Ait, Brahim Y., Baker, A., Bustyn, Y., Comas-Bru, L., Fohlmeister, J., Goldsmith, Y., Harrison, S.P., Hatvani, I.G., Rehfeld, K., Ritzau, M., Skiba, V., Stoll, H.M., Szűcs, J. G., Tanos, P., Treble, P.C., Azevedo, V., Baker, J.L., Borsato, A., Chawchai, S., Columbu, A., Endres, L., Hu, J., Kern, Z., Kimbrough, A., Koç, K., Markowska, M., Martrat, B., Masood, Ahmad S., Nehme, C., Novello, V.F., Pérez-Mejías, C., Ruan, J., Sekhon, N., Sinha, N., Tadros, C.V., Tiger, B.H., Warken, S., Wolf, A., Zhang, H., members S. W. G., 2024. SISALv3: a global speleothem stable isotope and trace element database. *Earth Syst. Sci. Data* 16, 1933–1963.
- Kaushal, N., Yang, L., Tanzil, J.T.I., Lee, J.N., Goodkin, N.F., Martin, P., 2020. Sub-annual fluorescence measurements of coral skeleton: relationship between skeletal luminescence and terrestrial humic-like substances. *Coral Reefs* 39, 1257–1272.
- Kawabata, T., Takeda, Y., Hori, M., Kandori, K., Yaji, T., 2021. Partitioning of sodium into calcium carbonates synthesized at 10–40 °C: influence of organic ligands and temperature. *Chem. Geol.* 559, 119904.
- Kele, S., Breitenbach, S.F.M., Capezzuoli, E., Nele, Meckler A., Ziegler, M., Millan, I.M., Kluge, T., Deák, J., Hanselmann, K., John, C.M., Yan, H., Liu, Z., Bernasconi, S.M., 2015. Temperature dependence of oxygen- and clumped isotope fractionation in carbonates: a study of travertines and tufts in the 6–95 °C temperature range. *Geochim. Cosmochim. Acta* 168, 172–192.
- Kele, S., Demény, A., Siklósy, Z., Németh, T., Tóth, M., Kovács, M.B., 2008. Chemical and stable isotope composition of recent hot-water travertines and associated thermal waters, from Egerszálók, Hungary: Depositional facies and non-equilibrium fractionation. *Sediment. Geol.* 211, 53–72.
- Kelemen, P.B., Benson, S.M., Pilorgé, H., Psarras, P., Wilcox, J., 2019. An Overview of the Status and Challenges of CO_2 Storage in Minerals and Geological Formations. *Frontiers in Climate* 1.
- Kelemen, P.B., Matter, J., 2008. In situ carbonation of peridotite for CO_2 storage. *Proc. Natl. Acad. Sci.* 105, 17295–17300.
- Kelemen, P.B., McQueen, N., Wilcox, J., Renforth, P., Dipple, G., Vankeuren, A.P., 2020. Engineered carbon mineralization in ultramafic rocks for CO_2 removal from air: Review and new insights. *Chem. Geol.* 550, 119628.
- Kell-Duivestein, I.J., Baldermann, A., Mavromatis, V., Dietzel, M., 2019. Controls of temperature, alkalinity and calcium carbonate reactant on the evolution of dolomite and magnesite stoichiometry and dolomite cation ordering degree - An experimental approach. *Chem. Geol.* 529, 119292.
- Kelleher, I.J., Redfern, S.A.T., 2002. Hydrous calcium magnesium carbonate, a possible precursor to the formation of sedimentary dolomite. In: *Molecular Simulation*, 6–7 ed, pp. 557–572.
- Kellermeier, M., Melero-García, E., Glaab, F., Klein, R., Drechsler, M., Rachel, R., García-Ruiz, J.M., Kunz, W., 2010. Stabilization of Amorphous Calcium Carbonate in Inorganic Silica-Rich Environments. *J. Am. Chem. Soc.* 132, 17859–17866.

- Kelson, J.R., Huntington, K.W., Schauer, A.J., Saenger, C., Lechner, A.R., 2017. Toward a universal carbonate clumped isotope calibration: Diverse synthesis and preparatory methods suggest a single temperature relationship. *Geochim. Cosmochim. Acta* 197, 104–131.
- Kelson, J.R., Huth, T.E., Passey, B.H., Levin, N.E., Petersen, S.V., Ballato, P., Beverly, E.J., Breecker, D.O., Hoke, G.D., Hudson, A.M., Ji, H., Licht, A., Oerter, E.J., Quade, J., 2023. Triple oxygen isotope compositions of globally distributed soil carbonates record widespread evaporation of soil waters. *Geochim. Cosmochim. Acta* 355, 138–160.
- Ketrae, R., Saidani, B., Gil, O., Leytey, L., Baraud, F., 2009. Efficiency of five scale inhibitors on calcium carbonate precipitation from hard water: Effect of temperature and concentration. *Desalination* 249, 1397–1404.
- Kettler, R.M., He, Y., Ke, S., Teng, F.-Z., Loope, D.B., 2022. Iron isotope evidence for siderite precursors to iron oxide concretions from the Navajo Sandstone, Utah (USA). *Chem. Geol.* 612, 121146.
- Khan, M.D., Song, Y., Shakya, S., Lim, C., Ahn, J.W., 2023. In situ carbonation mediated immobilization of arsenic oxyanions. *J. Mol. Liq.* 383, 121911.
- Khandoosi, S., Hazlett, R., Fustic, M., 2023. A critical review of CO₂ mineral trapping in sedimentary reservoirs – from theory to application: Pertinent parameters, acceleration methods and evaluation workflow. *Earth Sci. Rev.* 244, 104515.
- Kharaka, Y.K., Cole, D.R., Horvorka, S.D., Gunter, W.D., Knauss, K.G., Freifeld, B.M., 2006. Gas-water-rock interactions in Frio Formation following CO₂ injection: Implications for the storage of greenhouse gases in sedimentary basins. *Geology* 34, 577–580.
- Khasani, Deendarlanto, Itoi, R., 2021. Numerical study of the effects of CO₂ gas in geothermal water on the fluid-flow characteristics in production wells. *Engineering Applications of Computational Fluid Mechanics* 15, 111–129.
- Kile, D.E., Eberl, D.D., Hoch, A.R., Reddy, M.M., 2000. An assessment of calcite crystal growth mechanisms based on crystal size distributions. *Geochim. Cosmochim. Acta* 64, 2937–2950.
- Kim, J., Kimura, Y., Puchala, B., Yamazaki, T., Becker, U., Sun, W., 2023a. Dissolution enables dolomite crystal growth near ambient conditions. *Science* 382, 915–920.
- Kim, J.J., Lee, S.S., Fenter, P., Myneni, S.C.B., Nikitin, V., Peters, C.A., 2023b. Carbonate Coprecipitation for Cd and Zn Treatment and Evaluation of Heavy Metal Stability Under Acidic Conditions. *Environ. Sci. Technol.* 57, 3104–3113.
- Kim, S.-T., O'Neil, J.R., 1997. Equilibrium and nonequilibrium oxygen isotope effects in synthetic carbonates. *Geochim. Cosmochim. Acta* 61, 3461–3475.
- Kitano, Y., Okumura, M., 1973. Coprecipitation of fluoride with calcium carbonate. *Geochem. J.* 7, 37–49.
- Kitano, Y., Okumura, M., Idogaki, M., 1975. Incorporation of sodium, chloride and sulfate with calcium carbonate. *Geochem. J.* 9, 75–84.
- Kitano, Y., Okumura, M., Idogaki, M., 1980. Abnormal behaviors of copper (II) and zinc ions in parent solution at the early stage of calcite formation. *Geochem. J.* 14, 167–175.
- Kitano, Y., Oomori, T., 1971. The coprecipitation of uranium with calcium carbonate. *Journal of the Oceanographical Society of Japan* 27, 34–42.
- Klaebe, R., Swart, P., Frei, R., 2021. Chromium isotope heterogeneity on a modern carbonate platform. *Chem. Geol.* 573, 120227.
- Klochko, K., Cody, G.D., Tossell, J.A., Dera, P., Kaufman, A.J., 2009. Re-evaluating boron speciation in biogenic calcite and aragonite using ¹¹B MAS NMR. *Geochim. Cosmochim. Acta* 73, 1890–1900.
- Kluge, T., John, C.M., 2015. Effects of brine chemistry and polymorphism on clumped isotopes revealed by laboratory precipitation of mono- and multiphase calcium carbonates. *Geochim. Cosmochim. Acta* 160, 155–168.
- Kluge, T., John, C.M., Boch, R., Kele, S., 2018. Assessment of Factors Controlling Clumped Isotopes and δ¹⁸O Values of Hydrothermal Vent Calcites. *Geochem. Geophys. Geosyst.* 19, 1844–1858.
- Kluge, T., John, C.M., Jourdan, A.-L., Davis, S., Crawshaw, J., 2015. Laboratory calibration of the calcium carbonate clumped isotope thermometer in the 25–250 °C temperature range. *Geochim. Cosmochim. Acta* 157, 213–227.
- Knez, S., Pohar, C., 2005. The magnetic field influence on the polymorph composition of CaCO₃ precipitated from carbonized aqueous solutions. *J. Colloid Interface Sci.* 281, 377–388.
- Knight, A.W., Harvey, J.A., Shohel, M., Lu, P., Cummings, D., Ilgen, A.G., 2023. The combined effects of Mg²⁺ and Sr²⁺ incorporation during CaCO₃ precipitation and crystal growth. *Geochim. Cosmochim. Acta* 345, 16–33.
- Kobayashi, K., Hashimoto, Y., Wang, S.-L., 2020. Boron incorporation into precipitated calcium carbonates affected by aqueous pH and boron concentration. *J. Hazard. Mater.* 383, 121183.
- Koishi, A., Fernandez-Martinez, A., Van Driessche, A.E.S., Michot, L.J., Pina, C.M., Pimentel, C., Lee, B., Montes-Hernandez, G., 2019. Surface Wetting Controls Calcium Carboxylate Crystallization Kinetics. *Chem. Mater.* 31, 3340–3348.
- Koltai, G., Kluge, T., Krüger, Y., Spötl, C., Rinyu, L., Audra, P., Honiat, C., Leél-Óssy, S., Dublyansky, Y., 2024. Geothermometry of calcite spar at 10–50 °C. *Sci. Rep.* 14, 1553.
- Koltai, G., Ostermann, M., Cheng, H., Spötl, C., 2018. Can vein-filling speleothems constrain the timing of deep-seated gravitational slope deformation? A case study from the Vinschgau (Italian Alps). *Landslides* 15, 2243–2254.
- König, J., Spaehr, D., Bayarjargal, L., Gavryushkin, P.N., Sagatova, D., Sagatov, N., Milman, V., Liermann, H.-P., Winkler, B., 2022. Novel Calcium sp³ Carbonate CaC₂O₅-I⁴⁻2d May Be a Carbon Host in Earth's Lower Mantle. *ACS Earth and Space Chemistry* 6, 73–80.
- Konrad, F., Gallien, F., Gerard, D.E., Dietzel, M., 2016. Transformation of Amorphous Calcium Carbonate in Air. *Cryst. Growth Des.* 16, 6310–6317.
- Konrad, F., Purgstaller, B., Gallien, F., Mavromatis, V., Gane, P., Dietzel, M., 2018. Influence of aqueous Mg concentration on the transformation of amorphous calcium carbonate. *J. Cryst. Growth* 498, 381–390.
- Kontrec, J., Kralj, D., Brećević, L., Falini, G., Fermani, S., Noethig-Laslo, V., Miroslavljević, K., 2004. Incorporation of inorganic anions in calcite. *Eur. J. Inorg. Chem.* 2004, 4579–4585.
- Koraimann, G., Bischof, K., 2022. Characterisation of microbial biofilms from tunnel drainage water. *Geomechanics and Tunnelling* 15, 358–368.
- Kosednar-Legenstein, B., Dietzel, M., Leis, A., Stingl, K., 2008. Stable carbon and oxygen isotope investigation in historical lime mortar and plaster – Results from field and experimental study. *Appl. Geochem.* 23, 2425–2437.
- Kovács, Z., Demangel, I., Richoz, S., Hipppler, D., Baldermann, A., Krystyn, L., 2020. New constraints on the evolution of ⁸⁷Sr/⁸⁶Sr of seawater during the Upper Triassic. *Glob. Planet. Chang.* 192, 103255.
- Kumar, S., Naiya, T.K., Kumar, T., 2018. Developments in oilfield scale handling towards green technology-A review. *J. Pet. Sci. Eng.* 169, 428–444.
- Kusturica, A., van Laaten, N., Drake, H., Schäfer, T., 2022. LA-ICP-MS analysis of trace and rare-earth element distribution in calcite fracture fillings from Forsmark, Simpevarp and Laxemar (Sweden). *Environ. Earth Sci.* 81, 371.
- Labeyrie, J., Delibrias, G., 1964. Dating of old mortars by the carbon-14 method [58]. *Nature* 201, 742.
- Lacelle, D. (2007) Environmental setting, (micro)morphologies and stable C–O isotope composition of cold climate carbonate precipitates—a review and evaluation of their potential as paleoclimatic proxies. *Quat. Sci. Rev.* 26, 1670–1689.
- Lacelle, D., Lauriol, B., Clark, I., 2009. Formation of seasonal ice bodies and associated cryogenic carbonates in Caverne de l'Ours, Quebec, Canada: Kinetic isotope effects and pseudo-biogenic crystal structures. *Journal of Cave and Karst* 71, 48–62.
- Lachniet, M.S., 2009. Climatic and environmental controls on speleothem oxygen-isotope values. *Quat. Sci. Rev.* 28, 412–432.
- Lachniet, M.S., Bernal, J.P., Asmerom, Y., Polyak, V., 2012. Uranium loss and aragonite–calcite age discordance in a calcitized aragonite stalagmite. *Quat. Geochronol.* 14, 26–37.
- Lackner, K.S., 2003. A Guide to CO₂ Sequestration. *Science* 300, 1677–1678.
- Lakshtanov, L.Z., Stipp, S.L.S., 2007. Experimental study of nickel(II) interaction with calcite: Adsorption and coprecipitation. *Geochim. Cosmochim. Acta* 71, 3686–3697.
- Lalk, E., Pape, T., Gruen, D.S., Kaul, N., Karolewski, J.S., Bohrmann, G., Ono, S., 2022. Clumped methane isotopologue-based temperature estimates for sources of methane in marine gas hydrates and associated vent gases. *Geochim. Cosmochim. Acta* 327, 276–297.
- Lam, R.S.K., Charnock, J.M., Lennie, A., Meldrum, F.C., 2007. Synthesis-dependant structural variations in amorphous calcium carbonate. *CrystEngComm* 9, 1226–1236.
- Lammers, L.N., Kulasinski, K., Zarzycki, P., DePaolo, D.J., 2020. Molecular simulations of kinetic stable calcium isotope fractionation at the calcite-aqueous interface. *Chem. Geol.* 532.
- Land, L.S., 1998. Failure to Precipitate Dolomite at 25 °C from Dilute Solution Despite 1000-Fold Odersaturation after 32 Years. *Aquat. Geochem.* 4, 361–368.
- Lechner, M., Pogge von Strandmann, P.A.E., Jenkyns, H.C., Prosser, G., Parente, M., 2015. Lithium-isotope evidence for enhanced silicate weathering during OAE 1a (Early Aptian Selli event). *Earth Planet. Sci. Lett.* 432, 210–222.
- Lécuyer, C., Gardien, V., Rigaudier, T., Fourel, F., Martineau, F., Cros, A., 2009. Oxygen isotope fractionation and equilibration kinetics between CO₂ and H₂O as a function of salinity of aqueous solutions. *Chem. Geol.* 264, 122–126.
- Lécuyer, C., O'Neil, J.R., 1994. Stable isotope compositions of fluid inclusions in biogenic carbonates. *Geochim. Cosmochim. Acta* 58, 353–363.
- Lee, M., Kolbus Colin, M., Yepes Andres, D., Gomez Michael, G., 2019. Investigating ammonium by-product removal following stimulated ureolytic microbially-induced calcite precipitation. *Geo-Congress 2019*, 260–272. <https://doi.org/10.1061/9780784482117.026>.
- Lee, Y.J., Reeder, R.J., 2006. The role of citrate and phthalate during Co(II) coprecipitation with calcite. *Geochim. Cosmochim. Acta* 70, 2253–2263.
- Leenheer, J.A., Crouté, J.P., 2003. Characterizing aquatic dissolved organic matter. *Environ. Sci. Technol.* 37, 18A–26A.
- Leggett, S.A., Rasbury, E.T., Grossman, E.L., Hemming, N.G., Penman, D.E., 2020. The Brachiopod δ¹¹B Record Across the Carboniferous-Permian Climate Transition. *Paleoceanography and Paleoclimatology* 35.
- Leis, A., Wagner, H., Eichinger, S., Domberger, G., Wedenig, M., Dietzel, M., Boch, R., 2022. Use of green inhibitors for hardness stabilisation of tunnel drainage systems. *Geomechanics and Tunnelling* 15, 402–413.
- Lemaître, N., Bayon, G., Ondréas, H., Caprais, J.-C., Freslon, N., Bollinger, C., Rouget, M.-L., de Prunelé, A., Ruffine, L., Olu-Le, Roy K., Sarthou, G., 2014. Trace element behaviour at cold seeps and the potential export of dissolved iron to the ocean. *Earth Planet. Sci. Lett.* 404, 376–388.
- Lerm, S., Westphal, A., Miethling-Graff, R., Alawi, M., Seibt, A., Wolfgramm, M., Würdemann, H., 2013. Thermal effects on microbial composition and microbiologically induced corrosion and mineral precipitation affecting operation of a geothermal plant in a deep saline aquifer. *Extremophiles* 17, 311–327.
- Letulle, T., Gaspard, D., Daëron, M., Arnaud-Godet, F., Vinçon-Laugier, A., Suan, G., Lécuyer, C., 2023. Multi-proxy assessment of brachiopod shell calcite as a potential archive of seawater temperature and oxygen isotope composition. *Biogeosciences* 20, 1381–1403.
- Leukel, S., Panthöfer, M., Mondeshki, M., Kieslich, G., Wu, Y., Krautwurst, N., Tremel, W., 2018. Mechanochemical Access to Defect-Stabilized Amorphous Calcium Carbonate. *Chem. Mater.* 30, 6040–6052.
- Lev, L., Stein, M., Ito, E., Fruchter, N., Ben-Avraham, Z., Almogi-Labin, A., 2019. Sedimentary, geochemical and hydrological history of Lake Kinneret during the past 28,000 years. *Quat. Sci. Rev.* 209, 114–128.

- Levitt, Nicholas P., Eiler, John M., Romanek, Christopher S., Beard, Brian L., Xu, H., Johnson, Clark M., 2018. Near Equilibrium ^{13}C - ^{18}O Bonding During Inorganic Calcite Precipitation Under Chemo-Stat Conditions. *Geochim. Geophys. Geosyst.* 19, 901–920.
- Li, A., Zhang, H., Liu, Q., Zeng, H., 2022e. Effects of chemical inhibitors on the scaling behaviors of calcite and the associated surface interaction mechanisms. *J. Colloid Interface Sci.* 618, 507–517.
- Li, C., Zhang, C., Zhang, W., 2019a. The inhibition effect mechanisms of four scale inhibitors on the formation and crystal growth of CaCO_3 in solution. *Sci. Rep.* 9, 13366.
- Li, H., Eksteen, J., Kuang, G., 2019b. Recovery of lithium from mineral resources: State-of-the-art and perspectives – A review. *Hydrometallurgy* 189, 105129.
- Li, H., Kipp, M.A., Kim, S.L., Kast, E.R., Eberle, J.J., Tissot, F.L.H., 2024b. Exploring uranium isotopes in shark teeth as a paleo-redox proxy. *Geochim. Cosmochim. Acta* 365, 158–173.
- Li, H., Liu, X., Tripati, A., Feng, S., Elliott, B., Whicker, C., Arnold, A., Kelley, A.M., 2020. Factors controlling the oxygen isotopic composition of lacustrine authigenic carbonates in Western China: implications for paleoclimate reconstructions. *Sci. Rep.* 10.
- Li, J., Azmy, K., Kendall, B., 2022d. The Mo- and U-isotope signatures in alternating shales and carbonate beds of rhythmites: A comparison and implications for redox conditions across the Cambrian-Ordovician boundary. *Chem. Geol.* 602.
- Li, N., Zhang, F., Gao, J., Cao, M., Wei, G.Y., Wang, H., Zhang, Z., Cheng, M., Xiong, G., Zhou, J., Zhang, H., Peng, Y., Li, C., Shen, S.Z., 2022b. Assessing bulk carbonates as archives for seawater sulfur isotopic composition using shallow water cores from the South China Sea. *Palaeogeography, Palaeoclimatology, Palaeoecology*, p. 598.
- Li, Q., Wu, P., Wang, S., Huang, J., Lu, W., Tan, D., Gu, S., Fan, B., 2023b. The non-coevolution of DIC and alkalinity and the CO₂ degassing in a karst river affected by acid mine drainage in Southwest China. *Sci. Total Environ.* 900.
- Li, S., Li, G.K., Li, W., Chen, Y., Raymo, M.E., Chen, J., 2023a. Effects of Secondary Carbonate Precipitation and Dissolution on Changjiang (Yangtze) River Chemistry and Estimates of Silicate Weathering Rates. *Glob. Biogeochem. Cycles* 37.
- Li, W., Beard, B.L., Li, C., Xu, H., Johnson, C.M., 2015b. Experimental calibration of Mg isotope fractionation between dolomite and aqueous solution and its geological implications. *Geochim. Cosmochim. Acta* 157, 164–181.
- Li, W., Ji, Z., Luo, X., Li, Y., 2024a. Isotope fractionation of alkaline and alkaline-earth elements (Li, K, Rb, Mg, Ca, Sr, Ba) during diffusion in aqueous solutions. *Geochim. Cosmochim. Acta* 370, 104–112.
- Li, W., Liu, X.M., Hu, Y., Teng, F.Z., Hu, Y., 2021b. Potassium isotopic fractionation during clay adsorption. *Geochim. Cosmochim. Acta* 304, 160–177.
- Li, W., Liu, X.-M., Wang, K., Fodrie, F.J., Yoshimura, T., Hu, Y.-F., 2021a. Potassium phases and isotopic composition in modern marine biogenic carbonates. *Geochim. Cosmochim. Acta* 304, 364–380.
- Li, W., Liu, X.-M., Wang, K., Hu, Y., Suzuki, A., Yoshimura, T., 2022a. Potassium incorporation and isotope fractionation in cultured scleractinian corals. *Earth Planet. Sci. Lett.* 581, 117393.
- Li, W., Liu, X.M., Wang, K., McManus, J., Haley, B.A., Takahashi, Y., Shakouri, M., Hu, Y., 2022c. Potassium isotope signatures in modern marine sediments: Insights into early diagenesis. *Earth Planet. Sci. Lett.* 599.
- Li, X., Gao, B., Yue, Q., Ma, D., Rong, H., Zhao, P., Teng, P., 2015a. Effect of six kinds of scale inhibitors on calcium carbonate precipitation in high salinity wastewater at high temperatures. *J. Environ. Sci.* 29, 124–130.
- Li, Z., Huang, Y., Jiang, L., Tang, H., Jiao, G., Gou, H., Gou, W., Ni, S., 2024c. Metal stable isotopes fractionation during adsorption. *Ecotoxicol. Environ. Saf.* 283, 116770.
- Licht, A., Kelson, J., Bergel, S., Schauer, A., Petersen, S.V., Capirala, A., Huntington, K.W., Dupont-Nivet, G., Win, Z., Aung, D.W., 2022. Dynamics of Pedogenic Carbonate Growth in the Tropical Domain of Myanmar. *Geochemistry, Geophysics, Geosystems*, p. 23.
- Liendo, F., Arduino, M., Deorsola, F.A., Bensaid, S., 2022. Factors controlling and influencing polymorphism, morphology and size of calcium carbonate synthesized through the carbonation route: A review. *Powder Technol.* 398.
- Lin, Y.-B., Wei, H.-Z., Zhang, F., Hohl, S.V., Wei, G.-Y., Li, T., Xiong, G.-L., Li, N., Jiang, S.-Y., 2022. Evaluation of shallow-water corals and associated carbonate sediments as seawater Ba isotope archives in the South China Sea. *Palaeogeogr. Palaeoclimatol. Palaeoecol.* 605, 111196.
- Lin, Z., Sun, X., Strauss, H., Eroglu, S., Böttcher, M.E., Lu, Y., Liang, J., Li, J., Peckmann, J., 2021. Molybdenum isotope composition of seep carbonates – Constraints on sediment biogeochemistry in seepage environments. *Geochim. Cosmochim. Acta* 307, 56–71.
- Lindeman, I., Hansen, M., Scholz, D., Breitenbach, S.F.M., Hartland, A., 2022. Effects of organic matter complexation on partitioning of transition metals into calcite: Cave-analogue crystal growth experiments. *Geochim. Cosmochim. Acta* 317, 118–137.
- Lindroos, A., Ringbom, Å., Heinemeier, J., Hodgins, G., Sonck-Koota, P., Sjöberg, P., Lancaster, L., Kaisti, R., Brock, F., Ranta, H., Caroselli, M., Lugli, S., 2018. Radiocarbon Dating Historical Mortars: Lime Lumps and/or Binder Carbonate? *Radiocarbon* 60, 875–899.
- Lipar, M., Martín-Pérez, A., Tičar, J., Pavšek, M., Gabrovec, M., Hrvatin, M., Komac, B., Zorn, M., Hajna, N.Z., Zhao, J.X., Drysdale, R.N., Ferk, M., 2021. Subglacial carbonate deposits as a potential proxy for a glacier's former presence. *Cryosphere* 15, 17–30.
- Lippmann, F., 1973. Sedimentary carbonate minerals. In: Minerals, Rocks and Inorganic Materials, 6. Springer Verlag, 228p.
- Lisiecki, L.E., Stern, J.V., 2016. Regional and global benthic $\delta^{18}\text{O}$ stacks for the last glacial cycle. *Paleoceanography* 31, 1368–1394.
- Little, S.H., Wilson, D.J., Rehkämper, M., Adkins, J.F., Robinson, L.F., van de Flierdt, T., 2021. Cold-water corals as archives of seawater Zn and Cu isotopes. *Chem. Geol.* 578, 120304.
- Littlewood, J.L., Shaw, S., Peacock, C.L., Bots, P., Trivedi, D., Burke, I.T., 2017. Mechanism of Enhanced Strontium Uptake into Calcite via an Amorphous Calcium Carbonate Crystallization Pathway. *Cryst. Growth Des.* 17, 1214–1223.
- Liu, C., Li, W., 2023. Magnesium isotope fractionation between calcite and aqueous solutions under elevated temperatures of 98–170 °C. *Geochim. Cosmochim. Acta* 344, 160–177.
- Liu, D., Chen, T., Dai, Z., Papineau, D., Qiu, X., Wang, H., Benzerara, K., 2024a. A non-classical crystallization mechanism of microbially-induced disordered dolomite. *Geochim. Cosmochim. Acta* 381, 198–209.
- Liu, D., Xu, Y., Papineau, D., Yu, N., Fan, Q., Qiu, X., Wang, H., 2019b. Experimental evidence for abiotic formation of low-temperature proto-dolomite facilitated by clay minerals. *Geochim. Cosmochim. Acta* 247, 83–95.
- Liu, H., Liu, Z., Macpherson, G.L., Yang, R., Chen, B., Sun, H., 2015. Diurnal hydrochemical variations in a karst spring and two ponds, Maolan Karst Experimental Site, China: Biological pump effects. *J. Hydrol.* 522, 407–417.
- Liu, H., Wen, Z., Liu, Z., Yang, Y., Wang, H., Xia, X., Ye, J., Liu, Y., 2024b. Unlocking the potential of amorphous calcium carbonate: a star ascending in the realm of biomedical application. *Acta Pharm. Sin. B* 14, 602–622.
- Liu, J., Chen, J., Wang, Z., Cai, H., Yuan, W., Wang, Z., Huang, F., Liu, C., 2023a. Magnesium isotope fractionation during natural travertine deposition from Baishuitai, SW China. *Applied Geochemistry* 157, 105777.
- Liu, R., Huang, S., Zhang, X., Song, Y., He, G., Wang, Z., Lian, B., 2021. Bio-mineralisation, characterization, and stability of calcium carbonate containing organic matter. *RSC Adv.* 11, 14415–14425.
- Liu, S., Sui, Y., Dong, B., 2022a. Reinforcement of reclaimed sand by stimulating native microorganisms for biomineralization. *Frontiers in Bioengineering and Biotechnology* 10.
- Liu, Y., 2015. Theory and computational methods of non-traditional stable isotope fractionation. *Earth Science Frontiers* 22, 1–28.
- Liu, Y.-J., Li, S.-L., Chen, B.-P.-W., Chien, C.-L., Chan, J.C.C., 2022b. Porous Mg-stabilized amorphous calcium carbonate as carrier for hydrophobic drugs. *J. Chin. Chem. Soc.* 69, 1688–1697.
- Liu, Z., Shao, C., Jin, B., Zhang, Z., Zhao, Y., Xu, X., Tang, R., 2019a. Crosslinking ionic oligomers as conformable precursors to calcium carbonate. *Nature* 574, 394–398.
- Loewenthal, R.E., Marais, G.V., 1976. Carbonate Chemistry of Aquatic Systems: Theory and Application. Ann Arbor Science.
- Lopez-Berganza, J.A., Chen, S., Espinosa-Marzal, R.M., 2019. Tailoring Calcite Growth through an Amorphous Precursor in a Hydrogel Environment. *Crystal Growth and Design* 19, 3192–3205.
- Lorens, R.B., 1981. Sr, Cd, Mn and Co distribution coefficients in calcite as a function of calcite precipitation rate. *Geochim. Cosmochim. Acta* 45, 553–561.
- Lourteau, T., Berriche, H., Kécili, K., Heim, V., Bricault, D., Litaudon, M., Cachet, X., Roussi, F., Perrot, H., Horner, O., Cheap-Charpentier, H., 2019. Scale inhibition effect of *Hylocereus undatus* solution on calcium carbonate formation. *J. Cryst. Growth* 524, 125161.
- Louvel, M., Etschmann, B., Guan, Q., Testemale, D., Brugger, J., 2022. Carbonate complexation enhances hydrothermal transport of rare earth elements in alkaline fluids. *Nat. Commun.* 13, 1456.
- Lu, W., Barbosa, C.F., Rathburn, A.E., Xavier, P.D.M., Cruz, A.P.S., Thomas, E., Rickaby, R.E.M., Zhang, Y.G., Lu, Z., 2021. Proxies for paleo-oxygenation: A downcore comparison between benthic foraminiferal surface porosity and I/Ca. *Palaeogeography, Palaeoclimatology, Palaeoecology*, p. 579.
- Lu, Y., Paulmann, C., Mihailova, B., Malcherek, T., Birgel, D., López, Correa M., Lin, Z., Lu, L., Milker, Y., Peckmann, J., 2023b. Fibrous dolomite formation at a Miocene methane seep may reflect Neoproterozoic aragonite-dolomite sea conditions. *Communications Earth & Environment* 4, 346.
- Lu, Y.-C., Song, S.-R., Liu, L.-W., Peng, T.-R., Chen, B.-C., Tu, R.K.-C., Lin, L.-H., Wang, P.-L., 2023a. Applicability of carbonate clumped isotope thermometry in the Tuchang-Jentsje geothermal field. *Geothermics* 112, 102728.
- Lu, Y.-C., Song, S.-R., Taguchi, S., Wang, P.-L., Yeh, E.-C., Lin, Y.-J., MacDonald, J., John, C.M., 2018. Evolution of hot fluids in the Chingshui geothermal field inferred from crystal morphology and geochemical vein data. *Geothermics* 74, 305–318.
- Lucarelli, J.K., Purgstaller, B., Ulrich, R.N., Parvez, Z., Leis, A., Goetschl, K.E., Eagle, R.A., Dietzel, M., Tripati, A., 2023. Dual clumped ($\Delta 47$ - $\Delta 48$) isotope data for amorphous carbonates and transformation products reveal a novel mechanism for disequilibrium clumped isotope effects. *Geochim. Cosmochim. Acta* 359, 119–134.
- Ludwig, K., Kelley, D., Butterfield, D., Nelson, B., Früh-Green, G., 2006. Formation and evolution of carbonate chimneys at the Lost City Hydrothermal Field. *Geochim. Cosmochim. Acta* 70, 3625–3645.
- Luettkemeyer, P.B., Kirschner, D.L., Huntington, K.W., Chester, J.S., Chester, F.M., Evans, J.P., 2016. Constraints on paleofluid sources using the clumped-isotope thermometry of carbonate veins from the SAFOD (San Andreas Fault Observatory at Depth) borehole. *Tectonophysics* 690, Part A, 174–189.
- Luetscher, M., Boch, R., Sodemann, H., Spötl, C., Cheng, H., Edwards, R.L., Frisia, S., Hof, F., Müller, W., 2015. North Atlantic storm track changes during the Last Glacial Maximum recorded by Alpine speleothems. *Nat. Commun.* 6, 6344.
- Luetscher, M., Ziegler, F., 2012. CORA - a dedicated device for carbon dioxide monitoring in cave environments. *Int. J. Speleol.* 41, 275–283.
- Lundin, Johnson M., Noreland, D., Gane, P., Schoelkopf, J., Ridgway, C., Millqvist, Fureby A., 2017. Porous calcium carbonate as a carrier material to increase the dissolution rate of poorly soluble flavouring compounds. *Food Funct.* 8, 1627–1640.

- Luo, L., Capezzuoli, E., Rogerson, M., Vaselli, O., Wen, H., Lu, Z., 2022. Precipitation of carbonate minerals in travertine-depositing hot springs: Driving forces, microenvironments, and mechanisms. *Sediment. Geol.* 438.
- Ly, Y., Liu, S.A., Wu, H., Hohl, S.V., Chen, S., Li, S., 2018. Zn-Sr isotope records of the Ediacaran Doushantuo Formation in South China: diagenesis assessment and implications. *Geochim. Cosmochim. Acta* 239, 330–345.
- Ma, C., Xu, F., Zhu, Z., Yang, H., Nong, P., Kang, Z., Tang, S., Zhang, L. and Zhu, Y. (2022) Dissolution and Solubility of the Calcite–Otvatite Solid Solutions $[(\text{Ca}_{1-x}\text{Cd}_x)\text{CO}_3]$ at 2° C. *Minerals* 12(6).
- Ma, M., Wang, Y., Cao, X., Lu, W., Guo, Y., 2019. Temperature and supersaturation as key parameters controlling the spontaneous precipitation of calcium carbonate with distinct physicochemical properties from pure aqueous solutions. *Cryst. Growth Des.* 19, 6972–6988.
- Ma, S., Yang, Y., Lei, X., Yue, B., 2023. Water scaling predication for typical sandstone geothermal reservoirs in the Xi'an Depression. *Energy Geoscience* 4, 100182.
- Ma, Y., Aichmayer, B., Paris, O., Fratzl, P., Meibom, A., Metzler, R.A., Polit, Y., Addadi, L., Gilbert, P.U.P.A., Weiner, S., 2009. The grinding tip of the sea urchin tooth exhibits exquisite control over calcite crystal orientation and Mg distribution. *Proc. Natl. Acad. Sci.* 106, 6048–6053.
- Macedo R. G. M. d. A., Marques N. D. N., Palucci L. C. S., Cunha J. V. M., Villette M. A., Castro B. B. and Balaban R. D. C. (2019) Water-soluble carboxymethylchitosan as green scale inhibitor in oil wells. *Carbohydr. Polym.* 215, 137–142.
- Mackenzie, F.T., 2003. Carbonate mineralogy and geochemistry. In: Middleton, G.V., Church, M.J., Coniglio, M., Hardie, L.A., Longstaffe, F.J. (Eds.), *Encyclopedia of Sediments and Sedimentary Rocks*. Springer, Netherlands, Dordrecht, pp. 93–100.
- MacKenzie, F.T., Andersson, A.J., 2013. Geochemical perspectives: The marine carbon system and ocean acidification during phanerozoic time. *Geochemical Perspectives* 2, 1–239.
- Magette, E., Turner, A., Peng, Y., Herrmann, A.D., 2023. Syndepositional Uptake of Uranium, Molybdenum and Vanadium into Modern Bahamian Carbonate Sediments during Early Diagenesis; Geosciences (Switzerland) 13 (3).
- Maher, T.D., Santos, I.R., Tait, D.R., 2014. Mapping methane and carbon dioxide concentrations and $d^{13}\text{C}$ values in the atmosphere of two Australian coal seam gas fields. *Water Air Soil Pollut.* 225, 2216.
- Malone, M.J., Baker, P.A., 1999. Temperature dependence of the strontium distribution coefficient in calcite: An experimental study from 40° to 200°C and application to natural diagenetic calcites. *J. Sediment. Res.* 69, 216–223.
- Mangenot, X., Gasparrini, M., Rouchon, V., Boniface, M., 2018. Basin-scale thermal and fluid flow histories revealed by carbonate clumped isotopes (Δ_{47}) – Middle Jurassic carbonates of the Paris Basin depocentre. *Sedimentology* 65, 123–150.
- Marchegiano, M., Peral, M., Vendrickx, J., Martens, K., García-Alix, A., Snoek, C., Goderis, S., Claeys, P., 2024. The Ostracod Clumped-Isotope Thermometer: A Novel Tool to Accurately Quantify Continental Climate Changes. *Geophys. Res. Lett.* 51 e2023GL107426.
- Marin-Troya, P., Espinosa, C., Monasterio-Guillot, L., Alvarez-Lloret, P., 2023. Carbonate Minerals & Precipitation in the Presence of Background Electrolytes: Sr, Cs, and Li with Different Transporting Anions. *Crystals* 13, 796.
- Markó A., Driba, D., Zsele, F., Osvald, M., Brehme, M. (2021) Analysis of Geothermal Reinjection Problems with Hydrogeochemical Modelling. *Proceedings World Geothermal Congress 2020+1*, 7.
- Marriott, C.S., Henderson, G.M., Belshaw, N.S., Tudhope, A.W., 2004. Temperature dependence of $\delta^7\text{Li}$, $\delta^{44}\text{Ca}$ and Li/Ca during growth of calcium carbonate. *Earth Planet. Sci. Lett.* 222, 615–624.
- Martin-Chivelet, J., Muñoz-García, M.B., Cruz, J.A., Ortega, A.I., Turrero, M.J., 2017. Speleothem Architectural Analysis: Integrated approach for stalagmite-based paleoclimate research. *Sediment. Geol.* 353, 28–45.
- Martin-Garcia, R., Alonso-Zarza, A.M., Martín-Pérez, A., 2009. Loss of primary texture and geochemical signatures in speleothems due to diagenesis: Evidences from Castañoar Cave, Spain. *Sediment. Geol.* 221, 141–149.
- Maskenskaya, O.M., Drake, H., Broman, C., Hogmalm, J.K., Czuppon, G., Åström, M.E., 2014. Source and character of syntectonic hydrothermal calcite veins in Paleoproterozoic crystalline rocks revealed by fine-scale investigations. *Geofluids* 14, 495–511.
- Maskenskaya, O.M., Drake, H., Mathurin, F.A., Åström, M.E., 2015. The role of carbonate complexes and crystal habit on rare earth element uptake in low-temperature calcite in fractured crystalline rock. *Chem. Geol.* 391, 100–110.
- Matera, P.F., Ventrucci, G., Zucchi, M., Brogi, A., Capezzuoli, E., Liotta, D., Yu, T.-L., Shen, C.-C., Huntington, K.W., Rinyu, L., Kele, S., 2021. Geothermal Fluid Variation Recorded by Banded Ca-Carbonate Veins in a Fault-Related, Fissure-Ridge-Type Travertine Depositional System (Iano, southern Tuscany, Italy). *Geofluids* 2021, 8817487.
- Mathieson, A., Midgley, J., Wright, I., Saoula, N., Ringrose, P., 2011. In Salah CO₂ Storage JIP: CO₂ sequestration monitoring and verification technologies applied at Krechba, Algeria. *Energy Procedia* 4, 3596–3603.
- Matter, J.M., Stute, M., Snæbjörnsdóttir, S.Ó., Oelkers, E.H., Gislason, S.R., Aradottir, E.S., Sigfusson, B., Gunnarsson, I., Sigurdardóttir, H., Gunnlaugsson, E., Axelsson, G., Alfredsson, H.A., Wolff-Boenisch, D., Mesfin, K., Taya, D.F., d. l. R., Hall, J., Dideriksen, K. and Broecker, W.S., 2016. Rapid carbon mineralization for permanent disposal of anthropogenic carbon dioxide emissions. *Science* 352, 1312–1314.
- Mattey, D., Lowry, D., Duffet, J., Fisher, R., Hodge, E., Frisia, S., 2008. A 53 year seasonally resolved oxygen and carbon isotope record from a modern Gibraltar speleothem: Reconstructed drip water and relationship to local precipitation. *Earth Planet. Sci. Lett.* 269, 80–95.
- Mattey, D.P., Atkinson, T.C., Barker, J.A., Fisher, R., Latin, J.P., Durell, R., Ainsworth, M., 2016. Carbon dioxide, ground air and carbon cycling in Gibraltar karst. *Geochim. Cosmochim. Acta* 184, 88–113.
- Mattey, D.P., Atkinson, T.C., Hoffmann, D.L., Boyd, M., Ainsworth, M., Durell, R., Latin, J.P., 2021. External controls on CO₂ in Gibraltar cave air and ground air: Implications for interpretation of $d^{13}\text{C}$ in speleothems. *Sci. Total Environ.* 777, 146096.
- Mavromatis, V., Brazier, J.-M., Goetschl, K.E., 2022. Controls of temperature and mineral growth rate on Mg incorporation in aragonite. *Geochim. Cosmochim. Acta* 317, 53–64.
- Mavromatis, V., Gautier, Q., Bosc, O., Schott, J., 2013. Kinetics of Mg partition and Mg stable isotope fractionation during its incorporation in calcite. *Geochim. Cosmochim. Acta* 114, 188–203.
- Mavromatis, V., Goetschl, K.E., Greigg, C., Konrad, F., Purgstaller, B., Dietzel, M., 2018. Barium partitioning in calcite and aragonite as a function of growth rate. *Geochim. Cosmochim. Acta* 237, 65–78.
- Mavromatis, V., González, A.G., Dietzel, M., Schott, J., 2019. Zinc isotope fractionation during the inorganic precipitation of calcite – Towards a new pH proxy. *Geochim. Cosmochim. Acta* 244, 99–112.
- Mavromatis, V., Immenhauser, A., Buhl, D., Purgstaller, B., Baldermann, A., Dietzel, M., 2017a. Effect of organic ligands on Mg partitioning and Mg isotope fractionation during low-temperature precipitation of calcite in the absence of growth rate effects. *Geochim. Cosmochim. Acta* 207, 139–153.
- Mavromatis, V., Montouillout, V., Noireaux, J., Gaillardet, J., Schott, J., 2015. Characterization of boron incorporation and speciation in calcite and aragonite from co-precipitation experiments under controlled pH, temperature and precipitation rate. *Geochim. Cosmochim. Acta* 150, 299–313.
- Mavromatis, V., Purgstaller, B., Dietzel, M., Buhl, D., Immenhauser, A., Schott, J., 2017b. Impact of amorphous precursor phases on magnesium isotope signatures of Mg-calcite. *Earth Planet. Sci. Lett.* 464, 227–236.
- Mavromatis, V., Purgstaller, B., Louvat, P., Faure, L., Montouillout, V., Gaillardet, J., Schott, J., 2021. Boron isotope fractionation during the formation of amorphous calcium carbonates and their transformation to Mg-calcite and aragonite. *Geochim. Cosmochim. Acta* 315, 152–171.
- Mavromatis, V., van Zuilen, K., Blanchard, M., van Zuilen, M., Dietzel, M., Schott, J., 2020. Experimental and theoretical modelling of kinetic and equilibrium Ba isotope fractionation during calcite and aragonite precipitation. *Geochim. Cosmochim. Acta* 269, 566–580.
- McCormack, J., Baldermann, A., Bontognali, T.R.R., Wolf, A., Kwiecien, O., 2024. Hydrochemical mixing-zones trigger dolomite formation in an alkaline lake. *Sedimentology* 71, 871–886.
- McCrea, J.M., 1950. On the isotopic chemistry of carbonates and a paleotemperature scale. *J. Chem. Phys.* 18, 849–857.
- Mechal, A., Birk, S., Dietzel, M., Leis, A., Winkler, G., Mogessie, A., Kebede, S., 2017. Groundwater flow dynamics in the complex aquifer system of Gidabo River Basin (Ethiopian Rift): a multi-proxy approach. *Hydrogeol. J.* 25, 519–538.
- Meckler, A.N., Affolter, S., Dublyansky, Y.V., Krüger, Y., Vogel, N., Bernasconi, S.M., Frenz, M., Kipfer, R., Leuenberger, M., Spötl, C., Carolin, S., Cobb, K.M., Moerman, J., Adkins, J.F., Fleitmann, D., 2015. Glacial–interglacial temperature change in the tropical West Pacific: A comparison of stalagmite-based paleothermometers. *Quat. Sci. Rev.* 127, 90–116.
- Mehrabi H. and Tavakoli V. (2024) Editorial for the Special Issue: Deposition, Diagenesis, and Geochemistry of Carbonate Sequences. *Minerals* 14, 269.
- Mehta, N., Coutaud, M., Bouchet, J., van Zuilen, K., Bradbury, H.J., Moynier, F., Gorge, C., Skouri-Panet, F., Benzerara, K., 2023. Barium and strontium isotope fractionation by cyanobacteria forming intracellular carbonates. *Geochim. Cosmochim. Acta* 356, 165–178.
- Mehta, N., Gaëtan, J., Giura, P., Azais, T., Benzerara, K., 2022. Detection of biogenic amorphous calcium carbonate (ACC) formed by bacteria using FTIR spectroscopy. *Spectrochim. Acta A Mol. Biomol. Spectrosc.* 278, 121262.
- Meister, P., 2015. For the deep biosphere, the present is not always the key to the past: what we can learn from the geological record. *Terra Nova* 27, 400–408.
- Meister, P., Frisia, S., 2019. Dolomite formation by nanocrystal aggregation in the dolomia principale of the brenta dolomites (Northern Italy). *Riv. Ital. Paleontol. Stratigr.* 125, 183–196.
- Meister, P., Frisia, S., Dódonov, I., Pekker, P., Molnár, Z., Neuhuber, S., Gier, S., Kovács, I., Demény, A., Pósfai, M., 2023. Nanoscale Pathway of Modern Dolomite Formation in a Shallow, Alkaline Lake. *Cryst. Growth Des.* 23, 3202–3212.
- Meister, P., McKenzie, J.A., Bernasconi, S.M., Brack, P., 2013. Dolomite formation in the shallow seas of the Alpine Triassic. *Sedimentology* 60, 270–291.
- Mercedes-Martin, R., Rogerson, M., Prior, T.J., Brasier, A.T., Reijmer, J.J.G., Billing, I., Matthews, A., Love, T., Lepley, S., Pedley, M., 2021. Towards a morphology diagram for terrestrial carbonates: Evaluating the impact of carbonate supersaturation and alginic acid in calcite precipitate morphology. *Geochim. Cosmochim. Acta* 306, 340–361.
- Mergelsberg, S., Kerisit, S., Ilton, E., Qafoku, O., Thompson, C., Loring, J., 2020b. Low temperature and limited water activity reveal a pathway to magnesite via amorphous magnesium carbonate. *Chem. Commun. (Cambridge, England)* 56.
- Mergelsberg, S.T., De Yoreo, J.J., Miller, Q.R.S., Marc Michel, F., Ulrich, R.N., Dove, P. M., 2020a. Metastable solubility and local structure of amorphous calcium carbonate (ACC). *Geochim. Cosmochim. Acta* 289, 196–206.
- Mergelsberg, S.T., Riechers, S.L., Graham, T.R., Prange, M.P., Kerisit, S.N., 2021. Effect of Cd on the Nucleation and Transformation of Amorphous Calcium Carbonate. *Cryst. Growth Des.* 21, 3384–3393.
- Merle, M., Soulié, J., Sassoye, C., Roblin, P., Rey, C., Bonhomme, C., Combes, C., 2022. Pyrophosphate-stabilised amorphous calcium carbonate for bone substitution: toward a doping-dependent cluster-based model. *CrystEngComm* 24, 8011–8026.

- Meyer, M.C., Aldenderfer, M.S., Wang, Z., Hoffmann, D.L., Dahl, J.A., Degeling, D., Haas, W.R., Schlütz, F., 2017. Permanent human occupation of the central Tibetan Plateau in the early Holocene. *Science* 355, 64.
- Michalski, J.R., Goudge, T.A., Crowe, S.A., Cuadros, J., Mustard, J.F., Johnson, S.S., 2022. Geological diversity and microbiological potential of lakes on Mars. *Nature Astronomy* 6, 1133–1141.
- Mickler, P.J., Carlson, P., Banner, J.L., Breecker, D.O., Stern, L., Guilfoyle, A., 2019. Quantifying carbon isotope disequilibrium during in-cave evolution of drip water along discreet flow paths. *Geochim. Cosmochim. Acta* 244, 182–196.
- Middelburg, J.J., 2019. Marine Carbon Biogeochemistry - A primer for Earth System Scientists. Springer Open.
- Midgley S. D., Di Tommaso D., Fleitmann D. and Grau-Crespo R. (2021) Sulfate and Molybdate Incorporation at the Calcite-Water Interface: Insights from Ab Initio Molecular Dynamics. *ACS Earth and Space Chemistry* 5, 2066–2073.
- Midgley, S.D., Fleitmann, D., Grau-Crespo, R., 2022. Bromate incorporation in calcite and aragonite. *Geochim. Cosmochim. Acta* 324, 17–25.
- Mikhailova, K., Vasileva, K., Fedorov, P., Ershova, V., Vereshchagin, O., Rogov, M., Pokrovsky, B., 2019. Glendonite-like carbonate aggregates from the lower ordovician koporye formation (Russian part of the Baltic Klint): detailed mineralogical and geochemical data and paleogeographic implications. *Minerals* 9, Mills, J.V., DePaolo, D.J., Lammers, L.N., 2021. The influence of Ca:CO₃ stoichiometry on Ca isotope fractionation: Implications for process-based models of calcite growth. *Geochim. Cosmochim. Acta* 298, 87–111.
- Misra, S., Froehlich, P.N., 2012. Lithium isotope history of Cenozoic seawater: changes in silicate weathering and reverse weathering. *Science* 335, 818–823.
- Mitchell, A.C., Ferris, F.G., 2005. The coprecipitation of Sr into calcite precipitates induced by bacterial ureolysis in artificial groundwater: Temperature and kinetic dependence. *Geochim. Cosmochim. Acta* 69, 4199–4210.
- Mittermayr, F., Baldermann, A., Baldermann, C., Grathoff, G.H., Klammer, D., Köhler, S. J., Leis, A., Warr, L.N., Dietzel, M., 2017. Environmental controls and reaction pathways of coupled de-dolomitization and thaumasite formation. *Cem. Concr. Res.* 95, 282–293.
- Miyajima, Y., Araoka, D., Yoshimura, T., Ota, Y., Suzuki, A., Yoshioka, H., Suzumura, M., Smrká, D., Peckmann, J., Bohrmann, G., 2023. Lithium isotope systematics of methane-seep carbonates as an archive of fluid origins and flow rates. *Geochim. Cosmochim. Acta* 361, 152–170.
- Mizuno, T., Milodowski, A.E., Iwatsuki, T., 2022. Precipitation sequence of fracture-filling calcite in fractured granite and changes in the fractionation process of rare earth elements and yttrium. *Chem. Geol.* 603.
- Mohd Darus, D., Aimi Noorliyana, H., Azmi, R., Kamarudin, H., 2015. Reactions of limestone on the slaking process under different conditions of parameters. *Mater. Sci. Forum* 819, 393–398. <https://doi.org/10.4028/www.scientific.net/MSF.819.393>.
- Möller, P., De Lucia, M., 2020. Incorporation of Rare Earths and Yttrium in Calcite: A Critical Re-evaluation. *Aquat. Geochem.* 26, 89–117.
- Molnár, Z., Dódoný, I., Pósfai, M., 2023. Transformation of amorphous calcium carbonate in the presence of magnesium, phosphate, and mineral surfaces. *Geochim. Cosmochim. Acta* 345, 90–101.
- Mondal, S., Chakrabarti, R., Ghosh, P., 2022. A multi-proxy ($\delta^{44/40}\text{Ca}$, Sr/Ca, and Δ_{47}) study of fish otoliths for determination of seawater temperature. *Chem. Geol.* 605, 120950.
- Montoya-Pino, C., Weyer, S., Anbar, A.D., Pross, J., Oschmann, J., van de Schootbrugge, B., Arz, H.W., 2010. Global enhancement of ocean anoxia during Oceanic Anoxic Event 2: a quantitative approach using U isotopes. *Geology* 38, 315–318.
- Moore, C.H., 1989. Carbonate diagenesis and porosity. Elsevier, 338p.
- Moore C. H. and Wade W. J. (2013) Chapter 10 – Burial Diagenetic Environment. In: *Developments in Sedimentology* (eds. C. H. Moore and W. J. Wade). Elsevier. pp. 239–284.
- Morgan, J.L.L., Wasylenski, L.E., Nuester, J., Anbar, A.D., 2010. Fe Isotope Fractionation during Equilibration of Fe–Organic Complexes. *Environ. Sci. Technol.* 44, 6095–6101.
- Morse J. W. (2004) Formation and Diagenesis of Carbonate Sediments. In: *Treatise on Geochemistry, Volume 7, Sediments, Diagenesis, and Sedimentary Rocks*, Mackenzie F. T., Holland, H. D., Turekian, K. K. (eds.) 7, 67–85.
- Morse, J.W., Arvidson, R.S., Lüttge, A., 2007. Calcium carbonate formation and dissolution. *Chem. Rev.* 107, 342–381.
- Morse, J.W., Bender, M.L., 1990. Partition coefficients in calcite: Examination of factors influencing the validity of experimental results and their application to natural systems. *Chem. Geol.* 82, 265–277.
- Morse, J.W., Mackenzie, F.T., 1990. Geochemistry of Sedimentary Carbonates. Developments in Sedimentology, Amsterdam- New York - Tokyo, pp. 1–707.
- Moseley, G.E., Spötl, C., Brandstätter, S., Erhardt, T., Luetscher, M., Edwards, R.L., 2020. NALPS19: sub-orbital-scale climate variability recorded in northern Alpine speleothems during the last glacial period. *Clim. Past* 16, 29–50.
- Moynier, F., Fujii, T., 2017. Calcium isotope fractionation between aqueous compounds relevant to low-temperature geochemistry, biology and medicine. *Sci. Rep.* 7, 44255.
- Mpelwa, M., Tang, S.-F., 2019. State of the art of synthetic threshold scale inhibitors for mineral scaling in the petroleum industry: a review. *Pet. Sci.* 16.
- Mucci, A., Morse, J.W., 1984. The solubility of calcite in seawater solutions of various magnesium concentration, It = 0.697 m at 25 °C and one atmosphere total pressure. *Geochim. Cosmochim. Acta* 48, 815–822.
- Mueller, M., Jacquemyn, C., Walter, B.F., Pederson, C.L., Schurr, S.L., Igboekwe, O.A., Jöns, N., Riechelmann, S., Dietzel, M., Devriendt, L.S., Immenhauser, A., 2021. Constraints on the preservation of proxy data in carbonate archives – lessons from a marine limestone to marble transect, Latemar, Italy. *Sedimentology* 69, 423–460.
- Mueller, M., Walter, B.F., Giebel, R.J., Beranoaguirre, A., Swart, P.K., Lu, C., Riechelmann, S., Immenhauser, A., 2024. Towards a better understanding of the geochemical proxy record of complex carbonate archives. *Geochim. Cosmochim. Acta* 376, 68–99.
- Müller, I.A., Rodriguez-Blanco, J.D., Storck, J.-C., do Nascimento G. S., Bontognali T. R. R., Vasconcelos C., Benning L. G. and Bernasconi S. M., 2019. Calibration of the oxygen and clumped isotope thermometers for (proto-)dolomite based on synthetic and natural carbonates. *Chem. Geol.* 525, 1–17.
- Murphy, J.G., Ahm, A.-S.C., Swart, P.K., Higgins, J.A., 2022. Reconstructing the lithium isotopic composition ($\delta^7\text{Li}$) of seawater from shallow marine carbonate sediments. *Geochim. Cosmochim. Acta* 337, 140–154.
- Müsing, K., Clarkson, M.O., Vance, D., 2022. The meaning of carbonate Zn isotope records: Constraints from a detailed geochemical and isotope study of bulk deep-sea carbonates. *Geochim. Cosmochim. Acta* 324, 26–43.
- Nambiar, R., Hauzer, H., Gray, W.R., Henehan, M.J., Cotton, L., Erez, J., Rosenthal, Y., Renema, W., Müller, W., Evans, D., 2023. Controls on potassium incorporation in foraminifera and other marine calcifying organisms. *Geochim. Cosmochim. Acta* 351, 125–138.
- Naviaux, J.D., Subhas, A.V., Dong, S., Rollins, N.E., Liu, X., Byrne, R.H., Berelson, W.M., Adkins, J.F., 2019. Calcite dissolution rates in seawater: lab vs. in-situ measurements and inhibition by organic matter. *Mar. Chem.* 215, 103684.
- Négrel, P., Petelet-Giraud, E., Guerrot, C., Millot, R., 2021. Ca and Sr isotope constraints on chemical weathering processes: A view through the Ebro river basin. Spain. *Chemical Geology* 578, 120324.
- Nehrke, G., Reichart, G.J., Van Cappellen, P., Meile, C., Bijma, J., 2007. Dependence of calcite growth rate and Sr partitioning on solution stoichiometry: Non-Kessel crystal growth. *Geochim. Cosmochim. Acta* 71, 2240–2249.
- Nelson, C.J., Jacobson, A.D., Kitch, G.D., Weisenberger, T.B., 2021. Large calcium isotope fractionations by zeolite minerals from Iceland. *Communications Earth & Environment* 2, 206.
- Németh, P., Töchterle, P., Dublyansky, Y., Stalder, R., Molnár, Z., Klébert, S., Spötl, C., 2022. Tracing structural relicts of the ikaite-to-calcite transformation in cryogenic cave glendonite. *Am. Mineral.* 107, 1960–1967.
- Neuhuber, S., Gier, S., Draganits, E., Steier, P., Bolka, M., Ottner, F., Spötl, C., Hippler, D., Meister, P., 2024. Radiocarbon ages of microcrystalline authigenic carbonate in Lake Neusiedl (Austria) suggest millennial-scale growth of Mg-calcite and protodolomite. *Sedimentology* n/a 1–29.
- Niedermaier, A., Köhler, S.J., Dietzel, M., 2013. Impacts of aqueous carbonate accumulation rate, magnesium and polyaspartic acid on calcium carbonate formation (6–40 °C). *Chem. Geol.* 340, 105–120.
- Nielsen, L.C., De Yoreo, J.J., DePaolo, D.J., 2013. General model for calcite growth kinetics in the presence of impurity ions. *Geochim. Cosmochim. Acta* 115, 100–114.
- Nielsen, L.C., DePaolo, D.J., 2013. Ca isotope fractionation in a high-alkalinity lake system: Mono Lake, California. *Geochim. Cosmochim. Acta* 118, 276–294.
- Nielsen, L.C., DePaolo, D.J., De Yoreo, J.J., 2012. Self-consistent ion-by-ion growth model for kinetic isotopic fractionation during calcite precipitation. *Geochim. Cosmochim. Acta* 86, 166–181.
- Nielsen, M.H., Aloni, S., De Yoreo, J.J., 2014. In situ TEM imaging of CaCO₃ nucleation reveals coexistence of direct and indirect pathways. *Science* 345, 1158–1162.
- Nims, M.K., Linley, T.J., Moran, J.J., 2023. Temperature-dependent oxygen isotope fractionation in otoliths of juvenile Chinook salmon (*Oncorhynchus tshawytscha*). *Appl. Geochem.* <https://doi.org/10.1016/j.apgeochem.2023.105723>, 105723.
- Ning, M., Huang, K., Lang, X., Ma, H., Yuan, H., Peng, Y., Shen, B., 2019. Can crystal morphology indicate different generations of dolomites? Evidence from magnesium isotopes. *Chem. Geol.* 516, 1–17.
- Nir, O., Vengosh, A., Harkness, J.S., Dwyer, G.S., Lahav, O., 2015. Direct measurement of the boron isotope fractionation factor: Reducing the uncertainty in reconstructing ocean paleo-pH. *Earth Planet. Sci. Lett.* 414, 1–5.
- Nogara, J., Zarrouk, S.J., 2018. Corrosion in geothermal environment: Part 1: Fluids and their impact. *Renew. Sust. Energ. Rev.* 82, 1333–1346.
- Nooitgedacht, C.W., van der Lubbe, H.J.L., de Graaf, S., Ziegler, M., Staudigel, P.T., Reijmer, J.J.G., 2021. Restricted internal oxygen isotope exchange in calcite veins: Constraints from fluid inclusion and clumped isotope-derived temperatures. *Geochim. Cosmochim. Acta* 297, 24–39.
- Oelkers, E.H., Gislason, S.R., 2010. Water-CO₂-rock interaction during carbon sequestration. *European Mineralogical Union, Notes in Mineralogy* 10, chapter 9 10, 325–344.
- Oelkers, E.H., Gislason, S.R., 2023. CARBON CAPTURE AND STORAGE: FROM GLOBAL CYCLES TO GLOBAL SOLUTIONS. *Geochemical Perspectives* 12, 179–349.
- Oelkers, E.H., Pogge von Strandmann, P.A.E., Mavromatis, V., 2019. The rapid resetting of the Ca isotopic signatures of calcite at ambient temperature during its congruent dissolution, precipitation, and at equilibrium. *Chem. Geol.* 512, 1–10.
- Oelkers E. H. and Schott J. (2009) Thermodynamics and kinetics of water-rock interaction. *Rev. Mineral. Geochem.* 70, 569pp.
- Okazaki, T., Kuramitz, H., Watanabe, T., Ueda, A., 2021. Scale sensor: Rapid monitoring of scale deposition and inhibition using fiber optics in a geothermal system and comparison with other monitoring devices. *Geothermics* 93, 102069.
- Okumura, M., Kitano, Y., 1986. Coprecipitation of alkali metal ions with calcium carbonate. *Geochim. Cosmochim. Acta* 50, 49–58.
- Okumura, M., Kitano, Y., Idogaki, M., 1986. Behavior of bromide ions during the formation of calcium carbonate. *Mar. Chem.* 19, 109–120.
- Olsen, E.K., Watkins, J.M., Devriendt, L.S., 2022. Oxygen isotopes of calcite precipitated at high ionic strength: CaCO₃-DIC fractionation and carbonic anhydride inhibition. *Geochim. Cosmochim. Acta* 325, 170–186.

- Onac, B.P., Cleary, D.M., Dumitru, O.A., Polyak, V.J., Povară, I., Wynn, J.G., Asmerom, Y., 2023. Cryogenic ridges: a new speleothem type. *Int. J. Speleol.* 52, 1–8.
- Onuk, P., Dietzel, M., Hauzenberger, C.A., 2014. Formation of helictite in the cave Dragon Belly (Sardinia, Italy)—microstructure and incorporation of Mg, Sr, and Ba. *Geochemistry* 74, 443–452.
- O'Neil, J.R., Clayton, R.N., Mayeda, T.K., 1969. Oxygen isotope fractionation in divalent metal carbonates. *J. Chem. Phys.* 51, 5547–5558.
- Oomori, T., Kaneshima, H., Maezato, Y., Kitano, Y., 1987. Distribution coefficient of Mg^{2+} ions between calcite and solution at 10–50°C. *Mar. Chem.* 20, 327–336.
- Oriols, N., Salvador, N., Pradell, T., Buti, S., 2020. Amorphous calcium carbonate (ACC) in fresco mural paintings. *Microchem. J.* 154.
- Oriols, N., Salvador, N., Pradell, T., Jiménez, N., Cotte, M., Gonzalez, V., Buti, S., 2022. Carbonation of fresco mural paintings with a dolomitic mortar. *Cem. Concr. Res.* 157, 106828.
- Osácar, M.C., Arenas, C., Auqué, L., Sancho, C., Pardo, G., Vázquez-Urbez, M., 2016. Discerning the interactions between environmental parameters reflected in $\delta^{13}\text{C}$ and $\delta^{18}\text{O}$ of recent fluvial tufas: Lessons from a Mediterranean climate region. *Sediment. Geol.* 345, 126–144.
- Oster, J.L., Ronay, E.R., Sharp, W.D., Breitenbach, S.F.M., Furbish, D.J., 2023. Controls on Speleothem Initial $^{234}\text{U}/^{238}\text{U}$ Ratios in a Monsoon Climate. *Geochem. Geophys. Geosyst.* 24, e2023GC010899.
- Ostermann, M., Sanders, D., Prager, C., Kramers, J., 2007. Aragonite and calcite cementation in “boulder-controlled” meteoric environments on the Fern Pass rockslide (Austria): implications for radiometric age dating of catastrophic mass movements. *Facies* 53, 189–208.
- O'Sullivan, E.M., Nägler, T.F., Turner, E.C., Kamber, B.S., Babechuk, M.G., O'Hare, S.P., 2022. Mo isotope composition of the 0.85 Ga ocean from coupled carbonate and shale archives: Some implications for pre-Cryogenian oxygenation. *Precambrian Res.* 378.
- Osvald, M., Maróti, G., Pap, B., Szanyi, J., 2017. Biofilm Forming Bacteria during Thermal Water ReInjection. *Geofluids* 2017, 7.
- Otero, J., Charol, A.E., Starinieri, V., 2019. Sticky rice-nanolime as a consolidation treatment for lime mortars. *J. Mater. Sci.* 54, 10217–10234.
- Ott, H., de Kloe, K., van Bakel, M., Vos, F., van Pelt, A., Legerstee, P., Bauer, A., Eide, K., van der Linden, A., Berg, S., Makurat, A., 2012. Core-flood experiment for transport of reactive fluids in rocks. *Rev. Sci. Instrum.* p. 83.
- Ott, H., Oedai, S., 2015. Wormhole formation and compact dissolution in single- and two-phase CO₂-brine injections. *Geophys. Res. Lett.* 42, 7.
- Owen, R.A., Day, C.C., Hu, C.Y., Liu, Y.H., Pointing, M.D., Blättler, C.L., Henderson, G. M., 2016. Calcium isotopes in caves as a proxy for aridity: Modern calibration and application to the 8.2 kyr event. *Earth Planet. Sci. Lett.* 443, 129–138.
- Özgür, N., Uzun, E., 2022. Hydrogeological Features of Geothermal Waters and Travertine Deposits in Pamukkale, Western Anatolia, Turkey. In: *Advances in Science, Technology and Innovation*, pp. 633–635.
- Ozjurt, N.N., Lutz, H.O., Hunjak, T., Mance, D., Roller-Lutz, Z., 2014. Characterization of the Gacka River basin karst aquifer (Croatia): Hydrochemistry, stable isotopes and tritium-based mean residence times. *Sci. Total Environ.* 487, 245–254.
- Paces, J.B., Ludwig, K.R., Peterman, Z.E., Neymark, L.A., 2002. $^{234}\text{U}/^{238}\text{U}$ evidence for local recharge and patterns of ground-water flow in the vicinity of Yucca Mountain, Nevada, USA. *Appl. Geochem.* 17, 751–779.
- Pagel, M., Bonifacie, M., Schneider, D.A., Gautheron, C., Brigaud, B., Calmels, D., Cros, A., Saint-Bezar, B., Landrein, P., Sutcliffe, C., Davis, D., Chaduteau, C., 2018. Improving paleohydrological and diagenetic reconstructions in calcite veins and breccia of a sedimentary basin by combining Δ_{47} temperature, $\delta^{18}\text{O}_{\text{water}}$ and U-Pb age. *Chem. Geol.* 481, 1–17.
- Palmer, M.R., Elderfield, H., 1985. Sr isotope composition of sea water over the past 75 Myr. *Nature* 314, 526–528.
- Paris, G., Fehrenbacher, J.S., Sessions, A.L., Spero, H.J., Adkins, J.F., 2014. Experimental determination of carbonate-associated sulfate $\delta^{34}\text{S}$ in planktonic foraminifera shells. *Geochem. Geophys. Geosyst.* 15, 1452–1461.
- Parkhurst, D. L. and Appelo, C. A. J. (2013) Description of input and examples for PHREEQC version 3—a computer program for speciation, batch-reaction, one-dimensional transport, and inverse geochemical calculations. *US Geol Surv Tech Methods* 6.
- Passchier, C., Sürmelihindı, G., Spötl, C., 2016b. A high-resolution palaeoenvironmental record from carbonate deposits in the Roman aqueduct of Patara, SW Turkey, from the time of Nero. *Sci. Rep.* 6, 28704.
- Passchier, C., Sürmelihindı, G., Spötl, C., Mertz-Kraus, R., Scholz, D., 2016a. Carbonate deposits from the ancient aqueduct of Béziers, France — A high-resolution palaeoenvironmental archive for the Roman Empire. *Palaeogeogr. Palaeoclimatol. Palaeoecol.* 461, 328–340.
- Passey, B.H., Ji, H., 2019. Triple oxygen isotope signatures of evaporation in lake waters and carbonates: A case study from the western United States. *Earth Planet. Sci. Lett.* 518, 1–12.
- Patel, A.S., Raudsepp, M.J., Wilson, S., Harrison, A.L., 2024. Water activity controls the stability of amorphous Ca-Mg- and Mg-carbonates. *Cryst. Growth Des.* 24, 2000–2013.
- Paulo, C., McKenzie, J.A., Raoof, B., Bollmann, J., Fulthorpe, R., Strohmenger, C.J., Dittrich, M., 2020. Organomineralization of Proto-Dolomite by a Phototrophic Microbial Mat Extracellular Polymeric Substances: Control of Crystal Size and Its Implication for Carbonate Depositional Systems. *Am. J. Sci.* 320, 72–95.
- Pauwels, J., Salah, S., Vasile, M., Laenen, B., Cappuyns, V., 2021. Characterization of scaling material obtained from the geothermal power plant of the Balmatt site. *Mol. Geothermics* 94, 102090.
- Pearson, A.R., Hartland, A., Frisia, S., Fox, B.R.S., 2020. Formation of calcite in the presence of dissolved organic matter: Partitioning, fabrics and fluorescence. *Chem. Geol.* 539, 119492.
- Peck, W.H., Keller, D., Arnold, V.S., McDonald, F., Kuentz, L.C., Nugent, P.M., 2023. Passive carbon sequestration associated with wollastonite mining, Adirondack Mountains, New York. *Am. Mineral.* 108, 1997–2003.
- Pederson, C., Mavromatis, V., Dietzel, M., Rollion-Bard, C., Nehrke, G., Jöns, N., Jochum, K.P., Immenhauser, A., 2019. Diagenesis of mollusc aragonite and the role of fluid reservoirs. *Earth Planet. Sci. Lett.* 514, 130–142.
- Pedley, M., 2014. The morphology and function of thrombolitic calcite precipitating biofilms: A universal model derived from freshwater mesocosm experiments. *Sedimentology* 61, 22–40.
- Peng, H., Liu, P., Zheng, H., Belshaw, N.S., Hu, S., Zhu, Z., 2023. Cadmium isotope fractionation during adsorption onto calcite. *Chem. Geol.* 620, 121341.
- Peral, M., Bassinot, F., Daerón, M., Blamart, D., Bonnin, J., Jorissen, F., Kissel, C., Michel, E., Waelbroeck, C., Rebaubin, H., Gray, W.R., 2022. On the combination of the planktonic foraminiferal Mg/Ca, clumped (Δ_{47}) and conventional ($\delta^{18}\text{O}$) stable isotope paleothermometers in palaeoceanographic studies. *Geochim. Cosmochim. Acta* 339, 22–34.
- Perry, E., Gysi, A.P., 2020. Hydrothermal calcite-fluid REE partitioning experiments at 200°C and saturated water vapor pressure. *Geochim. Cosmochim. Acta* 286, 177–197.
- Pertlik, F., 1986. Structures of hydrothermally synthesized cobalt(II) carbonate and nickel(II) carbonate. *Acta Crystallogr. C42*, 4–5.
- Petchey, F., Piper, P.J., Dabell, K., Brock, F., Turner, H., Lam, T.M.D., 2022. DATING THAC LAC: CRYPTIC CaCO_3 DIAGENESIS IN ARCHAEOLOGICAL FOOD SHELLS AND IMPLICATIONS FOR ^{14}C . *Radiocarbon* 64, 1093–1107.
- Petersen S. V., Defliese W. F., Saenger C., Daerón M., Huntington K. W., John C. M., Kelson J. R., Bernasconi S. M., Colman A. S., Kluge T., Olack G. A., Schauer A. J., Bajnai D., Bonifacie M., Breitenbach S. F. M., Fiebig J., Fernandez A. B., Henkes G. A., Hodell D., Katz A., Kele S., Lohmann K. C., Passey B. H., Peral M. Y., Petrizzi D. A., Rosenheim B. E., Tripathi A., Venturelli R., Young E. D. and Winkelstern I. Z. (2019) Effects of Improved ^{17}O Correction on Interlaboratory Agreement in Clumped Isotope Calibrations, Estimates of Mineral-Specific Offsets, and Temperature Dependence of Acid Digestion Fractionation. *Geochemistry, Geophysics, Geosystems* 20.
- Phillips, S.C., Hong, W.-L., Johnson, J.E., Fahnestock, M.F., Bryce, J.G., 2018. Authigenic carbonate formation influenced by freshwater inputs and methanogenesis in coal-bearing strata offshore Shimokita, Japan (IODP site C0020). *Mar. Pet. Geol.* 96, 288–303.
- Piazza, G., Bracchi, V.A., Langone, A., Meroni, A.N., Basso, D., 2022. Growth rate rather than temperature affects the B/Ca ratio in the calcareous red alga Lithothamnion coralliooides. *Biogeosciences* 19, 1047–1065.
- Picazo, S., Malvoisin, B., Baumgartner, L., Bouvier, A.S., 2020. Low temperature serpentinite replacement by carbonates during seawater influx in the Newfoundland margin. *Minerals* 10.
- Pimentel, C., Pina, C.M., Sainz-Díaz, C.I., 2022. New insights into dolomite and dolomite-analogue structures from first principles calculations. *ACS Earth Space Chemi.* 6, 2360–2367.
- Pina, C.M., Pimentel, C., Crespo, Á., 2020. Dolomite cation order in the geological record. *Chem. Geol.* 547, 119667.
- Pina, C.M., Pimentel, C., Crespo, Á., 2022. The Dolomite Problem: A Matter of Time. *ACS Earth and Space Chemistry* 6, 1468–1471.
- Pirajno, F., 2012. Hydrothermal mineral deposits: principles and fundamental concepts for the exploration geologist. Springer Science & Business Media.
- Pirajno, F., 2020. Subaerial hot springs and near-surface hydrothermal mineral systems past and present, and possible extraterrestrial analogues. *Geosci. Front.* 11, 1549–1569.
- Plummer, L.N., Busenberg, E., 1982. The solubilities of calcite, aragonite, and vaterite in CO₂-H₂O solutions between 0 and 90°C and an evaluation of the aqueous model for the system CaCO₃-CO₂-H₂O. *Geochim. Cosmochim. Acta* 46, 1011–1040.
- Plummer, L.N., Wigley, T.M.L., Parkhurst, D.L., 1978. Kinetics of Calcite Dissolution in CO₂-Water Systems at 5-Degrees-C to 60-Degrees-C and 0.0 to 1.0 Atm CO₂. *Am. J. Sci.* 278, 179–216.
- Popov, K.I., Kovaleva, N.E., Rudakova, G.Y., Kombarova, S.P., Larchenko, V.E., 2016. Recent state-of-the-art of biodegradable scale inhibitors for cooling-water treatment applications (Review). *Therm. Eng.* 63, 122–129.
- Power, I.M., Harrison, A.L., Dipple, G.M., Wilson, S.A., Kelemen, P.B., Hitch, M., Southam, G., 2013. Carbon mineralization: From natural analogues to engineered systems. *Rev. Mineral. Geochem.* 305–360.
- Prendergast, A.L., Pryor, A.J.E., Reade, H., Stevens, R.E., 2018. Seasonal records of palaeoenvironmental change and resource use from archaeological assemblages. *J. Archaeol. Sci. Rep.* 21, 1191–1197.
- Present, T.M., Adkins, J.F., Fischer, W.W., 2020. Variability in Sulfur Isotope Records of Phanerozoic Seawater Sulfate. *Geophys. Res. Lett.* 47.
- Present, T.M., Gutierrez, M., Paris, G., Kerans, C., Grotzinger, J.P., Adkins, J.F., 2019. Diagenetic controls on the isotopic composition of carbonate-associated sulphate in the Permian Capitan Reef Complex, West Texas. *Sedimentology* 66, 2605–2626.
- Present, T.M., Paris, G., Burke, A., Fischer, W.W., Adkins, J.F., 2015. Large Carbonate Associated Sulfate isotopic variability between brachiopods, micrite, and other sedimentary components in Late Ordovician strata. *Earth Planet. Sci. Lett.* 432, 187–198.
- Prieto M. (2011) Thermodynamics of ion partitioning in solid solution-aqueous solution systems. In: *Ion Partitioning in Ambient-Temperature Aqueous Systems* (eds. M. Prieto and H. Stoll). Mineralogical Society of Great Britain & Ireland. 10.

- Prieto, M., Cubillas, P., Fernández-González, Á., 2003. Uptake of dissolved Cd by biogenic and abiogenic aragonite: A comparison with sorption onto calcite. *Geochim. Cosmochim. Acta* 67, 3859–3869.
- Prieto, M., Heberling, F., Rodríguez-Galán, R.M., Brandt, F., 2016. Crystallization behavior of solid solutions from aqueous solutions: An environmental perspective. *Prog. Cryst. Growth Charact. Mater.* 62, 29–68.
- Prochaska, W., 2012. Siderite and magnesite mineralizations in Palaeozoic strata of the Eastern Alps (Austria). *Journal of Alpine Geology* 54, 309–322.
- Prokhorov, I., Kluge, T., Janssen, C., 2019. Laser absorption spectroscopy of rare and doubly substituted carbon dioxide isotopologues. *Anal. Chem.* 91, 15491–15499.
- Prud'homme, C., Lécuyer, C., Antoine, P., Hatté, C., Moine, O., Fourel, F., Amiot, R., Martineau, F., Rousseau, D.D., 2018. $\delta^{13}\text{C}$ signal of earthworm calcite granules: A new proxy for palaeoprecipitation reconstructions during the Last Glacial in western Europe. *Quat. Sci. Rev.* 179, 158–166.
- Pruess, K., 2006. Enhanced geothermal systems (EGS) using CO_2 as working fluid—A novel approach for generating renewable energy with simultaneous sequestration of carbon. *Geothermics* 35, 351–367.
- Purgstaller, B., Dietzel, M., Baldermann, A., Mavromatis, V., 2017b. Control of temperature and aqueous $\text{Mg}^{2+}/\text{Ca}^{2+}$ ratio on the (trans-)formation of ikaite. *Geochim. Cosmochim. Acta* 217, 128–143.
- Purgstaller, B., Goetschl, K.E., Mavromatis, V., Dietzel, M., 2019. Solubility investigations in the amorphous calcium magnesium carbonate system. *CrystEngComm* 21, 155–164.
- Purgstaller, B., Konrad, F., Dietzel, M., Immenhauser, A., Mavromatis, V., 2017a. Control of $\text{Mg}^{2+}/\text{Ca}^{2+}$ Activity Ratio on the Formation of Crystalline Carbonate Minerals via an Amorphous Precursor. *Crystal Growth and Design* 17, 1069–1078.
- Purgstaller, B., Mavromatis, V., Goetschl, K.E., Steindl, F.R., Dietzel, M., 2021. Effect of temperature on the transformation of amorphous calcium magnesium carbonate with near-dolomite stoichiometry into high Mg-calcite. *CrystEngComm* 23, 1969–1981.
- Purgstaller, B., Mavromatis, V., Immenhauser, A., Dietzel, M., 2016. Transformation of Mg-bearing amorphous calcium carbonate to Mg-calcite – In situ monitoring. *Geochim. Cosmochim. Acta* 174, 180–195.
- Putton, L.M.A., Shields, G.A., Brasier, M.D., Grime, G.W., 1999. Metabolism controls Sr/Ca ratios in fossil aragonitic mollusks. *GEOLOGY* 27, 1083–1086.
- Putnis A. (2003) Introduction to mineral sciences. *Introduction to mineral sciences*.
- Qi, C., Lin, J., Fu, L.H., Huang, P., 2018. Calcium-based biomaterials for diagnosis, treatment, and theranostics. *Chem. Soc. Rev.* 47, 357–403.
- Quandt, D., Micheuz, P., Kurz, W., Krenn, K., 2018. Microtextures and fluid inclusions from vein minerals hosted in the Pillow Lavas of the Troodos supra-subduction zone. *Lithosphere* 10, 566–578.
- Quandt, D., Micheuz, P., Kurz, W., Kluge, T., Boch, R., Hipppler, D., Krenn, K., Hauzenberger, C.A., 2019. Geochemistry of vein calcites hosted in the troodos pillow lavas and their implications for the timing and physicochemical environment of fracturing, fluid circulation, and vein mineral growth. *Geochim. Geophys. Geosyst.* 20, 5913–5938.
- Quesnel, B., Boulayais, P., Gautier, P., Cathelineau, M., John, C.M., Dierick, M., Agrinier, P., Drouillet, M., 2016. Paired stable isotopes (O, C) and clumped isotope thermometry of magnesite and silica veins in the New Caledonia Peridotite Nappe. *Geochim. Cosmochim. Acta* 183, 234–249.
- Railsback, L.B., 2018. A comparison of growth rate of late Holocene stalagmites with atmospheric precipitation and temperature, and its implications for paleoclimatology. *Quat. Sci. Rev.* 187, 94–111.
- Raiswell, R., Brimblecombe, P., 1977. The partition of manganese into aragonite between 30 and 60° C. *Chem. Geol.* 19, 145–151.
- Ram, S., Erez, J., 2021. The Distribution Coefficients of Major and Minor Elements in Coral Skeletons Under Variable Calcium Seawater Concentrations. *Frontiers. Earth Sci.* 9.
- Randolph, J.B., Saar, M.O., 2011. Combining geothermal energy capture with geologic carbon dioxide sequestration. *Geophys. Res. Lett.* 38, L10401.
- Rangel G., Pereira, V., Ponte, C., Thorhallsson, S. (2019) Raming calcite deposits of well PV8 while discharging: a successful operation at Ribeira Grande geothermal field, São Miguel Island, Azores. *European Geothermal Congress, Den Haag, The Netherlands, 11.-14. June.*
- Rashid, F., Hussein, D., Lawrence, J.A., Khanqa, P., 2020. Characterization and impact on reservoir quality of fractures in the Cretaceous Qamchuqa Formation, Zagros folded belt. *Mar. Pet. Geol.* 113, 104117.
- Rasool, M.H., Ahmad, M., 2023. Reactivity of basaltic minerals for CO_2 sequestration via in situ mineralization: a review. *Minerals* 13, 1154.
- Raudsepp, M.J., Wilson, S., Morgan, B., 2023. Making Salt from Water: The Unique Mineralogy of Alkaline Lakes. *Elements* 19, 22–29.
- Raudsepp, M.J., Wilson, S., Morgan, B., Patel, A., Johnston, S.G., Gagen, E.J., Fallon, S.J., 2022. Non-classical crystallization of very high magnesium calcite and magnesite in the Coorong Lakes, Australia. *Sedimentology* 69, 2246–2266.
- Raudsepp, M.J., Wilson, S., Zeyen, N., Arizaleta, M.L., Power, I.M., 2024. Magnesite everywhere: Formation of carbonates in the alkaline lakes and playas of the Cariboo Plateau, British Columbia, Canada. *Chemical Geology* 648, 121951.
- Raza, A., Gholami, R., Rabiei, M., Rasouli, V., Rezaee, R., Fakharl, N., 2019. Impact of geochemical and geomechanical changes on CO_2 sequestration potential in sandstone and limestone aquifers. *Greenhouse Gases: Science and Technology* 9, 905–923.
- Razum, I., Bajo, P., Brunović, D., Ilijanić, N., Hasan, O., Röhl, U., Miko, M.Š., Miko, S., 2021. Past climate variations recorded in needle-like aragonites correlate with organic carbon burial efficiency as revealed by lake sediments in Croatia. *Sci. Rep.* 11, 7568.
- Reeder, R.J., 1990. Carbonates: mineralogy and chemistry. *Rev. Mineral.* 11, 399 pp.
- Reeder, R.J., Nugent, M., Lamble, G.M., Tait, C.D., Morris, D.E., 2000. Uranyl Incorporation into Calcite and Aragonite: XAFS and Luminescence Studies. *Environ. Sci. Technol.* 34, 638–644.
- Refsnider, K.A., Miller, G.H., Hillaire-Marcel, C., Fogel, M.L., Ghaleb, B., Bowden, R., 2012. Subglacial carbonates constrain basal conditions and oxygen isotopic composition of the Laurentide Ice Sheet over Arctic Canada. *Geology* 40, 135–138.
- Regattieri, E., Zanchetta, G., Isola, I., Zanella, E., Drysdale, R.N., Hellstrom, J.C., Zerbini, A., Dallai, L., Tema, E., Lanci, L., Costa, E., Magri, F., 2019. Holocene Critical Zone dynamics in an Alpine catchment inferred from a speleothem multiproxy record: disentangling climate and human influences. *Sci. Rep.* 9, 17829.
- Regenspurg, S., Alawi, M., Norden, B., Vieth-Hillebrand, A., Blöcher, G., Kranz, S., Scheit, T., Horn, F., Burckhardt, O., Rach, O., Saadat, A., 2020. Effect of cold and hot water injection on the chemical and microbial composition of an aquifer and implication for its use as an aquifer thermal energy storage. *Geothermics* 84, 101747.
- Remmelzwaal, S.R.C., Sadekov, A.Y., Parkinson, I.J., Schmidt, D.N., Titelboim, D., Abramovich, S., Roepert, A., Kienhuis, M., Polerecky, L., Goring-Harford, H., Kimoto, K., Allen, K.A., Holland, K., Stewart, J.A., Middelburg, J.J., 2019. Post-depositional overprinting of chromium in foraminifera. *Earth Planet. Sci. Lett.* 515, 100–111.
- Renard, F., Røyne, A., Putnis, C.V., 2019. Timescales of interface-coupled dissolution-precipitation reactions on carbonates. *Geosci. Front.* 10, 17–27.
- Rennie, V.C.F., Turchyn, A.V., 2014. The preservation of $\delta^{34}\text{S}_{\text{SO}_4}$ and $\delta^{18}\text{O}_{\text{SO}_4}$ in carbonate-associated sulfate during marine diagenesis: A 25 Myr test case using marine sediments. *Earth Planet. Sci. Lett.* 395, 13–23.
- Rezaei, M., Gabitov, R., Sadekov, A., Perez-Huerta, A., Borrelli, C., Stiles, A., 2024. Elemental Uptake by Different Calcite Crystal Faces: An In Situ Study. *Crystals* 14, 442.
- Richardson, J.A., Lepland, A., Hints, O., Prave, A.R., Gilhooly, W.P., Bradley, A.S., Fike, D.A., 2021. Effects of early marine diagenesis and site-specific depositional controls on carbonate-associated sulfate: Insights from paired S and O isotopic analyses. *Chem. Geol.* 584.
- Richardson, J.A., Newville, M., Lanzirotti, A., Webb, S.M., Rose, C.V., Catalano, J.G., Fike, D.A., 2019. The source of sulfate in brachiopod calcite: Insights from μ -XRF imaging and XANES spectroscopy. *Chem. Geol.* 529.
- Riding, R., 2000. Microbial carbonates: the geological record of calcified bacterial-algal mats and biofilms. *Sedimentology* 47, 179–214.
- Riechelmann, S., Mavromatis, V., Buhl, D., Dietzel, M., Hoffmann, R., Jöns, N., Kell-Duivestein, I., Immenhauser, A., 2018. Echinoid skeletal carbonate as archive of past seawater magnesium isotope signatures – Potential and limitations. *Geochim. Cosmochim. Acta* 235, 333–359.
- Riechelmann, S., Mavromatis, V., Buhl, D., Dietzel, M., Immenhauser, A., 2020. Controls on formation and alteration of early diagenetic dolomite: a multi-proxy $\delta^{44/40}\text{Ca}$, $\delta^{26}\text{Mg}$, $\delta^{18}\text{O}$ and $\delta^{13}\text{C}$ approach. *Geochim. Cosmochim. Acta* 283, 167–183.
- Riechers, S.L., Ilton, E.S., Qafoku, O., Du, Y., Kerisit, S.N., 2022. Cobalt hydroxide–cobalt carbonate competitive growth on carbonate surfaces. *Chem. Geol.* 605, 120951.
- Rieder, M., Wegner, W., Horschinegg, M., Klackl, S., Preto, N., Breda, A., Gier, S., Klötzli, U., Bernasconi, S.M., Arp, G., Meister, P., 2019. Precipitation of dolomite from seawater in a Carnian coastal plain (Dolomites, northern Italy): Evidence from carbonate petrography and Sr isotopes. *Solid Earth* 10, 1243–1267.
- Rimstidt, J.D., Balog, A., Webb, J., 1998. Distribution of trace elements between carbonate minerals and aqueous solutions. *Geochim. Cosmochim. Acta* 62, 1851–1863.
- Rinder, T., Dietzel, M., Leis, A., 2013. Calcium carbonate scaling under alkaline conditions - Case studies and hydrochemical modelling. *Appl. Geochem.* 35, 132–141.
- Riotte, J., Chabaux, F., 1999. $(^{234}\text{U})/(^{238}\text{U})$ activity ratios in freshwaters as tracers of hydrological processes: the Strengbach watershed (Vosges, France). *Geochim. Cosmochim. Acta* 63, 1263–1275.
- Ripken, M., Gallien, F., Schlotterbach, T., Lengauer, C.L., 2018. Structural and physicochemical characterization of basic calcium carbonate (BCC), $\text{Ca}_3(\text{CO}_3)_2(\text{OH})_2\text{H}_2\text{O}$. *Eur. J. Mineral.* 30, 85–96.
- Ripperdan R. L. (2001) Stratigraphic variation in marine carbonate carbon isotope ratios, in: J. W. Valley and D. R. C. Cole (Eds.), *Reviews of Mineralogy and Geochemistry*, pp. 637–662.
- Ritter, S.M., Schröter, M.I., Schröder-Ritzrau, A., Scholz, C., Frank, N., 2017. Geochemical Insights Into an Active Calcareous Tufa Depositing System in Southern Germany. *Procedia Earth and Planetary Science* 17, 328–331.
- Robles-Fernández, A., Areias, C., Daffonchio, D., Vahrenkamp, V.C., Sánchez-Román, M., 2022. The Role of Microorganisms in the Nucleation of Carbonates. *Environmental Implications and Applications. Minerals* 12, 1562.
- Rodler, A., Sánchez-Pastor, N., Fernández-Díaz, L., Frei, R., 2015. Fractionation behavior of chromium isotopes during coprecipitation with calcium carbonate: Implications for their use as paleoclimatic proxy. *Geochim. Cosmochim. Acta* 164, 221–235.
- Rodriguez-Blanco, J.D., Shaw, S., Benning, L.G., 2015. A route for the direct crystallization of dolomite. *Am. Mineral.* 100, 1172–1181.
- Rodriguez-Navarro, C., Benning, L.G., 2013. Control of Crystal Nucleation and Growth by Additives. *Elements* 9, 203–209.
- Rodriguez-Navarro, C., Ilić, T., Ruiz-Agudo, E., Elert, K., 2023. Carbonation mechanisms and kinetics of lime-based binders: An overview. *Cem. Concr. Res.* 173, 107301.
- Roepert, A., Polerecky, L., Geerken, E., Reichart, G.J., Middelburg, J.J., 2020. Distribution of chlorine and fluorine in benthic foraminifera. *Biogeosciences* 17, 4727–4743.
- Rogerson, M., Pedley, H.M., Wadhawan, J.D., Middleton, R., 2008. New insights into biological influence on the geochemistry of freshwater carbonate deposits. *Geochim. Cosmochim. Acta* 72, 4976–4987.

- Rogov, M., Ershova, V., Gaina, C., Vereshchagin, O., Vasileva, K., Mikhailova, K., Krylov, A., 2023. Glendonites throughout the Phanerozoic. *Earth Sci. Rev.* 241, 104430.
- Rollion-Bard, C., Blamart, D., Trebosc, J., Tricot, G., Mussi, A., Cuif, J.-P., 2011. Boron isotopes as pH proxy: A new look at boron speciation in deep-sea corals using ^{11}B MAS NMR and EELS. *Geochim. Cosmochim. Acta* 75, 1003–1012.
- Romanillo, S.J., Herrmann, A.D., Anbar, A.D., 2016. Syndepositional diagenetic control of molybdenum isotope variations in carbonate sediments from the Bahamas. *Chem. Geol.* 438, 84–90.
- Rosenheim, B.E., Swart, P.K., Thorrold, S.R., Willenz, P., Berry, L., Latkoczy, C., 2004. High-resolution Sr/Ca records in sclerosponges calibrated to temperature in situ. *Geology* 32, 145–148.
- Rosewitz, J.A., Wang, S., Scarlata, S.F., Rahbar, N., 2021. An enzymatic self-healing cementitious material. *Appl. Mater. Today* 23, 101035.
- Rovan, L., Zuliani, T., Horvat, B., Kanduč, T., Vreća, P., Jamil, Q., Čermelj, B., Buranakić, E., Cukrov, N., Strok, M., Lojen, S., 2021. Uranium isotopes as a possible tracer of terrestrial authigenic carbonates. *Sci. Total Environ.* 797, 149103.
- Roza-Llera, A., Di Lorenzo, F., Churakov, S.V., Jiménez, A., Fernández-Díaz, L., 2024. Pb removal efficiency by calcium carbonates: biogenic versus abiogenic materials. *Cryst. Growth Des.* 24, 79–92.
- Ruiz-Hernandez, S.E., Grau-Crespo, R., Ruiz-Salvador, A.R., De Leeuw, N.H., 2010. Thermochemistry of strontium incorporation in aragonite from atomistic simulations. *Geochim. Cosmochim. Acta* 74, 1320–1328.
- Rutledge, R.L., Gilleadeau, G.J., Remírez, M.N., Kaufman, A.J., Lyons, T.W., Bates, S., Algeo, T.J., 2024. Productivity and organic carbon loading control uranium isotope behavior in ancient reducing settings: implications for the paleoredox proxy. *Geochim. Cosmochim. Acta* 368, 197–213.
- Ryan, B.H., Kaczmarek, S.E., Rivers, J.M., 2020. Early and pervasive dolomitization by near-normal marine fluids: New lessons from an Eocene evaporative setting in Qatar. *Sedimentology* 67, 2917–2944.
- Ryb, U., Lloyd, M.K., Stolper, D.A., Eiler, J.M., 2017. The clumped-isotope geochemistry of exhumed marbles from Naxos, Greece. *Earth Planet. Sci. Lett.* 470, 1–12.
- Sade, Z., Hegyi, S., Halevy, I., 2022a. Equilibration Times of Dissolved Inorganic Carbon During pH Transitions. *Frontiers. Earth Sci.* 9.
- Sade, Z., Hegyi, S., Hansen, M., Scholz, D., Halevy, I., 2022b. The effects of drip rate and geometry on the isotopic composition of speleothems: Evaluation with an advection-diffusion-reaction model. *Geochim. Cosmochim. Acta* 317, 409–432.
- Saenger, C., Wang, Z., 2014. Magnesium isotope fractionation in biogenic and abiogenic carbonates: implications for paleoenvironmental proxies. *Quat. Sci. Rev.* 90, 1–21.
- Sakoparnig, M., Galan, I., Steindl, F.R., Kusterle, W., Juhart, J., Grengg, C., Briendl, L., Sacher, A., Thumann, M., Mittermayr, F., 2021. Durability of clinker reduced shotcrete: Ca^{2+} leaching, sintering, carbonation and chloride penetration. *Materials and Structures/Materiaux et Constructions* 54.
- Sanna, A., Uibu, M., Caramanna, G., Kuusik, R., Maroto-Valer, M.M., 2014. A review of mineral carbonation technologies to sequester CO_2 . *Chem. Soc. Rev.* 43, 8049–8080.
- Sanni, O.S., Bukuaghangin, O., Charpentier, T.V.J., Neville, A., 2019. Evaluation of laboratory techniques for assessing scale inhibition efficiency. *J. Pet. Sci. Eng.* 182, 106347.
- Santos, H.S., Nguyen, H., Venâncio, F., Ramteke, D., Zevenhoven, R., Kinnunen, P., 2023. Mechanisms of Mg carbonates precipitation and implications for CO_2 capture and utilization/storage. *Inorganic Chemistry Frontiers* 10, 2507–2546.
- Saraswati, P.K., 2024. Geochemical Proxies. In: Saraswati, P.K. (Ed.), *Larger Benthic Foraminifera Through Space and Time*. Springer Nature Switzerland, Cham, pp. 125–146.
- Saslow, S.A., Kerisit, S.N., Varga, T., Johnson, K.C., Avalos, N.M., Lawter, A.R., Qafoku, N.P., 2019. Chromate Effect on Iodate Incorporation into Calcite. *ACS Earth and Space Chemistry* 3, 1624–1630.
- Saunders, P., Rogerson, M., Wadhawan, J.D., Greenway, G., Pedley, H.M., 2014. Mg/Ca ratios in freshwater microbial carbonates: Thermodynamic, kinetic and vital effects. *Geochim. Cosmochim. Acta* 147, 107–118.
- Saunder, G., Pokrovski, G.S., Poitrasson, F., 2011. First experimental determination of iron isotope fractionation between hematite and aqueous solution at hydrothermal conditions. *Geochim. Cosmochim. Acta* 75, 6629–6654.
- Savard, M.M., Jautzy, J.J., Lavioie, D., Dhillon, R.S., Defliese, W.F., 2021. Clumped and oxygen isotopes reveal differential disequilibrium in the formation of carbonates from marine methane seeps. *Geochim. Cosmochim. Acta* 298, 43–54.
- Sawada, K., 1997. The mechanisms of crystallization and transformation of calcium carbonates. *Pure Appl. Chem.* 69, 921–928.
- Schäffer, R., Götz, E., Schlatter, N., Schubert, G., Weinert, S., Schmidt, S., Kolb, U., Sasse, I., 2022. Fluid–rock interactions in geothermal reservoirs, Germany: thermal autoclave experiments using sandstones and natural hydrothermal brines. *Aquat. Geochim.* 28 (2), 63–110.
- Schauble, E.A., Ghosh, P., Eiler, J.M., 2006. Preferential formation of ^{13}C – ^{18}O bonds in carbonate minerals, estimated using first-principles lattice dynamics. *Geochim. Cosmochim. Acta* 70, 2510–2529.
- Scheller, E.L., Ingalls, M., Eiler, J.M., Grotzinger, J.P., Ryb, U., 2023. The mechanisms and stable isotope effects of transforming hydrated carbonate into calcite pseudomorphs. *Geochim. Cosmochim. Acta* 354, 146–164.
- Schlager, W., 2005. Carbonate Sedimentology and Sequence. Stratigraphy no. 8. viii, 200. *SEPM Concepts in Sedimentology and Paleontology Series Series*.
- Schlidt V., Evans D. and S. V. (2023) The fractionation of Li isotopes into amorphous calcium magnesium carbonate (ACMC) and during its transformation into calcite, Goldschmidt Conference.
- Schmidt, C.A., Tambutté, E., Venn, A.A., Zou, Z., Castillo, Alvarez C., Devriendt, L.S., Bechtel, H.A., Stifler, C.A., Anglemeyer, S., Breit, C.P., Foust, C.L., Hopanchuk, A., Klaus, C.N., Kohler, I.J., LeCloud, I.M., Mezera, J., Patton, M.R., Purisch, A., Quach, V., Sengkhammee, J.S., Sristy, T., Vattem, S., Walch, E.J., Albéric, M., Politi, Y., Fratzl, P., Tambutté, S., Gilbert, P.U.P.A., 2024. Myriad Mapping of nanoscale minerals reveals calcium carbonate hemihydrate in forming nacre and coral biominerals. *Nat. Commun.* 15, 1812.
- Schneider, A., Crémère, A., Panieri, G., Lepland, A., Knies, J., 2017. Diagenetic alteration of benthic foraminifera from a methane seep site on Vestnesa Ridge (NW Svalbard). *Deep-Sea Res. I Oceanogr. Res. Pap.* 123, 22–34.
- Schölderle, F., Lipus, M., Pfarrang, D., Reinsch, T., Haberer, S., Einsiedl, F., Zosseder, K., 2021. Monitoring cold water injections for reservoir characterization using a permanent fiber optic installation in a geothermal production well in the Southern German Molasse Basin. *Geotherm. Energy* 9, 21.
- Scholle, P.A., Bedout, D.G., Moore, C.H., 1983. Carbonate depositional environments. *Am. Assoc. Pet. Geol. Mem.* 33, 1983, 708 pp.
- Scholz, D., Tolzmann, J., Hoffmann, D.L., Jochum, K.P., Spötl, C., Riechelmann, D.F.C., 2014. Diagenesis of speleothems and its effect on the accuracy of $^{230}\text{Th}/\text{U}$ -ages. *Chem. Geol.* 387, 74–86.
- Schöne, B.R., Marali, S., Jantschke, A., Mertz-Kraus, R., Butler, P.G., Fröhlich, L., 2023. Can element chemical impurities in aragonitic shells of marine bivalves serve as proxies for environmental variability? *Chem. Geol.* 616, 121215.
- Schroder, P., Silverstein, M., DiGregorio, D., Blättler, C.L., Loyd, S., Bradbury, H.J., Edwards, R.L., Marlow, J., 2024. Carbonate chimneys at the highly productive point Dume methane seep: Fine-scale mineralogical, geochemical, and microbiological heterogeneity reflects dynamic and long-lived methane-metabolizing habitats. *Geobiology* 22, e12608.
- Schultz, B., Thibault, N., Huggett, J., 2022. The minerals ikaite and its pseudomorph glendonite: Historical perspective and legacies of Douglas Shearman and Alec K. Smith. *Proceedings of the Geologists' Association* 133, 176–192.
- Seaton, N.C.A., Whitney, D.L., Teysier, C., Toraman, E., Heizler, M.T., 2009. Recrystallization of high-pressure marble (Sivrihisar, Turkey). *Tectonophysics* 479, 241–253.
- Segovia-Campos, I., Martignier, A., Filella, M., Jaquet, J.-M., Ariztegui, D., 2022. Micropearls and other intracellular inclusions of amorphous calcium carbonate: an unsuspected biomineralization capacity shared by diverse microorganisms. *Environ. Microbiol.* 24, 537–550.
- Sevilgen, D.S., Venn, A.A., Hu, M.Y., Tambutté, E., de Beer, D., Planas-Bielsa, V., Tambutté, S., 2019. Full *in vivo* characterization of carbonate chemistry at the site of calcification in corals. *Sci. Adv.* 5, eaau7447.
- Seyedali, M., Coogan, L.A., Gillis, K.M., 2021. The effect of solution chemistry on elemental and isotopic fractionation of lithium during inorganic precipitation of calcite. *Geochim. Cosmochim. Acta* 311, 102–118.
- Sha, L., Mahata, S., Duan, P., Luz, B., Zhang, P., Baker, J., Zong, B., Ning, Y., Brahim, Y., A., Zhang, H., Edwards, R.L., Cheng, H., 2020. A novel application of triple oxygen isotope ratios of speleothems. *Geochim. Cosmochim. Acta* 270, 360–378.
- Shaked, H., Polishchuk, I., Nagel, A., Bekenstein, Y., Pokroy, B., 2021. Long-term stabilized amorphous calcium carbonate—an ink for bio-inspired 3D printing. *Mater. Today Bio.* 11, 100120.
- Shalev, N., Bontognali, T.R.R., Vance, D., 2020. Sabkha dolomite as an archive for the magnesium isotope composition of seawater. *Geology* 49, 253–257.
- Shalev, N., Bontognali, T.R.R., Wheat, C.G., Vance, D., 2019. New isotope constraints on the Mg oceanic budget point to cryptic modern dolomite formation. *Nat. Commun.* 10, 5646.
- Shan, D., Zhu, M., Han, E., Xue, H., Cosnier, S., 2007. Calcium carbonate nanoparticles: A host matrix for the construction of highly sensitive amperometric phenol biosensor. *Biosens. Bioelectron.* 23, 648–654.
- Shang, L.-M., Jiang, J., Yu, S.-H., 2021. Formation of magnesium calcite mesocrystals in the inorganic environment only by using Ca^{2+} and Mg^{2+} and its biological implications. *Science China Materials* 64, 999–1006.
- Shao, M., Zhang, S., Pei, Y., Song, S., Lei, T., Yun, H., 2023. Soil texture and microorganisms dominantly determine the subsoil carbonate content in the permafrost-affected area of the Tibetan Plateau. *Front. Microbiol.* 14.
- Shao, Y., Farkas, J., Mosley, L., Tyler, J., Wong, H., Chamberlayne, B., Raven, M., Samanta, M., Holmden, C., Gillanders, B.M., Kolevica, A., Eisenhauer, A., 2021. Impact of salinity and carbonate saturation on stable Sr isotopes ($^{88}\text{Sr}/^{86}\text{Sr}$) in a lagoon-estuarine system. *Geochim. Cosmochim. Acta* 293, 461–476.
- Shen, C.-C., Wu, C.-C., Cheng, H., Lawrence, Edwards R., Hsieh, Y.-T., Gallet, S., Chang, C.-C., Li, T.-Y., Lam, D.D., Kano, A., Hori, M., Spötl, C., 2012. High-precision and high-resolution carbonate ^{230}Th dating by MC-ICP-MS with SEM protocols. *Geochim. Cosmochim. Acta* 99, 71–86.
- Shen, J., Smith, A.C., Barnett, M.J., Morgan, A., Wynn, P.M., 2022. Distinct Microbial Communities in the Soils, Waters, and Speleothems of a Hyperalkaline Cave System. *Journal of Geophysical Research: Biogeosciences* 127 e2022JG006866.
- Shenton, B.J., Grossman, E.L., Passey, B.H., Henkes, G.A., Becker, T.P., Lay, J.C., Perez-Huerta, A., Becker, S.P., Lawson, M., 2015. Clumped isotope thermometry in deeply buried sedimentary carbonates: The effects of bond reordering and recrystallization. *GSA Bull.* 127, 1036–1051.
- Shiraishi, F., Enø, Y., Nakamura, Y., Hanzawa, Y., Asada, J., Bahniuk, A.M., 2019. Relative influence of biotic and abiotic processes on travertine fabrics, Satono-yu hot spring, Japan. *Sedimentology* 66, 459–479.
- Shu, S., Chen, H., Meng, H., 2022. Modelling Microbially Induced Carbonate Precipitation (MICP) in Microfluidic Porous Chips. *Geofluids* 2022, 3616473.
- Shuai, Y., Xie, H., Zhang, S., Zhang, Y., Eiler, J.M., 2021. Recognizing the pathways of microbial methanogenesis through methane isotopologues in the subsurface biosphere. *Earth Planet. Sci. Lett.* 566, 116960.
- Sierralta, M., Kele, S., Melcher, F., Hambach, U., Reinders, J., van Geldern, R., Frechen, M., 2010. Uranium-series dating of travertine from Sütő: Implications for reconstruction of environmental change in Hungary. *Quat. Int.* 222, 178–193.

- Silantyev, S.A., Krasnova, E.A., Badyukov, D.D., Zhilkina, A.V., Kuzmina, T.G., Gryaznova, A.S., Shcherbakov, V.D., 2022. Carbonation of Serpentinites of the Mid-Atlantic Ridge: 1. Geochemical Trends and Mineral Assemblages. *Petrology* 30, S25–S52.
- Siman-Tov, S., Affek, H.P., Matthews, A., Aharonov, E., Reches, Z., e., 2016. Shear heating and clumped isotope reordering in carbonate faults. *Earth Planet. Sci. Lett.* 445, 136–145.
- Simonet, Roda M., Griesshaber, E., Ziegler, A., Rupp, U., Yin, X., Henkel, D., Häussermann, V., Laudien, J., Brand, U., Eisenhauer, A., Checa, A.G., Schmahl, W. W., 2019. Calcite fibre formation in modern brachiopod shells. *Sci. Rep.* 9, 598.
- Simoni, M., Hanein, T., Woo, C.L., Tyner, M., Nyberg, M., Martinez, J.-C., Quintero-Mora, N.I., Provost, J.L., Kinoshita, H., 2022. Decarbonisation of calcium carbonate in sodium hydroxide solutions under ambient conditions: effect of residence time and mixing rates. *Phys. Chem. Chem. Phys.* 24, 16125–16138.
- Smith, M.E., Moore, E.W., Swart, P.K., 2022. Constraining diagenesis within shallow water carbonate environments: Insights from clumped and sulfur isotopes. *Chem. Geol.* 614, 121183.
- Smrzka, D., Zwicker, J., Lu, Y., Sun, Y., Feng, D., Monien, P., Bohrmann, G., Peckmann, J., 2021. Trace element distribution in methane-seep carbonates: The role of mineralogy and dissolved sulfide. *Chem. Geol.* 580, 120357.
- Soete, J., Kleipool, L.M., Claes, H., Claes, S., Hamaekers, H., Kele, S., Özkul, M., Foubert, A., Reijmer, J.J.G., Swennen, R., 2015. Acoustic properties in travertines and their relation to porosity and pore types. *Mar. Pet. Geol.* 59, 320–335.
- Šolcová, A., Petr, L., Hájková, P., Petřík, J., Tóth, P., Rohovec, J., BÁTORA, J., Horská, M., 2018. Early and middle Holocene ecosystem changes at the Western Carpathian/Pannonian border driven by climate and Neolithic impact. *Boreas* 47, 897–909.
- Son, S., Li, W., Lee, J.Y., Kwon, K.D., 2020. On the coordination of Mg²⁺ in aragonite: Ab-initio absorption spectroscopy and isotope fractionation study. *Geochim. Cosmochim. Acta* 286, 324–335.
- Souchez, R.A., Lemmens, M., 1985. Subglacial carbonate deposition: An isotopic study of a present-day case. *Palaeogeogr. Palaeoclimatol. Palaeoecol.* 51, 357–364.
- Speer A. (1983) Chapter 5. CRYSTAL CHEMISTRY and PHASE RELATIONS of ORTHORHOMBIC CARBONATES. In *Carbonates* (ed. J. R. Richard). De Gruyter, Berlin, Boston. pp. 145–190.
- Spinthaki, A., Kamaratou, M., Skordalou, G., Petros, G., Petrou, I., Tramaux, A., David, G., Demadis, K.D., 2021. Searching for a universal scale inhibitor: A multi-scale approach towards inhibitor efficiency. *Geothermics* 89, 101954.
- Spötl, C., Baker, J.L., Skiba, V., Honiat, A., Fohlmeister, J., Luetscher, M., Trüssel, M., 2024. Speleothems in subglacial caves: An emerging archive of glacial climate history and mountain glacier dynamics. *Quat. Sci. Rev.* 333, 108684.
- Spötl C., Boch, R. (2019) Uranium series dating of speleothems. In Encyclopedia of Caves (ed. W. White, Culver, D., Pipan, T.). Elsevier. pp. 1096–1102.
- Spötl, C., Koltai, G., Dublyansky, Y., 2023. Mode of formation of cryogenic cave carbonates: Experimental evidence from an Alpine ice cave. *Chem. Geol.* 638.
- Staudigel, P., Davies, A.J., Bernecker, M., Tagliavento, M., van der Lubbe, H.J.L., Nootgedacht, G., Loos, N., Bernasconi, S.M., Vonhof, H., Fiebig, J., 2023. Fingerprinting Kinetic Isotope Effects and Diagenetic Exchange Reactions Using Fluid Inclusion and Dual-Clumped Isotope Analysis. *Geochim. Geophys. Geosyst.* 24, e2022GC010766.
- Staudigel P., Feng D., Peckmann J., Bernecker M., Davies A., Tagliavento M. and Fiebig J. (2024) Resolving and correcting for kinetic biases on methane seep paleotemperature using carbonate Δ_{47}/Δ_{48} analysis. *Science Advances* 10, eadn0155.
- Steßansson, A., Arnórsson, S., Sveinbjörnsdóttir, Á.E., Heinemaier, J., Kristmannsdóttir, H., 2019. Isotope ($\delta^{18}\text{O}$, $\delta^{13}\text{C}$, $\delta^{14}\text{C}$) and chemical (B, Cl) Constraints on water origin, mixing, water-rock interaction and age of low-temperature geothermal water. *Appl. Geochem.* 108, 104380.
- Stipp, S.L., Hochella, M.F., Parks, G.A., Leckie, J.O., 1992. Cd²⁺ uptake by calcite, solid-state diffusion, and the formation of solid-solution: Interface processes observed with near-surface sensitive techniques (XPS, LEED, and AES). *Geochim. Cosmochim. Acta* 56, 1941–1954.
- Stipp, S.L.S., Parks, G.A., Nordstrom, D.K., Leckie, J.O., 1993. Solubility-product constant and thermodynamic properties for synthetic otavite, CdCO_{3(s)}, and aqueous association constants for the Cd(II)-CO₂-H₂O system. *Geochim. Cosmochim. Acta* 57, 2699–2713.
- Stirling, C.H., Andersen, M.B., 2009. Uranium-series dating of fossil coral reefs: Extending the sea-level record beyond the last glacial cycle. *Earth Planet. Sci. Lett.* 284, 269–283.
- Stoll, H.M., Rosenthal, Y., Falkowski, P., 2002. Climate proxies from Sr/Ca of coccolith calcite: Calibrations from continuous culture of *Emiliania huxleyi*. *Geochim. Cosmochim. Acta* 66, 927–936.
- Stolper, D.A., Lawson, M., Davis, C.L., Ferreira, A.A., Neto, E.V.S., Ellis, G.S., Lewan, M. D., Martini, A.M., Tang, Y., Schoell, M., Sessions, A.L., Eiler, J.M., 2014. Formation temperatures of thermogenic and biogenetic methane. *Science* 344, 1500–1503.
- Strohm, S.B., Inckemann, S.E., Gao, K., Schweikert, M., Lemloh, M.L., Schmahl, W.W., Jordan, G., 2022. On the nucleation of ikaite (CaCO₃·6H₂O) – A comparative study in the presence and absence of mineral surfaces. *Chem. Geol.* 611.
- Strohm, S.B., Saldi, G.D., Mavromatis, V., Schmahl, W.W., Jordan, G., 2023. A study on ikaite growth in the presence of phosphate. *Aquat. Geochem.* 29, 219–233.
- Stumm, W., Morgan, J.J., 1996. Aquatic Chemistry - Chemical Equilibria and Rates in Natural Waters, 3rd Edition. John Wiley & Sons, Inc., New York.
- Su, Z., Deng, Z., Wang, Y., Ji, C., Li, F., Yang, G., Huang, L., 2023. Effects of the Sr/Ca ratio on the bioremediation of strontium based on microbially-induced carbonate precipitation. *Journal of Environmental Chemical Engineering* 11, 108990.
- Sun, Z., Gong, C., Ren, J., Zhang, X., Wang, G., Liu, Y., Ren, Y., Zhao, Y., Yu, Q., Wang, Y., Hou, J., 2020. Toxicity of nickel and cobalt in Japanese flounder. *Environ. Pollut.* 263, 114516.
- Sürmelihindi, G., Passchier, C., 2024. Writ in water—unwritten histories obtained from carbonate deposits in ancient water systems. *Geoarchaeology* 39, 63–88.
- Sürmelihindi, G., Passchier, C., 2024. Writ in water—Unwritten histories obtained from carbonate deposits in ancient water systems. *Geoarchaeology* 39, 63–88.
- Sürmelihindi, G., Passchier, C.W., Rigal, D., Wilson, A., Spötl, C., 2023. Roman aqueduct maintenance in the water supply system of Divona, France. *Scientific Reports*, p. 13.
- Sürmelihindi, G., Passchier, C.W., Spötl, C., Kessener, P., Bestmann, M., Jacob, D.E., Baykan, O.N., 2013. Laminated carbonate deposits in Roman aqueducts: Origin, processes and implications. *Sedimentology* 60, 961–982.
- Swanson, E.M., Wernicke, B.P., Eiler, J.M., Losh, S., 2012. Temperatures and fluids on faults based on carbonate clumped-isotope thermometry. *Am. J. Sci.* 312, 1–21.
- Swart, P.K., 2015. The geochemistry of carbonate diagenesis: The past, present and future. *Sedimentology* 62, 1233–1304.
- Swart, P.K., Eberli, G.P., McKenzie, J.A., 2012. Perspectives in carbonate geology: a tribute to the career of Robert Nathan Ginsburg. *John Wiley & Sons*.
- Sverson, D.D., Pester, N.J., Craddock, P.R., Seyfried Jr., W.E., 2014. Fe isotope fractionation during phase separation in the NaCl-H₂O system: An experimental study with implications for seafloor hydrothermal vents. *Earth Planet. Sci. Lett.* 406, 223–232.
- Szanyi, J., Nádor, A., Madarász, T., 2021. 150 years of geothermal energy research and utilization in Hungary. *Foldtan Kozlony* 151, 79–102.
- Tada, R., Siever, R., 1989. Pressure solution during diagenesis. *Annu. Rev. Earth Planet. Sci.* 17, 89–118.
- Tagliavento M., Davies A. J., Bernecker M., Staudigel P. T., Dawson R. R., Dietzel M., Goetschl K., Guo W., Schulz A. S., Therrien F., Zelenitsky D. K., Gerdes A., Müller W. and Fiebig J. (2023) Evidence for heterothermic endothermy and reptile-like eggshell mineralization in Troodon, a non-avian maniraptoran theropod. *Proceedings of the National Academy of Sciences of the United States of America* 120.
- Takai, K., Nakamura, K., Toki, T., Tsunogai, U., Miyazaki, M., Miyazaki, J., Hirayama, H., Nakagawa, S., Nunoura, T., Horikoshi, K., 2008. Cell proliferation at 122°C and isotopically heavy CH₄ production by a hyperthermophilic methanogen under high-pressure cultivation. *Proc. Natl. Acad. Sci.* 105, 10949–10954.
- Tanaka, K., Ohde, S., 2010. Fluoride in coral aragonite related to seawater carbonate. *Geochim. J.* 44, 371–378.
- Tang, J., Dietzel, M., Böhml, F., Köhler, S.J., Eisenhauer, A., 2008a. Sr²⁺/Ca²⁺ and ⁴⁴Ca/⁴⁰Ca fractionation during inorganic calcite formation: II. Ca isotopes. *Geochimica et Cosmochimica Acta* 72, 3733–3745.
- Tang, J., Dietzel, M., Fernandez, A., Tripati, A.K., Rosenheim, B.E., 2014. Evaluation of kinetic effects on clumped isotope fractionation (Δ_{47}) during inorganic calcite precipitation. *Geochim. Cosmochim. Acta* 134, 120–136.
- Tang, J., Köhler, S.J., Dietzel, M., 2008b. Sr²⁺/Ca²⁺ and ⁴⁴Ca/⁴⁰Ca fractionation during inorganic calcite formation: I. Sr incorporation. *Geochimica et Cosmochimica Acta* 72, 3718–3732.
- Tang, Y., Elzinga, E.J., Jae, Lee Y., Reeder, R.J., 2007. Coprecipitation of chromate with calcite: Batch experiments and X-ray absorption spectroscopy. *Geochim. Cosmochim. Acta* 71, 1480–1493.
- Tegethoff, F.W., 2001. Calcium carbonate - From the Cretaceous Period into the 21th Century. Birkhäuser, Basel, Boston, Berlin.
- Templeton, A., Benzerara, K., 2015. Emerging Frontiers in Geomicrobiology. *Elements* 11, 423–429.
- Teng, F.Z., Dauphas, N., Watkins, J.M., 2017. Non-traditional stable isotopes: Retrospective and prospective. *Rev. Mineral. Geochim.* 1–26.
- Terakado, Y., Masuda, A., 1988. The coprecipitation of rare-earth elements with calcite and aragonite. *Chem. Geol.* 69, 103–110.
- Terakado, Y., Taniguchi, M., 2006. A new method for the study of trace element partitioning between calcium carbonate and aqueous solution: A test case for Sr and Ba incorporation into calcite. *Geochem. J.* 40, 161–170.
- Tesoriero, A.J., Pankow, J.F., 1996. Solid solution partitioning of Sr²⁺, Ba²⁺, and Cd²⁺ to calcite. *Geochim. Cosmochim. Acta* 60, 1053–1063.
- Thaler, C., Paris, G., Dellinger, M., Dissard, D., Berland, S., Marie, A., Labat, A., Bartolini, A., 2023. Impact of seawater sulfate concentration on sulfur concentration and isotopic composition in calcite of two cultured benthic foraminifera. *Biogeosciences* 20, 5177–5198.
- Thien, B., Kulik, D., Curti, E., 2014. A unified approach to model uptake kinetics of trace elements in complex aqueous – Solid solution systems. *Appl. Geochim.* 41, 135–150.
- Thobey, M., Konhauser, K.O., Fralick, P.W., Altermann, W., Visscher, P.T., Lalonde, S.V., 2019. Global importance of oxic molybdenum sinks prior to 2.6 Ga revealed by the Mo isotope composition of Precambrian carbonates. *Geology* 47, 559–562.
- Thomazo, C., Buoncristiani, J.F., Vennin, E., Pellenard, P., Cocquerez, T., Mugnier, J.L., Gérard, E., 2017. Geochemical processes leading to the precipitation of subglacial carbonate crusts at bossons glacier, mont blanc massif (French alps). *Frontiers. Earth Sci.* 5.
- Thorsnes, T., Chand, S., Brunstad, H., Lepland, A., Lågstad, P., 2019. Strategy for Detection and High-Resolution Characterization of Authigenic Carbonate Cold Seep Habitats Using Ships and Autonomous Underwater Vehicles on Glacially Influenced Terrain. *Frontiers in Marine. Science* 6.
- Tiefenthaler, J., Mazzotti, M., 2022. Experimental Investigation of a Continuous Reactor for CO₂ Capture and CaCO₃ Precipitation. *Frontiers. Chem. Eng.* 4.
- Tobler, D.J., Rodriguez, Blanco J., D., Sørensen H. O., Stipp S. L. S. and Dideriksen K., 2016. Effect of pH on Amorphous Calcium Carbonate Structure and Transformation. *Crystal Growth and Design* 16, 4500–4508.
- Töchterle, P., Dublyansky, Y., Stöbener, N., Mandić, M., Spötl, C., 2017. High-resolution isotopic monitoring of cave air CO₂. *Rapid Commun. Mass Spectrom.* 31, 895–900.

- Toker, E., Kayseri-Özer, M.S., Özkul, M., Kele, S., 2015. Depositional system and palaeoclimate interpretations of Middle to Late Pleistocene travertines: Kocabasa, Denizli, south-west Turkey. *Sedimentology* 62, 1360–1383.
- Tong, X., Mänd, K., Li, Y., Zhang, L., Peng, Z., Wu, Q., Li, P., Zhai, M., Robbins, L.J., Wang, C., Konhauser, K.O., 2021. Iron and Carbon Isotope Constraints on the Formation Pathway of Iron-Rich Carbonates within the Dagushan Iron Formation. *North China Craton. Minerals* 11, 94.
- Toroz, D., Song, F., Uddin, A., Chass, G.A., Di Tommaso, D., 2022. A Database of Solution Additives Promoting Mg^{2+} Dehydration and the Onset of $MgCO_3$ Nucleation. *Cryst. Growth Des.* 22, 3080–3089.
- Torres, J., Tissot, F., Santos, P., Ferrari, C., Kremer, C., Kremer, E., 2016. Interactions of W(VI) and Mo(VI) Oxyanions with Metal Cations in Natural Waters. *J. Solut. Chem.* 45, 1598–1611.
- Tosca, N.J., Tutolo, B.M., 2023. Alkalinity in Theory and Practice. *Elements* 19, 7–9.
- Toyama, K., Terakado, Y., 2014. Experimental study of rare earth element partitioning between calcite and sodium chloride solution at room temperature and pressure. *Geochem. J.* 48, 463–477.
- Tran, H., Rott, E., Sanders, D., 2019. Exploring the niche of a highly effective biocalcifier: calcification of the eukaryotic microalgae *Oocardium stratum* Nägeli 1849 in a spring stream of the Eastern Alps. *Facies* 65, 37.
- Tremaine, D.M., Froelich, P.N., Wang, Y., 2011. Speleothem calcite farmed in situ: Modern calibration of $\delta^{18}\text{O}$ and $\delta^{13}\text{C}$ paleoclimate proxies in a continuously-monitored natural cave system. *Geochim. Cosmochim. Acta* 75, 4929–4950.
- Tripathi, A.K., Hill, P.S., Eagle, R.A., Mosenfelder, J.L., Tang, J., Schauble, E.A., Eiler, J. M., Zeebe, R.E., Uchikawa, J., Coplen, T.B., Ries, J.B., Henry, D., 2015. Beyond temperature: Clumped isotope signatures in dissolved inorganic carbon species and the influence of solution chemistry on carbonate mineral composition. *Geochim. Cosmochim. Acta* 166, 344–371.
- Tsao, C., Yu, P.-T., Li, S.-L., Hsu, I.J., Chuang, Y.-C., Chang, C.-K., Chen, S.-J., Chan, J.C. C., 2020. Ambient Formation of Spherulites of Mg-Calcite in an Aqueous Lipid Solution through the Interplay between Multiple Pathways. *J. Phys. Chem. C* 124, 20538–20546.
- Tsusue, A., Holland, H.D., 1966. The coprecipitation of cations with CaCO_3 -III. The coprecipitation of Zn^{2+} with calcite between 50 and 250 °C. *Geochim. Cosmochim. Acta* 30, 439–453.
- Tucker M. E., Wright V. P. and Dickson J. A. D. (1990) *Carbonate Sedimentology*.
- Turchyn, A.V., Depaolo, D.J., 2019. Seawater chemistry through phanerozoic time. *Annu. Rev. Earth Planet. Sci.* 47, 197–224.
- Tutolo, B.M., Luhmann, A.J., Kong, X.-Z., Saar, M.O., Seyfried Jr., W.E., 2015. CO_2 sequestration in feldspar-rich sandstone: Coupled evolution of fluid chemistry, mineral reaction rates, and hydrogeochemical properties. *Geochim. Cosmochim. Acta* 160, 132–154.
- Uchikawa, J., Chen, S., Eiler, J.M., Adkins, J.F., Zeebe, R.E., 2021. Trajectory and timescale of oxygen and clumped isotope equilibration in the dissolved carbonate system under normal and enzymatically-catalyzed conditions at 25 °C. *Geochim. Cosmochim. Acta* 314, 313–333.
- Uchikawa, J., Harper, D.T., Penman, D.E., Zachos, J.C., Zeebe, R.E., 2017. Influence of solution chemistry on the boron content in inorganic calcite grown in artificial seawater. *Geochim. Cosmochim. Acta* 218, 291–307.
- Uchikawa, J., Penman, D.E., Harper, D.T., Farmer, J.R., Zachos, J.C., Planavsky, N.J., Zeebe, R.E., 2023. Sulfate and phosphate oxyanions alter B/Ca and $\delta^{11}\text{B}$ in inorganic calcite at constant pH: Crystallographic controls outweigh normal kinetic effects. *Geochim. Cosmochim. Acta* 343, 353–370.
- Uchikawa, J., Penman, D.E., Zachos, J.C., Zeebe, R.E., 2015. Experimental evidence for kinetic effects on B/Ca in synthetic calcite: Implications for potential $\text{B}(\text{OH})_4^-$ and $\text{B}(\text{OH})_3$ incorporation. *Geochim. Cosmochim. Acta* 150, 171–191.
- Uemura, R., Kina, Y., Shen, C.C., Omine, K., 2020. Experimental evaluation of oxygen isotopic exchange between inclusion water and host calcite in speleothems. *Clim. Past* 16 (1), 17–27. <https://doi.org/10.5194/cp-16-17-2020>.
- Urbanová, P., Boaretto, E., Artioli, G., 2020. The state-of-the-art of dating techniques applied to ancient mortars and binders: a review. *Radiocarbon* 62, 503–525.
- Urey, H.C., 1947. The thermodynamic properties of isotopic substances. Liversidge lecture, delivered before the Chemical Society in the Royal Institution on December 18th, 1946. *Journal of the Chemical Society (Resumed)* 10.1039/jr9470000562, 562–581.
- Udowski, E., 1982. Reactions and equilibria in the systems $\text{CO}_2\text{-H}_2\text{O}$ and $\text{CaCO}_3\text{-CO}_2\text{-H}_2\text{O}$ (0 ° to 50 °C). A review. *Neues Jahrbuch für Mineralogie, Abhandlungen* 144, 148–171.
- Udowski, E., 1994. Synthesis of Dolomite and Geochemical Implications. In: *Dolomites*. 345–360.
- Udowski, E., Hoefs, J., 1993. Oxygen isotope exchange between carbonic acid, bicarbonate, carbonate, and water: A re-examination of the data of McCREA(1950) and an expression for the overall partitioning of oxygen isotopes between the carbonate species and water. *Geochim. Cosmochim. Acta* 57, 3815–3818.
- Uwakwe, O.C., Riechelmann, S., Hoffmann, R., Spötl, C., Jantschke, A., Hansen, M., Immenhauser, A., 2023. Experimental precipitation of cryogenic carbonate. *Chem. Geol.* 635.
- Valdez, B., Schorr, M., Quintero, M., Carrillo, M., Zlatev, R., Stoytcheva, M., De Dios, Ocampo J., 2009. Corrosion and scaling at Cerro Prieto geothermal field. *Anti-Corrosion Methods and Materials* 56, 28–34.
- Válek, J., Hughes, J.J., Groot, C.J.W.P., 2013. Historic mortars: Characterisation, assessment and repair. A state-of-the-art summary. *RILEM Bookseries* 7, 1–12.
- Valera-Fernández, D., Cabadas-Báez, H., Solleiro-Rebolledo, E., Landa-Arreguin, F.J., Sedov, S., 2020. Pedogenic carbonate crusts (calcretes) in karstic landscapes as archives for paleoenvironmental reconstructions – A case study from Yucatan Peninsula, Mexico. *Catena* 194.
- Valley, J.W., Cole, D.R., 2001. Stable Isotope Geochemistry. De Gruyter, Berlin, Boston.
- Valley, J.W., Eiler, J.M., Graham, C.M., Gibson, E.K., Romanek, C.S., Stolper, E.M., 1997. Low-temperature carbonate concretions in the Martian meteorite ALH84001: evidence from stable isotopes and mineralogy. *Science* 275 (5306), 1633–1638.
- Van Balen, K., 2005. Carbonation reaction of lime, kinetics at ambient temperature. *Cem. Concr. Res.* 35, 647–657.
- van Dijk, I., Barras, C., de Nooijer, L.J., Mouret, A., Geerken, E., Oron, S., Reichart, G.J., 2019. Coupled calcium and inorganic carbon uptake suggested by magnesium and sulfur incorporation in foraminiferal calcite. *Biogeosciences* 16, 2115–2130.
- van Dijk, I., de Nooijer, L.J., Barras, C., Reichart, G.J., 2020. Mn Incorporation in Large Benthic Foraminifera: Differences Between Species and the Impact of pCO₂. *Frontiers. Earth Sci.* 8.
- van Dijk, I., de Nooijer, L.J., Wolthers, M., Reichart, G.J., 2017. Impacts of pH and $[\text{CO}_3^{2-}]$ on the incorporation of Zn in foraminiferal calcite. *Geochim. Cosmochim. Acta* 197, 263–277.
- Van Driessche, A.E.S., Kellermeier, M., Benning, L.G., Gebauer, D., 2017. New Perspectives on Mineral Nucleation and Growth - From Solution Precursors to Solid Materials. Springer International Publishing, Switzerland, p. 380.
- Van, H.T., Nguyen, L.H., Nguyen, V.D., Nguyen, X.H., Nguyen, T.H., Nguyen, T.V., Vigneswaran, S., Rinklebe, J., Tran, H.N., 2019. Characteristics and mechanisms of cadmium adsorption onto biogenic aragonite shells-derived biosorbent: Batch and column studies. *J. Environ. Manag.* 241, 535–548.
- Van Strydonck M. (2016) ¹⁴C dating of mortar: a historic review. In: *Proceedings of the 4th Historic Mortars Conference HMC2016:648–655*. pp. 648–655.
- Vasylyiev, G., Vasylyeva, S., Novosad, A., Gerasymenko, Y., 2018. Ultrasonic modification of carbonate scale electrochemically deposited in tap water. *Ultrasound. Sonochem.* 48, 57–63.
- Veizer, J., Ala, D., Azmy, K., Bruckschen, P., Buhl, D., Bruhn, F., Carden, G.A.F., Diener, A., Ebnet, S., Godderis, Y., Jasper, T., Korte, C., Pawellek, F., Podlaha, O.G., Strauss, H., 1999. ⁸⁷Sr/⁸⁶Sr, $\delta^{13}\text{C}$ and $\delta^{18}\text{O}$ evolution of Phanerozoic seawater. *Chem. Geol.* 161, 59–88.
- Verrecchia, E.P., Freytet, P., Verrecchia, K.E., Dumont, J.-L., 1995. Spherulites in calcrete laminar crusts: biogenic CaCO_3 precipitation as a major contributor to crust formation. *J. Sediment. Res.* 65, 690–700.
- Vijay, K., Murmu, M., Deo, S.V., 2017. Bacteria based self healing concrete – A review. *Constr. Build. Mater.* 152, 1008–1014.
- Voegelin, A.R., Nägler, T.F., Beukes, N.J., Lacassie, J.P., 2010. Molybdenum isotopes in late Archean carbonate rocks: Implications for early Earth oxygenation. *Precambrian Res.* 182, 70–82.
- Voigt, M., Mavromatis, V., Oelkers, E.H., 2017. The experimental determination of REE partition coefficients in the water-calcite system. *Chem. Geol.* 462, 30–43.
- von Blanckenburg, F., von Wirén, N., Guelke, M., Weiss, D.J., Bullen, T.D., 2009. Fractionation of Metal Stable Isotopes by Higher Plants. *Elements* 5, 375–380.
- Vroom, J.M., De Grauw, K.J., Gerritsen, H.C., Bradshaw, D.J., Marsh, Ph.D., Watson, G. K., Birmingham, J.J., Allison, C., 1999. Depth Penetration and Detection of pH Gradients in Biofilms by Two-Photon Excitation Microscopy. *Appl. Environ. Microbiol.* 65, 3502–3511.
- Waite, A.J., Swart, P.K., Rosenberg, B.E., Rosenberg, A.D., 2018. Improved calibration of the Sr/Ca-temperature relationship in the sclerosponge *Ceratoporella nicholsoni*: Re-evaluating Sr/Ca derived records of post-industrial era warming. *Chem. Geol.* 488, 56–61.
- Walker, J.M., Greene, H.J.M., Moazzam, Y., Quinn, P.D., Parker, J.E., Langer, G., 2024. An uneven distribution of strontium in the coccolithophore *Scyphosphaera apsteini* revealed by nanoscale X-ray fluorescence tomography. *Environ. Sci. Process. Impacts* 26, 966–974.
- Wallace, A.F., Hedges, L.O., Fernandez-Martinez, A., Raiteri, P., Gale, J.D., Waychunas, G.A., Whitlam, S., Banfield, J.F., De Yoreo, J.J., 2013. Microscopic evidence for liquid-liquid separation in supersaturated CaCO_3 solutions. *Science* 341, 885–889.
- Wang, C., Reinhard, C.T., Rybacki, K.S., Hardisty, D.S., Ossa Ossa, F., Wang, X., Hofmann, A., Asael, D., Robbins, L.J., Zhang, L., Planavsky, N.J., 2021b. Chromium isotope systematics and the diagenesis of marine carbonates. *Earth Planet. Sci. Lett.* 562, 116824.
- Wang, H., Alfredsson, V., Tropsch, J., Etzl, R., Nylander, T., 2013a. Formation of CaCO_3 Deposits on Hard Surfaces—Effect of Bulk Solution Conditions and Surface Properties. *ACS Appl. Mater. Interfaces* 5, 4035–4045.
- Wang, J., Jacobson, A.D., Sageman, B.B., Hurtgen, M.T., 2023b. Application of the $\delta^{44}/\delta^{40}\text{Ca}-\delta^{88}/\delta^{86}\text{Sr}$ multi-proxy to Namibian Marinoa cap carbonates. *Geochim. Cosmochim. Acta* 353, 13–27.
- Wang, J., Jacobson, A.D., Zhang, H., Ramezani, J., Sageman, B.B., Hurtgen, M.T., Bowring, S.A., Shen, S.-Z., 2019b. Coupled $\delta^{44}/\delta^{40}\text{Ca}$, $\delta^{88}/\delta^{86}\text{Sr}$, and $\delta^{87}\text{Sr}/\delta^{86}\text{Sr}$ geochemistry across the end-Permian mass extinction event. *Geochim. Cosmochim. Acta* 262, 143–165.
- Wang, J., Tarhan, L.G., Jacobson, A.D., Oehlert, A.M., Planavsky, N.J., 2023a. The evolution of the marine carbonate factory. *Nature* 615, 265–269.
- Wang, L., Cheng, W.-C., Xue, Z.-F., Zhang, B., Lv, X.-J., 2023d. Immobilizing of lead and copper using chitosan-assisted enzyme-induced carbonate precipitation. *Environ. Pollut.* 319, 120947.
- Wang, S., Liu, K., Wang, J., Li, Y., Li, Z., Yang, H., Mo, T., 2023c. Geochemistry of syntaxial calcite veins in ultra-deep sandstone reservoirs from the Kuqa depression, western China. *J. Struct. Geol.* 173, 104895.
- Wang, S., Lu, K., Wang, T., Wu, J., Zheng, H., Huang, Y., 2020. A method for isotope exchange kinetics in mineral-water system—an in-situ study on oxygen isotope exchange in $\text{Na}_2\text{CO}_3\text{-H}_2\text{O}$ system. *Spectrochim. Acta A Mol. Biomol. Spectrosc.* 241, 118648.

- Wang, W., Wu, Z., Huang, F., 2021c. Equilibrium barium isotope fractionation between minerals and aqueous solution from first-principles calculations. *Geochim. Cosmochim. Acta* 292, 64–77.
- Wang, W., Zhou, C., Liu, Y., Wu, Z., Huang, F., 2019a. Equilibrium Mg isotope fractionation among aqueous Mg^{2+} , carbonates, brucite and lizardite: Insights from first-principles molecular dynamics simulations. *Geochim. Cosmochim. Acta* 250, 117–129.
- Wang, X., Edwards, R.L., Auler, A.S., Cheng, H., Kong, X., Wang, Y., Cruz, F.W., Dorale, J.A., Chiang, H.-W., 2017. Hydroclimate changes across the Amazon lowlands over the past 45,000 years. *Nature* 541, 204–207.
- Wang, Z., Chen, J., Cai, H., Yuan, W., Yuan, S., 2021a. Coprecipitation of metal ions into calcite: an estimation of partition coefficients based on field investigation. *Acta Geochimica* 40, 67–77.
- Wang, Z., Hu, P., Gaetani, G., Liu, C., Saenger, C., Cohen, A., Hart, S., 2013b. Experimental calibration of Mg isotope fractionation between aragonite and seawater. *Geochim. Cosmochim. Acta* 102, 113–123.
- Wanner, C., Eichinger, F., Jahrfeld, T., Diamond, L.W., 2017. Causes of abundant calcite scaling in geothermal wells in the Bavarian Molasse Basin, Southern Germany. *Geothermics* 70, 324–338.
- Warren, J., 2016. Evaporites. In: White, W.M. (Ed.), *Encyclopedia of Geochemistry: A Comprehensive Reference Source on the Chemistry of the Earth*. Springer International Publishing, Cham, pp. 1–8. https://doi.org/10.1007/978-3-319-39193-9_100-1.
- Warsinger, D.M., Swaminathan, J., Guillen-Burrieza, E., Arafat, H.A., Lienhard, V.J.H., 2015. Scaling and fouling in membrane distillation for desalination applications: A review. *Desalination* 356, 294–313.
- Wassenburg, J.A., Riechelmann, S., Schröder-Ritzrau, A., Riechelmann, D.F.C., Richter, D.K., Immenhauser, A., Terente, M., Constantin, S., Hachenberg, A., Hansen, M., Scholz, D., 2020. Calcite Mg and Sr partition coefficients in cave environments: Implications for interpreting prior calcite precipitation in speleothems. *Geochim. Cosmochim. Acta* 269, 581–596.
- Wassenburg, J.A., Samanta, A., Sha, L., Lee, H., Scholz, D., Cheng, H., Stoll, B., Ait, Brahim Y., Budsky, A., Breitenbach, S.F.M., 2024. Trace element partitioning controls on cave drip water compositions through prior calcite and aragonite precipitation. *Communications Earth & Environment* 5, 488.
- Wassenburg, J.A., Vonhof, H.B., Cheng, H., Martinez-Garcia, A., Ebner, P.-R., Li, X., Zhang, H., Sha, L., Tian, Y., Edwards, R.L., Fiebig, J., Haug, G.H., 2021. Penultimate deglaciation Asian monsoon response to North Atlantic circulation collapse. *Nat. Geosci.* 14, 937–941.
- Watkins, J.M., DePaolo, D.J., Watson, E.B., 2017. Kinetic fractionation of non-traditional stable isotopes by diffusion and crystal growth reactions. *Rev. Mineral. Geochem.* 82, 85–125.
- Watkins, J.M., Hunt, J.D., 2015. A process-based model for non-equilibrium clumped isotope effects in carbonates. *Earth Planet. Sci. Lett.* 432, 152–165.
- Watkins, J.M., Nielsen, L.C., Ryerson, F.J., DePaolo, D.J., 2013. The influence of kinetics on the oxygen isotope composition of calcium carbonate. *Earth Planet. Sci. Lett.* 375, 349–360.
- Watson, E.B., 2004. A conceptual model for near-surface kinetic controls on the trace-element and stable isotope composition of abiogenic calcite crystals. *Geochim. Cosmochim. Acta* 68, 1473–1488.
- Webb, G.E., Kamber, B.S., 2000. Rare earth elements in Holocene reefal microbialites: a new shallow seawater proxy. *Geochim. Cosmochim. Acta* 64, 1557–1565.
- Wedenig, M., Boch, R., Leis, A., Wagner, H., Dietzel, M., 2021. Green Inhibitor Performance against $CaCO_3$ Scaling: Rate-Modeling Aided Test Procedure. *Cryst. Growth Des.* 21, 1959–1971.
- Wedenig, M., Eichinger, S., Boch, R., Leis, A., Wagner, H., Dietzel, M., 2023. Understanding of tunnel drainage scale formation by in-situ monitoring. *Tunn. Undergr. Space Technol.* 131, 104853.
- Wei D., Gao Z., Zhang L., Fan T., Wang J., Zhang C., Zhu D., Ju J. and Luo W. (2023b) Application of blocky calcite vein LA-MC-ICP-MS U-Pb dating and geochemical analysis to the study of tectonic-fault-fluid evolutionary history of the Tabei Uplift, Tarim Basin. *Sediment. Geol.* 453.
- Wei, G., Sun, M., Li, X., Nie, B., 2000. Mg/Ca, Sr/Ca and U/Ca ratios of a porites coral from Sanya Bay, Hainan Island, South China Sea and their relationships to sea surface temperature. *Palaeogeogr. Palaeoclimatol. Palaeoecol.* 162, 59–74.
- Wei, G.-Y., Zhang, F., Yin, Y.-S., Lin, Y.-B., Pogge von Strandmann, P.A.E., Cao, M., Li, N., Xiong, G., Chen, X., Fan, C., Xu, C., Tan, F., Zhang, X., Yang, H., Ling, H.-F., Shen, S.-Z., 2023a. A 13 million-year record of Li isotope compositions in island carbonates: Constraints on bulk inorganic carbonate as a global seawater Li isotope archive. *Geochim. Cosmochim. Acta* 344, 59–72.
- Wei, G.-Y., Zhang, F., Yin, Y.-S., Lin, Y.-B., Pogge von Strandmann, P.A.E., Cao, M., Li, N., Xiong, G., Chen, X., Fan, C., Xu, C., Tan, F., Zhang, X., Yang, H., Ling, H.-F., Shen, S.-Z., 2023c. A 13 million-year record of Li isotope compositions in island carbonates: Constraints on bulk inorganic carbonate as a global seawater Li isotope archive. *Geochim. Cosmochim. Acta* 344, 59–72.
- Wei, H.Z., Zhao, Y., Liu, X., Wang, Y.J., Lei, F., Wang, W.Q., Li, Y.C., Lu, H.Y., 2021. Evolution of paleo-climate and seawater pH from the late Permian to postindustrial periods recorded by boron isotopes and B/Ca in biogenic carbonates. *Earth Sci. Rev.* 215.
- Wei, Y., Deng, W., Ma, J., Chen, X., Zeng, T., Wei, G., 2022. Evaluation of coral skeletal $\delta^{88}Sr$ as a paleoclimate proxy in the northern South China Sea. *Palaeogeogr. Palaeoclimatol. Palaeoecol.* 592, 110906.
- Weidendorfer, D., Schmidt, M.W., Mattsson, H.B., 2017. A common origin of carbonatite magmas. *Geology* 45, 507–510.
- Weidlich, R., Bialik, O.M., Rüggeberg, A., Grobety, B., Vennemann, T., Neuman, A., Makovsky, Y., Fouquet, A., 2023. Occurrence and genesis of cold-seep authigenic carbonates from the south-eastern Mediterranean Sea. *Depositional Rec.* 9, 844–870.
- Weiner S. and Dove P. M. (2003) 1. An Overview of Biomineralization Processes and the Problem of the Vital Effect. In *Biomineralization* (eds. M. D. Patricia, J. D. Y. James and W. Steve). De Gruyter, Berlin, Boston. pp. 1–30.
- Weise, A., Kluge, T., 2020. Isotope exchange rates in dissolved inorganic carbon between 40 °C and 90 °C. *Geochim. Cosmochim. Acta* 268, 56–72.
- Weissbach, T., Kluge, T., Affolter, S., Leuenberger, M.C., Vonhof, H., Riechelmann, D.F.C., Fohlemeister, J., Juhl, M.-C., Hemmer, B., Wu, Y., Warken, S.F., Schmidt, M., Frank, N., Aeschbach, W., 2023. Constraints for precise and accurate fluid inclusion stable isotope analysis using water-vapour saturated CRDS techniques. *Chem. Geol.* 617, 121268.
- Welch, S.A., Beard, B.L., Johnson, C.M., Braterman, P.S., 2003. Kinetic and equilibrium Fe isotope fractionation between aqueous Fe(II) and Fe(III). *Geochim. Cosmochim. Acta* 67, 4231–4250.
- Wen, T., Pinti, D.L., Castro, M.C., López-Hernández, A., Hall, C.M., Shouakar-Stash, O., Sandoval-Medina, F., 2018. A noble gas and $^{87}Sr/^{86}Sr$ study in fluids of the Los Azufres geothermal field, Mexico – Assessing impact of exploitation and constraining heat sources. *Chem. Geol.* 483, 426–441.
- Wendt, K.A., Pythoud, M., Moseley, G.E., Dublyansky, Y.V., Edwards, R.L., Spötl, C., 2019. Paleohydrology of southwest Nevada (USA) based on groundwater $^{234}U/^{238}U$ over the past 475 k.y. *GSA Bull.* 132, 793–802.
- Wenz, S., Scholz, D., Sürmelihindi, G., Passchier, C.W., Jochum, K.P., Andreae, M.O., 2016. 230Th/U-dating of carbonate deposits from ancient aqueducts. *Quat. Geochronol.* 32, 40–52.
- Weremeichik, J.M., Gabitov, R.I., Thien, B.M.J., Sadekov, A., 2017. The effect of growth rate on uranium partitioning between individual calcite crystals and fluid. *Chem. Geol.* 450, 145–153.
- Westphal, A., Eichinger, F., Eichinger, L., Würdemann, H., 2019. Change in the microbial community of saline geothermal fluids amended with a scaling inhibitor: effects of heat extraction and nitrate dosage. *Extremophiles* 23, 283–304.
- Westphal, H., Riegl, B., Eberli, G.P., 2010. Carbonate Depositional Systems: Assessing Dimensions and Controlling Parameters: The Bahamas. Springer Science & Business Media, Belize and the Persian/Arabian Gulf.
- White, A.F., 1977. Sodium and potassium coprecipitation in aragonite. *Geochim. Cosmochim. Acta* 41, 613–625.
- White, W.B., Culver, D.C., Pipan, T., 2019. *Encyclopedia of Caves*, 3rd ed. Academic Press, Elsevier, London, UK.
- White, W.M., 2023. *Isotope Geochemistry*, second ed. Wiley.
- Whiticar, M.J., Suess, E., Wefer, G., Müller, P.J., 2022. Calcium Carbonate Hexahydrate (Kaite): History of Mineral Formation as Recorded by Stable Isotopes. *Minerals* 12, 1627.
- Wiederhold, J.G., 2015. Metal Stable Isotope Signatures as Tracers in Environmental Geochemistry. *Environ. Sci. Technol.* 49, 2606–2624.
- Wiesli, R.A., Beard, B.L., Johnson, C.M., 2004. Experimental determination of Fe isotope fractionation between aqueous Fe(II), siderite and "green rust" in abiotic systems. *Chem. Geol.* 211, 343–362.
- Winkelbauer, H.A., Hoogakker, B.A.A., Chance, R.J., Davis, C.V., Anthony, C.J., Bischoff, J., Carpenter, L.J., Chereny, S.R.N., Hamilton, E.M., Holdship, P., Peck, V. L., Poulton, A.J., Stinchcombe, M.C., Wishner, K.F., 2023. Planktic foraminifera iodine/calcium ratios from plankton tows. *Frontiers in Marine. Science* 10.
- Winkelstern, I.Z., Kaczmarek, S.E., Lohmann, K.C., Humphrey, J.D., 2016. Calibration of dolomite clumped isotope thermometry. *Chem. Geol.* 443, 32–38.
- Wolff-Boenisch, D., Evans, K., 2014. Review of available fluid sampling tools and sample recovery techniques for groundwater and unconventional geothermal research as well as carbon storage in deep sedimentary aquifers. *J. Hydrol.* 513, 68–80.
- Wolthers, M., Nehrke, G., Gustafsson, J.P., Van Cappellen, P., 2012. Calcite growth kinetics: Modeling the effect of solution stoichiometry. *Geochim. Cosmochim. Acta* 77, 121–134.
- Won, Y.-H., Jang, H.S., Chung, D.-W., Stanciu, L.A., 2010. Multifunctional calcium carbonate microparticles: Synthesis and biological applications. *J. Mater. Chem.* 20, 7728–7733.
- Wostbrock, J. A. G. and Sharp Z. D. (2021) Triple Oxygen Isotopes in Silica–Water and Carbonate–Water Systems. *Rev. Mineral. Geochem.* 86, 367–400.
- Wright, V.P., 1992. A revised classification of limestones. *Sediment. Geol.* 76, 177–185.
- Wright, V.P., 2007. Calcrite. In *Geochemical Sediments and Landscapes*. 10–45.
- Würdemann, H., Westphal, A., Kleyböcker, A., Miethling-Graff, R., Teitz, S., Kasina, M., Seibt, A., Wolfgramm, M., Eichinger, F., Lerm, S., 2016. Microbial metabolic processes affect the operation of geothermal plants and the success of countermeasures. *Grundwasser* 21, 93–106.
- Würdemann, H., Westphal, A., Lerm, S., Kleyböcker, A., Teitz, S., Kasina, M., Miethling-Graff, R., Seibt, A., Wolfgramm, M., 2014. Influence of Microbial Processes on the Operational Reliability in a Geothermal Heat Store – Results of Long-term Monitoring at a Full Scale Plant and First Studies in a Bypass System. *Energy Procedia* 59, 412–417.
- Wynn, P.M., Ambler, S., Grefe, I., Soto, D.X., Surridge, B.W.J., Gabitov, R.I., Barker, P.A., Anwar, J., Quin, A., Pereira, M.G., Grant, H.K., 2021. Contemporary systematics of vadose zone nitrate capture by speleothem carbonate. *Chem. Geol.* 571, 120172.
- Wynn, P.M., Fairchild, I.J., Baker, A., Baldini, J.U.L., McDermott, F., 2008. Isotopic archives of sulphate in speleothems. *Geochim. Cosmochim. Acta* 72, 2465–2477.
- Wynn, P.M., Fairchild, I.J., Borsato, A., Spötl, C., Hartland, A., Baker, A., Frisia, S., Baldini, J.U.L., 2018. Sulphate partitioning into calcite: Experimental verification of pH control and application to seasonality in speleothems. *Geochim. Cosmochim. Acta* 226, 69–83.

- Xie, X., Yan, L., Li, J., Guan, L., Chi, Z., 2021. Cadmium isotope fractionation during Cd-calcite coprecipitation: Insight from batch experiment. *Sci. Total Environ.* 760, 14330.
- Xie, Z., Huang, K.-J., Xia, Y., Cline, J., Tan, Q., Liu, J., Xiao, J., Yan, B., 2022. Heavy $\delta^{26}\text{Mg}$ values in carbonate indicate a magmatic-hydrothermal origin of Carlin-type Au deposit. *Geochim. Cosmochim. Acta* 333, 166–183.
- Xiong, Z., Ding, L., Xie, J., 2019. Carbonate clumped isotope (Δ_{47}) thermometry and its application in paleoelevation reconstruction. *Kexue Tongbao/Chinese Science Bulletin* 64, 1722–1737.
- Xto, J., Wetter, R., Borca, C.N., Frieh, C., van Bokhoven, J.A., Huthwelker, T., 2019b. Droplet-based in situ X-ray absorption spectroscopy cell for studying crystallization processes at the tender X-ray energy range. *RSC Adv.* 9, 34004–34010.
- Xto, J.M., Du, H., Borca, C.N., Amstad, E., van Bokhoven, J.A., Huthwelker, T., 2019a. Tuning the Incorporation of Magnesium into Calcite during Its Crystallization from Additive-Free Aqueous Solution. *Cryst. Growth Des.* 19, 4385–4394.
- Xu, J., Balhoff, M.T., 2023. Emergence of Power-Law Particle Size Distribution in Microfluidic Calcium Carbonate Precipitation: An Extended Yule Process with a Ripening Effect. *Phys. Rev. Lett.* 131.
- Xu, L., Xie, J., Zhang, S., Choi, S., Kim, N.-H., Gao, D., Jin, X., Jia, S., Gao, Y., 2022b. Fossil turtle eggs from the Upper Cretaceous Gaogou Formation, Xiaguan-Gaoqiu Basin, Neixiang County, Henan Province, China: interpretation of the transformation from aragonite to calcite in fossil turtle eggshell. *Cretac. Res.* 134, 105166.
- Xu, N., Li, Y., Zheng, L., Gao, Y., Yin, H., Zhao, J., Chen, Z., Chen, J., Chen, M., 2014. Synthesis and application of magnesium amorphous calcium carbonate for removal of high concentration of phosphate. *Chem. Eng. J.* 251, 102–110.
- Xu, W., Zhou, G., Wan, C., Zhang, L., Tao, J., Xu, C., Yan, X., 2022a. Geochemical Characteristics and Fluid Properties of the Qixia Formation Dolomites of the Middle Permian in the Shuangyushu Block, NW Sichuan Basin, China. *Frontiers in Earth Science* 10.
- Xu, Z., Zhao, Y., Wang, J., Chang, H., 2019. Inhibition of calcium carbonate fouling on heat transfer surface using sodium carboxymethyl cellulose. *Appl. Therm. Eng.* 148, 1074–1080.
- Yamazaki, A., Yano, M., Harii, S., Watanabe, T., 2021. Effects of light on the Ba/Ca ratios in coral skeletons. *Chem. Geol.* 559, 119911.
- Yan, H., Liu, Z., Sun, H., 2017. Effect of in-stream physicochemical processes on the seasonal variations in $\delta^{13}\text{C}$ and $\delta^{18}\text{O}$ values in laminated travertine deposits in a mountain stream channel. *Geochim. Cosmochim. Acta* 202, 179–189.
- Yan, H., Liu, Z., Sun, H., 2020. Large degrees of carbon isotope disequilibrium during precipitation-associated degassing of CO_2 in a mountain stream. *Geochim. Cosmochim. Acta* 273, 244–256.
- Yan, W., Liang, B., Li, W., Huang, H., Shi, D., Chen, Z., Li, Z., Yu, M., Wei, G., Huang, K., 2024. Study on the growth mechanism of porous spherical calcium carbonate synthesized by carbonization controlled by amino acids. *J. Solid State Chem.* 329.
- Yan, X., Li, W., Zhu, C., Peacock, C.L., Liu, Y., Li, H., Zhang, J., Hong, M., Liu, F., Yin, H., 2023. Zinc Stable Isotope Fractionation Mechanisms during Adsorption on and Substitution in Iron (Hydroxides). *Environ. Sci. Technol.* 57, 6636–6646.
- Yan, Z., Gowthaman, S., Nakashima, K., Kawasaki, S., 2022. Polymer-assisted enzyme induced carbonate precipitation for non-ammonia emission soil stabilization. *Sci. Rep.* 12, 8821.
- Yang, F., Zhang, B., Pan, C., Zeng, Y., 2009. Traditional mortar represented by sticky rice lime mortar—One of the great inventions in ancient China. *Science in China Series E: Technological Sciences* 52, 1641–1647.
- Yao, X., Xie, C., Dong, X., Oganov, A.R., Zeng, Q., 2018. Novel high-pressure calcium carbonates. *Phys. Rev. B* 98, 014108.
- Yardley, B.W.D., Ewing, R.C., Whittleston, R.A., 2016. Deep-Mined Geological Disposal of Radioactive Waste. *Elements* 12, 225–296.
- Ye, F., Tian, C.M., He, B., Zhao, M., Wang, J., Han, X.B., Song, G.F., 2021. Experimental Study on Scaling and Clogging in Drainage System of Tunnels Under Construction. *Zhongguo Gonglu Xuebao/China Journal of Highway and Transport* 34, 159–170.
- Yin, X., Liu, F., Liu, Q., Zhang, Y., Gao, C., Zhang, S., Ridley, M.K., Liu, Y., 2023. Boron isotope fractionation between B(OH)_3 and B(OH)_4^- in aqueous solution: A theoretical investigation beyond the harmonic and Born–Oppenheimer approximations. *Chem. Geol.* 627, 121455.
- Yokoyama, Y., Mitsunobu, S., Tanaka, K., Itai, T., Takahashi, Y., 2009. A Study on the Coprecipitation of Arsenite and Arsenate into Calcite Coupled with the Determination of Oxidation States of Arsenic Both in Calcite and Water. *Chem. Lett.* 38, 910–911.
- Yoshimura, T., Tamenori, Y., Suzuki, A., Kawahata, H., Iwasaki, N., Hasegawa, H., Nguyen, L.T., Kuroyanagi, A., Yamazaki, T., Kuroda, J., Ohkouchi, N., 2017. Altervalent substitution of sodium for calcium in biogenic calcite and aragonite. *Geochim. Cosmochim. Acta* 202, 21–38.
- Yoshimura, T., Tanimizu, M., Inoue, M., Suzuki, A., Iwasaki, N., Kawahata, H., 2011. Mg isotope fractionation in biogenic carbonates of deep-sea coral, benthic foraminifera, and hermatypic coral. *Anal. Bioanal. Chem.* 401, 2755–2769.
- Yoshimura, T., Wakaki, S., Iwasaki, N., Ishikawa, T., Ohkouchi, N., 2022. Stable Sr isotope ($^{88}\text{Sr}/^{86}\text{Sr}$) fractionation in calcite precious corals. *Frontiers in Marine Science* 9.
- Young E. D. and Galy A. (2004) The isotope geochemistry of magnesium. In: C.M. Johnson, B.L. Beard, F. Albarede (Eds): *Stable isotope geochemistry. Chapter 6. Reviews of Mineralogy and Geochemistry*. 55, 197–230.
- Yu, P.-T., Tsao, C., Wang, C.-C., Chang, C.-Y., Wang, C.-H., Chan, J.C.C., 2017. High-Magnesium Calcite Mesocrystals: Formation in Aqueous Solution under Ambient Conditions. *Angew. Chem. Int. Ed.* 56, 16202–16206.
- Yu, X., Fang, Z., He, X., Yi, L., Deng, C., Yan, W., Qin, L., 2023. Chromium isotopic compositions of a reef in the South China Sea: Biological effects and influence from early diagenetic Mn-oxides reduction. *Palaeogeogr. Palaeoclimatol. Palaeoecol.* 628, 111729.
- Yuan, C., Liu, S.-A., Chen, J., Fang, L., 2022. Zinc isotopic evidence for enhanced continental weathering and organic carbon burial during the late Cambrian SPICE event. *Palaeogeogr. Palaeoclimatol. Palaeoecol.* 608, 111302.
- Yuan, Y., Chen, T., Zhang, F., Liu, Y., Xiong, G., Wei, G.-Y., Dahl, T.W., Yan, W., Ling, H.-F., Cheng, H., Shen, S.-Z., 2023. Substantial incorporation of isotopically heavy reduced U species into marine carbonate sediments. *Geochim. Cosmochim. Acta* 358, 27–37.
- Yumol, L.M., Uchikawa, J., Zeebe, R.E., 2020. Kinetic isotope effects during CO_2 hydration: Experimental results for carbon and oxygen fractionation. *Geochim. Cosmochim. Acta* 279, 189–203.
- Zachara, J.M., Cowan, C.E., Resch, C.T., 1991. Sorption of divalent metals on calcite. *Geochim. Cosmochim. Acta* 55, 1549–1562.
- Zachara, J.M., Kittrick, J.A., Dake, L.S., Harsh, J.B., 1989. Solubility and surface spectroscopy of zinc precipitates on calcite. *Geochim. Cosmochim. Acta* 53, 9–19.
- Zacherl, L., Baumann, T., 2023. Quantification of the effect of gas-water-equilibria on carbonate precipitation. *Geotherm. Energy* 11, 11.
- Zaihua, L., Svensson, U., Dreybrodt, W., Daoxian, Y., Buhmann, D., 1995. Hydrodynamic control of inorganic calcite precipitation in Huanglong Ravine, China: Field measurements and theoretical prediction of deposition rates. *Geochim. Cosmochim. Acta* 59, 3087–3097.
- Žák K., Onac B. P., Kadebskaya O. I., Filippi M., Dublyansky Y. and Luetscher M. (2018) Chapter 6 - Cryogenic Mineral Formation in Caves. In *Ice Caves* (eds. A. Perșoiu and S.-E. Lauritzen). Elsevier. pp. 123–162.
- Zakrzewska M., Rzepa G., Musialowski M., Goszcz A., Stasiuk R. and Debiec-Andrzejewska K. (2023) Reduction of bioavailability and phytotoxicity effect of cadmium in soil by microbial-induced carbonate precipitation using metabolites of ureolytic bacterium *Ochrobactrum sp. POC9*. *Frontiers in Plant Science* 14.
- Zamanian, K., Pustovoytov, K., Kuzyakov, Y., 2016. Pedogenic carbonates: Forms and formation processes. *Earth Sci. Rev.* 157, 1–17.
- Zammit, C.M., Shuster, J.P., Gagen, E.J., Southam, G., 2015. The Geomicrobiology of Supergene Metal Deposits. *Elements* 11, 337–342.
- Zaquin, T., Pinkas, I., Di Bisceglie, A.P., Mucaria, A., Milita, S., Fermani, S., Goffredo, S., Mass, T., Falini, G., 2022. Exploring coral calcification by calcium carbonate overgrowth experiments. *Cryst. Growth Des.* 22, 5045–5053.
- Zarei, T., Fuchs, E.C., Agostinho, L.L.F., Gebauer, D., Woisetschläger, J., Offerhaus, H.L., 2024. Intrinsic CO_2 nanobubbles in alkaline aqueous solutions. *Colloids Surf. A Physicochem. Eng. Asp.* 701, 134895.
- Zarrouk, S.J., Moon, H., 2014. Efficiency of geothermal power plants: A worldwide review. *Geothermics* 51, 142–153.
- Zeebe, E., Wolf-Gladrow, D., 2005. *CO_2 in seawater: Equilibrium, kinetics, isotopes* Elsevier. Amsterdam.
- Zeebe, R.E., 2009. Hydration in solution is critical for stable oxygen isotope fractionation between carbonate ion and water. *Geochim. Cosmochim. Acta* 73, 5283–5291.
- Zeebe, R.E., 2010. A new value for the stable oxygen isotope fractionation between dissolved sulfate ion and water. *Geochim. Cosmochim. Acta* 74, 818–828.
- Zeebe, R.E., 2014. Kinetic fractionation of carbon and oxygen isotopes during hydration of carbon dioxide. *Geochim. Cosmochim. Acta* 139, 540–552.
- Zeebe, R.E., 2020. Oxygen isotope fractionation between water and the aqueous hydroxide ion. *Geochim. Cosmochim. Acta* 289, 182–195.
- Zehner, J., Royne, A., Sikorski, P., 2021a. Calcite seed-assisted microbial induced carbonate precipitation (MICP). *PLoS One* 16, e0240763.
- Zehner, J., Royne, A., Sikorski, P., 2021b. A sample cell for the study of enzyme-induced carbonate precipitation at the grain-scale and its implications for biocementation. *Sci. Rep.* 11.
- Zeng, C., Hu, H., Feng, X., Wang, K., Zhang, Q., 2020. Activating CaCO_3 to enhance lead removal from lead-zinc solution to serve as green technology for the purification of mine tailings. *Chemosphere* 249, 126227.
- Zeyen, N., Benzerara, K., Beyssac, O., Daval, D., Muller, E., Thomazo, C., Tavera, R., López-García, P., Moreira, D., Duprat, E., 2021. Integrative analysis of the mineralogical and chemical composition of modern microbialites from ten Mexican lakes: What do we learn about their formation? *Geochim. Cosmochim. Acta* 305, 148–184.
- Zhang, C., Li, F., 2022. Magnesium isotope fractionation during carbonate precipitation associated with bacteria and extracellular polymeric substances. *Int. Biodeterior. Biodegradation* 173, 105441.
- Zhang, C., Yin, L., Ou, Y., Yang, G., Huang, L., Li, F., 2021. Contribution of selective bacterial extracellular polymeric substances to the polymorphism and morphologies of formed Ca/Mg carbonates. *Int. Biodeterior. Biodegradation* 160, 105213.
- Zhang F., Frýda J., Fakhraei M., Lin Y.-b., Wei G.-Y., Cao M., Li N., Zhou J., Frýdová B., Wei H. and Shen S.-Z. (2022a) Marine anoxia as a trigger for the largest Phanerozoic positive carbon isotope excursion: Evidence from carbonate barium isotope record. *Earth Planet. Sci. Lett.* 584, 117421.
- Zhang, G., Deng, Y., Chen, F., Li, M., Cao, J., Lai, H., Zhu, Y., Yang, S., Liang, Q., Kuang, Z., Fang, Y., Liu, Y., Jiang, X., Zhao, M., 2024. Copper and zinc isotopic compositions of methane-derived carbonates: implications for paleo-methane seepage and paleoenvironmental proxies. *GSA Bull.* 136, 4005–4017.
- Zhang, H., Brahim, Y.A., Li, H., Zhao, J., Kathayat, G., Tian, Y., Baker, J., Wang, J., Zhang, F., Ning, Y., Edwards, R.L., Cheng, H., 2019a. The Asian Summer Monsoon: Teleconnections and Forcing Mechanisms. A Review from Chinese Speleothem $d^{18}\text{O}$ Records. *Quaternary* 2, 38.
- Zhang, J., 2024. Oxygen Isotope Fractionation between Carbonate Minerals and Carbonic Acid Systems and Constraints for Environmental Science and Geological Processes. *Molecules* 29, 698.

- Zhang, J., Zhao, C., Zhou, A., Yang, C., Zhao, L., Li, Z., 2019b. Aragonite formation induced by open cultures of microbial consortia to heal cracks in concrete: Insights into healing mechanisms and crystal polymorphs. *Constr. Build. Mater.* 224, 815–822.
- Zhang, K., Shields, G.A., 2023. Early diagenetic mobilization of rare earth elements and implications for the Ce anomaly as a redox proxy. *Chem. Geol.* 635, 121619.
- Zhang, K., Tang, C.-S., Jiang, N.-J., Pan, X.-H., Liu, B., Wang, Y.-J., Shi, B., 2023. Microbial-induced carbonate precipitation (MICP) technology: a review on the fundamentals and engineering applications. *Environ. Earth Sci.* 82, 229.
- Zhang, S., DePaolo, D., 2020. Equilibrium calcite-fluid Sr/Ca partition coefficient from marine sediment and pore fluids. *Geochim. Cosmochim. Acta* 289.
- Zhang, T., Sun, R., Liu, Y., Chen, L., Zheng, W., Liu, C.-Q., Chen, J., 2022b. Copper and Zinc isotope signatures in scleratinian corals: Implications for Cu and Zn cycling in modern and ancient ocean. *Geochim. Cosmochim. Acta* 317, 395–408.
- Zhang, Y., Yin, H., Zhang, Q., Li, Y., Yao, P., 2016. Synthesis and characterization of novel polyaspartic acid/urea graft copolymer with acylamino group and its scale inhibition performance. *Desalination* 395, 92–98.
- Zhang, Z., Wang, J., 2023. Quantification of classical and non-classical crystallization pathways in calcite precipitation. *arXiv preprint arXiv:2203.11731v2*.
- Zhang, Z., Wang, J., 2024. Quantification of classical and non-classical crystallization pathways in calcite precipitation. *Earth Planet. Sci. Lett.* 636, 118712.
- Zhao, C., Zhang, Y., Cao, H., Zheng, X., Van Gerven, T., Hu, Y., Sun, Z., 2019b. Lithium carbonate recovery from lithium-containing solution by ultrasound assisted precipitation. *Ultras. Sonochem.* 52, 484–492.
- Zhao, D., Williams, J.M., Li, Z., Park, A.-H.A., Radlińska, A., Hou, P., Kawashima, S., 2023. Hydration of cement pastes with calcium carbonate polymorphs. *Cem. Concr. Res.* 173, 107270.
- Zhao, P., Tian, Y., You, J., Hu, X., Liu, Y., 2022b. Recent Advances of Calcium Carbonate Nanoparticles for Biomedical Applications. *Bioengineering (Basel)* 9 (11), 691.
- Zhao, T., Liu, W., Li, Y., Xu, Z., 2022a. Magnesium isotopic composition of rivers draining karst-dominated regions in Southwest China. *Chem. Geol.* 606, 121002.
- Zhao, T., Liu, W., Xu, Z., Sun, H., Zhou, X., Zhou, L., Zhang, J., Zhang, X., Jiang, H., Liu, T., 2019a. The influence of carbonate precipitation on riverine magnesium isotope signals: New constraints from Jinsha River Basin, Southeast Tibetan Plateau. *Geochim. Cosmochim. Acta* 248, 172–184.
- Zhao, Y., Wei, W., Li, S., Yang, T., Zhang, R., Somerville, I., Santosh, M., Wei, H., Wu, J., Yang, J., Chen, W., Tang, Z., 2021. Rare earth element geochemistry of carbonates as a proxy for deep-time environmental reconstruction. *Palaeogeogr. Palaeoclimatol. Palaeoecol.* 574, 110443.
- Zhong, S., Mucci, A., 1995. Partitioning of rare earth elements (REEs) between calcite and seawater solutions at 25°C and 1 atm, and high dissolved REE concentrations. *Geochim. Cosmochim. Acta* 59, 443–453.
- Zhong, S., Yin, Y., Liang, X., Deng, Q., 2024. Aragonite and Its Composites: Preparations, Properties and Applications. *European Journal of Inorganic Chemistry* 27 (20), e202300733.
- Zhou, J., Lundstrom, C.C., Fouke, B., Panno, S., Hackley, K., Curry, B., 2005. Geochemistry of speleothem records from southern Illinois: Development of (^{234}U)/(^{238}U) as a proxy for paleoprecipitation. *Chem. Geol.* 221, 1–20.
- Zhou, X., Rosenthal, Y., Haynes, L., Si, W., Evans, D., Huang, K.-F., Hönnisch, B., Erez, J., 2021. Planktic foraminiferal Na/Ca: A potential proxy for seawater calcium concentration. *Geochim. Cosmochim. Acta* 305, 306–322.
- Zhou, Y., Zhang, X., Wei, L., Liu, S., Zhang, B., Zhou, C., 2018. Experimental study on prevention of calcium carbonate crystallizing in drainage pipe of tunnel engineering. *Adv. Civ. Eng.* 2018, 9430517.
- Zhu, B., Ge, L., Yang, T., Jiang, S., Lv, X., 2019. Stable isotopes and rare earth element compositions of ancient cold seep carbonates from Enza River, northern Apennines (Italy): Implications for fluids sources and carbonate chimney growth. *Mar. Pet. Geol.* 109, 434–448.
- Zhu, C., Chen, T., Zhao, L., 2021. Magnesium partitioning into vaterite and its potential role as a precursor phase in foraminiferal Mg/Ca thermometer. *Earth Planet. Sci. Lett.* 567, 116989.
- Zhuang, D., Yan, H., Tucker, M.E., Zhao, H., Han, Z., Zhao, Y., Sun, B., Li, D., Pan, J., Zhao, Y., Meng, R., Shan, G., Zhang, X., Tang, R., 2018. Calcite precipitation induced by *Bacillus cereus* MRR2 cultured at different Ca^{2+} concentrations: Further insights into biotic and abiotic calcite. *Chem. Geol.* 500, 64–87.
- Zotzmann, J., Vetter, A., Regensburg, S., 2018. Evaluating efficiency and stability of calcite scaling inhibitors at high pressure and high temperature in laboratory scale. *Geotherm. Energy* 6, 18.
- Zou, Z., Bertinetti, L., Habraken, W.J.E.M., Fratzl, P., 2018. Reentrant phase transformation from crystalline ikaite to amorphous calcium carbonate. *CrystEngComm* 20, 2902–2906.
- Zou, Z., Habraken W. J. E. M., Matveeva G., Jensen A. C. S., Bertinetti L., Hood M. A., Sun C.-y., Gilbert P. U. P. A., Polishchuk I., Pokroy B., Mahamid J., Politi Y., Weiner S., Werner P., Bette S., Dinnebier R., Kolb U., Zolotoyabko E. and Fratzl P. (2019) A hydrated crystalline calcium carbonate phase: Calcium carbonate hemihydrate. *Science* 363, 396–400.
- Zou, Z., Yang, X., Albéric, M., Heil, T., Wang, Q., Pokroy, B., Politi, Y., Bertinetti, L., 2020. Additives Control the Stability of Amorphous Calcium Carbonate via Two Different Mechanisms: Surface Adsorption versus Bulk Incorporation. *Adv. Funct. Mater.* 30, 2000003.
- Zwicker, J., Smrzka, D., Vadillo, I., Jiménez-Gavilán, P., Giampouras, M., Peckmann, J., Bach, W., 2022. Trace and rare earth element distribution in hyperalkaline serpentinite-hosted spring waters and associated authigenic carbonates from the Ronda peridotite. *Appl. Geochim.* 147, 105492.